PhD degree in Systems Medicine (curriculum in Molecular Oncology)

European School of Molecular Medicine (SEMM),

University of Milan and University of Naples "Federico II"

Settore disciplinare: BIO/11

Weaponizing CRISPR/Cas9

Sara Tavella

IFOM - FIRC Institute of Molecular Oncology
Milan, Italy

Tutor: Dr. Fabrizio d'Adda di Fagagna

IFOM, Milan, IT

PhD Coordinator: Prof. Saverio Minucci

Anno accademico 2020-2021

Table of Contents

Figures Index

1 Abstract

One of the major limits of current therapies against cancer and viral infections is the non-specific toxicity that they often cause on healthy tissues because of their impact on important cellular mechanisms shared, to different extents, between diseased and healthy cells. For this reason, there is an unmet need for more specific and more effective therapies.

Wherefore, the aim of my project is the development of a novel strategy, with potential for therapy, that allows the induction of sequence-specific DNA lesions (DNA double-strand break, DSB), by the use of the CRISPR/Cas9 system targeting a genome sequence abnormality in diseased cells, while sparing normal cells. Potential applications of this approach can be cancer cells carrying genomic mutations or chromosomal rearrangements and infected cells carrying an integrated proviral genome. Importantly, whether the aberrant genome sequences are expressed or not is irrelevant for the efficacy of this approach.

As a proof of principle, I generated, in two parallel cell systems, an isogenic pair of cell lines with a healthy and a diseased counterpart. The "diseased" target sequence is an integrated proviral genome. To generate them, I infected HeLa and RKO cells with a lentiviral vector containing the sequence of the green fluorescent protein (GFP). I then treated these two cell systems with the purpose of inducing a DSB by retroviral transduction of the Cas9 endonuclease and its RNA guide targeting the integrated GFP sequences.

As a negative control, I treated these cell lines in parallel with a Cas9 carrying a scramble guide that does not recognize any sequence in the human genome. Upon these treatments, I observed a preferential reduction of proliferation and an increased mortality in cells bearing the target sequence and transduced with the targeting RNA guide compared to cells without the target sequence or transduced with the scramble guide.

I also observed that Cas9-mediated DNA damage is associated with the formation of micronuclei which often stain positive for cGAS and activate an inflammatory response.

These results suggest the possibility to "weaponize" the CRISPR/Cas9 system for the elimination of cells with an aberrant genome.

However, cells can survive DNA damage insults by repairing them. In order to address this mechanism of "resistance" to the treatment, I investigated if the generation of a sequence-specific DSB can be combined with the inhibition of its repair. Indeed, Cas9-induced DNA damage and inhibition of DNA repair by non-homologous end-joining (NHEJ) by the use of a pharmacological inhibitor of the DNA-dependent protein kinase (DNA-PK), a DNA repair factor involved in NHEJ, further kill target cells.

However, DNA-PK inhibition lacks sequence specificity in its activity, thus impacting on the repair of endogenous DNA damage too. For this reason, a sequence-specific DSB repair inhibitor would be desirable.

Our group has previously demonstrated that DSBs trigger the recruitment of RNA polymerase II that generates damage-induced long non-coding RNAs (dilncRNAs) at DSB. DilncRNAs are the precursors of small non-coding RNAs called DNA damage response RNAs (DDRNAs) and the interaction between dilncRNAs and DDRNAs is necessary for the recruitment of the proteins involved in DDR, including DNA repair. Noteworthy, antisense oligonucleotides (ASO) against these damage-induced RNA species impair their functions and inhibit the assembly of DDR factors in the form of foci and thus they are effective sequence-specific DNA repair inhibitors.

In cells treated with Cas9, I observed a reduction in DDR foci, compared to controls, upon treatment with sequence-specific ASO, confirming the efficacy of ASO also in my experimental system.

2 Introduction

2.1 DNA damage and DNA Damage Response (DDR)

Nuclear DNA is subjected to various events that can cause thousands of lesions per day (Jackson and Bartek 2009). Since genomic DNA is the most precious component of a cell, any kind of damage elicits a prompt cellular reaction (d'Adda di Fagagna 2008).

Generally, DNA lesions are efficiently repaired and cells resume normal proliferation; however, if not properly repaired, they can cause programmed cell death (apoptosis), irreversible cell-cycle arrest (cellular senescence), or permanent DNA modifications that can lead to cancer (d'Adda di Fagagna 2008; Hanahan and Weinberg 2011).

For this reason, cells have developed a pathway that senses DNA lesions, signals their presence and coordinates their repair through a signal amplification and effector cascade named DNA damage response (DDR) (d'Adda di Fagagna 2008; Jackson and Bartek 2009).

2.1.1 Types of DNA damage

Genomic lesions can be the consequence of exogenous and endogenous factors. Exogenous factors can be distinguished between physical and chemical insults. Ionizing radiations (IR), like X-rays used also for medical diagnoses, or environmental factors, such as the ultraviolet (UV) component of sunlight, are examples of physical genotoxins. Chemical genotoxic agents, instead, include food components, cigarette smoke and chemotherapy drugs (Ciccia and Elledge 2010).

Random endogenous DNA damage, like mismatches and small insertions or deletions, can occurs during DNA replication (Branzei and Foiani 2008). Also cellular metabolism can induce DNA damage because of the production of reactive oxygen species (ROS): superoxide anions, hydroxyl radicals and hydrogen peroxide, generated by oxidative respiration, and products of lipid peroxidation may lead to a variety of oxidative modifications of DNA, but also RNA, proteins and lipids (De Bont and van Larebeke 2004).

Meiotic recombination and telomere shortening are dangerous for DNA integrity (Jackson and Bartek 2009) too. Scheduled events can introduce DNA damage too. For example, a class of enzymes known as topoisomerases induces transient DNA breaks to release localized topological stress; during meiosis, genomic recombination is critical for a correct chromosome segregation in daughter cells (Borde and de Massy 2013); class switch and V(D)J recombination are two mechanisms required for the antibody repertoire diversification in the immune system (Soulas-Sprauel et al. 2007).

DNA lesions, generated by these stimuli, can be divided in two categories: informational, when bases are modified or lost, and structural, when the integrity of the sugar backbone is compromised (Vitelli et al. 2017). Informational damages include a variety of chemical

modifications that can lead to the complete loss of a base or to changes in its chemical nature; structural damages are more dangerous because they can promote chromosomal rearrangements due to the loss of large portions of the genome (Vitelli et al. 2017). These types of lesions can be single-strand breaks (SSBs), that are nicks in the sugar-phosphate backbone of one of the two strands; double-strand breaks (DSBs) which consist in the breakage of both strands; and DNA crosslinks, where the two strands are covalently linked (Chatterjee and Walker 2017).

2.1.2 Informational DNA damage repair

Lesions that involve base modifications are generally quickly repaired through different pathways.

DNA mismatch repair (MMR) pathway corrects base substitutions, insertions and deletions occurring during DNA replication; the steps involved are the recognition of the lesion by dedicated sensors that recruits endonucleases, the initiation of the repair, the excision of the lesion, the resynthesis of DNA by DNA polymerases to fill the gap and the ligation of the repaired strands by DNA ligases (Kunkel and Erie 2005; Li 2008).

Nucleotide excision repair (NER) pathway can remove different types of base lesions but it is mainly involved in the repair of bulky DNA adducts induced by either UV light or chemotherapeutic agents. NER is divided in two main branches: global genome NER (GG-NER) and transcription-coupled NER (TC-NER) (Gillet and Schärer 2006; Marteijn et al. 2014). In the first case, different sensors recognize the presence of single-stranded DNA due to the disruption of a base. In the second case, instead, lesions caused by stalled RNA polymerase II are sensed and the complex is translocated in order to allow the exposure and repair of the lesion (Marteijn et al. 2014).

Base excision repair (BER) pathway corrects lesions that can induce little distortions in the DNA helix structure, such as oxidation, deamination and alkylation (Krokan and Bjoras 2013). DNA glycosylases remove the damaged base generating an abasic site that is then cleaved by endonucleases; this induces a SSB, in turn repaired with the contribution of DNA polymerases and DNA ligases (Demin et al. 2021).

Translesion synthesis (TLS) is another pathway that cells can use to deal with single-strand DNA lesions. It is a DNA damage tolerance pathway that allows DNA replication past DNA lesions, through the switch between the canonical DNA polymerases and specialized translesion polymerases that have low-fidelity on undamaged templates, but are particularly efficient at pairing nucleotides to the damaged bases (Waters et al. 2009; Dash and Hadden 2021).

2.1.3 Structural DNA damage repair

Breaks in the DNA backbone like SSBs, but especially DSBs, are particularly deleterious because, if not properly repaired before cell division, they can cause the loss of critical amounts of genetic information and dramatic chromosomal rearrangements. These type of lesions are repaired by either non-homologous end joining (NHEJ) or by homologous recombination (HR) (Hustedt and Durocher 2017).

The canonical NHEJ (c-NHEJ) is the main pathway involved in the repair of DSBs in mammalian cells and it works in all the phases of the cell cycle (Hakem 2008). It is highly efficient and acts by re-ligating the DNA ends; however, it is prone to mutations. Ku proteins recognize DNA ends and recruit DNA-PK catalytic subunit (DNA-PKcs) which phosphorylates itself and several targets, as Artemis, a nuclease that contributes, together with specialized DNA polymerases, in the blunting of DNA ends. DNA ligase IV, another target of DNA-PKcs, ligates DNA ends in collaboration with X-ray repair cross-complementing protein 4 (XRCC4) and XRCC4-like factor (XLF) (Chang et al. 2017).

The alternative NHEJ (alt-EJ) pathway, also known as microhomology-mediated end joining (MMEJ), plays a role in the repair of residual DSBs. This mechanism relies on a different subset of proteins, among which DNA ligase 3 and DNA polymerase θ (Hustedt and Durocher 2017).

HR is an error-free pathway that occurs only in the S and G2 phases of cell cycle and it requires a homologous chromosome as template for repair (San Filippo, Sung, and Klein 2008; Symington and Gautier 2011). The steps are the resection of DSB ends, the formation of a presynaptic filament, the search for homology and the repair synthesis (Jasin and Rothstein 2013; Taylor et al. 2015). In mammals, DNA ends are sensed by the MRN complex, composed by the meiotic recombination 11 (Mre11), Rad50 and the Nijmegen breakage syndrome 1 (Nbs1) proteins, in complex with CtIP. Upon binding, MRN starts resecting DNA ends from the 5' terminus and creates a single-stranded DNA gap. EXO1, DNA2, BLM, and WRN are involved in the resection; together, their actions generate long 3′ ssDNA tails. CDK, ATM and ATR are responsible for the phosphorylation of CtIP and it is essential to start end resection (Sartori et al. 2007; Peterson et al. 2013). Also the interaction between BRCA1 and BARD1 is required for correct end resection; moreover, BRCA1 is important for the removal of 53BP1, which is recruited to DSB sites to blocks 5′ end resection in G1 phase (Mirman and de Lange 2020). The replication protein A (RPA) is rapidly recruited at the single-stranded DNA to protect its integrity (Eid et al. 2010; Nimonkar et al. 2011; Sturzenegger et al. 2014). RPA is subsequently removed from ssDNA by the recombinase RAD51, together with the BRCA2-PALB2 complex (Zhao et al. 2017).

All these factors are necessary for the assembly of the presynaptic filament. RAD51, together with the ssDNA filament, searches for a homologous region and invades it, forming a displacement loop (D-loop) (Bonilla et al. 2020). RAD51 is removed from the heteroduplex to expose the 3′ of the invading ssDNA, where the DNA replication machinery, that includes PCNA and DNA polymerases, can initiate nascent DNA synthesis using the now paired strand as template (Northall et al. 2016). If the DSB has two free DNA ends, synthesis-dependent strand annealing (SDSA) can complete the repair; the invading strand now extended through DNA synthesis dissociates from the D-loop structure and reanneals with the other broken end without crossover events (San Filippo, Sung, and Klein 2008; A. Mehta and Haber 2014). Alternatively, the second broken end may be captured and annealed to the displaced strand of the D-loop, leading to the formation of a double Holliday junction (dHJ). Dissolution of this structure by proteins like BLM will result in non-crossover events, while resolution can lead to either crossover or non-crossover events, depending on the resolvases involved (A. Mehta and Haber 2014).

The choice between the different repair pathways is finely regulated and it depends on different factors including epigenetic markers and cell cycle phase; however, the mechanism is not yet fully understood (Swift et al. 2021). Ku70/Ku80 heterodimer promotes NHEJ and inhibits HR. In addition, it has been proposed that in G1 DNA ends are protected from resection by 53BP1 together with RIF1 and the shieldin complex (Zimmermann et al. 2013; Dev et al. 2018; Mirman et al. 2018; Noordermeer et al. 2018). End resection, instead, is promoted by CtIP and BRCA1 in G2 to allow HR (Cruz-García, López-Saavedra, and Huertas 2014). New proteins are constantly identified as key players in the choice of one of the two pathways, such as CYREN, described as a negative regulator of NHEJ in S/G2 (Arnoult et al. 2017) and Sp1, that instead impedes BRCA1 recruitment at the DNA ends in favor of 53BP1 (Swift et al. 2021).

2.1.4 The DNA damage response

The DNA Damage Response (DDR) pathway is a complex signaling cascade that coordinates DNA repair with a broad set of events (Ciccia and Elledge 2010; Polo and Jackson 2011) (Figure 1). Upon the generation of a DNA break, DDR is immediately activated, leading to a transient cell-cycle arrest that prevents the propagation of the damaged genome to daughter cells. Sensor proteins are activated and recruited to the site of the damage, where engage the apical kinases ATM, ATR and DNA-PK which phosphorylate their substrates on a serine or threonine followed by glutamine, the S/TQ motif (Blackford and Jackson 2017).

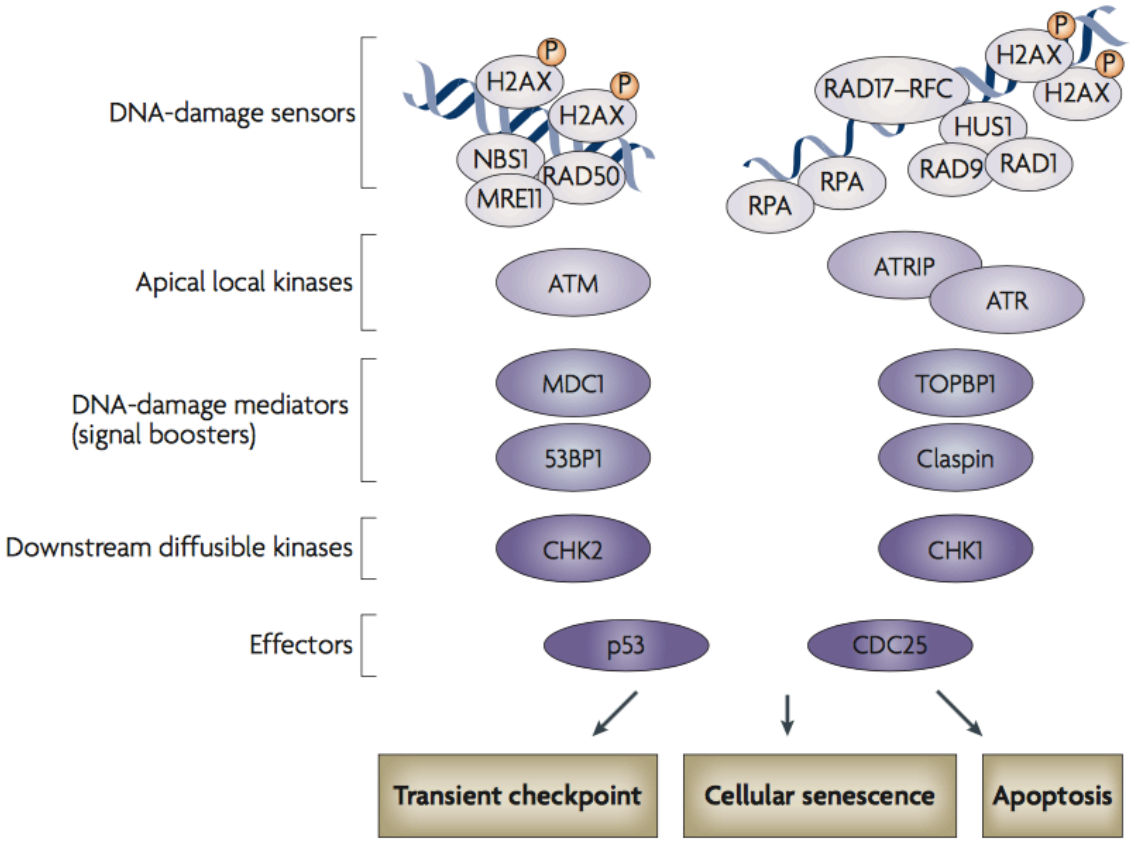

Adapted from d'Adda di Fagagna 2008

Figure 1. The DNA damage response pathway.
Ruptures in the DNA lead to the formation of either DSBs or SSBs. DNA breaks are sensed by the MRN and RPA complexes, respectively. These factors recruit either the apical kinases ATM or ATR, bound by ATRIP and the RAD9-RAD1- HUS1 complex. These kinases phosphorylate (P) the histone variant H2AX on Ser139 (γH2AX) to recruit DNA damage mediators such as MDC1, 53BP1, BRCA1, which boost the signal, generating a positive feedback loop. The diffusible downstream kinases CHK2 (mainly phosphorylated by ATM) and CHK1 (mainly phosphorylated by ATR) spread the signal to several effectors including p53 and CDC25, which coordinate several cellular events to avoid the propagation of the DNA damage to the daughter cells. After a lesion, the first response is a transient cell cycle arrest to allow the repair of DNA (DNA damage checkpoint). If the DNA damage is not properly repaired, prolonged DDR activation leads to apoptosis, a form of programmed cell death, or cellular senescence, a permanent cell cycle arrest.

The generation of a SSB activates the kinase ATR. Its activation depends on the presence of the ATR-interacting protein (ATRIP) and RPA at the lesion (Zou and Elledge 2003; Sun et al. 2020). Its activity is boosted by the heterotrimeric 9-1-1 complex (composed of RAD9, RAD1 and HUS1) (Parrilla-Castellar, Arlander, and Karnitz 2004). Upon DSB, instead, MRN recruits the ATM at the site of damage, where it undergoes auto-phosphorylation at serine 1981, causing its activation (J. H. Lee and Paull 2005; Shiloh 2006). DNA-PKcs is

recruited to the break site by the Ku70/80 heterodimer and undergoes an activating autophosphorylation on the S2056 and T2609 clusters (Blackford and Jackson 2017).
One of the first targets of these three apical kinases is the histone variant H2AX, which is phosphorylated at serine 139 (γH2AX): this phosphorylation is a key step for DDR since it allows the recruitment of additional ATM proteins in a positive feedback loop that fuel the spreading of γH2AX along the chromatin up to 1Mb away from the DNA lesion site (Meador et al. 2008; Iacovoni et al. 2010). γH2AX acts as recognition mark for the DSB and promotes the retention of other DDR proteins at the site of damage (Collins et al. 2020). The result is the formation of cytologically-detectable nuclear foci that contain the DDR proteins recruited to the site of damage (Lukas, Lukas, and Bartek 2011). The mediator of DNA-damage checkpoint 1 (MDC1) plays a crucial role in the establishment of this positive feedback loop (Lou et al. 2003; Stewart et al. 2003), by binding γH2AX through its C-terminal domain and further promoting MRN and ATM accumulation at the DSB, leading to an increase in the concentration of several DDR proteins at the DSB site (Spycher et al. 2008). MDC1 mediates also the recruitment of the E3 ubiquitin ligases RNF8 and RNF168 that mediate ubiquitylation of H2AX that is crucial for recruitment of downstream proteins, such as BRCA1 and 53BP1 (Panier and Durocher 2009; Bekker-Jensen and Mailand 2010). In addition to phosphorylation and ubiquitylation events, other reversible post-translational modifications like sumoylation and metylation are essential for DDR activation (Jackson and Durocher 2013). ATM and ATR, once activated, phosphorylate also the downstream protein kinases CHK2 and CHK1, respectively (Bartek, Lukas, and Lukas 2004; Bekker-Jensen and Mailand 2010). At this point, CHK1 and CHK2 diffuse in the nucleoplasm, where they can phosphorylate their substrates, and ultimately activating p53 and the CDC25 phosphatases. The phosphorylation of the CDC25 phosphatases leads to inactivation of the CDK-Cyclin complexes that are responsible for the progression throughout the cell-cycle phases (Swastika Sur and Devendra K. Agrawal 2016), but also p53-mediated transcription of the CDK1 inhibitor p21 promotes cell-cycle arrest (Branzei and Foiani 2008). DNA damage-induced cell-cycle arrest is usually transient and cells restart proliferating normally once damage has been repaired. However, in case of persistent DDR activation, cells may undergo apoptosis or enter a prolonged arrest known as cellular senescence (d'Adda di Fagagna 2008).

2.1.5 DNA damage checkpoints

Transient cell cycle arrest is mediated by DNA damage checkpoints upon the generation of DNA lesions. The CHK2 and CHK1 kinases are activated by ATM and ATR, respectively, and in turn they target cyclin-dependent kinases (CDKs), responsible for cell cycle

progression (Matthews, Bertoli, and de Bruin 2021). There are three distinct checkpoints that have to be regulated: the G1/S checkpoint, between the G1 and S phases; the intra-S phase checkpoint, within S phase; the G2/M checkpoint; between G2 and M phases (Branzei and Foiani 2008).

2.1.5.1 The G1/S checkpoint

In the presence of DNA damage in G1, the G1/S checkpoint prevents the transition to S phase to avoid the propagation of genetic errors; for this reason the initiation of DNA replication is inhibited (Matthews, Bertoli, and de Bruin 2021). To delay the G1/S transition, the phosphatase CDC25A is phosphorylated by CHK1 and CHK2 and degraded, inhibiting the cyclinE(A)CDK2 complexes. The delay can last several hours; however, the arrest can be prolonged in a p53-dependent mechanism. Indeed, p53 can accumulate in the cells after phosphorylation by ATM/ATR and CHK1/CHK2; moreover, these kinases phosphorylate also the ubiquitin ligase MDM2, that normally interacts with p53 to promote its turnover (Kastan and Bartek 2004). In this way, p53 is not exported in the cytoplasm and degraded, but it accumulates in the nucleus where it activates its target genes, as the gene encoding p21, which specifically binds and inhibits the CDK2-CyclinE complex, maintaining the G1/S arrest (Sancar et al. 2004). p21 also binds the CDK4-cyclinD complex, thus preventing the phosphorylation of the retinoblastoma tumor suppressor protein (Rb), which is necessary for the activation of E2F, a transcription factor which promotes cell cycle progression (Narasimha et al. 2014)

2.1.5.2 The intra-S checkpoint

The intra-S checkpoint is activated by stalled replication forks during the S phase or by unrepaired damage that escaped the G1/S checkpoint and causes a reversible inhibition of the firing of those DNA replication origins that have not yet been initiated. It can be triggered either by the ATM/ATR-CHK2/CHK1- CDC25A-CDK2 pathway (very similar to the G1/S checkpoint), or by a second pathway that requires the phosphorylation of the cohesin protein SMC1 by ATM with the aid of BRCA1, FANCD2 and NBS1 (Yazdi et al. 2002; Iyer and Rhind 2017). The so-called 53BP1 “nuclear bodies” mark DNA fragile sites and DNA lesions that arise during DNA replication stress. 53BP1 nuclear bodies are inherited by the daughter cell, shielding these regions of unrepaired damage into nuclear compartments that might enable repair before the subsequent S phase (Lukas et al. 2011).

2.1.5.3 The G2/M checkpoint

If DNA damage occurs during the G2 phase, or when cells progress into G2 with unrepaired lesions inflicted during the previous S or G1 phases, cells are prevented from entering into mitosis thanks to the G2/M checkpoint. The down-regulation of CDC25A and the up-regulation of Wee1, mediated by ATM/ATR and CHK2/CHK1, inhibit the progression to mitosis by controlling the activity of Cdk1/Cyclin B1 (Mailand et al. 2002). If the damage cannot be repaired, persistent DDR activation may induce apoptosis or senescence (d'Adda di Fagagna 2008).

2.1.6 Consequences of DNA damage

Persistent DNA damage can lead to different cellular responses, such as cellular senescence, cell death and the promotion of inflammation.

2.1.6.1 DNA damage and cellular senescence

Cells in a senescence state have permanently lost their proliferative capacity, despite their viability and metabolic activity, a condition initially described by Hayflick (Hayflick and Moorhead 1961). Markers of cellular senescence, in addition to an arrest in cell growth, are morphological cell changes, appearance of senescence-associated heterochromatin foci (SAHFs), senescence-associated DNA damage foci (SDFs) and release of pro-inflammatory cytokines, referred to as the senescent-associated secretory phenotype (SASP) (Di Micco et al. 2021). Different types of stresses can lead to cellular senescence, such as dysfunctional telomeres, DNA damage, and oncogene activation (d'Adda di Fagagna et al. 2003; Herbig et al. 2004; Di Micco et al. 2006). Our group previously demonstrated that persistent DDR activation at telomeres triggers cellular senescence (Fumagalli et al. 2012). Oncogene-induced senescence (OIS) is a mechanism where checkpoint-proficient cells undergoes senescence upon activation of an oncogene; it occurs *in vivo* and contributes to tumour suppression by preventing the expansion of oncogene-expressing cells (Evan and d'Adda di Fagagna 2009; Jackson and Bartek 2009). Altered DNA replication (Di Micco et al. 2006) and oxidative stress (Ogrunc and d'Adda di Fagagna, 2011) have been proposed to be the mechanisms responsible for the activation of DDR signaling following oncogene activation (Ogrunc and d'Adda di Fagagna 2011). Moreover, it has been shown that SASP can be a consequence of the activation of the cGAS-STING pathway because of detection of cytosolic DNA upon DNA damage (Dou et al. 2017; Glück et al. 2017).

2.1.6.2 DNA damage and cell death

Several stimuli, like unrepaired DNA damage, can trigger different cell death pathways that act as tumor suppression mechanisms. P53, the so-called guardian of the genome, is one of the major players in preserving genome integrity and, given its role in regulating cell cycle arrest and death, it is often mutated in human cancers (Levine and Abrams 2008).

Apoptosis is a programmed cell death mechanism where p53 mediates transcription activation and repression of several genes in response to different signals (Riley et al. 2008). p53 is involved in both cell intrinsic and extrinsic apoptotic pathways: in the first case, p53 is activated upon cellular stresses and it regulates the expression of pro-apoptotic genes like the p53-upregulated modulator of apoptosis (PUMA) and the apoptosis regulator BAX; in the second case, p53 is activated upon the binding of specific ligands to the so-called death receptors, that transmit apoptotic signals to the cells. Both the pathways result in the activation of a family of cysteine proteases, termed caspases, that lead to cell death (Peter 2011; Surova and Zhivotovsky 2013).

It has been shown that p53 can elicit an apoptotic response also independently from its effects on transcription by translocating in the cytoplasm, where it interacts with the anti-apoptotic proteins Bcl-X_L and Bcl-2, with consequential release of the cytochrome C from mitochondria that induces caspases activation and cell death (Manfredi 2003).

However, cells can adopt other mechanisms for cell death. For example, if checkpoints are compromised, irremediably damaged cells can enter mitosis prematurely, leading to mitotic catastrophe characterized by morphological alterations, such as micronuclei and multinucleation. These giant, polyploid cells can die by two independent mechanisms, either necrosis, when the integrity of nuclear and plasma membranes is lost, or apoptosis (Waldman et al. 1996; Vitale et al. 2011; Surova and Zhivotovsky 2013).

Autophagy is generally a pro-survival mechanism where cellular components are digested in lysosomes, for example when nutrients availability is limited, to provide precursors for the maintenance of cells. However, high levels of damage or prolonged exposure to a certain stress can result in cell death (Surova and Zhivotovsky 2013).

2.1.6.3 DNA damage generates micronuclei

It has been shown that the DNA damage caused by several factors, such as chromosome mis-segregations (Santaguida and Amon 2015), RNase H2 knock-out (MacKenzie et al. 2017) and irradiation (Harding et al. 2017) leads to the formation of micronuclei.

Micronuclei are small structures, generally 1–5 μm in diameter (Guo et al. 2020), composed by chromatin fragments that are surrounded by a nuclear envelope and released in the

cytoplasm; their presence is considered a biomarker of genotoxic stress and genomic instability (Krupina, Goginashvili, and Cleveland 2021). Upon generation, micronuclei can be either degraded or reincorporated into the nucleus, otherwise they can persist in the cytoplasm, leading to the death of micronucleated cells (Hintzsche et al. 2017). Micronuclei generally exhibit defects in the envelope and a suboptimal number of nuclear pores that impair the replication, transcription and repair of the DNA that they contain (Krupina, Goginashvili, and Cleveland 2021). Indeed, reduced levels of BrdU incorporation have been observed in micronuclei, compared to the primary nuclei, suggesting aberrant DNA replication (Crasta et al. 2012). Transcription can be affected too; for example, it can depend on the presence or absence of nuclear pore complexes on the membrane of micronuclei that can impair the exchange of proteins between the micronucleus and the cytoplasm. Moreover, also the micronuclear content can affect transcription: it has been reported that it occurs only when entire chromosomes are entrapped in micronuclei, while micronuclei containing DNA fragments does not show transcription activity (Hintzsche et al. 2017). In addition, even the DNA damage response is compromised: micronuclei have been stained positive for DDR markers as γH2AX and pRPA (S33), while downstream markers like 53BP1 are not efficiently recruited, with consequences on the DNA repair. Indeed, upon DNA damage induction, γH2AX foci are rapidly resolved in primary nuclei, while they persist in micronuclei (Crasta et al. 2012).

2.1.6.3.1 Micronuclei lead to inflammation through the cGAS-STING signaling axis

Defects in the membrane integrity of micronuclei cause the activation of the cGAS-STING pathway because of the detection of the DNA backbone by cGAS (Glück et al. 2017). In addition to micronuclei, also chromatin bridges, the result of fused chromosomes that fail to segregate, have been proposed to activate cGAS upon mitotic errors (Flynn, Koch, and Mitchison 2021). The cyclic GMP-AMP synthase (cGAS), once activated, dimerizes and catalyses the production of the second messenger cyclic GMP-AMP (cGAMP), which in turn activates the stimulator of interferon genes (STING), a transmembrane protein dimer located at the endoplasmic reticulum. This promotes a conformational change of STING, favouring its oligomerization. Once activated, with the contribution of other proteins, STING promotes the phosphorylation, dimerization and translocation of the interferon regulatory factor 3 (IRF3) transcription factor and the nuclear factor κB (NF-κB) into the nucleus, that results in the induction of inflammatory cytokines (Glück et al. 2017; Hopfner and Hornung 2020), small cell-signaling proteins that are then secreted to modulate the

immune and inflammatory response, and chemokines, a type of cytokines that attract leukocytes (Rodier et al. 2009).

2.2 DNA damage and transcription

It has been shown that in the proximity of a DSB site transcription is inhibited by an ATM-dependent mechanism to prevent collision or interference between the transcriptional and the repair machineries (Shanbhan et al. 2010; Pankotai et al. 2012; Marnef, Cohen, and Legube 2017). Our group has confirmed these observations by combining next generation sequencing with high-resolution mapping of DNA damage such as BLESS, BLISS and γH2AX ChIP-seq. However, we also found the presence of RNA pol II very close to the DNA lesions (Iannelli et al. 2017). Moreover, the chromatin state of the DNA surrounding the DSB is remodeled and decondensed, similarly to transcriptionally active loci (Ziv et al. 2006). Different evidences showed the role of RNA in the regulation of chromatin and transcription (Holoch and Moazed 2015), but we demonstrated the active role of RNA in preserving genome integrity (d'Adda di Fagagna 2014): RNA transcripts promote DDR signaling upon DNA damage generation to promote the efficient repair of the locus (Francia et al. 2012; Michelini et al. 2017).

2.2.1 dilncRNA transcription at the site of DSBs

When a DSB occurs, cells detect the damage and elicit a prompt response to promote its repair; this is known as the DNA-damage response. It was believed that the activation of this pathway requires the engagement of specialized DDR proteins only. However, our group has discovered that the induction of a DSB results in the assembly of what seems like a functional promoter at the site of damage: POL2A, the catalytic component of RNAPII, is recruited to DNA ends together with the preinitiation complex (PIC) and its associated components, MED1 and CDK9 (collectively named PMC). This recruitment spreads on the chromatin up to 2 kb from the broken DNA ends. In addition, POL2A and the PIC components colocalize with γH2AX, as proved by stochastical optical reconstruction microscopy (STORM) and by DNA-damage in situ ligation followed by proximity ligation assay (DI-PLA) (Pessina et al., 2019). RNAPII is responsible for the transcription of a novel class of RNA molecules named damage-induced long non-coding RNAs (dilncRNAs) from and toward the DNA ends of DSBs. These RNA can be detected by reverse transcription followed by quantitative PCR (RT- qPCR), and by single-molecule fluorescent in situ hybridization (smFISH) (Michelini et al. 2017). The MRN complex is responsible for the

recruitment of RNAPII at the site of damage. In addition, we also reported that, in an *in vitro* system, recombinant human MRN and purified native RNAPII are sufficient to reconstitute a minimal functional transcriptional apparatus at DSBs. This system also allowed us to demonstrate that RNAPII transcription of dilncRNAs is independent from MRN nuclease activity but, instead, dependent on its ability to melt DNA ends, as shown by a number of assays, including single-molecule FRET assays (Sharma et al. 2021).

DilncRNAs can then be processed in a DROSHA- and DICER-dependent manner to generate DNA damage response RNAs (DDRNAs) (Francia et al. 2012; 2016). The pairing between the long (dincRNA) and the short (DDRNA) RNA species is essential to promote the localization of DDRNAs at the DSB and the formation of a DDR focus, by recruiting several DDR factors such as of 53BP1, that interacts with DDRNAs and dilncRNAs through its Tudor domain (Michelini et al. 2017). DROSHA and DICER are RNA endonucleases involved in the maturation of miRNA; however, they play a role also in DDR. Indeed, depletion of DROSHA and DICER impairs the recruitment of repair factors to the damage site and also the repair efficiency by HR and NHEJ (Francia et al. 2012; Wei et al. 2012; Lu et al. 2018). A recent article from our lab reported that DROSHA is recruited at the site of damage by the MRN complex and it accumulates via protein-protein interactions and not via direct binding with RNA; moreover, its recruitment is independent from both H2AX and the kinase activity of ATM and DNA-PK, suggesting that it is an early event during DDR activation (Cabrini et al. 2021).

RNA species similar to the ones described by us were also reported in *Neurospora crassa*, *Arabidopsis thaliana*, *Drosophila melanogaster* and human cell lines (Wei et al. 2012; Yang and Qi 2015; Qi et al. 2016; Wang and Goldstein 2016). For instance, it has also shown that, in *S. pombe*, DNA damage induces *de novo* transcription and these newly synthesized RNA molecules anneal with their DNA templates resulting in transient DNA:RNA hybrids required for efficient DSB repair via HR (Ohle et al. 2016).

Recently, also our group has proposed that dilncRNAs contribute to HR-mediated repair of DSBs. Indeed, we have observed that dilncRNAs species can hybridize with resected DNA ends to form DNA:RNA hybrids. Hybrids formation favors the recruitment of HR proteins like BRCA1, BRCA2, and RAD5; DSB-induced DNA:RNA hybrids are recognized by BRCA1 and their levels are modulated by BRCA2 through the direct interaction and recruitment of RNase H2 to DSBs (D'Alessandro et al. 2018).

2.2.2 Inhibition of DDR signaling and repair by antisense oligonucleotides (ASO)

Experiments that prevent the transcription and the function of these ncRNAs showed their importance in DNA damage signaling and repair. For example, the inhibition of RNAPII by alpha-amanitin prevents global DDR activation and consequently DNA repair, without however affecting γH2AX foci accumulation and showing that the damage-induced transcription is one of the earliest events upon DSBs, occurring as fast as the phosphorylation of H2AX.

Our group has previously used antisense oligonucleotides (ASOs) to investigate the effects of the inhibition of the pairing between DDRNAs and dilncRNAs (figure 2). ASOs are short, single-stranded, synthetic molecules that are used to inhibit the functions of target RNAs through Watson-Crick base pairing (Rinaldi and Wood 2018). They usually carry chemical modifications to be sufficiently stable and effective *in vivo*. One of the modifications that we used in our experiments is the replacement of an oxygen atom with a sulfur to generate a phosphorothioate backbone that increases nucleases resistance (Michelini et al. 2018). In addition, our ASOs are mixmers of DNA and LNA (locked nucleic acid, in which a link between the 2′ oxygen and 4′ carbon of ribose is present) bases that increase the binding affinity to the RNA target (Khvorova and Watts 2017). Excitingly, we have found that the use of ASOs against the pairing of dilncRNAs and DDRNAs inhibits DDR signalling in a sequence-specific manner, thus without impacting ongoing DDR activation in the form of visible foci at other damaged sites in the same cell, both *in vitro* and *in vivo* (Rossiello et al. 2017; Michelini et al. 2017; Aguado et al. 2019). To prove the selectivity of ASOs treatments, we used a cell line in which DSBs were introduced in three Tet sequences arrays and in two Lac sequences arrays. We used γH2AX foci detected by immunofluorescence as an indication of the efficient generation of DSBs. We treated cells with ASOs against the RNAs transcribed at the DSBs induced in the Tet sequences. We observed that ASO impaired DDR activation, as monitored by 53BP1 focus formation, at Tet loci only, while leaving DDR activation at the Lac sites within the same cell unaffected.

To characterize the impact of ASOs-mediated dilncRNAs inactivation on DSB repair, we have taken advantage of a traffic light reporter system (TLR), that allows the monitoring of both HR and NHEJ events (Certo et al. 2011). This system generates a readout of HR-mediated gene targeting and NHEJ mediated gene disruption occurring at an individual DSB detectable by flow-cytometry. Indeed, depending on how a DSB is repaired, this system generates two different fluorescent proteins: either a functional green fluorescent protein (GFP), in the case of repair by HR, or a mCherry protein, in the case of repair NHEJ (Certo et al. 2011). Our data showed that ASOs against the dilncRNAs transcribed upon the

generation of DSBs inhibit their repair: we have detected a significant reduction of both the green and the red fluorescent signals by flow cytometry, indicating that ASOs can interfere both with HR and NHEJ (D'Alessandro et al. 2018).

It has been reported that the activity of super-enhancers and DNA-binding transcription factors is dependent on liquid-liquid phase separation (LLPS) events (Boehning et al. 2018; Boijja et al. 2018; Cho et al. 2018; H. Lu et al. 2018; Sabari et al. 2018). LLPS is a process where selected molecules are separated and concentrated, favoring subcellular compartmentalization and organization of the molecular events occurring inside the cell (Pessina et al. 2021). We showed that DNA damage response foci are membraneless structures formed via LLPS and modulated by dilncRNAs (Pessina et al. 2019). It was already demonstrated that 53BP1 accumulates at DSBs and phase separates (Kilic et al. 2019). What we discovered is that the phase separation of 53BP1 is mediated by the RNA transcribed at the site of the damage: RNA acts as a driving agent for protein condensation by promoting local concentration of RNA-interacting proteins which thus form liquid droplets through liquid-liquid de-mixing by phase separation. Both transcriptional inhibitors and ASOs against dilncRNAs and DDRNAs disrupt such liquid droplets of DDR factors. LLPS favors DNA-damage signaling and repair events by controlling the diffusion and concentration of DDR factors in proximity to DSBs (Pessina et al., 2019).

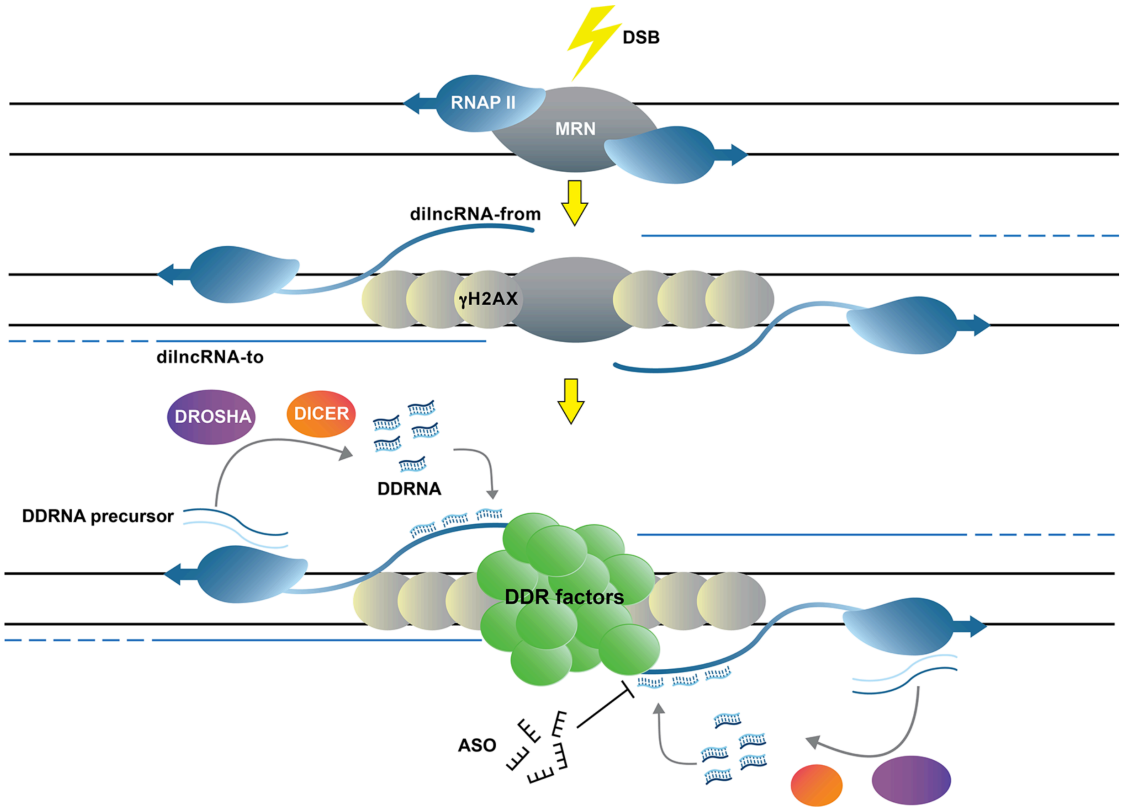

Adapted from Michelini et al. 2018

Figure 2. Proposed model for dilncRNA and DDRNA generation and activity at DSBs.
Upon generation of a DSB, the MRN complex senses the DNA damage and recruits RNAPII to the broken DNA ends, where it starts transcribing damage-induced long non coding RNAs (dilncRNA) from (blue) and towards (light blue) the break. These RNA molecules are then processed by DROSHA and DICER generating short DNA damage RNAs (DDRNAs). The pairing between nascent unprocessed single-stranded dilncRNA and DDRNAs allows the recruitment of DDR factors and the formation of a proper DDR focus. The treatment with antisense oligonucleotides (ASO) complementary to DDRNAs sequence, prevents the interaction between dilncRNAs and DDRNAs and inhibits DRR in a site- and sequence-specific manner.

2.3 The CRISPR/Cas9 technology

CRISPR is a powerful tool used for different applications, such as genome editing, and it composed by Cas9, a protein that acts as a pair of molecular scissors, and a RNA guide that brings Cas9 at the desired DNA sequence.

2.3.1 Genome editing before CRISPR discovery

Technologies used to manipulate DNA started developing immediately after the discovery of DNA itself. It was clear to scientists the potential of making site-specific changes in the genome of cells and organisms. Genome editing is the process where a sequence is changed by adding, removing or replacing pieces of DNA. It is based on the introduction of a DSB that elicits a DNA damage response. The way in which the damage is repaired can lead to different outcomes: for example, if the DSB is repaired by NHEJ, small mutations are inserted, resulting in the disruption of the target gene. Gene correction, instead, is the consequence of a DSB repair by HR, thanks to the delivery of a donor template (Urnov et al. 2010).

Different artificial nucleases have been developed to perform genome editing. The first endonucleases used to modify the genome in a sequence-specific manner were zinc finger proteins. A zinc finger is a small domain that can properly fold thanks to one or more zinc ions; the most common is characterized by a conserved region formed by 2 cysteines and 2 histidines that interacts with one zinc ion and it was described for the first time in 1985 in the Xenopus transcription factor IIIA (J. Miller, McLachlan, and Klug 1985). The Cys2-His2 zinc-finger domain is the most abundant DNA-binding region in the proteins of eukaryotes (zinc finger protein, ZFP) and recognize 3bp of DNA. ZFPs were then engineered with other ZFPs to bind longer DNA targets and they were fused together with the restriction enzyme FokI to create a DNA binding endonuclease able to cut in a sequence-specific manner (zinc finger nuclease, ZFN) (Kim, Cha, and Chandrasegaran 1996). Moreover, for an efficient cut, FokI has to dimerize and bind the DNA in the proper orientation and at the right distance to allow the formation of the dimer. The result of the cut is a 5' overhang (Vanamee, Santagata, and Aggarwal 2001). In 2009, two groups have discovered a new class of proteins, the transcription activator-like effectors (TALEs), that the *Xanthomonas* bacteria use to attack their plant hosts in order to control and regulate plants gene expression (Boch et al. 2009; Moscou and Bogdanove 2009). This discovery allowed the creation of an alternative tool to bind and cut DNA in a sequence-specific manner. Indeed, TALEs contain several DNA-binding domains composed by around 34 aminoacids and each repeat recognizes a single bp on DNA. TALEs were modified by fusing them with the catalytic

domain of the FokI enzyme, like it was done some years before with the ZFPs (Christian et al. 2010). The final product was named transcription activator-like effectors nuclease (TALEN) and DSBs are generated in the spacer sequence between the two nucleases monomers that bind the DNA on the two opposite strands allowing the generation of the FokI dimer that can cleave the target (Miller et al. 2011). The production and the validation of TALENs is generally easier then ZFNs; however, both techniques are expensive, difficult to handle and time consuming, which prevented their spreading for a routine usage (Doudna and Charpentier 2014).

2.3.2 The discovery of the CRISPR/Cas system

The discovery of the CRISPR/Cas9 system changed everything. The CRISPR system is considered the adaptive immunity of bacteria to viruses and plasmids. It consists of a set of CRISPR associated genes (cas) and a series of repeated sequences (direct repeats) that alternate with non-repetitive sequences (spacers). Cas genes are transcribed and translated into proteins, while the CRISPR loci are transcribed in non-coding RNAs that are then processed in short CRISPR RNAs (crRNAs). These RNAs bind and direct the Cas proteins to the target nucleic acid (Ran, et al. 2013; Hsu, Lander, and Zhang 2014). More in details, the process in composed by the following steps: bacteria can incorporate fragments of DNA (spacers) from bacteriophages or plasmids into the CRISPR loci; once the bacteria are invaded by the same bacteriophage or plasmid, they start transcribing the CRISPR regions into RNA molecules that are processed to form crRNAs. CrRNAs interact with the different Cas proteins and the complex binds and cut the foreign target nuclei acid (Makarova et al. 2011).

This CRISPR system was identified for the first time in 1987 by a group of Japanese researchers that found short repeats interspaced with short sequences of the genome of *Escherichia coli* (Ishino et al. 1987). In the following years, CRISPR loci were then detected in different bacteria and archaea and two key discoveries helped in understanding better their features and function. The first study identified the CRISPR associated genes (cas), flanking the CRISPR loci and encoding nucleases and helicases (Jansen et al. 2002). The second relevant discovery was made in 2005 by three independent groups: they showed that the non-repeating CRISPR spacers contains sequences that derive from the DNA of bacteriophages. The authors suggested that these integrated viral elements provide the immunity against infection (Mojica et al. 2005; Bolotin et al. 2005; Pourcel, Salvignol, and Vergnaud 2005). The evidence confirming the role of CRISPR in protecting bacteria from phage infection arrived in 2007 from a group working on the bacterial strain *Streptococcus thermophilus* (Barrangou et al. 2007). Additional studies identified three major classes of CRISPR systems

that use different mechanisms to recognize and cleave the invading nucleic acids: the type I locus is transcribed and processed in small CRISPR RNAs (crRNAs) that guide the Cas nuclease to the target DNA, while the type III locus, once transcribed and processed, can target both DNA and RNA (Makarova et al. 2011). The type II locus, instead, is characterized by the presence of a trans-activating crRNA (tracrRNA) that is transcribed upstream the CRISPR locus. Its presence is essential to mediate the maturation of the crRNAs by the host RNAse III (Deltcheva et al. 2011). In addition, this system requires, like the type I system, the presence of a small region near the target sequence of crRNAs on the foreign DNA, that is named protospacer adjacent motif (PAM) (Doudna and Charpentier 2014). The type I and III systems require several Cas proteins to interact with the crRNAs and reach their target. On the contrary, the type II system needs only the Cas9 protein, encoded by the cas9 gene, to help in the maturation of crRNAs and to recognize and cut the DNA target, together with the tracrRNA:crRNA complex (Doudna and Charpentier 2014; Jinek et al. 2012). In the years following its discovery, scientists started using this system in vitro to target the eukaryotic genome (Cong et al. 2013; Jinek et al. 2013; Mali et al. 2013). Cas9 from the *Streptococcus pyogenes* bacterium (SpCas9) is the most commonly used and its PAM sequence is NGG; however, also Cas9 proteins from other bacteria and archea have been tested as an alternative: for example, Cas9 from *Staphylococcus aureus* (SaCas9), Cas12a from *Acidaminococcus* and Lachnospiraceae, the RNA-editing Cas13a from *Leptotrichia shahii* (Ventura and Dow 2018). Moreover, a single guide RNA (sgRNA) was optimized by combining a 20-nt long crRNA, containing the sequence complementary to the target DNA, and a tracrRNA that interacts with the Cas9 protein (Jinek et al. 2012).

Cas9 is a large protein that contains two nuclease domains; one cleaves the DNA strand that is complementary to the 20 nucleotides crRNA and the other one cleaves the opposite DNA strand, generating a blunt DSB (Doudna and Charpentier 2014). The cut is possible because Cas9 is formed by two active sites that can cut DNA, one involving aspartic acid (D10) and the other one histidine (H840) (Jinek et al. 2014). The Cas9-sgRNA complex can bind the target DNA sequence after the recognition of a short nucleotide sequence, the PAM sequence; then it unwinds the dsDNA starting from the region proximal to PAM and it displaces the non-target DNA strand, allowing the formation of a RNA-DNA hybrid between the sgRNA and the template DNA. At this point Cas9 can cut both the template and the non-template DNA strands (Shibata et al. 2017). Although the crRNA binds the DNA sequence that is complementary, some mismatches are tolerated (Haeussler 2020). It has been shown that some mutations in the target sequence allows the binding of the RNA guide, especially if in the PAM-distal region (Hsu et al. 2013). Anyway, these events are rare; indeed, the 97 % of off-targets has less than five mismatches with the target DNA guide (Haeussler 2020).

To further limit the possibility of off-targets and optimize the use of the CRISPR/Cas9 system in genome editing, Cas9 was inactivated in two ways to increase its specificity: single inactivation and double inactivation. In the first case, only one of the two active sites is able to cut the DNA because the other one is replaced with alanine (A), creating the Cas9 nickase variant (nCas9) (Jinek et al. 2014). In this way, two nCas9, associated with two different RNA guides, are used to introduce two cuts on the opposite strands, at 40-50 nt distance, producing two long overhangs (Ran et al. 2013; Gupta et al. 2019). In the case of double inactivation, both the active sites of Cas9 are mutated, producing a Cas9 that is no more able to cut the DNA; this version is called dead Cas9 (dCas9). The dead Cas9 was then fused with the FokI nuclease (fCas9); two fCas9 proteins are necessary to efficiently bind and cleave the target DNA and a spacer sequence between the nucleases is required; in this way it is possible to further reduce the risk of off-targets (Tsai et al. 2014; Guilinger, Thompson, and Liu 2014). In addition, dCas9 is used also for other applications: for example, to evaluate the function of a gene in a transient way without inducing any DSB, Cas9 can be fused with the transcriptional repressor KRAB (Kruppel-associated box domain) to turn off transcription by blocking RNA polymerase activity (CRISPR interference; CRISPRi) (Gilbert et al. 2013; L. S. Qi et al. 2013; Gilbert et al. 2014); otherwise it can also be fused with synthetic transcription activators used to control expression of genes involved, for example, in tissue regeneration, genetic defects, tumor suppression, stem cell differentiation, long non coding RNA production (CRISPR activation, CRISPRa) (Konermann et al. 2015; Pickar-Oliver and Gersbach 2019). To target and control epigenetic markers in order to study gene regulation, dCas9 is fused with catalytic domains of enzymes that acetylate or demethylate histones (Pickar-Oliver and Gersbach 2019).
Another possible application of dCas9 is the labeling of DNA as an alternative to fluorescence in situ hybridization (FISH) (Jao, Wente, and Chen 2013). The endonuclease is fluorescently tagged and it is a powerful tool for live-cell imaging (Hsu, Lander, and Zhang 2014).

The advantage of the CRISPR/Cas9 tool, compared to ZFNs and TALENs, is that this system requires only the change of the guide RNA to be used in a different context; this is the reason why this technology rapidly spread in several laboratories for different applications and in different experimental systems (Doudna and Charpentier 2014; Hsu, Lander, and Zhang 2014).

2.3.3 Repair of Cas9-induced DNA damage

The use of the CRISPR/Cas9 system has opened some question about how fast the DSB generated by the endonuclease is repaired and by which pathway. Indeed, Cas9 can be repaired either by HR or NHEJ, with different levels of fidelity and different outcomes. If the DSB is repaired by NHEJ, it could lead to small deletions, frame shifts, or modified binding sites, which make it suitable for gene knockout mutations; while the repair by HR allows DNA knock-in or gene replacement in the presence of a donor template (Kim and Kim 2014). Roidos and colleagues, in 2020, have taken advantage of the 'Color Assay Tracing-Repair" (CAT-R) system to understand which pathway is more prone to repair a DSB generated by Cas9 (Roidos et al. 2020). The CAT-R is a fluorescent reporter system formed by a sequence encoding the mCherry protein and a sequence encoding for the GFP protein. It was inserted in a single locus in two cell lines, HEK-293 and RPE-1, that were also engineered to express Cas9 in a doxycycline inducible manner. The sgRNA of Cas9 was designed to target the GFP sequence and it has to be transfected to perform the experiment. Once Cas9 is expressed and the sgRNA is transfected, there are three possible outcomes after the repair of the DSB: loss of the GFP signal because of a frameshift due to small indels but expression of mCherry; loss of both the GFP and mCherry signal after large rearrangements; intact GFP and mCherry expression either if the DSB is repaired in an error-free manner or the cells are not properly transfected with the sgRNA. The authors observed that, after 72 hours, 49-50% of cells were positive for mCherry and negative for GFP expression, 43-44% of cells were negative for both mCherry and GFP expression, and only the 6-8% of cells were positive for both the signal. This result was confirmed also 5 and 7 days upon sgRNA transfection, meaning that a DSB induced by Cas9 is mainly repaired by pathways that lead to either small indels or large deletions. The combination of next-generation sequencing and Oxford Nanopore Technology have determined that indels of 1 bp were the most frequent in terms of small rearrangements; while, the majority of the large deletion events consisted in deletions bigger than 3kb and up to 8kb. Most of these big rearrangements were detected upstream the DSB, suggesting the binding of Cas9 to the DNA ends, causing an asymmetric processing of the extremities (Roidos et al. 2020).

Indeed, Richardson and colleagues already showed, in 2016, that Cas9 needs around 6 hours to fully dissociate from the DNA substrate and it first releases the 3' end of cleaved strand that is not complementary to the RNA guide (Richardson et al. 2016).

To address the same point, another group showed that Cas9 can stay associated with DNA upon cutting in vitro (Brinkman et al. 2018). The authors have incubated DNA fragments with the Cas9 carrying the sgRNA able to cut within those fragments and generate two

smaller DNA pieces. They have then run the products of the reaction by agarose gel and they have observed the two products of the reaction, but the smaller band was really faint; moreover, also a smear was present, indicating that the DNA did not run properly. Upon denaturation of Cas9 and DNA, the smear disappeared and the two bands were clearly visible, suggesting that the Cas9 digested correctly the target DNA but, in absence of the denaturation step, it stays bound to one of the DNA ends (Brinkman et al. 2018).

In addition, they characterized the kinetics and the repair fidelity of a DSB induced by Cas9, since little was known. They used the K562 cell line engineered in order to express an inducible Cas9; to switch off the activity of Cas9, the nuclease was bound to a destabilizing domain. They transfected cells with a plasmid expressing the sgRNA against the LBR gene, their target DNA sequence. 24 hours after transfection, they stabilized Cas9, collected cells at various time points after Cas9 induction, amplified the region around the cut by PCR and sequenced the products to determine the fraction of indels (Brinkman et al. 2018). They found that indels accumulated over time, showing that DSB induced by Cas9 are repaired in an error-prone manner. By transfecting again these cells with the same sgRNA, they did not observed an additional increase of indels, suggesting that the sgRNA was no more able to cut the target sequence once indels are acquired. Not only, they also observed, by using a mathematical model on their experimental results, that Cas9 activates really slowly, because the cutting half-life of Cas9 (the time that is required, in the absence of repair, to cut the 50% of the target sequences) is around 6 hours, very different from the kinetics of DSBs after IR, that generally takes 1 hour.

Playing with some inhibitors of the DNA damage response, like DNA-PK, they were able to determine the two main pathways involved in the repair of DSB in their system: NHEJ, responsible for 1bp insertion, and microhomology-mediated end joining (MMEJ), responsible for 7bp deletions. MMHJ is a mutagenic pathway that join together two DNA ends by using short homology sequences near to the ends (Mcvey et al. 2017; Brinkman et al. 2018).

Also Bothmer and colleagues, in 2017, characterized the different repair pathways involved upon DSB induced by Cas9. They studied the effects of three Cas9 variants targeting the HBB locus; they confirmed that the WT Cas9 induces DSBs that are generally repaired by NHEJ (Bothmer et al. 2017). Then, they used the paired nickase approach: two Cas9 proteins induce a nick in the DNA that, if it is not repaired before S phase, can be transformed into DSBs. If the nicks are made by the D10A Cas9 variant, the result is a 5’ overhang with the predominant engagement of a-NHEJ pathway; if the nicks are generated by the N863A Cas9 variant, the final result is a 3’ overhang that stimulates the HR pathway (Bothmer et al. 2017).

In addition to the Cas9 variant used to induce the DSB, also the chromatin context plays a role in the repair pathway choice (Schep et al. 2021). The study of scars left by the different DSB repair pathways in more than 1000 genomic loci revealed that DSBs in the euchromatic regions are mainly repaired by NHEJ while, in the heterochromatic contexts, the contribution of MMEJ is higher. Single-stranded template repair (SSTR) (Richardson et al. 2016) requires a single-stranded oligodeoxynucleotide (ssODN) donor sequence to mediate the repair and, in the case of Cas9-induced DSB, it competes with MMEJ for the repair of DSBs in the lamina-associated domains or in the regions with the histone modification H3K9me2 (Schep et al. 2021). The repair pathway choice can depend also on the cellular state: differentiated, quiescent, or actively cycling. For example, a DSB in a quiescent cell cannot be repair by HR but it will be repaired by NHEJ (Ferreira da Silva, Meyenberg, and Loizou 2021).
There are also evidences that show how the persistent binding of Cas9 to DNA ends can block the access to repair enzymes. Clarke and colleagues have discovered the RNA polymerase II can remove Cas9 from DNA but only if RNA pol II collides with Cas9 in the template orientation (RNA pol II is transcribing the DNA strand that is complementary with the sgRNA), facilitating the repair of the DNA damage. The removal of Cas9 from the DNA makes the protein a "multi-turnover" nuclease that can cut again the target DNA. If RNA pol II is in the non-template orientation, the collision with Cas9 will not remove the nuclease from the DNA (Clarke et al. 2018).

2.3.4 Different forms of Cas9 can be delivered in target cells

The CRISPR/Cas9 system can be expressed in target cells in at lest three different ways: by delivering a DNA plasmid expressing both the Cas9 protein and the sgRNA, a mRNA that encodes the Cas9 protein and a separate sgRNA, a ribonucleoprotein complex (RNP) that carries both the Cas9 and the sgRNA. The DNA plasmid requires both transcription and translation before Cas9 can start working. It has been shown that the Cas9 protein becomes detectable 5 hours after transfection with peaks at 24/48 hours. Its expression can last weeks and it is perfect for long-term experiments. However, the long half-life of Cas9 can generate off-target effects. The mRNA version of Cas9 can be directly translated in the cytoplasm of the target cells and the protein is already detectable after 1 hour; this approach is recommended for short experiments and to limit off-target effects. Finally, the ribonucleoprotein system is a complex composed by the Cas9 protein and the sgRNA; transcription and translation are not required. This is the most efficient system because it starts working as soon as it is delivered into the cell; moreover, due to its transient expression, the possibility of off-targets is reduced (Fajrial et al. 2020).

2.3.5 Different methods to deliver Cas9 in the target cells

The delivery of the CRISPR/Cas9 components can be relatively easy in the cellular models, while, *in vivo*, it is important to protect them by degradation. There are at least three ways to deliver CRISPR/Cas9: physical, viral and non-viral. The physical delivery needs external sources to transiently disrupt the cellular membrane and deliver Cas9 into the cells. Some examples are microinjection, electroporation and nucleoporation (a type of electroporation used to deliver material directly into the nucleus). These approaches are generally used for *in vitro* and *ex vivo* studies (Yan et al. 2021). The viral and non-viral approaches are instead suitable also for Cas9 delivery *in vivo*. The viral approach is the most used to deliver CRISPR/Cas9. Indeed, they can efficiently infect different type of cells, both dividing and non-dividing. There are three common viral vectors: adeno-associated viruses (AAVs), adenoviruses (AVs) and lentiviruses (LVs). The adeno-associated viruses (AAVs) are commonly found in humans and they have already been approved for some clinical trials because of their non-pathogenic features. After delivery, the DNA of the virus generally does not integrate in the host genome. Anyway, it can happen that the cargo of AAVs integrates into the AASV1 locus (adeno-associated virus integration site 1), without causing side effects. A limitation of AAV vectors is that they have a small size and they can only carry a small genetic cargo. Ways to overcome the problem can be either the use of the smaller Cas9 protein from the *S. aureus* instead of the most common one from *S. pyrogenes* or separation of the Cas9 gene and the sgRNA in two individual vectors (C. L. Xu et al. 2019). Adenovirus vectors can be used to deliver bigger genomic material than the AAVs and also their genome does not integrate in the host cell, reducing the risk of off-target effects. Different generations of AV vectors have been optimized but unfortunately these engineered viral vectors can still cause an activation of the host immune response. In addition, people already infected by AVs during their lives have generated antibodies against the most common types of AVs used for therapy (Xu et al. 2019). The third class of viral vectors are lentiviruses. These are the viral vectors that can carry the largest cargo and have been engineered to split in three plasmids the essential genes of the virus, to reduce as much as possible the probability to produce viable viral particles in the host cells and to activate the host immune system. However, the lentiviral vector integrates into the host genome. It can be an advantage if the purpose of the study is the creation of a cell line stably expressing Cas9 but, *in vivo*, the integration of the vector in random regions of the host genome can cause mutagenesis and tumorigenesis (Cheng, Zhang, and Ding 2021). For this reason, LVs vectors that do not integrate in the genome of the host cells have been created (Yáñez-Muñoz et al. 2006). Although the CRISPR/Cas9 system can be efficiently delivered by the viral

vectors, the use of viruses can induce a host immune response, off-target risks due to a long-term expression of Cas9 and, in the case of lentiviruses, mutagenesis caused by the random insertion of the cargo. For these reasons, more and more forms of non-viral vectors are now emerging (Luther et al. 2018). These vectors can offer advantages like low immunogenicity, flexibility in cargo size and delivery of all the CRISPR components with one vector, low costs, large scale production. Some of the methods are: lipid and lipid-derived nanoparticles, polymer-based nanoparticles, cell-penetrating peptides, nucleic acids nanoparticles and inorganic nanoparticles. Lipid and lipid-derived nanoparticles (LNPs) are composed by hydrophobic and hydrophilic portions; they are frequently used because of their efficiency (Yan et al. 2021). Polymer-based nanoparticles can form complexes with nucleic acids or proteins. They are efficient, safe and they are used to control the drug release (Behr et al. 2021). Cell-penetrating peptides can be used not only to create the backbone of the nanoparticle, but also to modify the surface of the vector in order to improve its capability to target and enter in the host cell. Anyway, their use can induce an immune response due to the possible toxicity of a foreign peptide in the host cell (Behr et al. 2021). The inorganic nanoparticles include several metallic and nonmetallic components. Gold and silica nanoparticles are examples of vectors used to deliver Cas9 into the cells; they easily conjugate with other components that are useful for the delivery of the cargo in the target organ or cell type. They are easy to produce, stable and generally not toxic, even if it depends on the properties of the nanoparticles like size, shape, charge and modifications of the surface (Lino et al. 2018; Behr et al. 2021).

2.3.6 Applications of the CRISPR/Cas9 system

The CRISPR/Cas9 system is used to investigate and treat genetic diseases, infectious diseases, cancers and immunological diseases. The translational potential of CRISPR in treating diseases is the possibility that a single treatment is enough to provide a long-term therapy (Wu et al. 2020). CRISPR can be used to generate disease models to understand the mechanisms that can cause diseases and to find new pharmacological approaches: for example, it was used for the creation of cellular and mouse models to study Alzheimer's disease (Paquet et al. 2016), atherosclerosis (Jarrett et al. 2018), obesity, diabetes (Roh et al. 2018) and cancer (Maddalo et al. 2014). More complex disease models were also generated in sheeps, rabbits, pigs and monkeys, showing the potential of the CRISPR/Cas9 tool to quickly generate animals with one or several modified genes (Wu et al. 2020). CRISPR/Cas9 is also used to perform genome-wide functional screenings; lentiviral delivery of several RNA guides in Cas9 expressing cells can be used to study alterations in thousands of genes in parallel. In this way, it is possible to study the phenotype caused by the complete loss of

function of specific genes (Wang et al. 2014) but also which genes, in cancer cells, can confer resistance to drug treatments, allowing the discovery of new targets and the development of new therapies (Shalem et al. 2014). Another application of Cas9 in cancer therapy is its use to disrupt genes essential for the proliferation and survival of cancer cells, in order to promote apoptosis and reduce tumor growth. This approach can be useful also to combat viral infections; indeed, Cas9 can target and insert mutations in genes essential for viral replication, suppressing the propagation of the virus (Chen et al. 2019).

The Cas9 system can also be used to correct point mutations that are the cause of genetic human diseases. For example, it can be co-delivered with a homologous donor template containing the right DNA sequence that can replace the mutated region in the genome after DSB induction by Cas9 and repair by HR (Pickar-Oliver and Gersbach 2019).

Alternatives that do not need the generation of DSBs have been developed to convert single nucleotides: base editors are a class of genome editing agents where a dCas9 has been fused with a deaminase enzyme (Anzalone, Koblan, and Liu 2020). Two examples are cytosine deaminases of the APOBEC family that convert C → T (or G → A) and adenine base editors (ABE) that convert A → T (H. Zhang et al. 2021). ABE has been used to correct a mutation in the nuclear lamin A gene (*LMNA*), responsible for the Hutchinson-Gilford progeria syndrome (HGPS), in patient-derived fibroblasts and in a mouse model of the disease (Koblan et al. 2021).

Also agriculture can benefit of the CRISPR/Cas9 technology. Indeed, the Cas9 system can be used to manipulate the genome of plants to increase their yield and quality, their resistance to diseases and herbicides (H. Zhu, Li, and Gao 2020), underlying the immense potential of this technology.

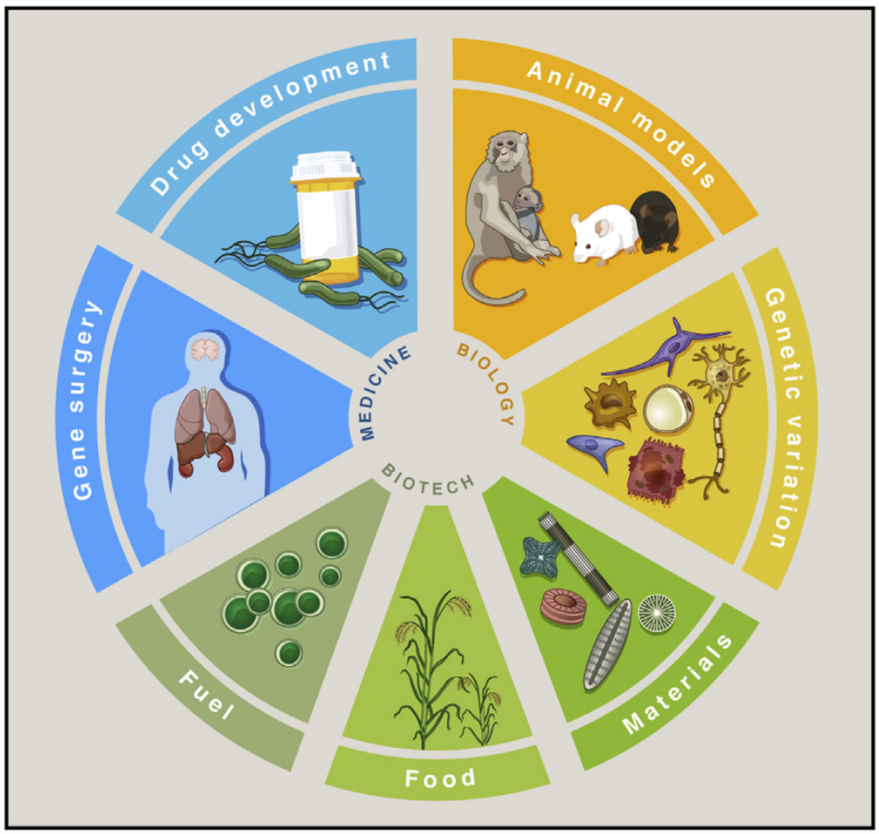

Adapted from Hsu et al. 2014

Figure 3. Applications of the CRISPR/Cas9 technology.
The CRISPR/Cas9 system can be used in different fields, such as biology, biotechnology and medicine. Clockwise from top: Cas9 can be used to create model organisms to study gene function or human diseases; to develop new drugs and generate synthetic materials; in agriculture to improve crops yield, quality and resistance to pathogens; to create biofuels; to cure genetic diseases directly in vivo; to create bacterial factories for the production of high amounts of drug precursors.

2.3.7 Cas9 delivery and applications *in vivo*

As already mentioned, there are viral and non-viral methods to vehicle Cas9 in cells, but the efficacy and safety are still under investigation. Nevertheless, progresses have been made to deliver Cas9 *in vivo*. The already assembled RNP complex formed by the Cas9 protein and the RNA guide has been identified as the best candidate to express the endonuclease in the target cells thanks to its rapid mechanism of action in different cell types, its fast degradation and reduced off-target effects (Kim et al. 2014; Hendel et al. 2015; Schumann et al. 2015; Liang et al. 2015).

Several model organisms have been successfully edited with Cas9. For example, germ line genome editing was efficiently achieved by injecting the mix of Cas9 and RNA guide in

one-cell-stage embryo to knock out different genes in zebrafish (Jao, Wente, and Chen 2013), mice (Hui Yang et al. 2013), frogs (Xiaogang Guo et al. 2014), monkeys (Niu et al. 2014); but also to insert a sequence of interest in the genome by HR upon delivery of a DNA donor template (Yang et al. 2013; Ventura and Dow 2017).

Cas9 was used by Chen and colleagues to target fusion genes in mouse xenografts. RNA guides were designed against the two genes involved in the genomic rearrangement and, combined with a Cas9 nickase, generated two nicks that allow the insertion of a suicide gene. In particular, they introduced the gene encoding a thymidine kinase, an enzyme that converts the prodrug ganciclovir in the mature form able to block DNA synthesis and induce apoptosis in the target cells; this construct remains episomal in the healthy cells because of the lack of induction of two proximal nicks. Cas9 was efficiently delivered by using a defective adenovirus, unable to replicate and self-propagate. that However, DNA damage can be generated in the genes involved in the rearrangement also in the healthy tissues; moreover, the authors agreed that non-viral approaches to vehicle Cas9 would be recommended (Chen et al. 2017).

For example, the RNP complex was efficiently delivered in different areas of adult mouse brains by directly injecting it in the region of interest to edit the genome of post-mitotic neurons (Staahl et al. 2017).

Lipid nanoparticles constitute a promising alternative to deliver Cas9 in different organs, such as muscles, liver and lung. Different chemistries of lipid nanoparticle have been proposed, with good results in terms of Cas9 delivery in the target cells and safety. For example, Wei and colleagues optimized a protocol for the systemically deliver of the RNP complex by using a specific lipid nanoparticles formulation that preserves the integrity of the endonuclease, while circulating in the bloodstream, allowing correct genome editing in lungs and liver upon intravenous injection (Wei et al. 2020).

Rosenblum and colleagues combined two treatments to deliver Cas9 in mice models affected by glioblastoma. Lipid nanoparticles (LNPs) were intracerebral injected to deliver Cas9 mRNA and the guide RNA to knock out a gene essential for cancer proliferation, leading to reduced tumor growth and increased mice survival. To target metastases, LNPs were coated with antibodies able to bind receptors expressed on the surface of target tumor cells, improving mice viability (Rosenblum et al. 2020).

LNPs were used also to treat Duchenne muscular dystrophy by transiently delivering the Cas9 mRNA and the guide RNA into skeletal muscles of a mouse model by repeated intramuscular injections to promote exon skipping and restoration of the correct reading frame of the dystrophin protein (Kenjo et al. 2021).

Excitingly, Cas9-based strategies are now also in clinical trials to treat the two genetic blood diseases sickle cell disease and β-thalassemia. Sickle cell disease is characterized by a mutation in the β-globin gene; the most common is a Glu > Val mutation that results in an aberrant sickle hemoglobin (HbS). β-thalassemia is the consequence of mutations in the β-globin gene, such as small insertions, deletions or single point mutations, that cause reduced or absent synthesis of the β-globin chain of hemoglobin. Vertex and CRISPR Therapeutics companies have developed the CTX001 strategy; 45 patients for both the diseases have been recruited to be transfused with Cas9-edited CD34+ human hematopoietic stem cells that re-express the fetal hemoglobin, thanks to a mutation in the *BCL11A* gene that eliminates its repression, to compensate the absence of a functional adult hemoglobin version (Wu et al. 2020). Available data reported that the treated patients experienced an improvement of the major symptoms (Urnov 2021).

Laber congenital amaurosis (LCA) is a rare genetic disease, caused by mutations in the CEP290 gene, that leads to vision loss in children. Allergan and Editas companies developed the EDIT-101 strategy to correct a point mutation in the *CEP290* gene by a single subretinal injection; they have recruited 18 patients and started a clinical trial named BRILLIANCE (Wu et al. 2020). This represents the first time that Cas9 is delivered directly in patients, an important and promising step towards new treatments *in vivo*.

2.3.8 CRISPR-associated concerns

Although the simplicity of the CRISPR/Cas9 system allows its use in several applications, some problems emerged for its use in the clinics.

The major concern is based on the evidence that the Cas9 endonuclease can generates off-targets because some mismatches between the RNA guide and the target DNA in the PAM-distal region can be tolerated (Kuscu et al. 2014). However, several strategies have been proposed to overcome this limitation. A possibility could be to shorten the length of the RNA guide to decrease the interface between DNA and RNA. Even if counterintuitive, different groups have shown the efficacy of this strategy in reducing off-target effects, without sacrificing the on-target activity of Cas9 (Fu et al. 2014). Cas9 variants constitute another alternative; for example, Cas9 nickases introduce nicks, normally repaired with high fidelity, but can generate DSBs when working in pairs, almost abrogating off-targets (Ran, Hsu, Lin, et al. 2013). The dCas9, instead, can be fused with the FokI nuclease domain to cut the DNA target more specifically because it has to dimerize (Guilinger, Thompson, and Liu 2014; Tsai et al. 2014). Another way is the use of the Cas9 protein already assembled with the RNA

guide to form a RNP complex that start cutting the DNA immediately after delivery and its rapid degradation reduces the chances of generating off-target effects (Kim et al. 2014).
However, there are studies reporting genome sequencing data showing that the off-targets events mediated by Cas9 are not frequent (Smith et al. 2014; Veres et al. 2014; Sternberg and Doudna 2015; Gekara 2017; Long et al. 2016).
Another concern related to the therapeutic use of Cas9 is the preexisting adaptive immune response that has been found in the human population against the endonuclease; indeed, Charlesworth and colleagues found antibodies and T cells against SaCas9 and SpCas9, the most commonly used variants of Cas9, in the serum of donors; indeed, these two species of bacteria frequently infect the human population. However, a possible solution could be the use of Cas9 orthologs from other bacterial species that do not infect humans (Charlesworth et al. 2019).
It has been shown that upon DSB generation by Cas9 in RPE1 cells and in human pluripotent stem cells, edited cells with a functional p53 protein were counter selected (Haapaniemi et al. 2018; Ihry et al. 2018). Stable inactivation of p53 restored cell proliferation and efficient gene editing in the presence of a DNA donor template. However, permanent loss of p53 could lead to chromosomal rearrangements and oncogenic events (Conti and Di Micco 2018). For this reason, a transient p53 inhibition was proposed as an alternative: Schiroli and colleagues confirmed p53 activation upon DSB generation by Cas9 in hematopoietic stem cells (HSCs), that resulted in cell cycle arrest. Transient p53 inactivation did not impact on genome stability but increases HSC proliferation and precise genome editing efficiency (Schiroli et al. 2019).
In addition, it has been reported that if Cas9 is cutting in an amplified gene, cells can undergo apoptosis. This concern emerged because of false positive results were generated in loss-of-function screenings when DSBs were induced by Cas9 in amplified regions of the genome. A possible explanation of the Cas9 anti-proliferative effect could be the consequences of many on-target DNA breaks (Aguirre et al. 2017; de Weck et al. 2018; Doench 2018).
A link between Cas9 and genome instability was identified also by Leibowitz et al, which observed that Cas9-induced DNA damage generated micronuclei and chromosome bridges in their experimental system, leading to chromothripsis, a rearrangement involving one or few chromosomes (Leibowitz et al. 2021).
However, the toxicity induced by the generation of sequence-specific DSBs with Cas9 could be an important aspect to be investigated more deeply. Indeed, the CRISPR/Cas9 system could be used to generate DSBs either in cancer cells, by targeting chromosomal rearrangements, or in cells infected with multiple copies of an integrated proviral genome, such as HIV.

It would be interesting to understand if sequence-specific DSBs induction is sufficient to impair proliferation and induce cell death selectively in cells carrying genomic aberrations, independently from its expression and function, while sparing normal cells that lack the DNA target sequence. Afterwards, it would be worth exploring if the combination of Cas9-induced DNA damage with molecules that inhibit DSB repair could boost the effects of the endonuclease on cell survival and death, opening the possibility to develop a potential therapeutic strategy.

This was the aim of my PhD work.

3 Material and methods

3.1 Cell line generation

HeLa and RKO GFP stable cell lines were generated by infecting HeLa and RKO WT cells (provided by the IFOM cell culture) with a lentivirus carrying the pLenti-CMV-MCS-GFP-SV-puro plasmid from AddGene (Witwicka et al. 2015) previously depleted of the promoter and enhancer region.

Lentiviruses are a subclass of retroviruses with the ability to integrate into the genome of non-dividing as well as dividing cells. Lentiviruses were produced by transfecting HEK 293T by calcium phosphate method with the vector expressing the gene of interest (10 μg of the pLenti-CMV-MCS-GFP-SV-puro plasmid for each plate of HEK 293T cells) together with the third-generation packaging vectors expressing the gag, pol, rev and env genes. The day after the transfection the growth medium was replaced with 5 ml of fresh medium to concentrate viral particles in the supernatants. 48 hours post-transfection, viral supernatants were collected, filtered with 0.45 μm filter, to remove cells that were dead or detached from the plate, and supplemented with 8 μg/ml polybrene. Target cells were incubated with the supernatant for 16 hours. After the infection with the highest viral titer, cells were grown under puromycin selection (1 μg/ml) to create the HeLa and RKO GFP stable cell lines. Cells was tested for the number of GFP construct integrations comparing it to the Actin gene, that is assumed to be present in two copies in the cell. The number of construct's copies was calculated according to this formula:

$$N° \text{ of integrations} = 2^{(Ct\ actin - Ct\ GFP)}$$

HeLa WT and GFP cells were grown under standard tissue culture conditions (37 °C, 5% CO_2) in DMEM, supplemented with 10% FBS, 2mM L-Glutamine and 1% Penicillin/Streptomycin. RKO WT and RKO GFP cells were grown under standard tissue culture conditions (37 °C, 5% CO_2) in MEM, supplemented with 10% FBS, 2mM L-Glutamine, 0.1 mM NEAA, 1 mM NaPyr and 1% Penicillin/Streptomycin.

3.2 Ionizing radiation (IR)

Ionizing radiation (IR) is a radiation able to ionize the target. The Gray (Gy) is the International System of Units of absorbed radiation dose, where 1 Gy is the absorption of 1 joule of radiation energy by 1 kilogram of matter. When DNA is targeted by IR DSBs and several other types of DNA damage are generated. Here, DSBs were generated by using X-rays, an electromagnetic type of IR, generated by a high-voltage X-rays generator tube (Faxitron X-Ray Corporation).

3.3 FISH for the GFP sequence

The integration sites of the pLenti-CMV-MCS-GFP-SV-puro plasmid were assessed by FISH analysis. The plasmid was labeled with Spectrum Green Nick Translation Kit (Vysis, Abbott Molecular) according to the manufacturer's instructions.
Hela, MCF10A, MBA MD 361 e BT474 cells were prepared using a standard cytogenetic methodology (Gasparini et al. 2010). Slides were pretreated with 2XSSC/0.5% NP40 at 37°C for 30 minutes and codenaturation occurred at 70°C for 2 minutes and 37°C overnight using Hybrite (Vysis). The FISH hybridization signals were analyzed in an Olympus BX51 microscope coupled to a charge-coupled device camera COHU 4912 (Olympus). The images were captured with a 100X (oil immersion) objective and were analyzed using the Mac Probe software (PowerGene Olympus).

3.4 CRISPR/Cas9 infection

All the cell lines were infected with the CRISPR/Cas9 lentiviral vector (lentiCRISPRv2 #98290, AddGene) (Stringer et al. 2019). Before infection different sgRNAs were cloned in the Cas9 lentiviral plasmid. The GFP sgRNAs were designed to target and cut the GFP sequence; the sgRNA was designed by using different CRISPR design tools ato compare the scores of efficiency and off-targets. The sequence for the scramble sgRNA used as a negative control was taken from Liao et al. (Liao et al. 2015).

3.4.1 sgRNAs cloning protocol

The lentiCRISPRv2 plasmid is one vector system containing two expression cassettes, both the hSpCas9 and the chimeric guide RNA. To insert the sgRNA of interest in the lentiCRISPRv2 vector, the plasmid is digested using BsmBI, and a pair of annealed oligos can be cloned into the scaffold of the single guide RNA scaffold (the sequences of the different sgRNAs are listed in the table 1). The oligos are designed based on the target site sequence (20bp) and flanked at their 3' ends by a 3bp NGG PAM sequence. 1 µg of the plasmid was first digested with 1µl of BsmBI enzyme (NEB #R0739) in 3.1 NEB Buffer (1X) adding water up to 30 µl final volume. After a 1-hour incubation at 55°C, the plasmid was dephosphorylated adding 1 µl of Alkaline Phosphatase, Calf Intestinal (CIP #M0290) and kept 30 minutes at 37oC, in order to prevent the ligation of the empty vector. The digestion was then loaded on 1% agarose gel and the larger band was purified using the Wizard® SV Gel and PCR Clean-Up System (Promega #A9281) according to manufacturer's instructions. In parallel, 1 µl of the forward and reverse oligonucleotides

from both the 100 µM stocks were annealed and phosphorylated adding 0.5 µl of T4 Polynucleotide Ligase (NEB #M0201S) and 1 µl of T4 DNA Ligase Reaction Buffer 10X (NEB #B0202S), already containing 1 mM ATP, to 10 µl of final volume reaction. The mix was incubated 30 minutes at 37°C, followed by 5 minutes at 95°C, and then left cooling inside the block at room temperature on the bench down to 25°C. The annealed and phosphorylated oligos were then diluted 1:200 in nuclease-free water and 1µl was used to set up the ligation reaction with 50 ng of the digested and purified plasmid and 1 µl of the Quick Ligase (M2200S) in its 2X Ligase Buffer for a total volume of 11 µl and kept for 10 minutes at room temperature. The ligation was then transformed into Stbl3 recombination-deficient bacteria (Invitrogen C7373-03), to avoid recombination due to the Long-Terminal Repeats (LTRs) contained in the lentiviral transfer plasmids. In detail, 5 µl of the ligation reaction was added to 50 µl of bacteria, thawed on ice without pipetting. After 30 minutes on ice, the cells were heat-shocked for 45 seconds at 42°C without shaking and then placed again on ice for 2 minutes before adding 250 µl of pre-warmed S.O.C. Medium to each bacteria vial. The vials were shacked for 1 hour at 37°C and then spread on a pre- warmed selective plate for overnight incubation at 37°C. The day after, some colonies were picked up, put in 5 ml of LB medium supplemented with ampicillin and placed in a horizontally shaking incubator at 37°C for the mini-inoculum. The mini-inoculum was used to generate a glycerol stock, and for bacterial DNA extraction (Wizard® Plus SV Minipreps Purification systems, Promega #A1460) to check by sequencing the presence of the insert inside the plasmid. Only the insert-positive clones were incubated overnight in 250 ml of LB selective medium at 37°C for a maxi inoculum of bacteria, from which DNA was extracted by using the NucleoBond Xtra Maxi kit for transfection-grade plasmid DNA by following the manufacturer's instructions.

ID	SEQUENCE
SGRNA SCRAMBLE FW	CACCGGCGCGAAGCTTAGGGATAAC
SGRNA SCRAMBLE RV	AAACGTTATCCCTAAGCTTCGCGCC
SGRNA GFP 45 FW	CACCGCGTCGCCGTCCAGCTCGACC
SGRNA GFP 45 RV	AAACGGTCGAGCTGGACGGCGACGC
SGRNA GFP 72 FW	CACCGGAGCTGGACGGCGACGTAAA
SGRNA GFP 72 RV	AAACTTTACGTCGCCGTCCAGCTCC
SGRNA GFP 131 FW	CACCGGGTGGTGCAGATGAACTTCA
SGRNA GFP 131 RV	AAACTGAAGTTCATCTGCACCACCC
SGRNA GFP 132 FW	CACCGCGGTGGTGCAGATGAACTTC
SGRNA GFP 132 RV	AAACGAAGTTCATCTGCACCACCGC

SGRNA GFP 133 FW	CACCGCTGAAGTTCATCTGCACCAC
SGRNA GFP 133 RV	AAACGTGGTGCAGATGAACTTCAGC
SGRNA GFP 149 FW	CACCGGGGCACGGGCAGCTTGCCGG
SGRNA GFP 149 RV	AAACCCGGCAAGCTGCCCGTGCCCC
SGRNA GFP 192 FW	CACCGAGCACTGCACGCCGTAGGTC
SGRNA GFP 192 RV	AAACGACCTACGGCGTGCAGTGCTC
SGRNA GFP 273 FW	CACCGTTCAAGTCCGCCATGCCCGA
SGRNA GFP 273 RV	AAACTCGGGCATGGCGGACTTGAAC
SGRNA GFP 335 FW	CACCGCAACTACAAGACCCGCGCCG
SGRNA GFP 335 RV	AAACCGGCGCGGGTCTTGTAGTTGC
SGRNA GFP 444 FW	CACCGCGGCCATGATATAGACGTTG
SGRNA GFP 444 RV	AAACCAACGTCTATATCATGGCCGC
SGRNA GFP 507 FW	CACCGCGCTGCCGTCCTCGATGTTG
SGRNA GFP 507 RV	AAACCAACATCGAGGACGGCAGCGC
SGRNA GFP 573 FW	CACCGCAGAACACCCCCATCGGCGA
SGRNA GFP 573 RV	AAACTCGCCGATGGGGGTGTTCTGC
SGRNA GFP 635 FW	CACCGCATGTGATCGCGCTTCTCGT
SGRNA GFP 635 RV	AAACACGAGAAGCGCGATCACATGC
SGRNA GFP 685 FW	CACCGTGGAGTTCGTGACCGCCGCC
SGRNA GFP 685 RV	AAACGGCGGCGGTCACGAACTCCAC

Table 1. Single guides RNAs list.

3.4.2 CRISPR/Cas9 lentiviral infection protocol

HEK293T cells were used as host cells for the production of lentiviral particles to transduce the GFP or CRISPR/Cas9 constructs in HeLa and RKO cells. HEK293T cells were transfected with both the plasmid of interest (either pLenti-CMV-MCS-GFP-SV-puro or Lenti CRISPR v2) and the plasmids coding the lentiviral packaging proteins to start the production of lentiviral particles. The transfection method was based on calcium phosphate, where calcium phosphate-DNA precipitates bind the cell surface and enter the cell by endocytosis. Precipitates are obtained by slowly mixing a solution containing calcium chloride and DNA with a HEPES-buffered saline solution containing sodium phosphate. In details, for a 10 cm dish, 10 µg of CRISPR/Cas9 plasmid and 3rd generation packaging plasmids (2,5 µg of pRSV-Rev, containing Rev; 2,8 µg packaging plasmid pMDLg/pRRE containing Gag and Pol; 5 µg envelope expressing plasmid pMD2.G) were resuspended in sterile H2O with 62,4 µl of CaCl2 (2M). Subsequently, 500 µl of this solution was added to

500 µl of 2xHBS, constantly mixing. After 5 minutes incubation at room temperature, 1 ml of the mixture was then added to the cells and left overnight at 37°C. The day after, the medium containing the viral particles was replaced with 5,5 ml of fresh medium. After another day in the incubator, the 5,5 ml of viral medium were collected from each 293T dish and used to infect one dish of the target cells. Before each infection, the viral titer was calculated using the Lenti-X GoStix Plus (Takara, Cat#631281), a method that allows a rapid, simple, and effective quantification of the lentivirus production in the cell supernatants. To perform the test, 20 µl of supernatant are applied on a GoStix cassette and, 10 minutes after, test and control bands appears, indicating the presence of the lentiviral capsid protein p24. The results on the cassette can then be analyzed using a free smartphone app, which quantifies lentivirus titer by comparing the intensities of the test and the control bands. The target cells were collected at different time points after infection for the analyses described in this thesis.

In the experiments where HeLa cells were treated with the pool of GFP RNA guides, 1 µg of each Cas9 plasmid was mixed to the other to obtain the final concentration of 10 µg.

3.5 BLESS (direct in situ breaks labelling, enrichment on streptavidin and next-generation sequencing)

BLESS (direct in situ breaks labeling, enrichment on streptavidin and next-generation sequencing) is a technique to detect and map DSBs at genome-wide level in a population of cells (Crosetto et al. 2013). In the experiments described in this thesis, a modified version of the protocol published by Crosetto and colleagues in 2013, optimized in our laboratory, was used. For a typical BLESS experiment 5-10 million cells, for each condition, were crosslinked with 2% formaldehyde for 30 minutes at RT. The crosslinking reaction was then quenched with the addition of 125mM Glycine. MCF10A GFP cells were fixed 24 hours after infection with the lentivirus carrying either the Cas9 protein and the GFP guide or the Cas9 protein and the scramble guide, then rinsed twice in 1X cold PBS, collected by scraping and centrifuged at 2000 rpm for 5 min at 4°C. Cells were washed twice in cold PBS and the pellet was flash-freezed at -80°C and stored until use. Pellets were resuspended in 1mL of Lysis buffer (Tris HCl pH 8 10mM, NaCl 10mM, EDTA 1mM, EGTA 1mM, NP- 40 0.2%, DTT 1mM, Proteases inhibitors (Roche)), and incubated for 90 minutes on a rotating wheel at 4°C. Cells were then collected by centrifugation (2000rpm for 5 minutes at 4°C) and resuspended in 1mL nucleus break buffer (Tris HCl pH 8 10mM, NaCl 150mM, EDTA

1mM, EGTA 1mM, SDS 0.3%, DTT 1mM) and incubated in a thermomixer at 37°C shaking at 800 rpm for 45 minutes. Cells were then collected by centrifugation (2000rpm for 5 minutes at RT) and resuspended in 500µL NEB Buffer 2 (Tris HCl pH 8 10mM, NaCl 50mM, MgCl2 10mM, DTT 1mM, 0.1% Triton) + 10µg/mL Proteinase K (Roche) and incubated in a thermomixer at 37°C shaking at 800 rpm for 45 minutes. Samples were quickly transferred to ice and 500uL NEB Buffer 2 + Protease Inhibitor was added to each sample. Isolated nuclei were centrifuged (3000rpm for 10 minutes at 4°C) and washed twice in NEB buffer 2 and once in Blunting buffer (Tris HCl pH 7.5 100mM, NaCl 50mM, MgCl2 10mM, DTT 5mM, 0.025% Triton X-100). The pellet of isolated nuclei was then subjected to a blunting reaction (42µL Blunting buffer 1X, 5µL dNTP 1mM, 2µL Blunting enzyme mix (Quick blunting kit, NEB) for 45 minutes at RT. After blunting, nuclei were resuspended in 1mL NEB Buffer 2, centrifuged (3000rpm for 10 minutes at 4°C) and washed twice. Then the pellet was washed twice in T4 Ligase buffer and finally the nuclei were subjected to the Ligation step with the biotinylated proximal linker (Linker P1B, see table 2) which would tag each exposed DSB in the nuclei (18.5µL T4 Ligase buffer 1x, 5µL of 10µM Linker P1B in T4 Ligase buffer 1x, 1.5 Ligase 400.000 U/µL (NEB)). In situ ligation was performed overnight as described in the published BLESS protocol, followed by DNA de-crosslinking and extraction. After ligation, the pellets were washed twice in 1mL Wash&Bind buffer (W&B, 5mM Tris HCl pH 7.5, 1mM EDTA, 1M NaCl, 0.1% Triton X-100); after each wash, the samples were centrifuged 10 minutes at 3000rpm, at RT). Then, the pellets were resuspended in 500uL of NEB Buffer 2 + 200µg/mL Proteinase K and incubated for 45 minutes in a thermomixer set at 55°C, shaking 800rpm. Afterwards the incubation was continued for 45 minutes at 65°C. The samples were spinned down for 1 minute and transferred in ice. Potassium Acetate (0.3 M), Glycogen and 0.7 volumes of ice-cold Isopropanol. After mixing the solution, samples were incubated for 1 hour at -20°C and later centrifuged 13000rpm for 20 minutes at 4°C. Pellets were washed twice with 70% ethanol and finally resuspended in 130 µL of pure water. Purified genomic DNA was fragmented with Covaris S220 (10% duty factor, 175W peak incident power, 200 Cycles/burst, 150s) to obtain a pool of 250 bp fragments. Covaris machines utilize the Adaptive Focused AcousticsTM (AFA) process to shear DNA, exploiting bursts of ultrasonic acoustic energy at very high frequency that lead to a strictly regulated fragment size distribution. Next, the sheared DNA fragments were diluted with 180 µL of pure water: 10µL of this solution was stored and used as Input for further analyses. The remaining sheared DNA fragments were captured on streptavidin beads (Dynabeads MyOne Strepdavidin C1, ThermoFisher Scientific): the samples were incubated for 30minutes with 10µL of beads on a rotating wheel at 4°C in W&B buffer. Magnetic beads were then washed twice in W&B buffer and

resuspended in 37.5µL pure water. The sheared fragments underwent a blunting reaction (5 µL Blunting buffer, 5 µL dNTP 1mM, 2 µL Quick blunting enzyme mix, 0.5 BSA 20mg/mL) for 45 minutes at RT, shaking at 1200rpm for 15 seconds every 15 minutes. Afterwards, the sheared DNA fragments were washed twice in W&B buffer and resuspended in 33 µL pure water. Next, they were ligated to the distal linker (Linker D3, see table 2): they were incubated overnight in 5µL Ligase buffer 10X, 10µL Linker D3 100mM, 2 µL T4 Ligase (400.000 U/µL, NEB), in a thermomixer set at 16°C, shaking for 45 seconds at 1200rpm every 45 minutes. The ligation product was washed twice in W&B buffer and resuspended in 21 µL pure water. BLESS linkers have a hairpin-like structure: the stem is composed of a barcode sequence, the I-SceI target site then there is the loop containing the biotinylated nucleotide. Digestion of the ligation product with I-SceI allowed linearization of the linkers, thus recovery of the fragments from the magnetic beads, followed library preparation. The digestion was performed by adding 2.5 µL Cut Smart Buffer 10x, 0.5 µL BSA 20mg/mL, 1 µL I-SceI (NEB): the samples were incubated at 37°C for 4 hours. In parallel, input samples were also digested with I-SceI using the same reaction mix. Finally, the supernatants were recovered and subjected to PCR amplification. Each sample was split into 5 PCR reactions: 5 µL I- SceI digested DNA, 1 µL PCR primer 1 (PCRP1, see table 3), 1 µL PCR primer 2 (PCRD3, see table 3), 1 µL dNTP 1mM, 5 µL 10x Q5 buffer, 0.5 µL Q5 polymerase (NEB). Each reaction was subjected to 18 cycles of PCR reaction. PCR products were recovered and the ones coming from the same sample were pooled together. Finally, both input samples and PCR products were purified with Wizard SV gel and PCR clean-up system (Promega) and resuspended in 35 µL pure water. The purified samples were analyzed with BLESS-quantitative PCR (BLESS-qPCR).

3.5.1 BLESS qPCR

To quantify the enrichment of DNA sequences at specific genomic regions, captured by BLESS, in the lab we optimized an approach based on ChIP-qPCR analyses. The qPCR primers were typically designed in the 300bp surroundings of the site of interested (table 3). qPCR with the selected primers was performed on the final BLESS product and on the genomic Input, that corresponds to 1:30 of the material recovered after sonication. The enrichment was expressed as % of input:

% of input = $\frac{LB}{IN} \times 100$

LB = 2^{-Ct} Library, corresponding to the BLESS product obtained after the PCR step

IN = 2^{-Ct} Input

In this way, the DNA enrichment for each sample is normalized on the amount of starting material. Note that this calculation does not take into account the input dilution and the PCR cycles used to amplify the material in the final step of BLESS protocol. However, since the same input dilution and number of PCR cycle were used, different BLESS experiments are comparable.

3.5.2 BLESS linkers and qPCR primers

ID	SEQUENCE
LINKER P1B	TACTACCTCGAGAGTTACGCTAGGGATAACAGGGTAATATAGTT T[BtndT]TTTCTATATTACCCTGTTATCCCTAGCGTAACTCTCGAGG TAGTA
LINKER D3	CGTCGTCTCGAGAGTTACGCTAGGGATAACAGGGTAATATAGTT TTTTTCTATATTACCCTGTTATCCCTAGCGTAACTCTCGAGACGA CG

Table 2. BLESS linkers list.

ID	SEQUENCE
PCRP1	CCCTAGCGTAACTCTCGAGGTAGTA
PCRD3	CTAGCGTAACTCTCGAGACGACG
GFP CUT RIGHT FW	TCGTGACCACCCTGACCTA
GFP CUT RIGHT RV	AAGTCGTGCTGCTTCATGTG
GFP CUT LEFT FW	CGACTCTAGAATGGTGAGCAAG
GFP CUT LEFT RV	GTTTACGTCGCCGTCCAG

Table 3. BLESS qPCR primers list.

3.6 Incucyte experiments

For the assays carried out in incucyte to characterize viability and cell death of HeLa and RKO cells after different treatments, I plated 150 000 cells per well in a 6 multiwell plates. 24 hours after, I treated cells to generate DNA damage (either 1Gy irradiation or Cas9 infection); one day upon DSB generation I plated cells into 96 multiwell plates and I

monitored cell proliferation with the help of Incucyte, a real-time quantitative live-cell imaging and analysis platform that enables visualization and quantification of cells behaviour over time. I also added 400x cytotox green dye (Sartorius, #4633) to count dead cells; this reagent makes real time measurements of mortality based on cell membrane integrity; indeed, when a cell is dead and the membrane integrity is lost, the dye enters the cell and fluorescently labels the nucleus. I have monitored cells behaviors either in Incucyte S3 or in Incucyte SX5 for a number of days that depends on the experiment and I precisely counted the number of alive and dead cells by using the cell-by-cell analysis software of Incucyte, that allows the cell count based on size, morphology and fluorescence of the cells.

3.7 Immunofluorescence

Immunofluorescence (IF) is a technique here applied to study protein sub-cellular localization at single-cell level. This technique allows the visualization by fluorescent microscopy of target proteins that are recognized by antibodies. Cells were grown on coverslips, washed twice for 5 minutes with PBS and fixed with 4% paraformaldehyde (PFA) for 10 minutes at RT. To allow accessibility of the target epitopes to the antibodies, cells were permeabilized with 0.2% Triton X-100 for 10 minutes at RT. Cells were incubated for 1 hour in blocking solution (PBG, 0.5% BSA, 0.2% cold water fish gelatin, Sigma) and then incubated with primary antibodies (see the dedicated section) diluted in PBG for 1 hour at RT, in a dark humidified chamber. Cells were washed twice for 5 minutes with PBG and incubated with fluorophore-conjugated secondary antibodies diluted 1:500 in PBG for 45 minutes at RT in a dark humidified chamber. The incubation with secondary antibodies was followed by 5 minutes incubation with 4'-6-Diamidino-2-phenylindole (DAPI, 1µg/ml, Sigma-Aldrich, excitation wavelength 358nm, emission wavelength 461nm). DAPI binds preferentially to AT clusters of DNA minor groove and it was used to visualize nuclei. Cells were briefly washed with PBS and water. Finally, coverslips were mounted with mowiol mounting medium (Calbiochem), which is a polyvinyl alcohol solution containing an "anti-fade" agent, capable of reducing photobleaching of the fluorophores conjugated to the secondary antibodies. Coverslips were air dried before microscope analyses.

3.7.1 Imaging

For all the experiments, immunofluorescence images were acquired using either the wide-field Olympus Upright Olympus AX70 or the wide-field Olympus Upright BX51 and the MetaMorph software (Soft Imaging System GmbH). Comparative immunofluorescence

analyses were performed in parallel with identical acquisition parameters using ImageJ software; five random fields of cells were taken for each condition at each timepoint, with the same exposition and same magnification (60x objective, 1x optical zoom). The quantification was performed using the ImageJ software, adjusting the brightness and contrast signal using the same parameters for all the images, which are set considering the signal of the control conditions as a reference. I have propagated the same brightness and contrast to all the images and I have analyzed the results. For DDR foci, the intensity of foci per nucleus was measured using CellProfiler software (Carpenter et al., genome biology, 2006). Briefly, images were first masked over DAPI-staining to select for nuclei and discard unspecific cytoplasmic signal. Next, foci were identified with the "enhance speckles" module and background signal filtered out using the manual thresholding strategy. The intensity of nuclear DDR foci was then calculated by multiplying the number of nuclear foci by their average intensity in each nucleus.

3.7.2 Antibodies

Anti-γH2AX (mouse monoclonal, Millipore 05-636, 1:1000); anti-53BP1 (goat polyclonal, Bethyl A303-906A, 1:1000); anti-CRISPR/Cas9 (mouse monoclonal, clone 7A9-3A3, Sigma-Aldirch ab191468, 1:1000); anti-cGAS (rabbit monoclonal, clone D1D3G, Cell Signaling 15102, 1:200) were used as primary antibodies. As secondary antibodies for immunofluorescence I used the donkey anti-mouse Alexa 488 IgG (Life Technologies, 1:500, excitation wavelength 495 nm, emission wavelength 519 nm); donkey anti-rabbit Cy3 IgG (Jackson Immuno Research, 1:500, excitation wavelength 550 nm, emission wavelength 570 nm), donkey anti-goat Alexa 647 IgG (Life Technologies, 1:500, excitation wavelength 650 nm, emission wavelength 665 nm).

3.8 RNA extraction and standard RT–qPCR

Total RNA was isolated from cells using the Maxwell® RSC simplyRNA Tissue Kit (Promega), according to the manufacturer's instructions. Samples were treated with DNase I (Qiagen) to remove any potential residual genomic DNA contamination. 1000 ng of total RNA was reverse-transcribed using the SuperScript VILO Reverse Transcriptase (Invitrogen) with random primers. Roche SYBR Green-based RT–qPCR experiments were performed on either Roche LightCycler 480 or Roche LightCycler 96. For each RT– qPCR reaction, 10 ng of cDNA was used (primer sequences are listed in table 4).

3.8.1 qPCR

A SYBR-green based system was used to perform qPCR. SYBR-Green is a fluorescent dye that binds the double-stranded DNA species produced during the PCR reaction, generating a fluorescent signal that is detected in real-time by the real-time qPCR machine. The low fluorescence detected during the initial PCR cycles defines the baseline fluorescence, above which a fixed fluorescence threshold is set. The cycle number at which the fluorescence is higher than the fixed threshold is the threshold cycle (Ct).

Usually, 10 ng of cDNA was used for RT-qPCR. The relative change in the level of the target molecule was calculated using the comparative CT method (i.e. $2^{\Delta\Delta Ct}$ method) (Livak and Schmittgen 2001). This method is based on the calculation of ΔCt between the target gene and reference (housekeeping) in the sample analysed (ΔCt_{sample}) and the control sample ($\Delta Ct_{control}$). $2^{\Delta\Delta Ct}$ (with $\Delta\Delta Ct = \Delta Ct_{sample}-\Delta Ct_{control}$) is the value indicating the level of expression of the target gene. SYBR-Green based RT-qPCR experiments were performed on either Roche LightCycler 480 or Roche LightCycler 96 machine using Roche SYBR and the following program:

1. Denaturation: 95°C 15 min, 1 cycle
2. Denaturation/Annealing/Extension: 95°C 15 sec > 60°C 20 sec > 72°C 30 sec, 50 cycles
3. Melting curve: 40°C > 90°C > 40°C, 1 cycle

ID	SEQUENCE
HUMAN GFP FW	GAAGCGCGATCACATGGT
HUMAN GFP RV	CCATGCCGAGAGTGATCC
HUMAN ACTIN FW	TGTGGGGTCCTGTGGTGT
HUMAN ACTIN RV	GAAGGGGACAGGCAGTGAG
HUMAN IL-6 FW	CCACTCACCTCTTCAGAACG
HUMAN IL-6 RV	CATCTTTGGAAGGTTCAGGTTG
HUMAN IL-8 FW	TTGGCAGCCTTCCTGATTTC
HUMAN IL-8 RV	TCTTTAGCACTCCTTGGCAAAAC
HUMAN CXCL10 FW	GCATCAGCATTAGTAATCAACCTG
HUMAN CXCL10 RV	TGGCCTTCGATTCTGGATTC
HUMAN TNF FW	ACCTCTCTCTAATCAGCCCTC
HUMAN TNF RV	CTACAGGCTTGTCACTCGG

Table 4. RT-qPCR primers list.

3.9 RNA-seq

Total RNA was isolated from cells using the Maxwell® RSC simplyRNA Tissue Kit (Promega), according to the manufacturer's instructions. Samples were treated with DNase I (Qiagen) to remove any potential residual genomic DNA contamination. The integrity of the RNA material was checked by using the bioanalyzer instrument; then, the library was prepared with the Illumina stranded mRNA prep Ligation kit for polyA transcripts and the RNA from HeLa GFP cells treated with either the scramble Cas9 or the GFP Cas9 was sequenced. The analyses were carried out by aligning reads on the human genome, looking at the differentially expressed genes between uncut and cut conditions, correcting the results for the batch effect and consulting different gene sets.

3.10 FACS analysis

For cell cycle analysis, at least 10^6 infected cells and supernatant were harvested and centrifuged at 1500 rpm for 10 minutes. Pellets were washed once in PBS 1X and cells were then fixed in 75% ethanol for 1 hour in ice. After washing with PBS 1X, cells were stained with Propidium Iodide (PI) (Sigma-Aldrich, 50 µg ml−1) in PBS 1X supplemented with RNase A (Sigma-Aldrich, 250 µg ml−1). Samples were acquired with Attune NxT, using a 561 nm laser and 695/40 filter for PI. The analysis was done using the FloJo software.

3.11 Colony formation assay

For the colony formation assay, I plated HeLa GFP cells in a 6 multiwell plate and the day after I infected them with a freshly prepared lentivirus expressing the Cas9 carrying either the scramble guide or the guide against the GFP sequence. Seven days after infection, I have counted the uncut condition and I have plated 400 cells, while for the cut condition I have plated the same volume of medium where cells were resuspended, in order to amplify the differences between treatments. I have left the plate in the incubator for one week, I have then fixed colonies with ethanol and I have stained them with crystal violet.

3.12 ASO transfection

Cells were transfected with antisense oligonucleotides accordingly to the following protocol. One day before transfection 150 000 cells per condition were plate in growth medium without antibiotics. The day of the transfection I have diluted and mixed GFP ASO (table 5)

in order to obtain the final concentration of 10 nM into 250 µl of serum-free medium (referred to 2 ml final medium) and I have gently mixed. I have boiled the ASO mix for 5 minutes at 95°C, then I have chilled it on ice for 5 minutes. I have diluted 4 µl of Lipofectamine® RNAiMAX transfection reagent (Life Technologies 13778075) into 250 µl of serum-free medium (Opti-MEM® I Reduced Serum Medium, GlutaMAX™ Supplement, Life Technologies 51985-026). I have combined the diluted LNA with the diluted RNAiMAX, I have mixed gently and I have incubated the mix for 20 minutes at room temperature. Just before the transfection, I have changed the medium to the cells with 1500 µl of medium without antibiotics per each well. I have added 500 µl of the complex LNA-RNAiMAX to each well. Finally, I have incubated cells at 37°C in a CO2 incubator and I have not changed medium for at least 24 hours.

I have used Locked Nucleic Acid (LNA), nucleic acids analogues in which a bridge between the 2' oxygen and 4' carbon "locks" the ribose in an ideal conformation for Watson-Crick binding. This makes LNA highly thermally stable and increases their binding affinity for a complementary sequence. For this reason, LNAs are used as antisense oligonucleotides (ASO) that bind the target nucleic acids and inhibit their further processing and/or function.

ID	SEQUENCE
A1	TCGGGGTAGCGGCTGAAGCA
A2	CGCCGTAGGTCAGGGTGGTC
A3	GCCAGGGCACGGGCAGCTTG
A4	CCGGTGGTGCAGATGAACTT
A5	TCAGCTTGCCGTAGGTATTA
B1	GGATCCACCGGTCGCCAC
B2	AGCAAGGGCGAGGAGCTGTT
B3	ACCGGGGTGGTGCCCA
B4	GAGCTGGACGGCGACGTAAA
B5	TTCAGCGTGTCCGGCTAGGG
CTRL ASO	CCCTAACCCTAACCCTAACCC

Table 5. ASO list.

3.13 Resazurin assay

ASO toxicity was assessed using the *In vitro* toxicology assay kit, resazurin based (Sigma-Aldrich) in a 1:10 concentration.

Metabolically active cells reduce resazurin (7-hydroxy-3H-phenoxazin-3-one-10-oxide, Sigma-Aldrich) into resorufin (7-Hydroxy-3H-phenoxazin-3-one), which absorbs at 570 nm. Cells were with resazurin for 1 hour in a 96-well cell culture plate, then absorbance was measured in a Perkin Elmer EnVision™ 2104 Microplate Reader at 570nm. Absorbance of media alone was subtracted from cell values to obtain a final value for each condition.

3.14 RNP delivery

To perform the experiment based on the RNP approach, I have tested two different ways to deliver the RNP complex: transfection and electroporation.

3.14.1 RNP transfection

I have used an Invitrogen TrueGuide Synthetic gRNAs against the GFP sequence ready-to-use, where the crRNA and tracrRNA were already combined together, and the TrueCut Cas9 Protein v2 (Invitrogen, A36499). RNP and sgRNA were delivered into the cells by using the recommended reagent lipofectamine CRISPRMAX Cas9 Transfection Reagent (CMAX00008). The sgRNA is a 20 nt long sequence that bind and cut the same region of the GFP gene that is recognized by the Cas9 of the lentiviral approach. The PAM sequence is TGG. I have plated 150 000 cells per condition in 6 multiwell plates and, as soon as they have attached to the plate, I prepared the reagents for Cas9 transfection. In the first tube I have combined 125 µl of serum-free medium with 6250 ng of RNP, 1200 ng of sgRNA and 12.5 µl of Lipofectamine Cas9 Plus reagent for each condition. In the second tube I have mixed 125 µl of serum-free medium and 7.5 µl of Lipofectamine CRISPRMAX reagent for each condition. I have waited 2 minutes at room temperature and then I have mixed the two tubes. The mixture was incubated for 20 minutes at room temperature and the final 250 µl of reagents were provided to the cells.

3.14.2 RNP electroporation

HeLa cells were electroporated using SE Cell Line 4D-Nucleofector X Kit and program CN-114 (Lonza), according to the manufacturer's instructions. Cells were electroporated with 1,25 mM of RNPs, pre-annealed at 95°C for 5 minutes and equilibrated for 10-20 minutes at RT before electroporation according to IDT protocol. Alt R Cas9 electroporation enhancer was added to improve the efficiency of the gene editing procedure according to (Schiroli et al. 2019).

3.15 Statistical analysis

P values were calculated with Prism 9 software. Statistical analyses were performed with either t-test or one-way ANOVA test, as indicated, and represented as a mean ±SEM. Asterisks in the figures indicate p values. *$p < 0.05$, **$p < 0.005$, ***$p < 0.0005$, ****$p < 0.0001$.

4 Results

4.1 Cas9 as a novel DNA damaging agent

DNA damaging agents such radiation and chemotherapy are the most frequent therapies used against cancer. A strategy to enhance the efficacy of these treatments is their combination with DDR inhibitors. However, detrimental side effects on normal tissues are often observed (O'Connor 2015). In order to selectively kill target cells, it is important to take advantage of the specific abnormalities that are present in cancer cells but not in normal cells. The CRISPR/Cas9 technology has the potential to be a great strategy for introducing sequence-specific DSBs, while sparing normal cells that lack the target DNA sequence. Other possible uses of the CRISPR/Cas9 technology can be cells infected with an integrated, even silent, proviral genome. Indeed, current antiviral therapies are only limiting the replication of the viruses, but they are unable to eradicate latent infections.
A potential limitation of this approach is the fact that DSB, if repaired, allow cells to survive. In order to improve the efficacy of CRISPR/Cas9-mediated approach proposed above, the generation of the sequence-specific DSB should be combined with inhibitors of their repair (figure 4).

I therefore tested if the CRISPR/Cas9 system, used as a sequence-specific DNA damaging agent, can have a synthetic lethal effect when combined with cells carrying genomic abnormalities targeted by the RNA guide of the endonuclease, while sparing normal cells lacking the aberrant target DNA sequence. I also combined the sequence-specific DNA damage induced by Cas9 with the inhibition of its repair to boost the effects of the two treatments in killing target cells.

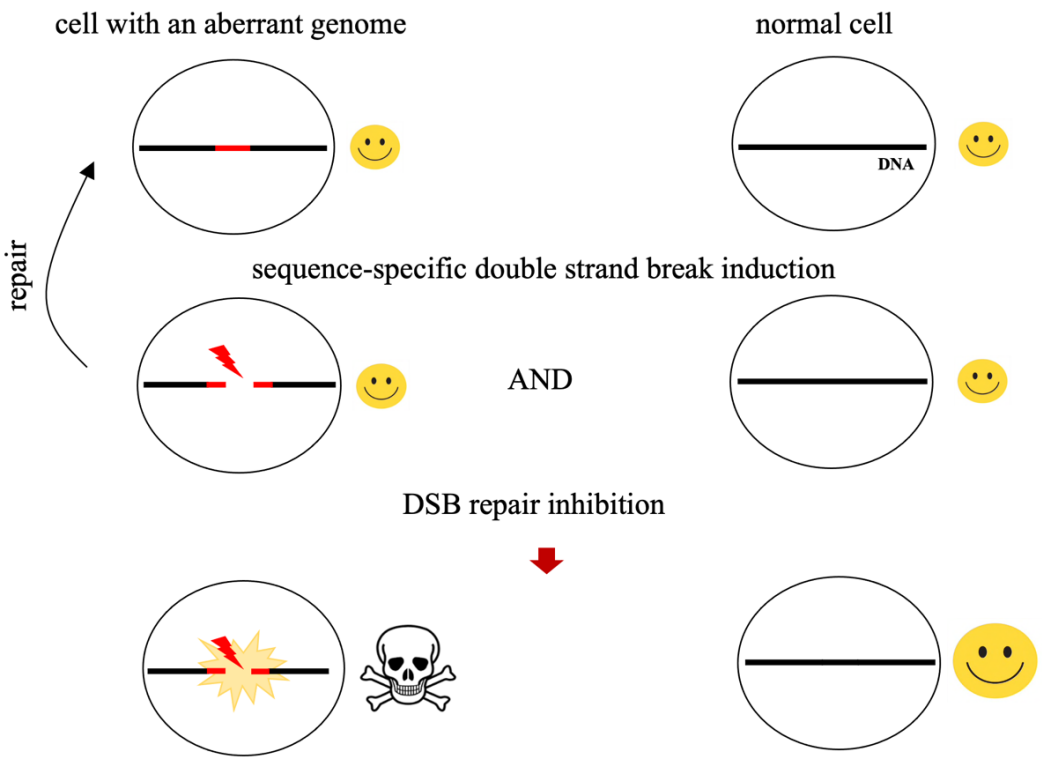

Figure 4. Schematic representation of an approach to target cells with aberrant genomes. Cas9 introduces a sequence-specific double strand break in a DNA sequence only present in cells with an aberrant genome, while sparing normal cells. However, the DSB can be repaired and cells can keep proliferating. Only targeting genomic aberrations with the CRISPR/Cas9 technology and inhibiting their repair can cause a lethal persistent DNA damage.

4.1.1 Generation of an experimental model system

The first thing that I decided to carry out was the identification of the cell lines most suitable for the generation of an experimental system to test my working hypothesis (figure 4). To determine the different degree of sensitivity to DNA damage, I irradiated six cells lines (HeLa, RKO, DLD-1, HCT116, U2OS, HaCaT) with different doses of ionizing radiations (IR; 5, 10 and 20 grays). I measured all the conditions 24 hours after irradiation by using an automated cell counter named Luna II. To count exactly how many cells survived to the treatment, I used trypan blue, a dye that allows the identification of dead cells because it is permeable only to damaged cell membranes. By distinguishing between alive and dead cells in this way, I observed that HeLa and RKO cells were those showing a most robust reduced viability in an IR dose-dependent manner (**figure 5A**). For this reason, I chose them to generate an experimental system harbouring the Green Fluorescent Protein (GFP) sequence, by lentiviral delivery. I next identified the pLenti-CMV-MCS-GFP-SV-puro lentiviral vector to introduce the GFP sequence in my target cell lines; in this plasmid the transcriptional promoter of the GFP was removed and the GFP gene is not actively transcribed. This was intentional as GFP expression can lead to some degree of toxicity in the cell – studies demonstrated that GFP expression can lead to cellular damage induced by reactive oxygen species (ROS) generation and consequential cell death by apoptosis (Ansari et al. 2016) – and its inactivation, by Cas9 targeting, could have provided an increased cell fitness advantage that may have confounded the interpretation of the results. In addition, this approach will inform whether efficacy can be observed also when targeting non transcribed regions, thus independently from their coding role.

I established a stable cell line by infecting HeLa and RKO cells with the pLenti-CMV-MCS-GFP-SV-puro Δpromoter lentiviral vector in order to obtain the integration of the GFP gene in multiple chromosomal sites, thus mimicking a cell system with a set of genomic aberrations absent in the parental cell line. Infected cells were selected by puromycin resistance and I named them HeLa GFP and RKO GFP cells **(figure 5B)**.

To have an estimate of how many copies of the GFP sequence have been integrated into the genome of these infected cells, I extracted genomic DNA from HeLa and RKO, both the WT and GFP cell lines. I designed primers against the GFP sequence and I performed a real time-qPCR to detect the relative amounts of the GFP gene DNA compared to a single-copy gene as actin (**figure 5C**). Comparing the Ct values of the GFP gene with the Ct of the actin gene, I was able to conclude that around 16 copies of the pLenti-CMV-MCS-GFP-SV-puro Δpromoter lentiviral vector have been integrated per cell.

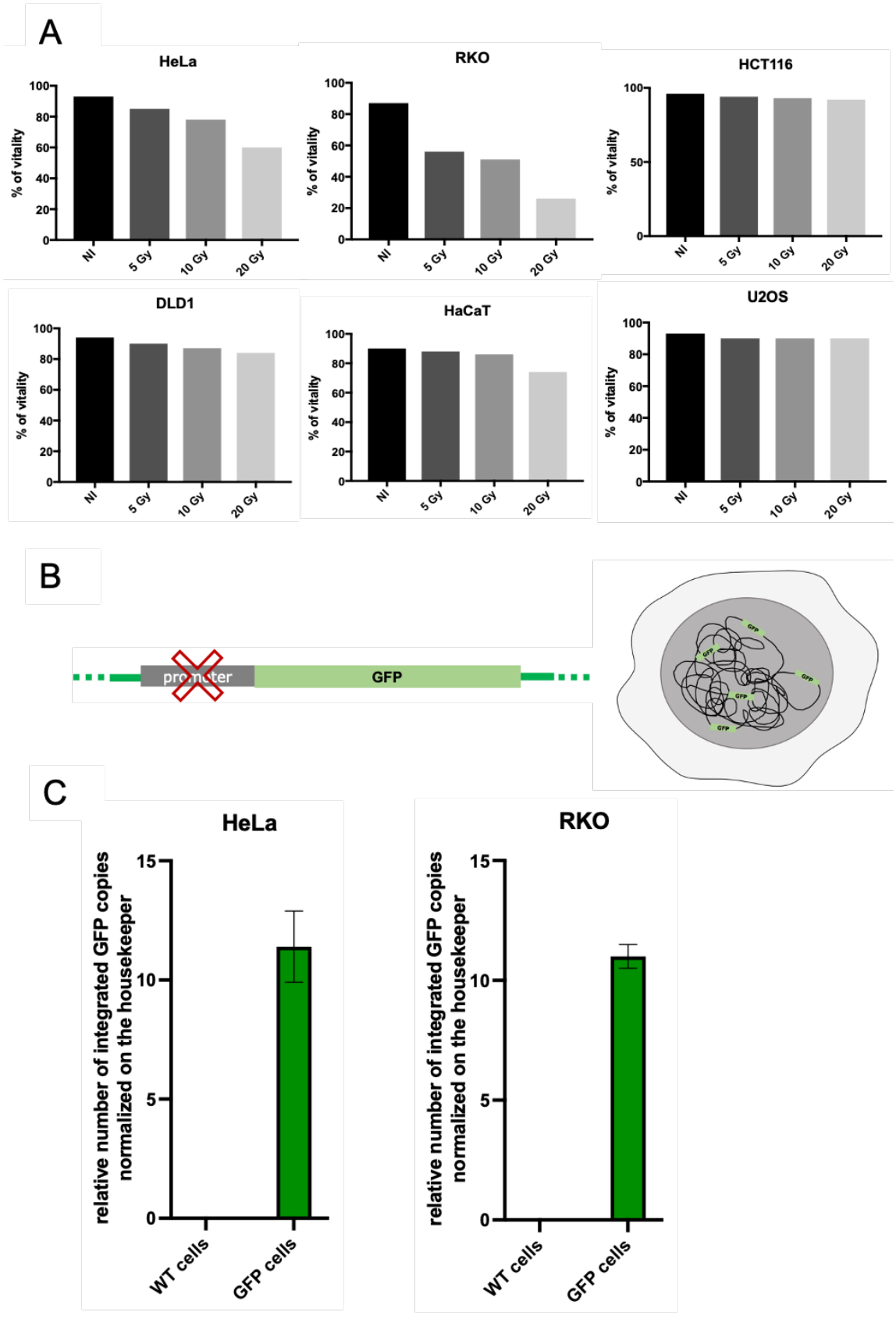

Figure 5. Creation of the experimental system.
(A) Percentage of viability of six cell lines 24 hours after irradiation with 5, 10, 20 Gy; the not irradiated controls are also shown. **(B)** Schematic representation of the cell line creation. HeLa and RKO WT cells were infected with a lentivirus carrying a promoterless GFP sequence; the GFP sequence integrated in multiple sites. **(C)** Relative number of integrated GFP copies in HeLa and RKO cells detected by qPCR, compared to actin.

To independently validate this measure and also to better understand how GFP copies are spatially distributed into the genome of the target cell lines, I collaborated with Patrizia Gasparini, from Fondazione IRCCS Istituto Nazionale dei Tumori in Milan, to perform fluorescence *in situ* hybridization (FISH) in my infected HeLa GFP cells (MBA MD 361 and BT474 were used as negative controls). She observed that the GFP copies seem to have been integrated at individual sites into the genome and not in clusters; moreover, around 16 copies of dots were qualitatively counted in GFP-infected cells, confirming what I detected by qPCR (figure 6).

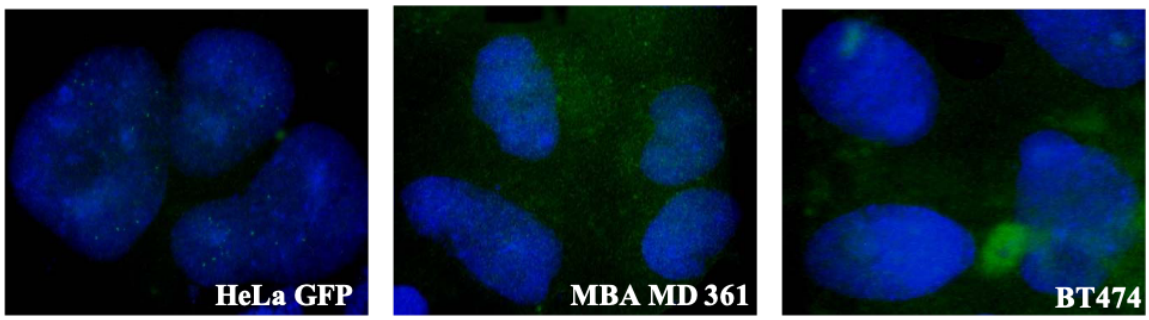

Figure 6. FISH for the GFP sequence on different cell lines.
FISH against the GFP sequence was performed in three different cell lines. HeLa GFP cells were positive for the FISH signal, as expected. Two negative controls, MBA MD 361 and BT474, were analyzed in parallel.

4.1.2 WT and GFP cells are equally sensitive to random DNA damage generated by IR

In order to confirm that the insertion of the GFP sequence in the genome of both HeLa and RKO cells was not altering their sensitivity to DNA damage compared to their WT versions, I irradiated HeLa WT, HeLa GFP, RKO WT and RKO GFP cell lines with 1Gy to induce random DNA damage and I monitored their survival in Incucyte, a real-time quantitative live-cell imaging and analysis platform that enables visualization and quantification of cells behaviour over time.

I plated the four cell lines in 6 wells plates and the day after I exposed them to 1Gy generated by a high-voltage X-rays generator tube (Faxitron X-ray Corporation). The conditions for both HeLa and RKO cells were: WT not irradiated cells, WT 1Gy irradiated cells, GFP not irradiated cells and GFP 1Gy irradiated cells. 24 hours upon irradiation, I plated all the conditions at the same cell density into a 96 well plate and I added to the medium of each well the Incucyte cytotox green dye: this reagent allows real time quantification of cell death based on cell membrane integrity; indeed, when a cell is dead and the membrane integrity is affected, the dye can enter the cell, bind the DNA and fluorescently labels the nucleus with a fluorescent signal. This system also allowed me, by taking advantage of its cell-by-cell analysis software, to count cells number for a more precise measurement of the effects of irradiation, thus also validating the approach.

I monitored proliferation of both HeLa WT and GFP cells (figure 7A) for 90 hours after plating and I first analyzed viability as the relative number of alive cells normalized on day 0, to determine the growth of cells during the experiment. As predicted, three independent experiments in HeLa cells shown that, four days after irradiation, a 40% reduction in the cell number of the irradiated conditions compared to the not irradiated controls can be observed. Importantly, this is quantitatively observed independently from the presence, or not, of the GFP sequence (figure 7B). The reduction in cell number correlated with an increase over time of the percentage of dead cells as recognized by the cytotox dye (figure 7C); already three days after DNA damage induction, HeLa irradiated cells were three times more dead than the not irradiated controls; again: this was independent from the presence of the GFP sequence (figure 7D).

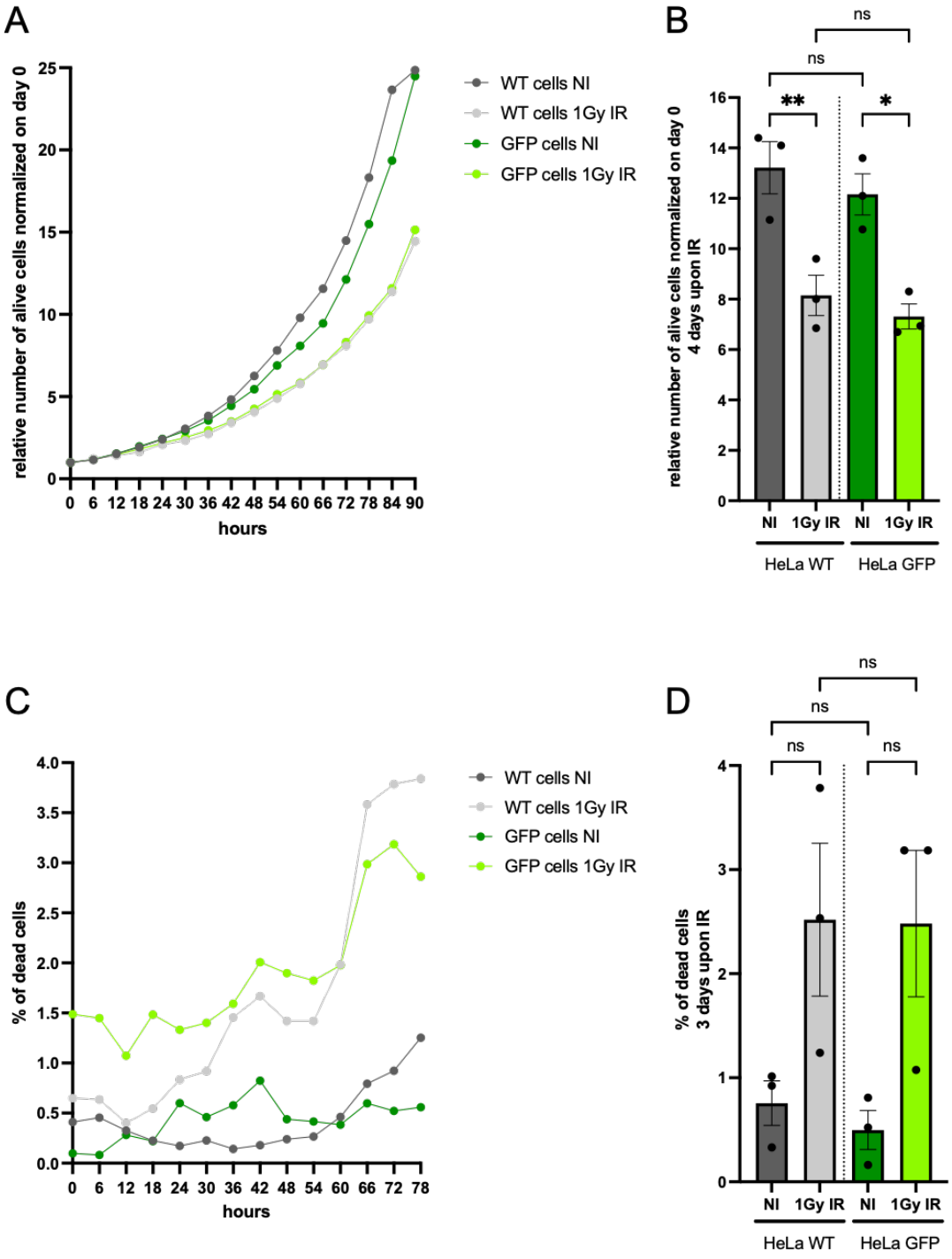

Figure 7. Irradiation kills HeLa cells, independently from the presence of the GFP sequence. **(A)** A representative growth curve showing the viability of not irradiated and 1Gy irradiated HeLa WT and GFP cells. **(B)** Viability of HeLa WT and GFP cells 4 days upon irradiation, n=3 independent experiments. Error bars represent the s.e.m. *p < 0.05, **p < 0.005. One-way ANOVA test. **(C)** A representative mortality curve showing the percentage of dead cells of not irradiated and 1Gy irradiated HeLa WT and GFP cells. **(D)** Mortality of HeLa WT and GFP cells 3 days upon irradiation, n=3 independent experiments. Error bars represent the s.e.m. One-way ANOVA test.

I recapitulated these results also in RKO cells: I monitored proliferation of these cells for 90 hours (figure 8A) and I observed that, four days after irradiation, around 60% reduction in the cell number of the irradiated conditions can be observed compared to the not irradiated controls, independently from the presence of the GFP sequence (figure 8B), indicating also that RKO cells are slightly more sensitive to DNA damage than HeLa cells under these settings. I monitored cell mortality in time by adding the cytotox dye (figure 8C) and already three days after the generation of DNA damage, irradiated cells were five times more dead than the not irradiated controls, independently from the presence of the GFP sequence (figure 8D).

The demonstration that HeLa and RKO cells, in the presence or not of the integrated GFP sequence, are equally sensitive to the generation of random DNA damage by IR allows me to confidently measure the effects of sequence-specific DSB induction by Cas9.

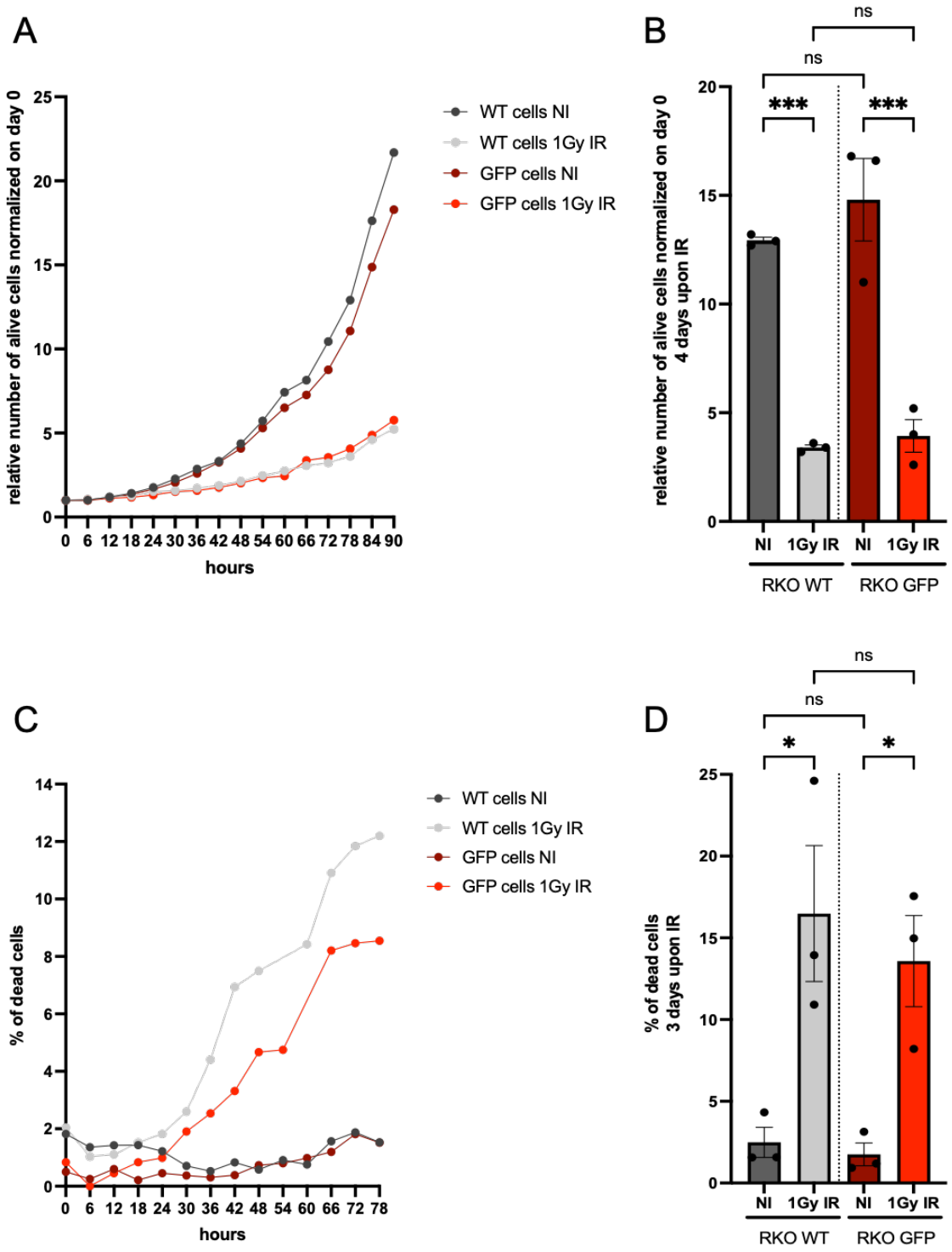

Figure 8. Irradiation kills RKO cells, independently from the presence of the GFP sequence. **(A)** A representative growth curve showing the viability of not irradiated and 1Gy irradiated RKO WT and GFP cells. **(B)** Viability of RKO WT and GFP cells 4 days upon irradiation, n=3 independent experiments. Error bars represent the s.e.m. ***p < 0.0005. One-way ANOVA test. **(C)** A representative mortality curve showing the percentage of dead cells of not irradiated and 1Gy irradiated RKO WT and GFP cells. **(D)** Mortality of RKO WT and GFP cells 3 days upon irradiation, n=3 independent experiments. Error bars represent the s.e.m. *p < 0.05. One-way ANOVA test.

4.1.3 Sequence-specific effects of Cas9 in GFP cells

After having demonstrated that WT and GFP cells have the same behavior upon DNA damage induction, I planned to explore the feasibility to induce a sequence-specific DSB with the CRISPR/Cas9 technology in cells carrying the GFP sequence, while sparing WT cells because of the lack of the target DNA sequence, and to study the cascade of events that follow DNA damage generation.

4.1.3.1 Cas9 generates DSBs and activates DDR

I designed five different CRISPR/Cas9 RNA guides targeting the GFP sequence to characterize the effects of the induction of a sequence-specific DNA damage in target cells (figure 9A). I cloned each individual guide into the lentiCRISPRv2 plasmid, performed the transformation into Stbl3 bacteria, extracted the DNA from bacteria and sequenced it to check the presence of the guide. To compare the efficiency of the guides, I performed a direct *in situ* breaks labeling, enrichment on streptavidin and next-generation sequencing technique named BLESS (Crosetto et al. 2013), that allowed me to detect the presence of a DSB in the GFP sequence. I thus infected GFP cells with the lentiCRISPR v2 vector containing Cas9 and one guide against the GFP sequence and collected them 24 hours after infection; every sgRNA guide was tested individually. In parallel, as a negative control, I infected GFP cells with a lentiCRISPR v2 vector containing Cas9 and a scramble guide (Liao et al. 2015) that did not recognize any sequence into the genome. The advantage of this technique is the *in situ* blunting and ligation of DSBs to a biotinylated double-stranded DNA linker that "tags" the DSB position. After that, DNA is extracted and fragmented to isolate the biotinylated linker by streptavidin beads. Following the additional ligation of a distal linker, the enriched sequences are amplified by using primers matching the linkers and I then checked the enrichment for the GFP sequence by qPCR using primers mapping 300bp far from the DSB. Primers for the qPCR were designed both on the right and on the left of the DSB (figure 9A). By this approach I observed that the RNA guides 149 and 133 are the most efficient ones in inducing sequence-specific DSBs within the GFP sequence, compared to the others **(**figure 9B**)**, and I then arbitrary chose the GFP 149 guide, that I will define as the GFP guide, to perform the experiments that I will describe from now on.

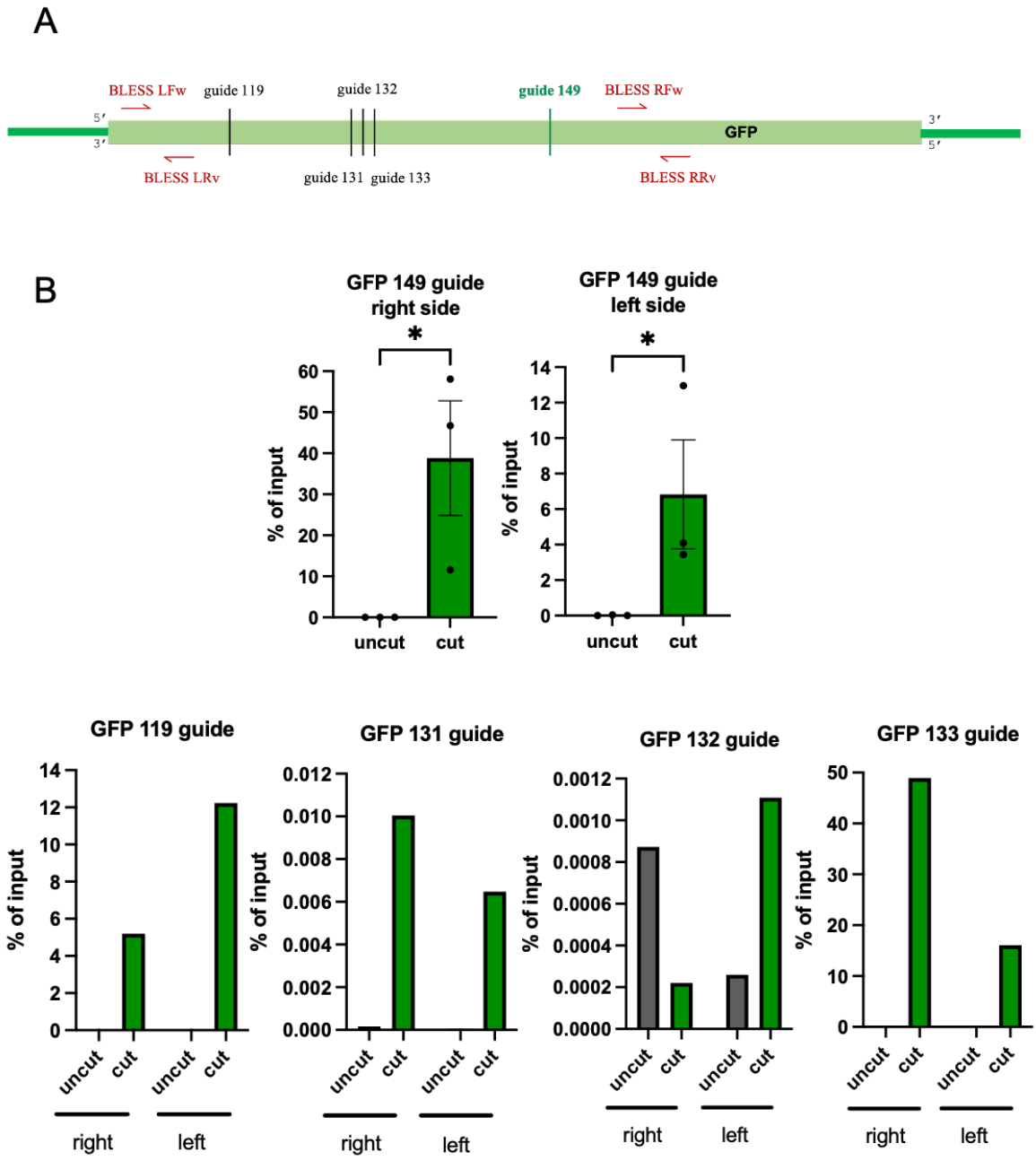

Figure 9. DSB detection by BLESS.
(A) Scheme showing were the Cas9 guides (in black) cut inside the GFP sequence and where the primers for BLESS anneal (in red). In green the guide 149. **(B)** RT-qPCR on DNA material obtained by BLESS to determine which Cas9 guide is cutting inside the GFP sequence, compared to a scramble guide. Primers were designed upstream and downstream the break. Error bars represent the s.e.m. *p < 0.05. t-test.

I further characterized DNA damage induction by Cas9 in the HeLa WT and GFP cells. Indeed, having observed that RKO cells are very sensitive to DNA damage and die quickly, I chose HeLa cells as a more convenient model to study DDR activation. First of all, I checked by immunofluorescence the activation of DDR in cells infected with either the Cas9 carrying the scramble guide or the Cas9 carrying the GFP guide by scoring for the formation of γH2AX and 53BP1 foci, together with the staining for the Cas9 protein (figure 10).

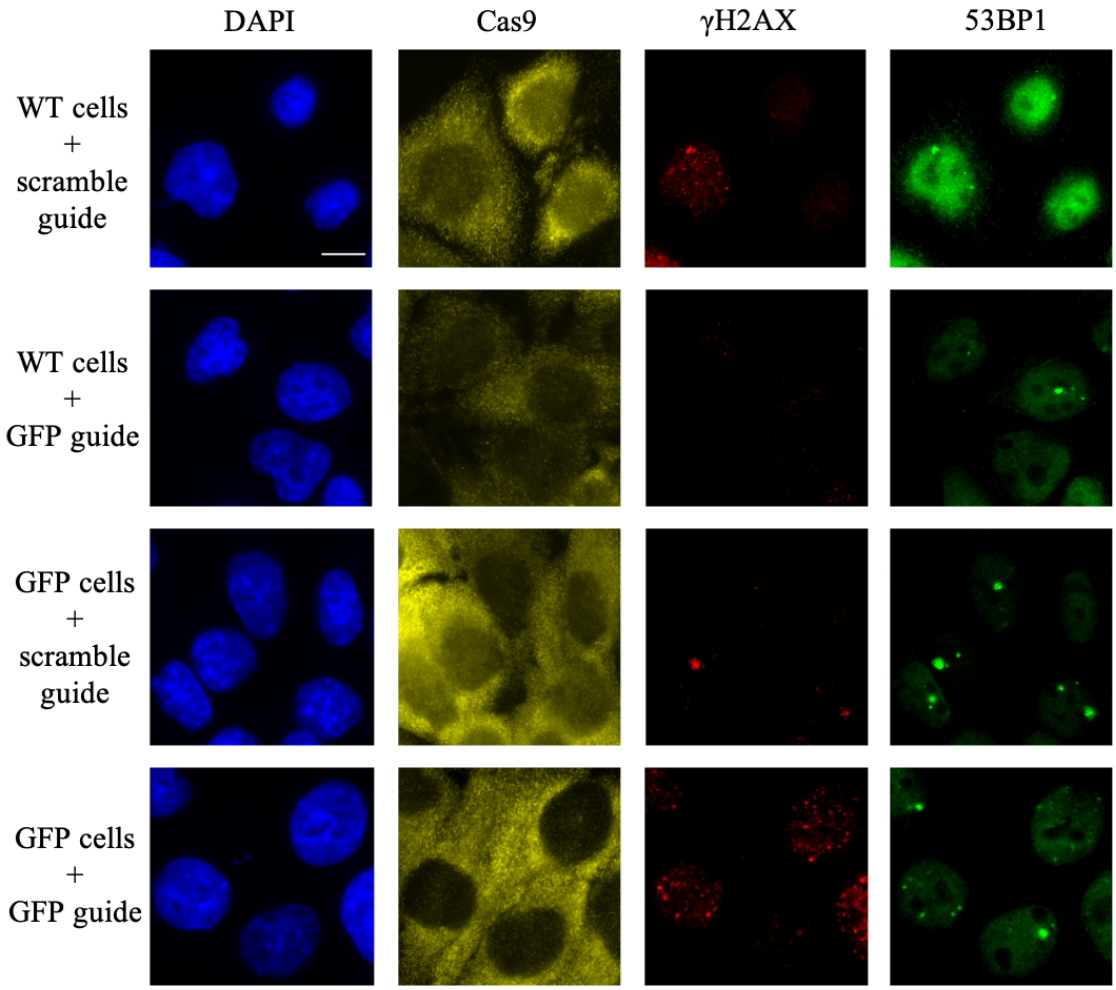

Figure 10. Cas9 induces DNA damage in HeLa GFP cells only.
Representative immunofluorescence images showing γH2AX, Cas9 and 53BP1 stainings in HeLa WT and GFP cells 4 days upon Cas9 treatment. Original magnification 60x, scale bar 10 μm.

Since I delivered Cas9 by infecting cells with a lentivirus that integrates into the host genome, I measured DDR induced by Cas9 four days upon infection, a time point in which the DNA damage caused by the integration of the Cas9 lentivirus into the genome is already reduced. I observed that, four days after infection, although all conditions tested were expressing the Cas9 protein (figure 10), DDR activation was observed only in HeLa GFP cells infected with the Cas9 expressing the specific GFP guide, as demonstrated by the independent software-based quantification (Cell Profiler) of γH2AX and 53BP1 foci in the figure 11, compared to the negative controls that include HeLa GFP cells treated with the Cas9 carrying the scramble guide and HeLa WT cells. The low levels of DDR in HeLa WT cells treated with the Cas9 carrying the GFP guide indicates that the RNA guide is specific for the GFP sequence; in the same way, the low DDR levels in HeLa cells infected with the Cas9 associated with the scramble guide shows that this guide is not recognizing any sequence in the HeLa genome.

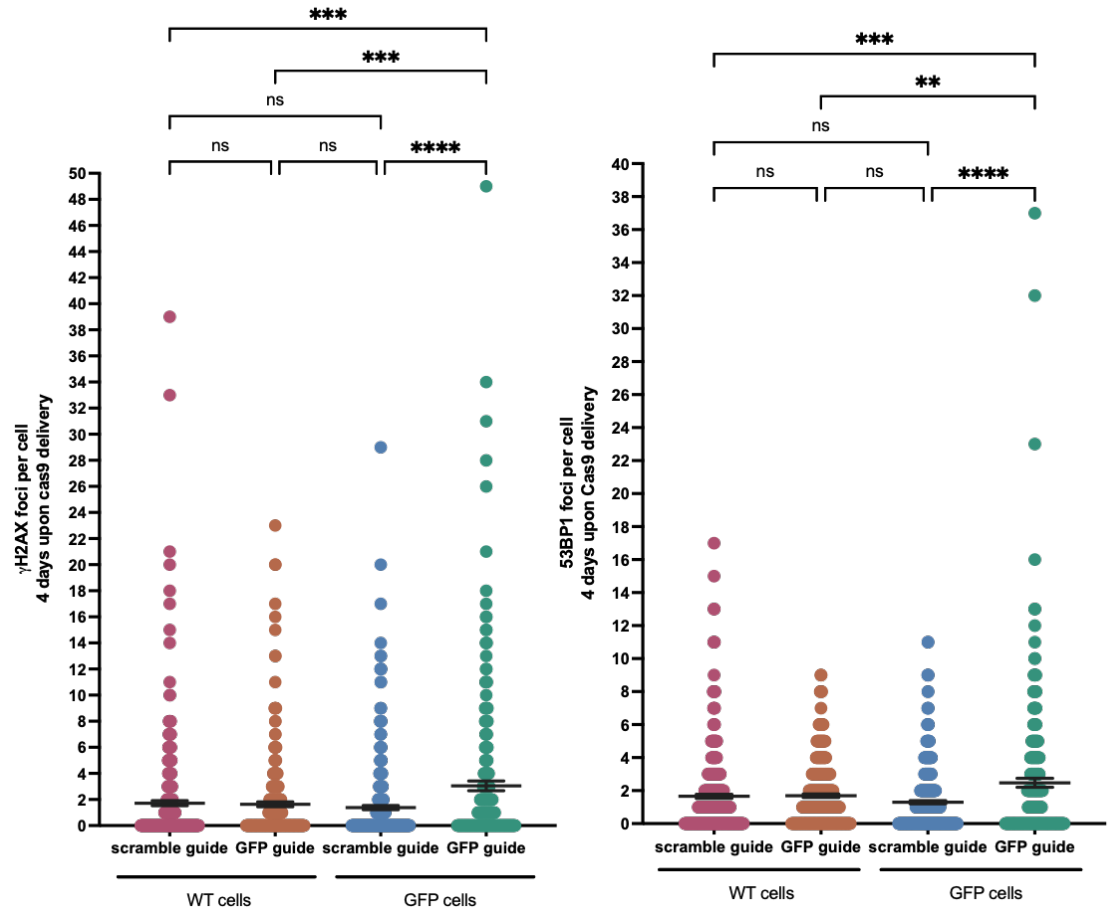

Figure 11. DNA damage induction upon Cas9 treatment.
Quantitative analyses of γH2AX and 53BP1 foci in HeLa WT and GFP cells 4 days upon Cas9 treatment. N=4 independent experiments. At least 60 cells per condition were analysed for each experiment. Error bars represent the s.e.m. **p < 0.005, ***p < 0.0005, ****p < 0.0001. One-way ANOVA test.

4.1.3.2 Cas9-induced DSBs cause multinucleation and increased cell size

I also noticed that HeLa GFP became bigger in size upon Cas9 cut. To confirm this observation, I took advantage of the cell-by-cell analysis software of Incucyte; in this way I was able to first count the number of cells for each condition and then to discriminate between cells there had an area either smaller or bigger than 1000 μm^2. The result showed that, 6 days after Cas9 delivery, HeLa GFP cells started becoming bigger upon cut, compared to the scramble condition (see discussion) **(**figure 12).

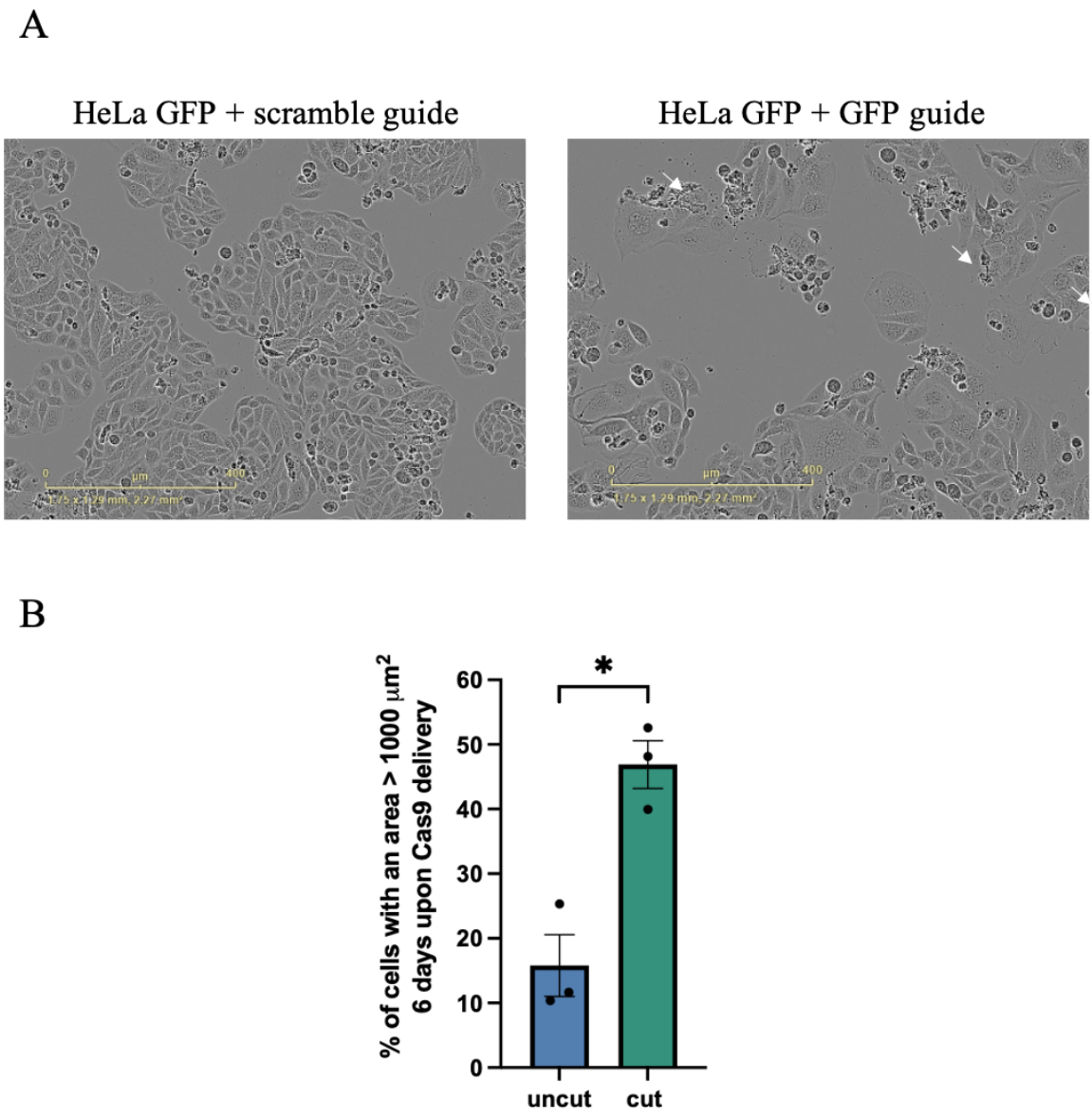

Figure 12. Cells increase their size upon Cas9-induced DSBs.
(A) Representative images of HeLa GFP cells increasing their size 6 days upon the treatment with the Cas9 carrying the GFP guide. Original magnification 60x, scale bar 10 µm. The white arrows indicate examples of big cells. **(B)** Quantification of the percentage of cells with an area > 1000 μm^2 using the Incucyte cell-by-cell analysis. N=3 independent experiments. Error bars represent the s.e.m. *p < 0.05. One-way ANOVA test.

This increase in cell size can be partially explained by the observation that, 4 days upon Cas9 delivery, a percentage of HeLa GFP cells presents more than one nucleus per cell (figure 13). This could be a consequence of mitotic errors due to cell cycle progression in the presence of unrepaired DNA damage (Hart, Adams, and Draviam 2021), but it could also indicate entrance in senescence, since senescent cells are larger and flatter than normal cells (Di Micco et al. 2021)

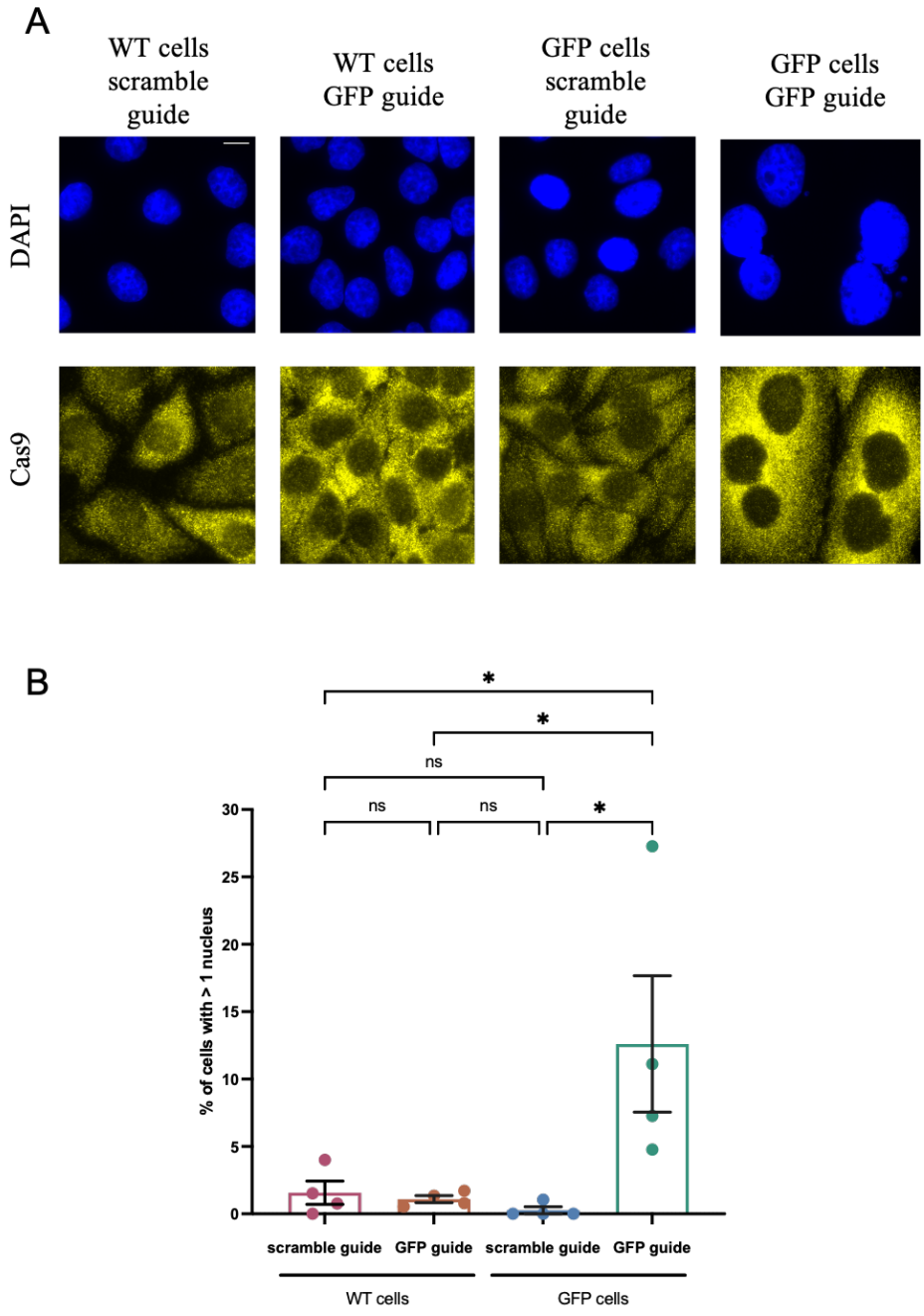

Figure 13. DNA damage by Cas9 induces cell multinucleation.
(A) Representative images of multinucleated HeLa GFP cells 4 days upon the treatment with the Cas9 carrying the GFP guide. Original magnification 60x, scale bar 10 µm. **(B)** Quantification of the percentage of cells with > 1 nucleus. N=4 independent experiments. Error bars represent the s.e.m. *p < 0.05. One-way ANOVA test.

In addition, since DNA damage impacts on cell cycle progression (Aguirre et al. 2017), I performed flow cytometry to characterize the distribution of cells among the different phases of the cell cycle. I plated HeLa GFP cells at the same confluence and, the day after, I infected cells with a lentivirus carrying either Cas9 and the scramble guide, as a negative control, or Cas9 and the guide against the GFP sequence. 3 days after infection I collected at least 1 million cells for both conditions, I fixed cells and I then stained them with propidium iodide (PI) supplemented with RNase A. PI is an agent that binds nucleic acids and it can be used to quantify the DNA content of cells and, consequentially, their cell cycle distribution. HeLa GFP cells showed an accumulation in the G2 phase upon cut induced by Cas9, compared to the uncut condition (figure 14).

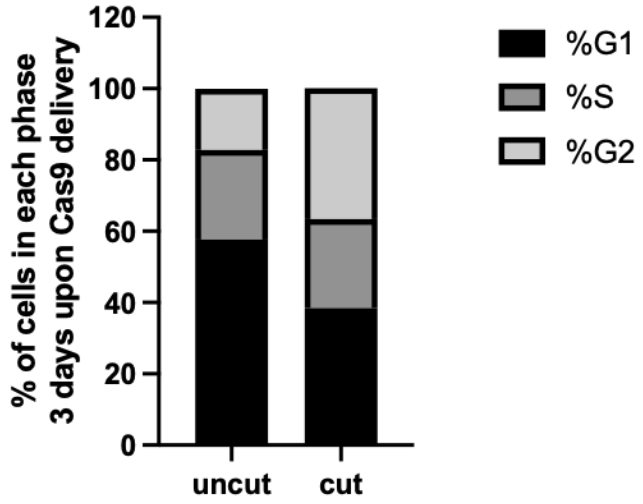

Figure 14. Cells accumulate in G2 upon Cas9 cut.
FACS analysis shows an accumulation of HeLa GFP cells in the G2 phase 3 days upon treatment with the Cas9 carrying the GFP guide, compared to the control. N=1 experiment.

4.1.3.3 Cas9-induced DNA damage causes the formation of cGAS positive micronuclei that lead to an inflammatory response

Four days after Cas9 delivery I observed, by DAPI staining, in addition to the appearance of multinucleated cells, an increase in the formation of micronuclei that was specific for HeLa GFP cells treated with the Cas9 expressing the GFP guide; in addition, the majority of these micronuclei were positive for cGAS (figure 15).

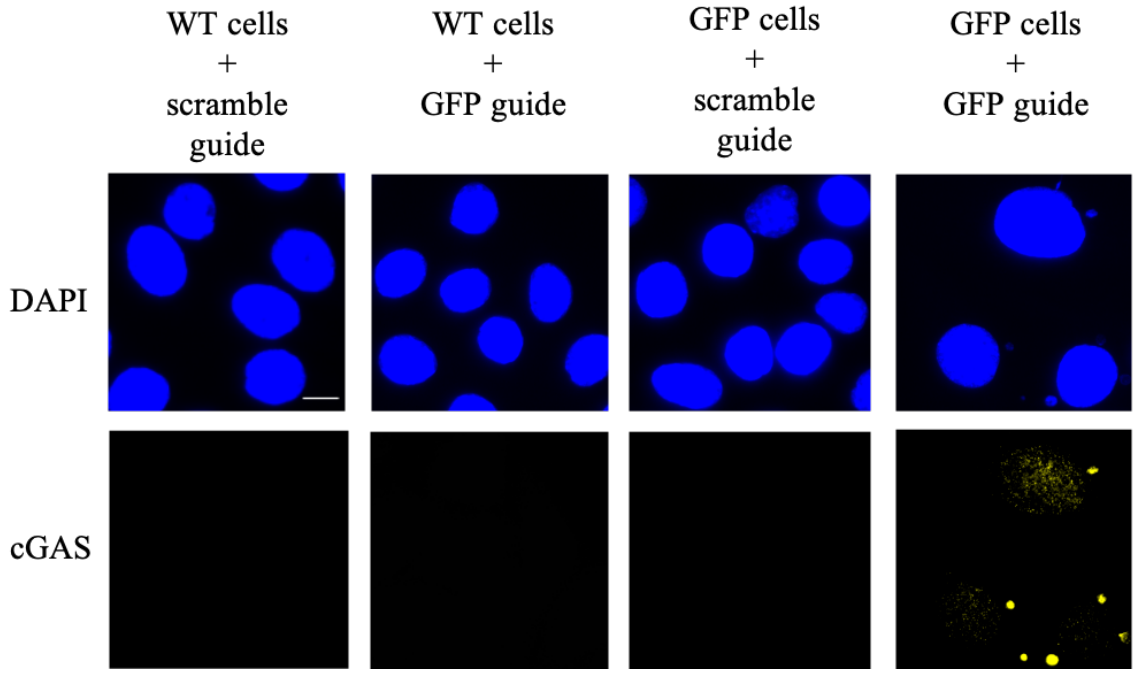

Figure 15. Cas9 induces cGAS positive micronuclei in HeLa GFP cells only.
Representative immunofluorescence images showing micronuclei formation and cGAS staining in HeLa WT and GFP cells 4 days upon Cas9 treatment. Original magnification 60x, scale bar 10 μm.

Strikingly, 70% of HeLa GFP cells treated with Cas9 containing the GFP guide have, at least, one micronucleus per cell, while less than the 10% of cells of the other conditions showed micronuclei formation. Moreover, the majority of the cells with micronuclei upon Cas9 cut displayed cGAS at micronuclei, suggesting the leakiness of their membranes (figure 16) (Harding et al. 2017). These results suggest that the chronic induction of DSBs by Cas9 can lead to the generation of cGAS-positive micronuclei.

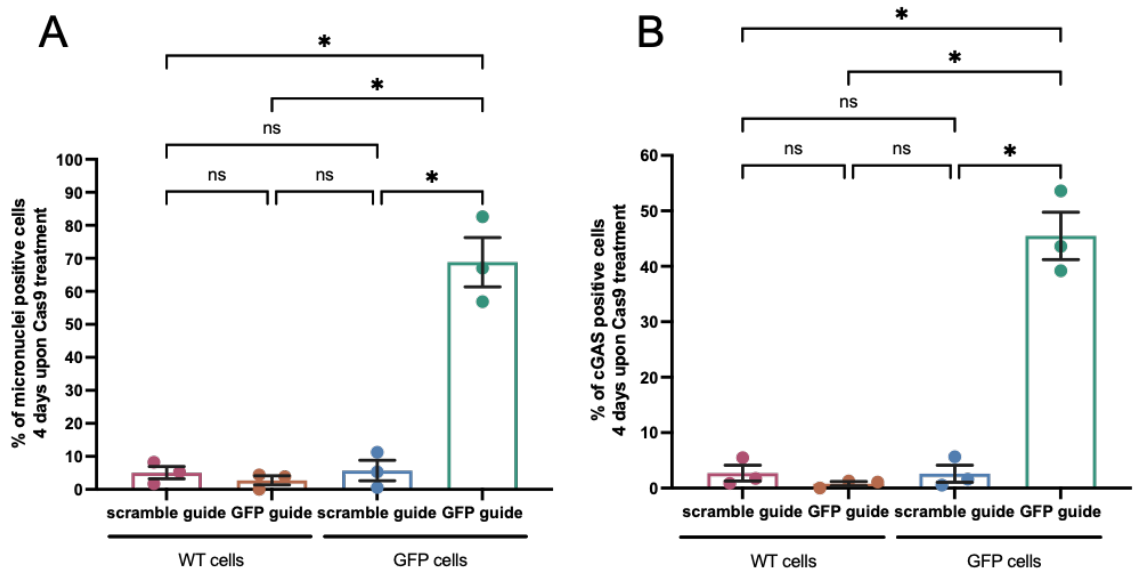

Figure 16. cGAS positive micronuclei formation upon Cas9 treatment.
(A) Quantitative analyses of the percentage of micronuclei positive cells 4 days upon Cas9 treatment. N=3 independent experiments. At least 60 cells per condition were analysed for each experiment. Error bars represent the s.e.m. *p < 0.05. One-way ANOVA test. **(B)** Quantitative analyses of the percentage of cGAS positive cells 4 days upon Cas9 treatment. N=3 independent experiments. Error bars represent the s.e.m. *p < 0.05. One-way ANOVA test.

The relocalization of cGAS to micronuclei caused by DNA damage can initiate an inflammatory response (Harding et al. 2017); for this reason, I also checked the expression of some cytokines and chemokines after DNA damage induction. I plated HeLa GFP cells and I infected them with lentiviruses expressing Cas9 and either the scramble guide or the GFP guide. 3 days after infection, I collected both the undamaged and the damaged conditions, I extracted total RNA from cells, I reverse transcribed the RNA into cDNA and I performed real time quantitative PCR (RT-qPCR) on my samples. In two or three independent experiments, I consistently observed an increase of the expression of IL-6, IL-8, CXCL10 and TNF in HeLa GFP cells treated with the Cas9 carrying the GFP guide, compared to the negative controls (figure 17), suggesting that the DNA damage caused by Cas9 is responsible for the activation of inflammatory pathways.

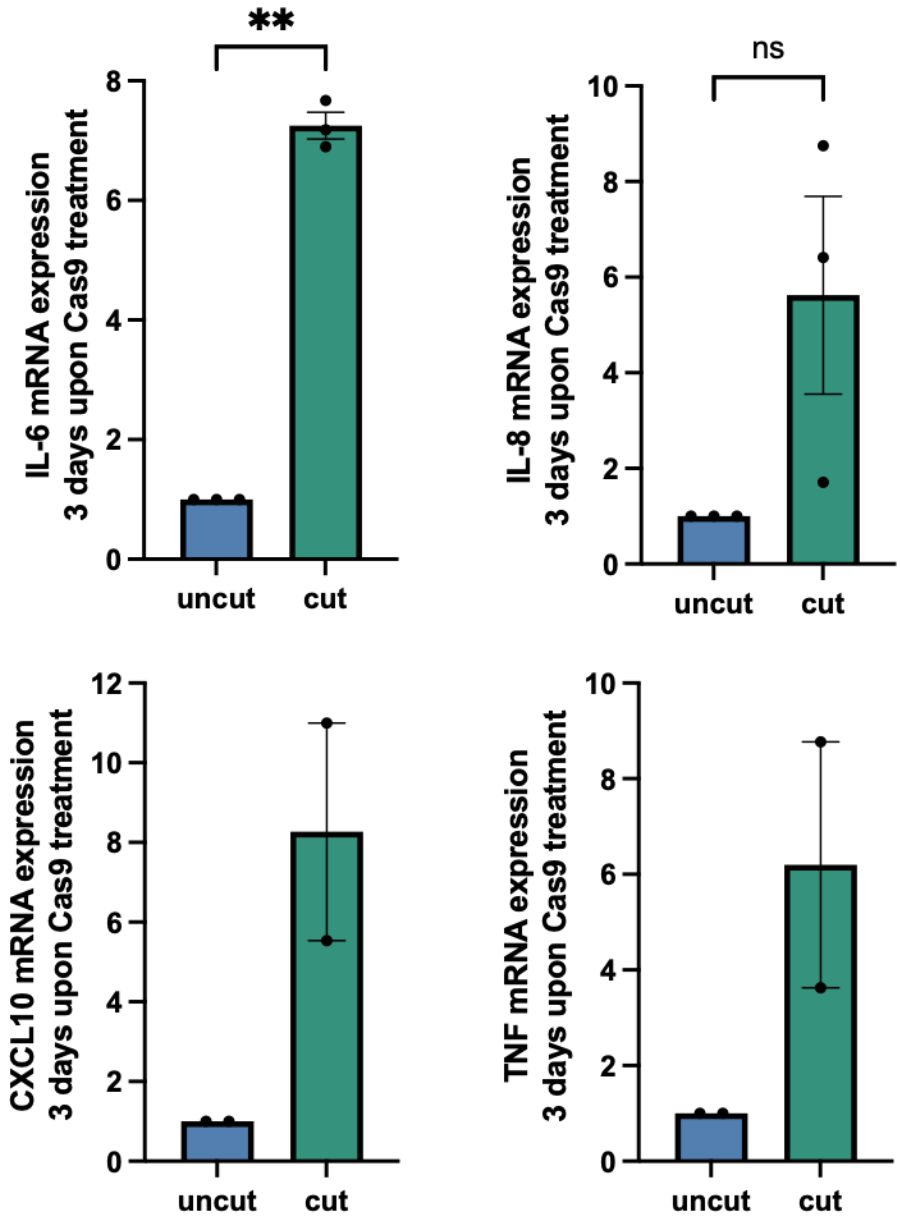

Figure 17. Cas9 treatment causes inflammation in the cut cells.
RT-qPCR for IL-6, IL-8, CXCL10 and TNF mRNA expression levels in HeLa GFP cells 3 days upon Cas9 treatment. N=3 independent experiments for IL-6 and IL-8; error bars represent the s.e.m. **p < 0.005. One-way ANOVA test. N=2 independent experiments for CXCL10 and TNF; error bars represent the s.d.

To further investigate the impact of the DNA damage induced by Cas9 on gene expression of HeLa GFP cells, in particular on the expression of inflammatory genes, I performed next generation sequencing for genome-wide analysis of differential gene expression on total RNA from HeLa GFP cells treated with Cas9 carrying either the GFP guide or the scramble guide. I first checked the integrity of the RNA material by bioanalyzer; then, after library preparation with the Illumina kit for polyA transcripts, RNA from HeLa GFP cells treated with either the Cas9 carrying the scramble guide or the Cas9 carrying the GFP guide was

sequenced by the IFOM genomic unit. The analyses of the reads obtained were carried out by the IFOM bioinformatic unit by aligning reads on the human genome, and looking at the differentially expressed genes between undamaged and damaged conditions, correcting the results for potential batch effects and analyzing different gene sets.

The RNA-seq experiment showed the activation of several inflammation pathways; the most significantly upregulated upon generation of DNA damage by Cas9 was the IL-17 signaling pathway, accordingly to the BioCarta gene set. This pathway, once activated, leads to the expression of cytokines and chemokines including IL-6, IL-8, CXCL10 and TNF, confirming what I observed by RT-qPCR. This result was visualized by using the KEGG gene set (figure 18).

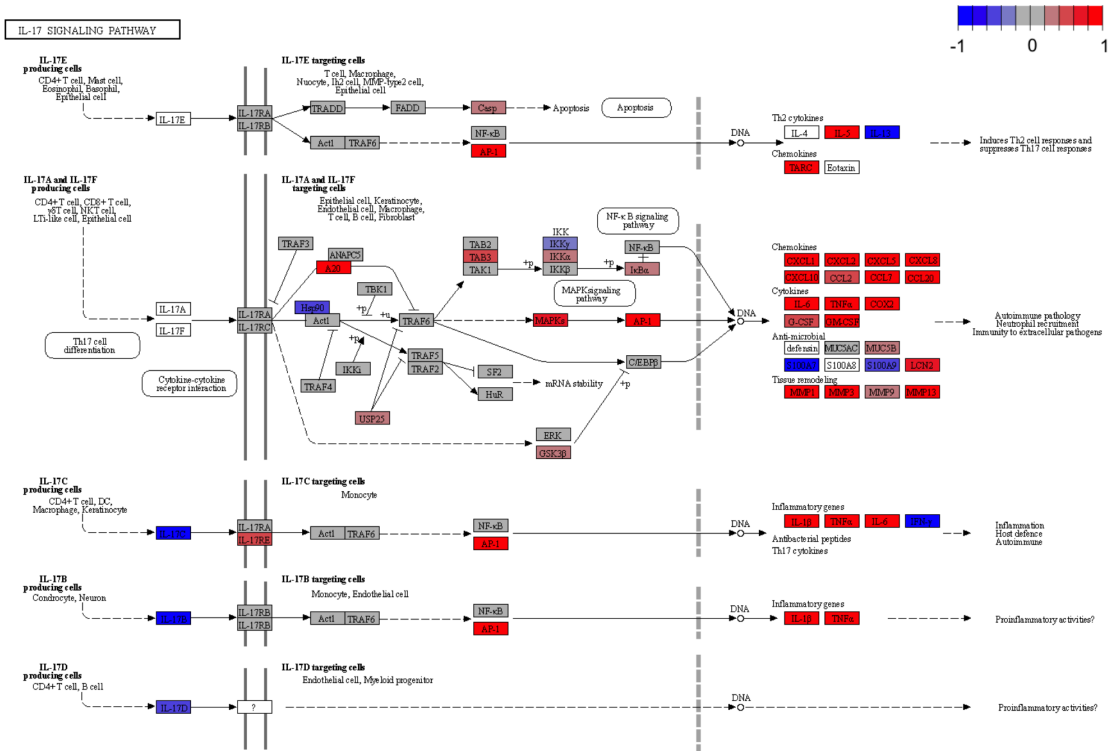

Figure 18. IL-17 signaling pathway.

KEGG visualization of the IL-17 signaling pathway. In red the upregulated genes and in blue the downregulated genes 3 days upon Cas9 delivery in HeLa GFP cells, compared to the uncut condition.

4.1.4 Sequence-specific DNA damage induced by Cas9 kills GFP cells

Next, I investigated if the DNA damage induced by Cas9 in the GFP sequences could selectively kill HeLa GFP and RKO GFP cells, while sparing WT cells that lack the Cas9-targeted DNA sequence.

4.1.4.1 Cas9-induced DNA damage kills HeLa GFP cells

I infected both HeLa WT and GFP cells with a lentiCRISPR v2 vector containing either the Cas9 with the scramble guide or the Cas9 carrying the guide against the GFP sequence.
Also for this round of experiments, I took advantage of Incucyte to monitor cell proliferation and survival over time. The experimental design was as follows:
Day 0 → I plated both HeLa WT and GFP cells in 6 multiwell plates
Day 1 → I infected cells with a freshly-prepared lentivirus expressing either Cas9 with the scramble guide or Cas9 with the guide against the GFP sequence
Day 2 → I replated all conditions at the same cell density in a 96 multiwell plate, I added the Incucyte cytotox green dye and I started the experiment in Incucyte
The conditions studied were: HeLa WT + scramble guide; HeLa WT + GFP guide; HeLa GFP + scramble guide; HeLa GFP + GFP guide. I followed cell viability for 96 hours (figure 19A). Four days after Cas9 delivery, I observed a decrease in the number of HeLa GFP cells infected with the Cas9 carrying the GFP guide, compared to the negative controls. This was reproduced in three independent biological replicates (figure 19B).
I also monitored cell death for 96 hours (figure 19C) and I observed an increase of cell death in HeLa GFP cells treated with the Cas9 cutting inside the GFP sequence. More precisely, four days after Cas9 delivery, I detected four times more dead cells in the HeLa GFP cells + GFP guide condition, compared to the negative controls (figure 19D).
I carried out in parallel the same experiment in HeLa WT and GFP cells to confirm the absence of possible Cas9 off-targets (Haeussler 2020), although I already observed by IF that there is no detectable DDR activation in terms of γH2AX and 53BP1 foci formation in HeLa WT cells, compared to the GFP version when infected with the Cas9 carrying the GFP guide. HeLa WT cells were infected with either the lentiCRISPR v2 vector containing Cas9 + scramble RNA or the lentiCRISPR v2 vector containing Cas9 + GFP guide. WT cells viability was not affected by these treatments, indicating the specificity of Cas9 in inducing DSBs and consequent cell death only in the cells with the GFP target sequence infected with the Cas9 cutting inside the GFP (figure 19).

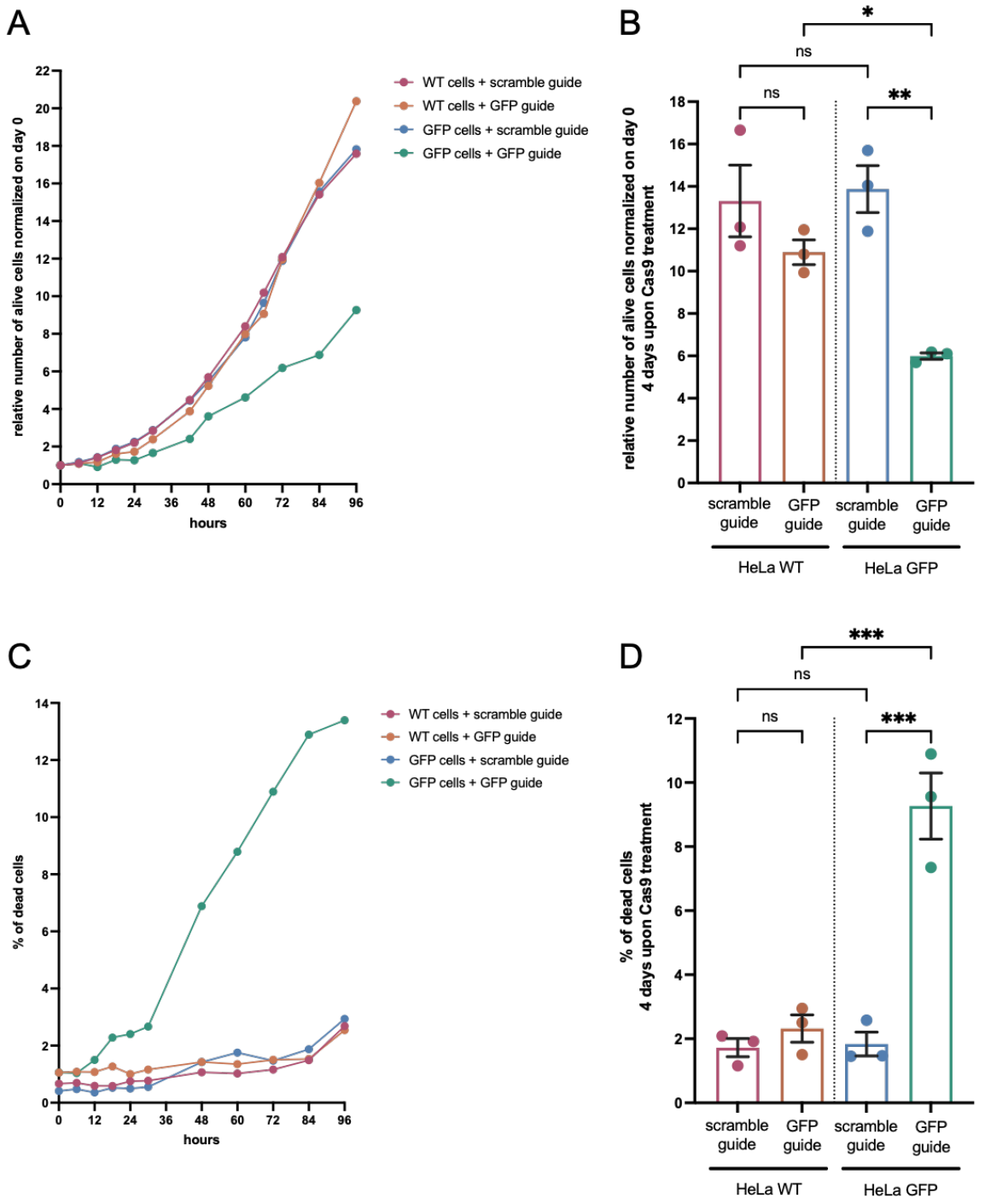

Figure 19. Cas9 carrying the GFP guide kills HeLa GFP only.
(A) A representative growth curve showing the viability of HeLa WT and GFP cells treated with either Cas9 carrying a scamble guide or Cas9 carrying the GFP guide. **(B)** Viability of HeLa WT and GFP cells 4 days upon Cas9 treatment, n=3 independent experiments. Error bars represent the s.e.m. *p < 0.05, **p < 0.005. One-way ANOVA test. **(C)** A representative mortality curve showing the percentage of dead HeLa WT and GFP cells after the treatment with either Cas9 carrying a scamble guide or Cas9 carrying the GFP guide. **(D)** Mortality of HeLa WT and GFP cells 4 days upon Cas9 treatment, n=3 independent experiments. Error bars represent the s.e.m. ***p < 0.0005. One-way ANOVA test.

These experiments were carried out in Incucyte only for five days because then the controls started to be too confluent and the cell count by the Incucyte software was no longer reliable. To study the long-term effects of Cas9 in HeLa GFP cells, I set up conditions to perform colony formation assays. Colony formation assay is a technique used to study cell survival based on the capability of a single cell to grow into a colony. Single cells can be seeded before or after a treatment and colonies form after one-two weeks. Generally, a colony consists of at least 50 cells (Franken et al. 2006). I plated HeLa GFP cells in a 6 multiwell plate, the day after I infected them with a freshly-prepared lentivirus expressing either Cas9 with the scramble guide or Cas9 with the guide against the GFP sequence and, seven days after DNA damage induction, I plated all the conditions in a new 6 multiwell plate. I counted HeLa GFP cells treated with Cas9 carrying the scramble guide and I plated 400 cells, while for HeLa GFP cells treated with Cas9 expressing the GFP guide I plated the same volume of medium, where cells were resuspended, of the negative control, in order to maintain the difference between the two treatments. I allowed cells to grow for one week, I then fixed colonies with ethanol and I stained them with crystal violet. The result of three independent experiments showed that in the cut conditions there were on average only ~100 colonies compared to the ~300 colonies of the uncut condition (figure 20). Since this technique allowed me to observe a bigger difference between the treatments compared to the experiments carried out in Incucyte, I am planning to perform colony formation assays to monitor cell survival at later time points.

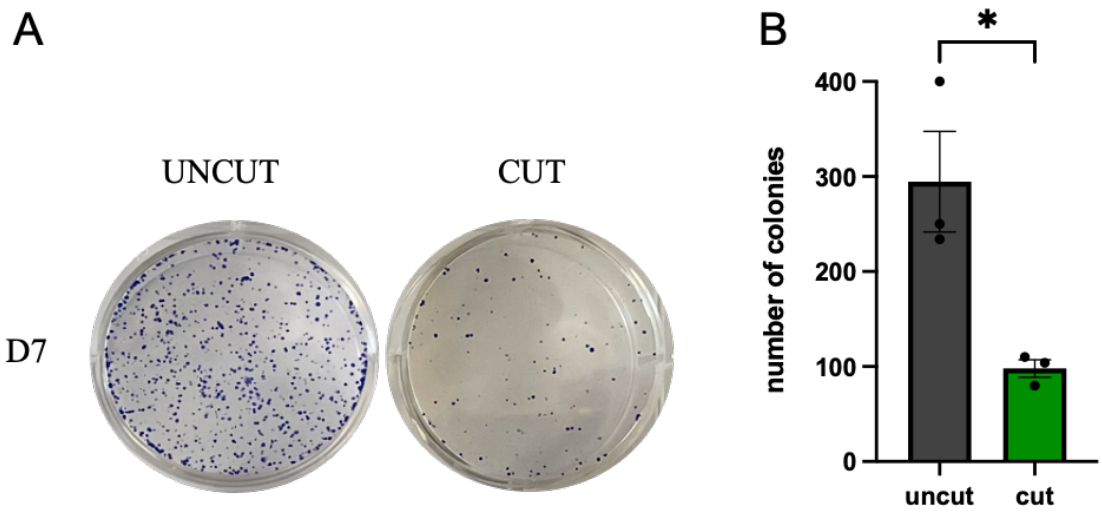

Figure 20. Cas9 cutting in the GFP sequence reduces the number of cells able to form colonies. **(A)** A representative experiment showing the difference, in terms of colonies, between uncut and cut HeLa GFP cells. **(B)** Quantification of the number of colonies in n=3 independent experiments. Error bars represent the s.e.m. *$p < 0.05$. t-test.

4.1.4.2 Cas9-induced DNA damage kills RKO GFP cells

Next, I recapitulated these results in RKO cells. I performed the experiment as in HeLa cells: I infected both RKO WT and GFP cells with a lentiCRISPR v2 vector containing either Cas9 with the scramble guide or Cas9 carrying the guide against the GFP sequence; I carried out in parallel the same experiment in RKO WT and GFP cells to confirm the absence of potential Cas9 off-targets. I next monitored cell proliferation and death over-time with Incucyte and I performed the experiment as follows:

Day 0 → I plated both RKO WT and GFP cells in 6 multiwell plates

Day 1 → I infected cells with a freshly-prepared lentivirus expressing either Cas9 with the scramble guide or Cas9 with the guide against the GFP sequence

Day 2 → I plated all the conditions at the same cell density in a 96 multiwell plate, I added the Incucyte cytotox green dye and I started the experiment in Incucyte

The conditions studied were: RKO WT + scramble guide; RKO WT + GFP guide; RKO GFP + scramble guide; RKO GFP + GFP guide. I followed cell viability for 90 hours (figure 21A) and, four days upon Cas9 delivery, I observed a decrease in the proliferation of RKO GFP cells infected with the Cas9 carrying the GFP guide, compared to the negative controls, in three independent experiments (figure 21B). I also monitored cell death for 90 hours (figure 21C) and I observed an increase of cell death in RKO GFP cells treated with the Cas9 cutting inside the GFP sequence. More precisely, four days after Cas9 delivery, I detected about five times more dead cells in the RKO GFP cells + GFP guide condition, compared to the negative controls (figure 21D).

RKO WT cells infected with either the lentiCRISPR v2 vector containing Cas9 + scramble RNA or the lentiCRISPR v2 vector containing Cas9 + GFP guide were not affected by the treatments, indicating the specificity of Cas9 in inducing DSB and consequent cell death only in the cells with the GFP target sequence infected with the Cas9 cutting inside the GFP (figure 21).

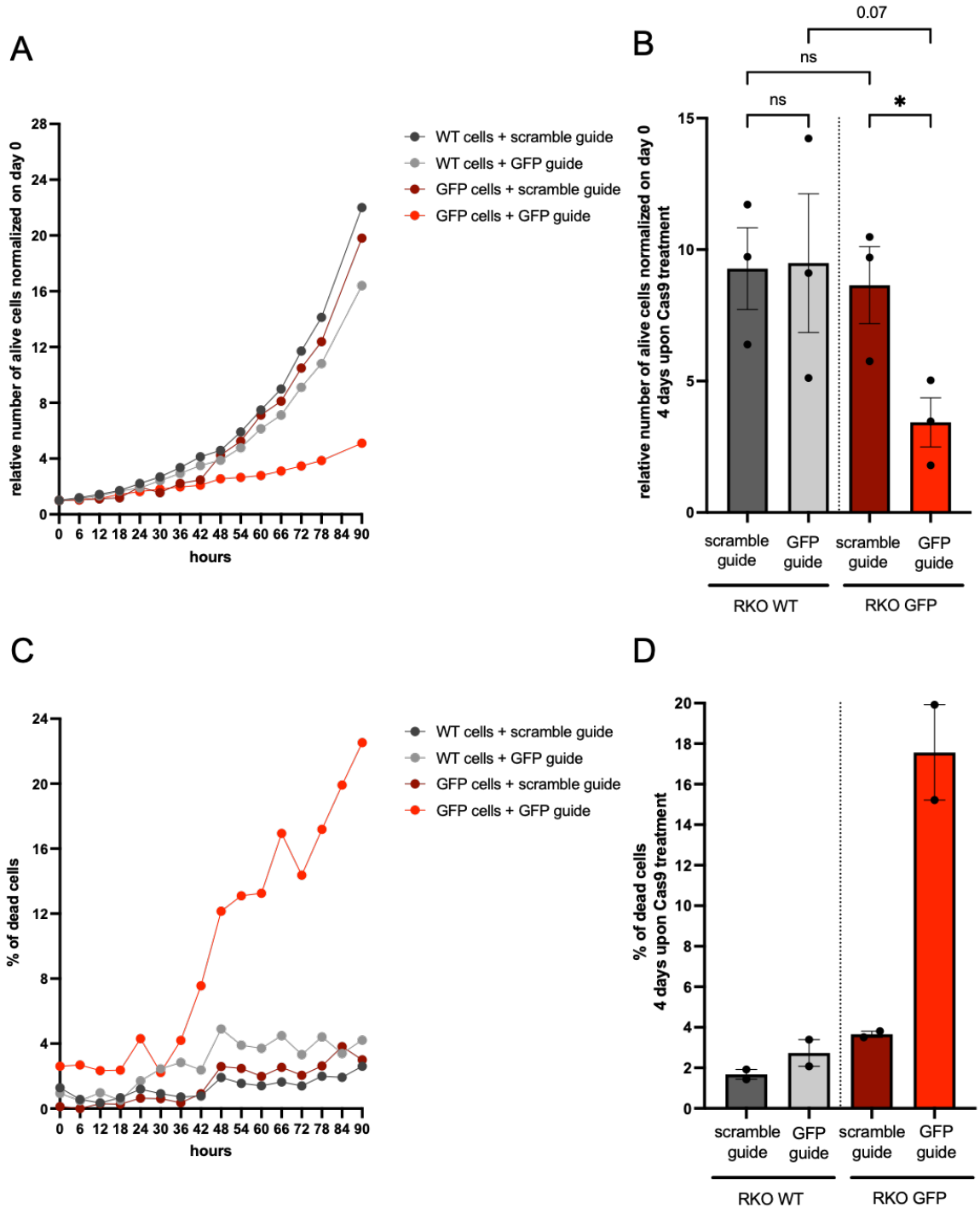

Figure 21. Cas9 carrying the GFP guide kills RKO GFP only.
(A) A representative growth curve showing the viability of RKO WT and GFP cells treated with either Cas9 carrying a scamble guide or Cas9 carrying the GFP guide. **(B)** Viability of RKO WT and GFP cells 4 days upon Cas9 treatment, n=3 independent experiments. Error bars represent the s.e.m. *p < 0.05. One-way ANOVA test. **(C)** A representative mortality curve showing the percentage of dead RKO WT and GFP cells after the treatment with either Cas9 carrying a scamble guide or Cas9 carrying the GFP guide. **(D)** Mortality of RKO WT and GFP cells 4 days upon Cas9 treatment, n=2 independent experiments.

4.1.5 Multiple Cas9 RNA guides against the GFP sequence do not seem more effective than an individual Cas9 RNA guide in impairing cell proliferation of GFP cells

To attempt to further increase the reduction in proliferation of GFP cells caused by the Cas9 and the GFP guide, I designed 9 additional RNA guides spanning the full length of the GFP sequence to test if the generation of several DSBs within the GFP sequence could improve target cells killing. I performed in parallel the experiment in both WT and GFP cells and I tested the hypothesis both in HeLa and RKO cells.

I compared the effects of three different treatments on cell survival and death: lentiviral infection of the Cas9 expressing the scramble guide, lentiviral infection of the Cas9 expressing the GFP guide previously used and lentiviral infection of different Cas9 plasmids, each expressing one of the ten GFP guides that I have designed. These 10 plasmids were mixed together to reach the same molar quantity of the other two treatments.

I plated HeLa and RKO cell lines in 6 multiwell plates and the day after I infected them with freshly-prepared lentiviruses.

The viability of HeLa WT cells was not affected by any of these treatments, indicating the specificity of the different GFP guides in targeting only the complementary DNA sequence. The single GFP guide halved the proliferation of HeLa GFP cells, compared to the undamaged condition and WT cells, as in previous experiments. However, the pool of GFP guides affected the proliferation of HeLa GFP cells to an extent similar to that observed upon treatment with only one guide (figure 22A-B).

The same result was achieved in RKO cells: as expected, the viability of the WT conditions was not impaired by any of the Cas9 treatments, indicating the specificity of the different GFP guides in recognizing only the GFP target sequence. The treatment of RKO GFP cells with the lentivirus carrying Cas9 and the single GFP guide halved the number of GFP cells, compared to the negative controls, as in previous experiments. Nevertheless, the treatment with the pool of GFP guides impacted on proliferation of RKO GFP cells as the single GFP guide (figure 22C-D).

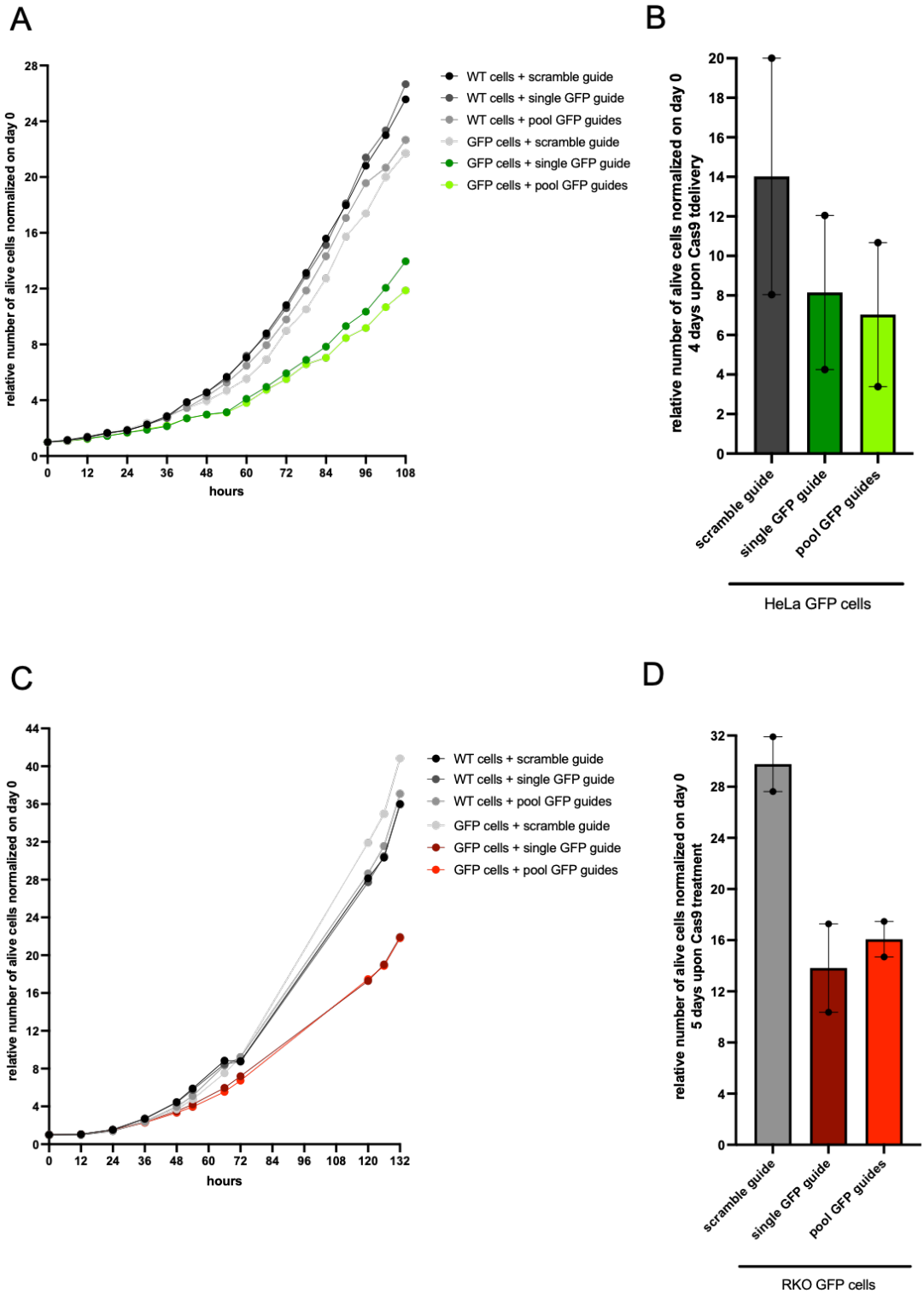

Figure 22. One cut and several cuts in the GFP sequence equally affect viability of HeLa and RKO GFP cells.

(A) A representative growth curve showing the viability of HeLa WT and GFP cells treated with Cas9 carrying a scamble guide, Cas9 carrying a single GFP guide or Cas9 carrying a pool of GFP guides. **(B)** Viability of HeLa GFP cells 4 days upon Cas9 treatment, n=2 independent experiments. Error bars represent the s.d. **(C)** A representative growth curve showing the viability of RKO WT and GFP cells treated with Cas9 carrying a scamble guide, Cas9 carrying a single GFP guide or Cas9 carrying a pool of GFP guides. **(D)** Viability of RKO GFP cells 5 days upon Cas9 treatment, n=2 independent experiments. Error bars represent the s.d.

4.2 DNA damage induction and inhibition of its repair

So far, my results allow me to propose the CRISPR/Cas9 system as a weapon against cells with an aberrant genome. Indeed, I demonstrated that by this approach it is possible to induce cell death in at least two different cancer cell lines by targeting the GFP sequence with the Cas9 endonuclease cutting within the GFP sequence. Indeed, HeLa and RKO GFP cells are not only two experimental systems that simulate cells with an integrated proviral genome; they are also cancer cells with several molecular changes that can confer them resistance to treatments, suggesting that if this approach works in these cell lines, it could work also in non-transformed infected cells and in other cancer types.
Anyway, this result could be improved by inhibiting the repair of the DSBs caused by Cas9.

4.2.1 Irradiation and DNA-PKi

In order to test if repair inhibition of Cas9-induced DSBs could increase mortality in GFP cells, I combined the Cas9 treatment with an inhibitor of NHEJ, the main pathway involved in the repair of DSBs. In particular, I tested the DNA-PK inhibitor NU7441 (Zhao et al. 2006). DNA-PK is a key protein in the DDR because, once recruited at the site of damage by Ku, it promotes DNA repair by NHEJ (O'Connor, Martin, and Smith 2007). It has already been demonstrated that inhibition of DNA-PK sensitizes cancer cells to DNA damaging agents, such as irradiation and chemotherapy, because their inability to repair DSBs (Lord, Garrett, and Ashworth 2006). For this reason, inhibitors of this DDR factor are already in phase I clinical trials for the treatment of advanced solid tumors (O'Connor 2015; van Bussel et al. 2021).

4.2.1.1 IR-induced DNA damage combined with DNA-PK inhibition kill HeLa WT and GFP cells equally

To validate the combinatory effects of DNA damage generation and inhibition of its repair, I treated HeLa WT and GFP cells with either the DNA-PKi NU7441 (1uM final concentration) or DMSO as a control; 1 hour later, I irradiated the two cell lines with 1Gy to verify that WT cells are equally sensitive to DNA damage repair inhibition compared to their GFP version. Cells were treated with DNA-PKi before irradiation in order to have cells fully exposed to the inhibitor when DNA damage is induced. 24 hours after irradiation, I plated cells in a 96 well plate and I added the green cytotox dye to start monitoring cell behavior in Incucyte. As observed previously, the irradiation of cells reduced the proliferation of all the cell lines, compared to the not irradiated controls, independently from

the presence of the GFP sequence, as monitored 4 days after irradiation by Incucyte. The most sensitive cells to DNA-PK inhibition were the irradiated conditions, independently from the presence of the GFP sequence, showing that DSB induction and inhibition of its repair act together in reducing cell viability (figures 23A-B). Of course, DNA-PKi is not a selective treatment for damaged cells; indeed, DNA-PK inhibition slightly affected also the viability of the not irradiated cells lines, probably because of the inhibition of the repair of endogenous DNA damage (figures 23A-B). Irradiation not only reduced cell proliferation; indeed, also in this setting of experiments, I observed an increase of HeLa cells positive for the cytotox dye 4 days after DNA damage induction, meaning that irradiation actually killed cells, independently from the presence of the GFP sequence. Moreover, the combination of irradiation and repair inhibition killed cells at least five times more than irradiation alone. In terms of cell death, the DNA-PKi was very specific in being toxic only in the cells that were actively damaged compared to the not irradiated conditions, as monitored by Incucyte 4 days after irradiation (figures 23C-D).

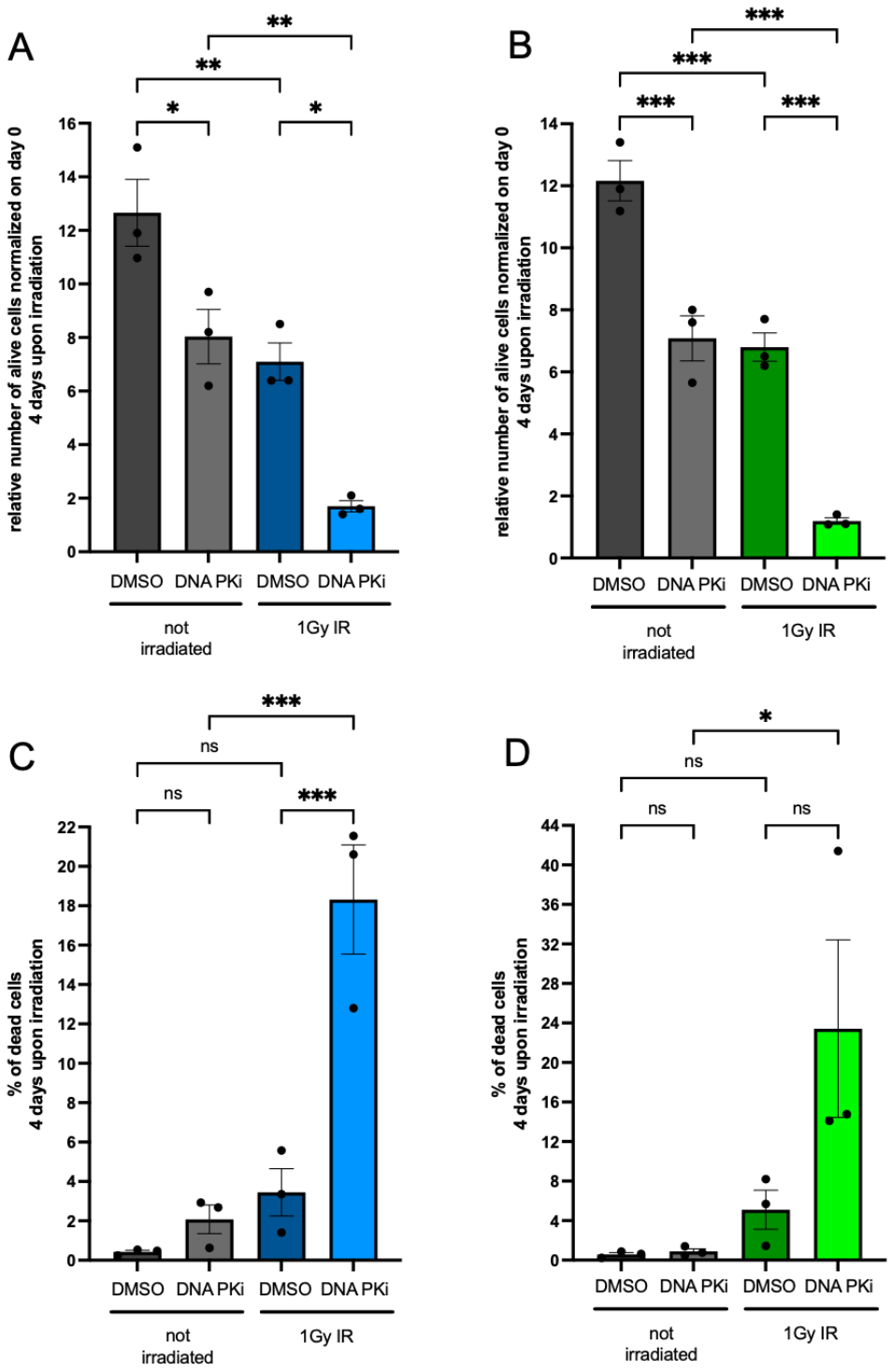

Figure 23. Irradiation and inhibition of the repair by DNA-PKi further kill both HeLa WT and GFP cells.

(A) Viability of HeLa WT cells 4 days upon irradiation, in combination with either DMSO or DNA-PKi. N=3 independent experiments. Error bars represent the s.e.m. *p < 0.05, **p < 0,005. One-way ANOVA test. **(B)** Viability of HeLa GFP cells 4 days upon irradiation, in combination with either DMSO or DNA-PKi. N=3 independent experiments. Error bars represent the s.e.m. ***p < 0.0005. One-way ANOVA test. **(C)** Mortality of HeLa WT cells 4 days upon irradiation, in combination with either DMSO or DNA-PKi. N=3 independent experiments. Error bars represent the s.e.m. ***p < 0.0005. One-way ANOVA test. **(D)** Mortality of HeLa GFP cells 4 days upon irradiation, in combination with either DMSO or DNA-PKi. N=3 independent experiments. Error bars represent the s.e.m. *p < 0.05. One-way ANOVA test.

4.2.1.2 IR-induced DNA damage and DNA-PKi equally kill RKO WT and GFP cells

I also performed the experiment in RKO WT and GFP cells to confirm the combinatory effect of DNA damage induction and repair inhibition in killing cells. I treated RKO cells with either DNA-PKi at the final concentration of 1 μM or DMSO as a control; after 1 hour, I irradiated the two cell lines with 1Gy to show that WT and GFP cells are equally sensitive to repair inhibition of IR-induced DNA damage.

Also in this case, irradiation alone already reduced the proliferation of all the cells lines, compared to the not irradiated controls, independently from the presence of the GFP sequence, as monitored 4 days after irradiation by Incucyte. The most sensitive cells to DNA-PK inhibition were the irradiated conditions, independently from the presence of the GFP sequence, showing that the combination of DSB induction and repair inhibition further reduce cell survival (figure 24A-B). The viability of irradiated RKO cells was slightly affected by the inhibition of DNA-PK, probably because of its impact on the repair of endogenous DNA damage; nevertheless, the strongest DNA-PK inhibitory effect was observed in irradiated cells (figure 24A-B). Irradiation not only reduced cell proliferation; indeed, 4 days after DNA damage induction, I observed six times more dead cells in the irradiated conditions compared to the negative controls. DNA-PK inhibition further killed cells, as monitored 4 days after irradiation by Incucyte, confirming that repair inhibition of DSBs caused by IR kills more cells than DNA damage generation only (figure 24C-D**)**. Moreover, DNA-PKi was very specific in being toxic only in the cells that were actively damaged, compared to the not irradiated conditions.

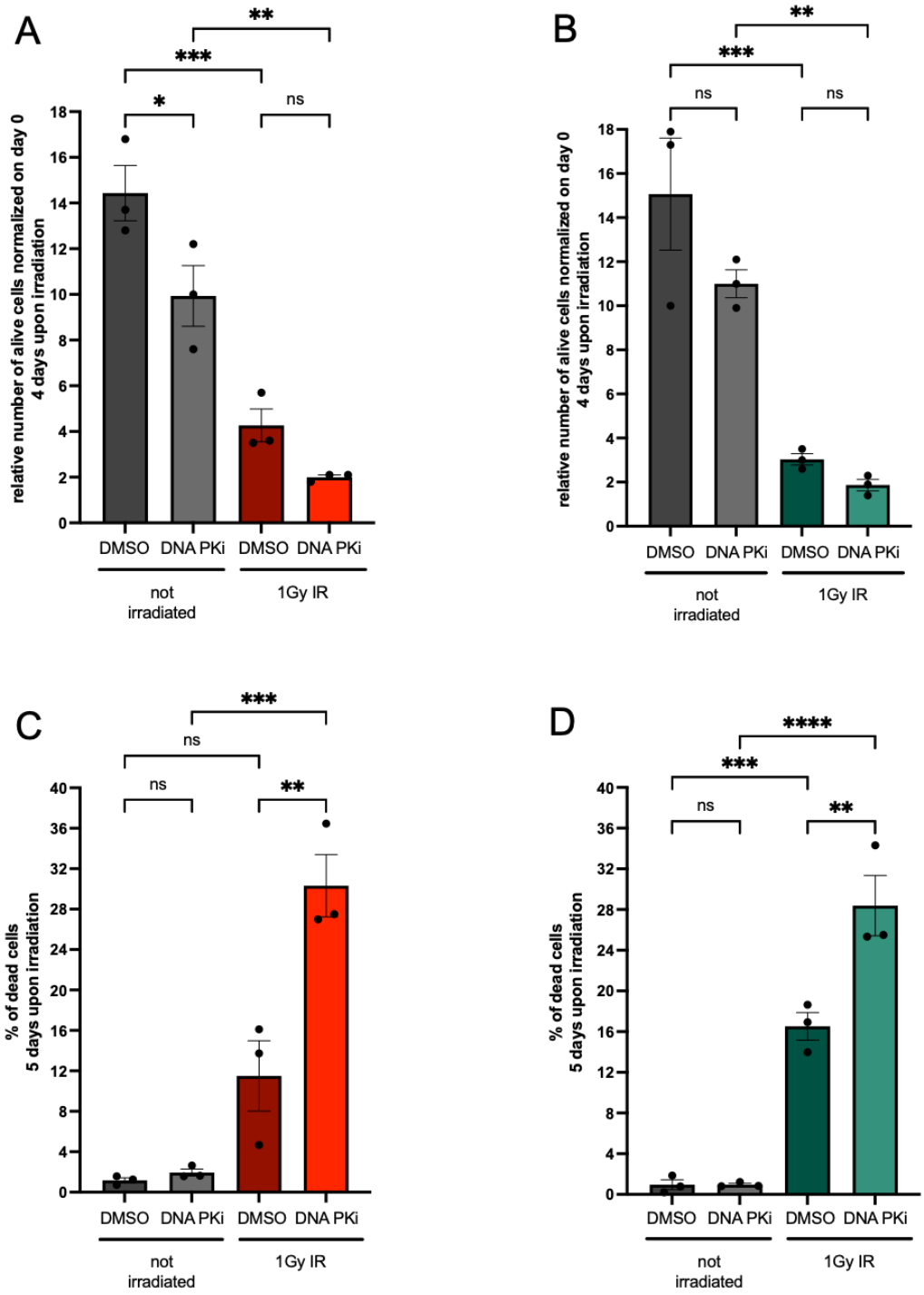

Figure 24. Irradiation and inhibition of the repair by DNA-PKi further kill both RKO WT and GFP cells.

(A) Viability of RKO WT cells 4 days upon irradiation, in combination with either DMSO or DNA-PKi. N=3 independent experiments. Error bars represent the s.e.m. *p < 0.05, **p < 0.005, ***p < 0.0005. One-way ANOVA test. **(B)** Viability of RKO GFP cells 4 days upon irradiation, in combination with either DMSO or DNA-PKi. N=3 independent experiments. Error bars represent the s.e.m. **p < 0.005, ***p < 0.0005. One-way ANOVA test. **(C)** Mortality of RKO WT cells 5 days upon irradiation, in combination with either DMSO or DNA-PKi. N=3 independent experiments. Error bars represent the s.e.m. **p < 0.005, ***p < 0.0005. One-way ANOVA test. **(D)** Mortality of RKO GFP cells 5 days upon irradiation, in combination with either DMSO or DNA-PKi. N=3 independent experiments. Error bars represent the s.e.m. **p < 0.005, ***p < 0.0005, ***p < 0.0001. One-way ANOVA test.

4.2.2 Sequence-specific DNA damage induction by Cas9 and DNA-PKi

Since I observed that the inhibition of repair of DNA damage caused by irradiation significantly increased cell death compared to DNA damage induction only, I adopted this experimental strategy in the Cas9 system to study the effects of repair inhibition of a sequence-specific DSB.

4.2.2.1 Cas9-induced DNA damage and DNA-PKi increase DDR in HeLa GFP cells

First, I tested if also the combination of DNA damage induced by Cas9 with DNA-PKi treatment induced DNA damage accumulation in terms of γH2AX and 53BP1 foci formation. I performed IF only on HeLa cells because I already showed that RKO cells are more sensitive to DNA damage and die with faster kinetics, making HeLa cells a more convenient model to study DDR activation. For this reason, I performed an IF in HeLa WT and GFP cells for γH2AX and 53BP1 and for Cas9 expression. I first plated cells in 6 multiwell plates, the day after I infected all the conditions with a fresh lentivirus carrying either Cas9 with the scramble guide or Cas9 with the guide against the GFP sequence.
3 days after Cas9 delivery, I treated cells with either DMSO or the DNA-PKi at the final concentration of 1 μM. I decided to treat cells with DNA-PKi 3 days after Cas9 delivery to avoid any interference with the integration of the lentivirus carrying the endonuclease into the genome of HeLa cells. One day after DNA-PKi treatment, and thus four days after Cas9 delivery, I fixed coverslips and I have stained them for γH2AX, 53BP1 and Cas9 (figure 25). For both HeLa WT and GFP I had four conditions: scramble guide + DMSO, scramble guide + DNA-PKi, GFP guide + DMSO, GFP guide + DNA-PKi treated cells. I confirmed, in the WT cells, that the treatment with Cas9 was not inducing γH2AX and 53BP1 foci formation, meaning that the Cas9 expressing the scramble guide was not producing off-targets in the cells lacking the GFP sequence (figure 26A). The addition of DNA-PKi in undamaged cells has slightly increased the levels of γH2AX but not the levels of 53BP1, suggesting that even if the inhibitor had a small impact on the repair of endogenous DNA damage, this was relatively low. On the contrary, in HeLa GFP cells, the delivery of the Cas9 cutting in the target gene increased the levels of γH2AX and 53BP1 foci, compared to the undamaged conditions, as I had observed previously. The addition of DNA-PKi further induced the formation of γH2AX and 53BP1 foci, compared not only to the undamaged conditions but also to GFP cells treated only with the Cas9 carrying the GFP guide (figure 26B). These results show that also the inhibition of repair of the sequence-specific DNA damages induced

by Cas9 leads to an accumulation of γH2AX and 53BP1 foci in HeLa GFP cells, compared to the uncut condition and WT cells.

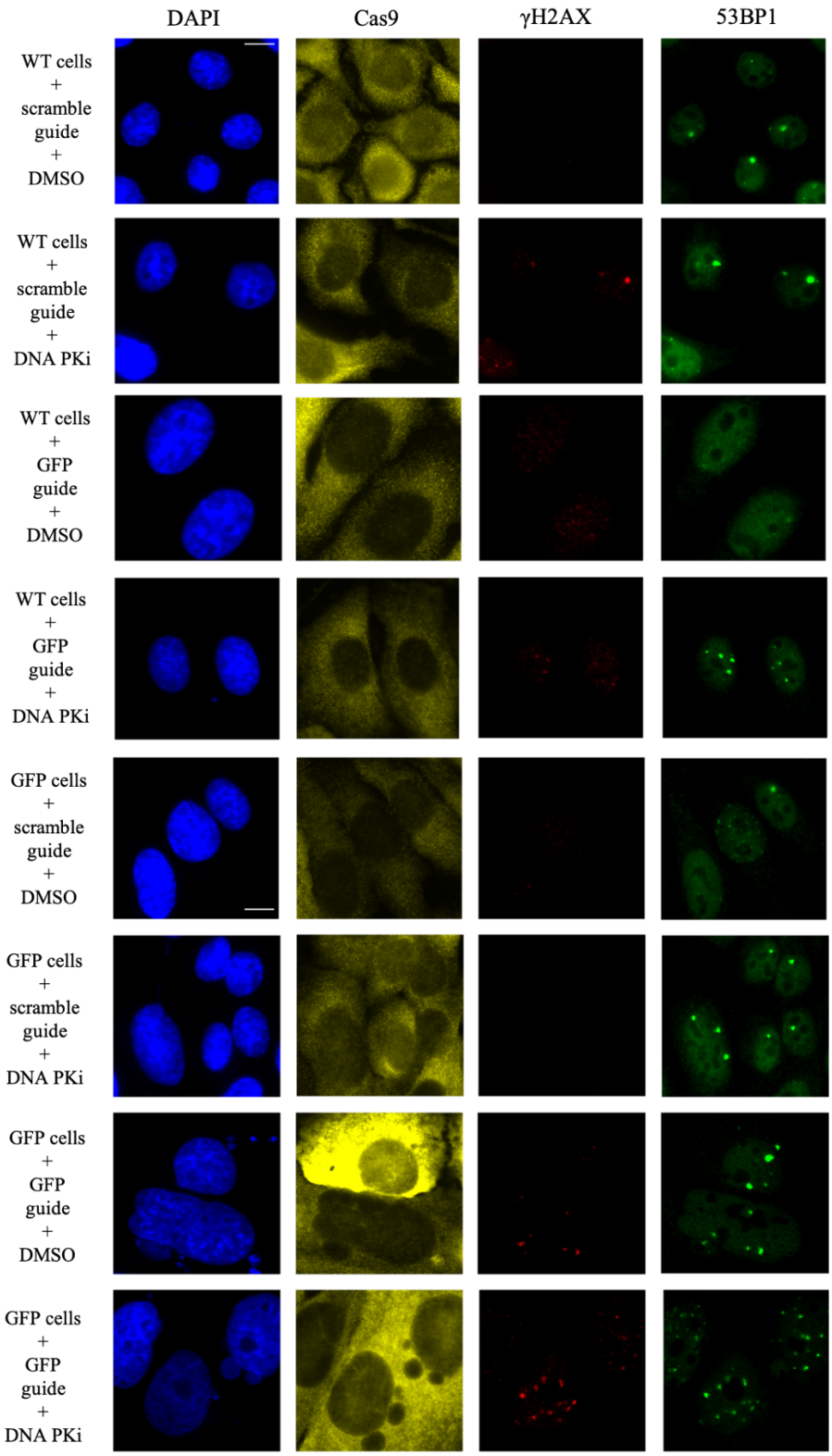

Figure 25. Cas9-induced DSB and repair inhibition through DNA-PK induce DNA damage accumulation.
Representative immunofluorescence images showing γH2AX, Cas9 and 53BP1 stainings in HeLa WT and GFP cells 4 days upon Cas9 treatment, in combination with either DMSO or DNA-PKi. Original magnification 60x, scale bar 10 μm.

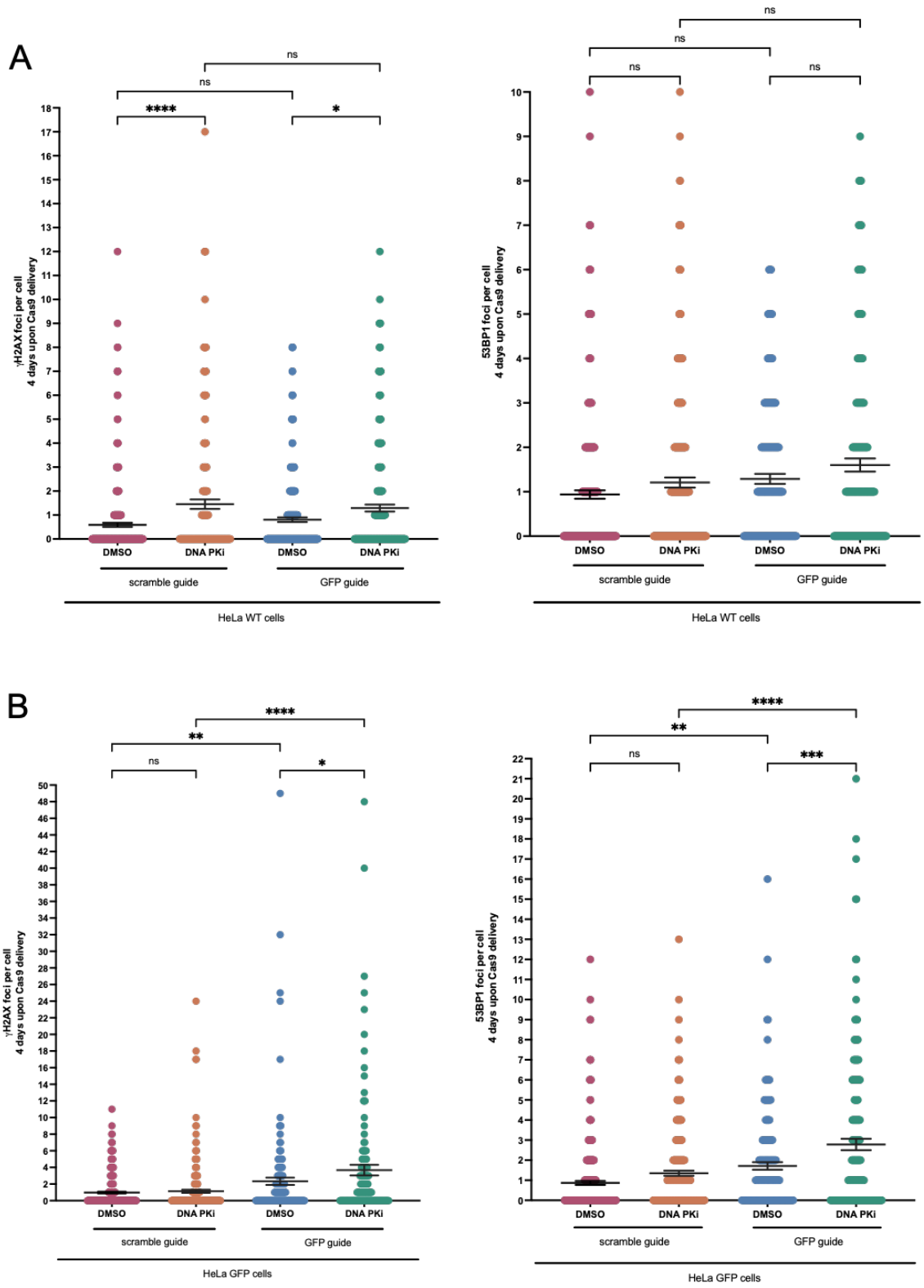

Figure 26. Cas9 cut and DNA-PKi combination increases DDR foci.
(A) Quantitative analyses of γH2AX and 53BP1 foci in HeLa WT cells 4 days upon Cas9 delivery, in combination with either DMSO or DNA-PKi. N=3 independent experiments. At least 50 cells per condition were analysed for each experiment. Error bars represent the s.e.m. *p < 0.05, ****p < 0.0001. One-way ANOVA test. **(B)** Quantitative analyses of γH2AX and 53BP1 foci in HeLa GFP cells 4 days upon Cas9 delivery, in combination with either DMSO or DNA-PKi. N=3 independent experiments. At least 50 cells per condition were analysed for each experiment. Error bars represent the s.e.m. *p < 0.05, **p < 0.005, ***p < 0.0005, ****p < 0.0001. One-way ANOVA test.

4.2.2.2 Cas9-induced DNA damage and DNA-PKi further increases cell death in GFP cells

To evaluate the impact of DNA-PKi on proliferation and mortality of both HeLa and RKO cells damaged by Cas9, I performed an experiment with a design similar to the one I just described. I first plated HeLa and RKO cells in 6 multiwells plates, the following day I infected all the conditions with a lentivirus carrying either the Cas9 with the scramble guide or the Cas9 with the guide against the GFP sequence. 24 hours after infection, I plated again all the conditions in a 96 well plate and I have added the green cytotox dye to start the experiment in Incucyte. 3 days after Cas9 delivery, I then added to the medium either DMSO or the DNA-PKi (NU7441) at the final concentration of 1 μM. At this point I had 4 different conditions for the four cell lines: scramble guide + DMSO, scramble guide + DNA-PKi, GFP guide + DMSO, GFP guide + DNA-PKi treated cells.

I monitored cell viability and mortality in Incucyte and I confirmed that, 5 days after Cas9 delivery, HeLa WT cells were not affected by the treatment with either the Cas9 carrying the scramble guide or the Cas9 associated with the GFP guide, indicating that the endonuclease was not inducing any DNA damage. The addition of DNA-PKi slightly affected cell proliferation, independently from the RNA guide carried by the Cas9, probably by impacting on random DNA damage in the cells (figure27A-B).

RKO WT cells shown the same behavior of HeLa WT cells: 5 days after lentiviral infection, cells did not show any impact on proliferation and cell death induced by the Cas9 treatment, as monitored by Incucyte. Also in this case, the DNA-PK inhibition had only a small impact of cell viability and death, that was identical between cells treated with the scramble Cas9 and cells treated with the GFP Cas9, further validating that, in the absence of the target, Cas9 is not inducing significant amounts of DNA damage (figure 27C-D).

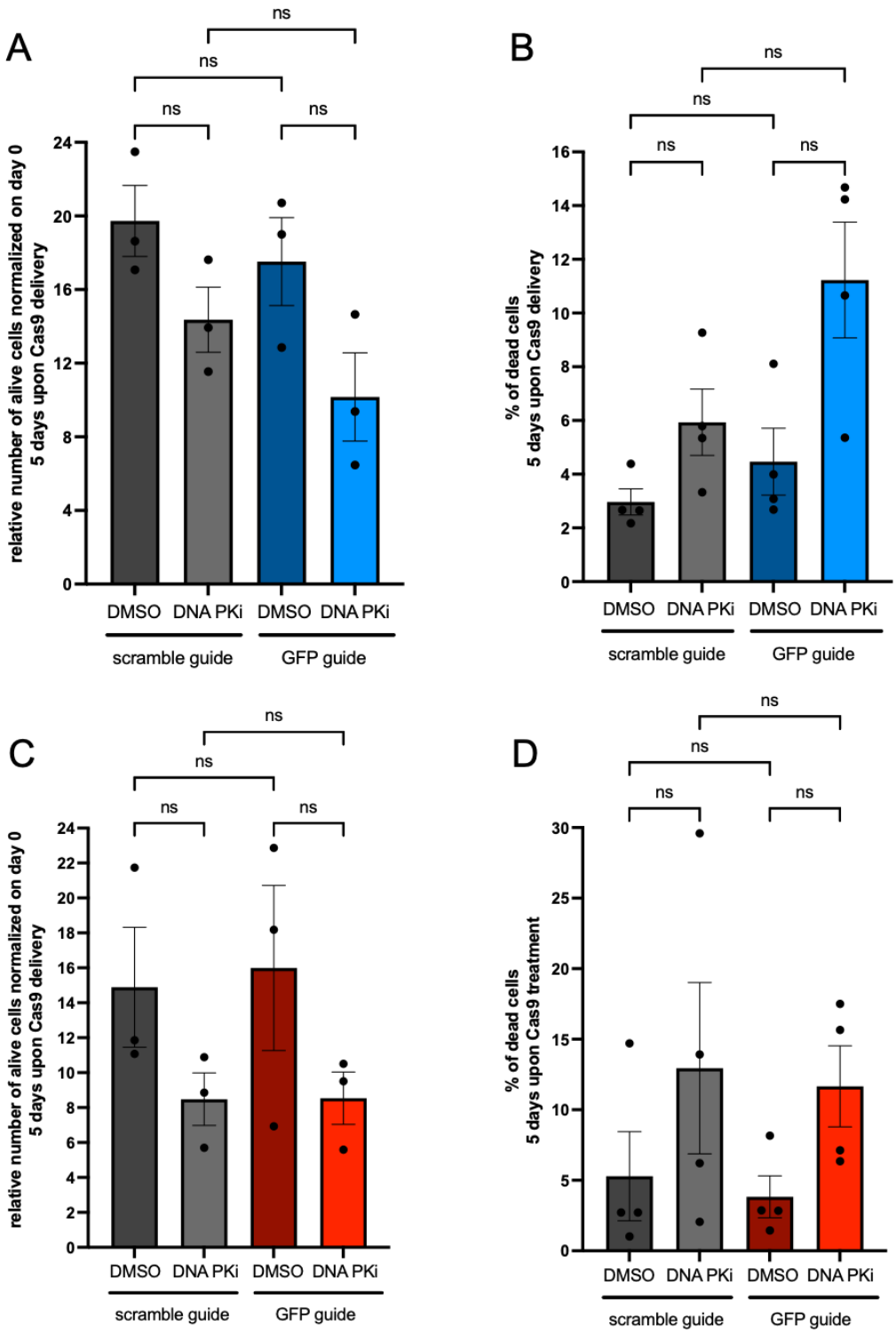

Figure 27. Inhibition of the repair by DNA-PKi does not affect HeLa and RKO WT cells viability, independently from the Cas9 treatment.
(A) Viability of HeLa WT cells 5 days upon Cas9 treatment, in combination with either DMSO or DNA-PKi. N=3 independent experiments. Error bars represent the s.e.m. One-way ANOVA test. **(B)** Mortality of HeLa WT cells 5 days upon Cas9 treatment, in combination with either DMSO or DNA-PKi. N=3 independent experiments. Error bars represent the s.e.m. **(C)** Viability of RKO WT cells 5 days upon Cas9 treatment, in combination with either DMSO or DNA-PKi. N=3 independent experiments. Error bars represent the s.e.m. One-way ANOVA test. **(D)** Mortality of RKO WT cells 5 days upon Cas9 treatment, in combination with either DMSO or DNA-PKi. N=3 independent experiments. Error bars represent the s.e.m.

I then performed the experiment in both HeLa and RKO GFP cells to test if the inhibition of the repair of a sequence-specific DSB can kill the target cells.

I followed the steps that I already described above and I monitored cell behaviors in Incucyte. Also in this set of experiments, 5 days after Cas9 delivery, I observed that Cas9 alone is sufficient to reduce proliferation and kill HeLa GFP cells when associated with the GFP guide (figure 28A-B). The inhibition of DNA-PK further impacts on cell viability and death: the proliferation of the cells where the DSBs repair was inhibited was halved compared to the cut alone condition and the mortality of these cells was doubled, demonstrating the combinatory effect of sequence-specific DNA damage generation by Cas9 and inhibition of its repair by DNA-PKi.

RKO GFP cells shown the same behavior: even if not always reaching full statistical significance, Cas9-induced DSBs were clearly sufficient to impact on cell proliferation and induce cell death (figure 28C-D). The combination of DSBs generation and inhibition of their repair further reduced cell proliferation and increased cell death.

These results indicate that Cas9 can efficiently kill only the cells with an exogenous DNA sequence integrated in their genome thanks to its specificity, but also the possibility to further improve its impact by inhibiting the repair of the sequence-specific damages by the use of a pharmacological inhibitor of DNA-PK.

A potential limitation is that DNA-PKi is not a sequence-specific treatment because, in addition to the sequence-specific DSBs induced by Cas9, it can also inhibit the repair of endogenous DNA damage. For this reason, a sequence-specific DSB repair inhibitor would be desirable.

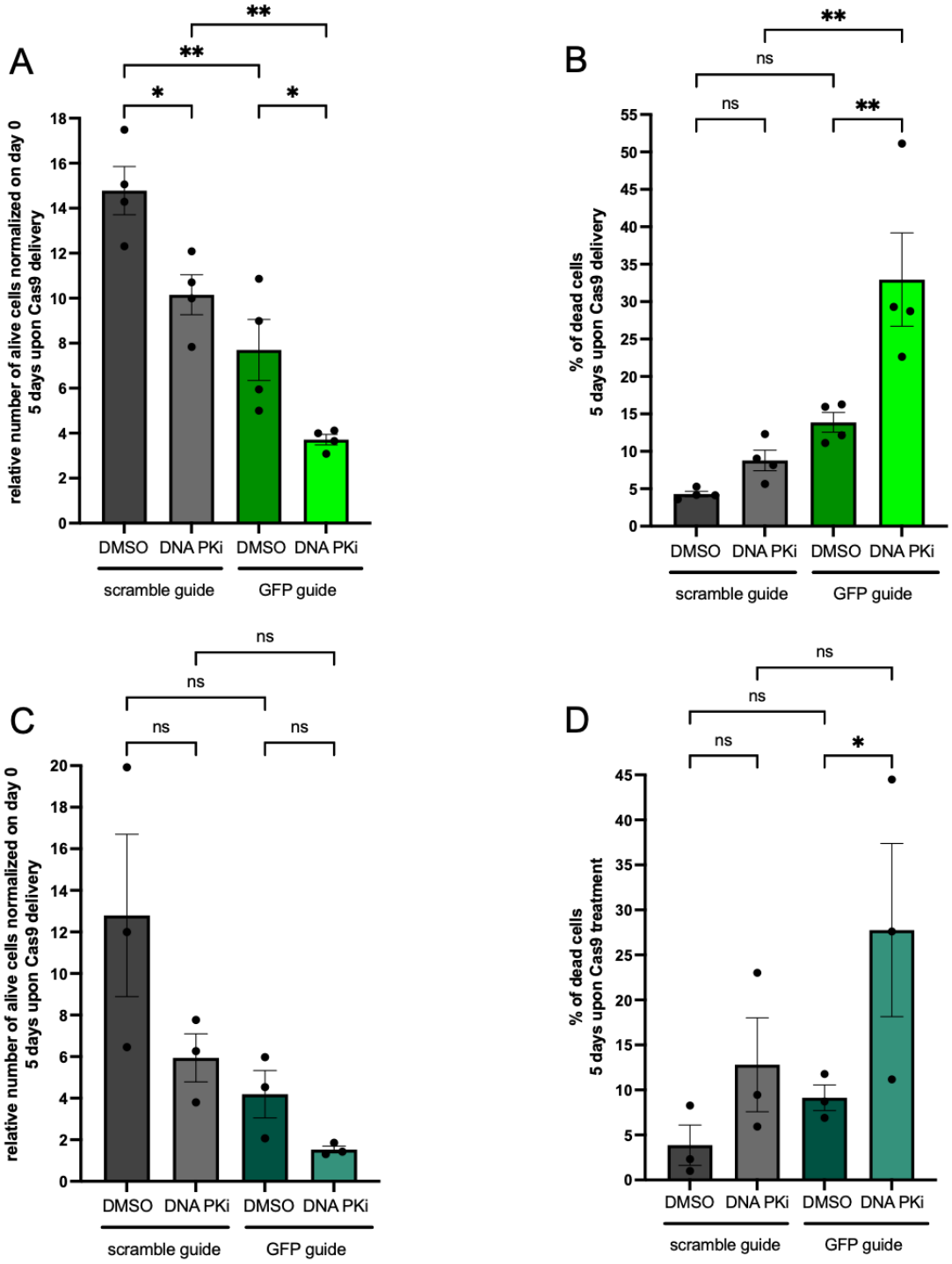

Figure 28. Inhibition of the repair by DNA-PKi synergize with sequence-specific DSB by Cas9 + GFP guide and kill HeLa and RKO GFP cells.

(A) Viability of HeLa GFP cells 5 days upon Cas9 treatment, in combination with either DMSO or DNA-PKi. N=3 independent experiments. Error bars represent the s.e.m. *p < 0.05, **p < 0.005. One-way ANOVA test. (B) Mortality of HeLa GFP cells 5 days upon Cas9 treatment, in combination with either DMSO or DNA-PKi. N=3 independent experiments. Error bars represent the s.e.m. **p < 0.005. One-way ANOVA test. (C) Viability of RKO GFP cells 5 days upon Cas9 treatment, in combination with either DMSO or DNA-PKi. N=3 independent experiments. Error bars represent the s.e.m. One-way ANOVA test. (D) Mortality of RKO GFP cells 5 days upon Cas9 treatment, in combination with either DMSO or DNA-PKi. N=3 independent experiments. Error bars represent the s.e.m. *p < 0.05. One-way ANOVA test.

4.2.3 Cas9-induced DNA damage and ASO

Our group previously demonstrated that RNA Polymerase II promotes the transcription of damage-induced long non-coding RNAs (dilncRNAs) at the sites of DNA double-strand breaks (DSBs) (Michelini et al. 2017; Pessina et al. 2019). DilncRNAs are the precursors of small non-coding RNAs called DNA damage response RNAs (DDRNAs) (Francia et al. 2012) and the interaction between dilncRNAs and DDRNAs is necessary for the stable recruitment of the proteins involved in the DNA damage response (DDR). Moreover, we also shown that antisense oligonucleotides (ASO) against these RNA species can impair their function by inhibiting the assembly of a proper DDR focus and the repair of DSBs (Michelini et al. 2017; D'Alessandro et al. 2018)

Based on these published results, I started investigating if the use of ASO against the dilncRNAs induced at the GFP site after the generation of DSBs by Cas9 has a combinatory effect in further killing cells – just like DNA-PK inhibition but with increased specificity given the locus-specific activity of ASO.

I started characterizing the effects of ASO in my experimental system. I designed ASO against the dilncRNAs transcribed from the DSB and then I tested them individually by transfecting each ASO at different concentrations in undamaged HeLa GFP cells; two days later I performed a resazurin-based cell viability assay. This assay measures the presence of metabolically-active cells able to reduce the non-fluorescent resazurin reagent into the fluorescent resorufin product. The fluorescent signal that is generated is proportional to the number of living cells in the sample and it is detected by a microplate fluorometer using specific excitation and emission wavelengths. I removed ASO that were spuriously toxic in the absence of DSBs and I focused on the remaining ones. These ASO organized into two groups: group A was composed of ASO binding the dilncRNAs transcribed from the right side of the break, while the group B was composed of ASOs (figure 29) binding the dilncRNAs transcribed from the left side of the break.

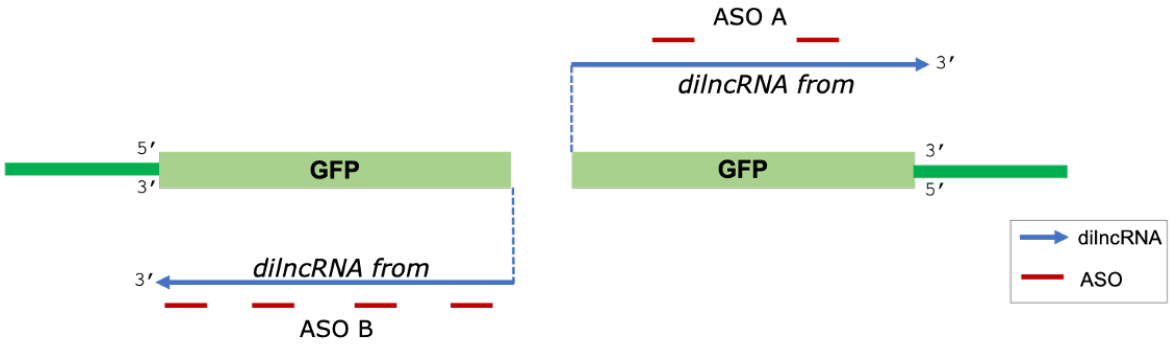

Figure 29. Schematic representation showing where GFP ASO bind dilncRNAs transcribed from the GFP DSB.
The group A is composed by two ASO binding the RNAs transcribed from the right side of the break, while the group B is composed by four ASO binding the RNA molecules transcribed from the left side of the break.

I combined them together to a final concentration of 10 nM. I also used a negative control ASO one that does not match with any sequence of the genome. I transfected HeLa and RKO GFP cells with 10nM ASO to have the following conditions: mock transfected cells, CTRL ASO transfected cells, GFP ASO transfected cells. I carried out the experiment as I have just described and I performed resazurin assays to check cell viability 2 days after transfection. These GFP ASO, used together, were not affecting cell viability compared to untreated conditions and the control ASO; in this way, I defined the maximal concentration of ASO that can be used without significant detrimental effects in undamaged cells (figure 30).

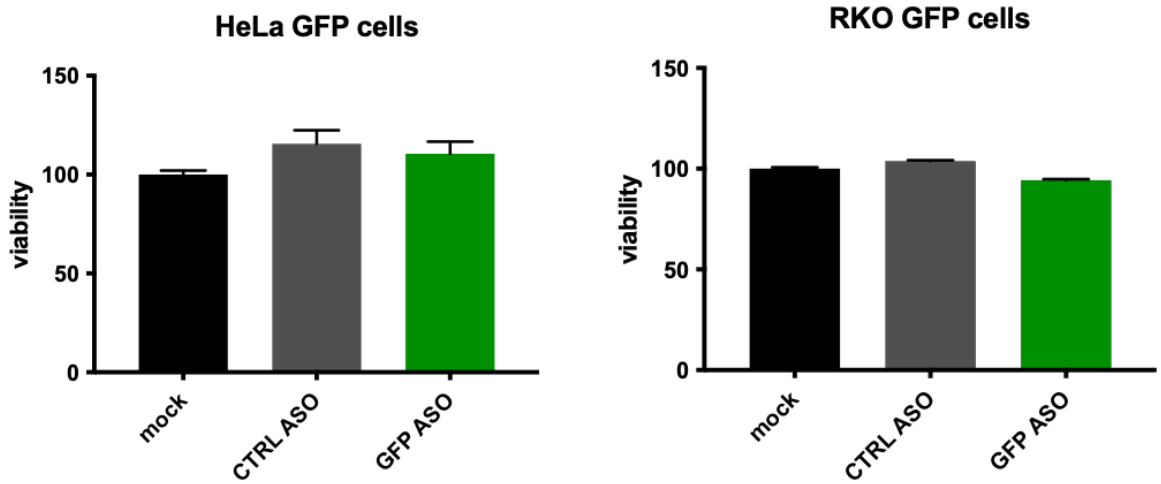

Figure 30. Viability assay for unspecific ASO toxicity.
Resazurin-based assay performed 2 days after transfection on HeLa and RKO GFP cells to determine the unspecific toxicity of 10 nM ASO in undamaged conditions. Mock is used as reference. N=3 technical experiments.

Our group previously published that ASOs can selectively block DDR activation at individual DNA damage sites within the same cell by impairing 53BP1 focus formation, while leaving γH2AX foci and also DDR activation at other sites within the same nucleus unaffected (Michelini et al. 2017)

I planned to confirm that GFP ASO were effective also in my experimental setting by determining by immunofluorescence their impact on DDR foci in HeLa GFP cells. I plated HeLa GFP cells in 6 multiwell plates, I transfected them the following day and 24 hours after transfection, I infected cells with the lentivirus expressing either the Cas9 carrying the scramble guide or the Cas9 expressing the GFP guide (figure 31).

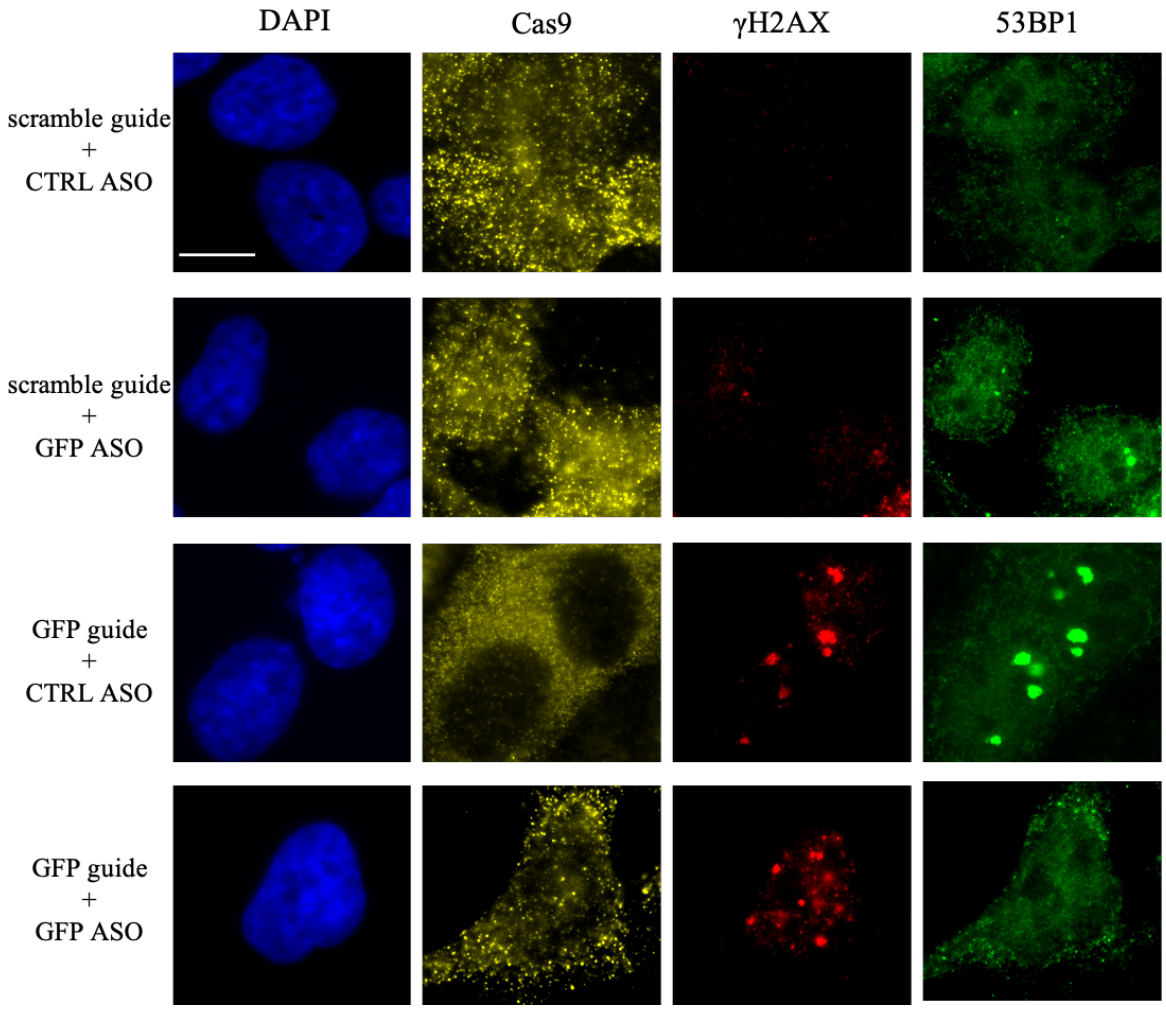

Figure 31. GFP ASO reduce 53BP1 foci number in a sequence-specific manner.
Representative immunofluorescence images showing γH2AX and 53BP1 stainings in HeLa GFP cells 3 days after Cas9 delivery. Original magnification 60x, scale bar 10 μm.

3 days upon delivery of Cas9, I fixed coverslips and I performed IF experiments to detect Cas9 expression and DDR foci formation. I observed an increase in 53BP1 foci formation in the cut condition compared to the uncut; instead ASO treated cells showed a statistically significant decrease of 53BP1 foci compared to controls, confirming that ASOs against the dilncRNAs impair DDR signalling in a sequence-specific manner also in the GFP system (figure 32A).

I detected an activation of DDR in terms of recruitment of 53BP1 at the site of damage 3 days after Cas9 delivery in the cells treated with the GFP guide, compared to the scramble guide; this activation was present also 7 days upon Cas9 treatment, as shown by the IF in figure 32B, suggesting that the endonuclease was still generating DNA damage. In addition, the reduction in 53BP1 foci formation between the cut condition and the cut condition treated with ASOs was maintained after 7 days, showing a long-term effect of ASOs in impairing the DDR signalling (figure 32B).

I then plated HeLa GFP cells in 6 multiwell plates to monitor in Incucyte cell proliferation and death upon Cas9 and ASO treatments. 24 hours after plating cells, I transfected HeLa GFP either with the control ASO or the GFP ASOs; the following day I infected cells with the lentivirus expressing either the Cas9 carrying the scramble guide or the Cas9 expressing the GFP guide. I delivered ASO before Cas9 in order to have the oligonucleotides ready to bind dilncRNAs as soon as they were transcribed upon DNA damage induction.

The preliminary results obtained so far, by Incucyte and colony formation assay, seem to suggest a combinatory effect of sequence-specific DNA damage induction by Cas9 and sequence-specific repair inhibition by ASO. However, these results are presently too preliminary to be discussed here and I hope that, if validated, they could support the therapeutic potential of the combination of Cas9 and ASO in the selective killing of target cells.

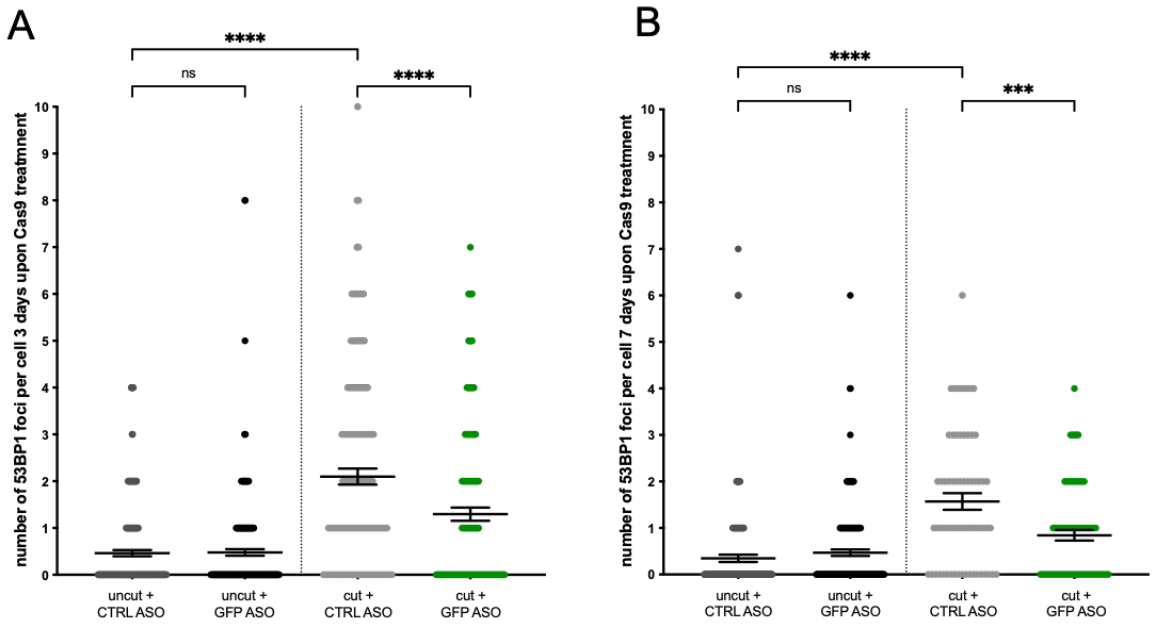

Figure 32. GFP ASO reduce 53BP1 foci in the cut conditions.
(A) Quantification of 53BP1 foci in HeLa GFP cells 3 days after being treated with either the Cas9 carrying the scramble guide or the Cas9 carrying the GFP guide, in combination with either a CTRL ASO or the GFP ASO**. (B)** Quantification of 53BP1 foci in HeLa GFP cells 7 days after being treated with either the Cas9 carrying the scramble guide or the Cas9 carrying the GFP guide, in combination with either a CTRL ASO or the GFP ASO. N=2 independent experiments. At least 50 cells per condition were analysed for each experiment. Error bars represent the s.e.m. **p < 0.005, ***p < 0.0005, ****p < 0.0001. One-way ANOVA test.

4.3 RNP complex as an alternative to the lentiviral system

Since the Cas9 protein can be delivered in the cells in different ways, I tested the use of the ribonucleoprotein complex (RNP) to induce sequence-specific DNA damage in HeLa GFP cells. The most common delivery methods for *in vitro* experiments are lipofection and electroporation, so I have started adopting these protocols with the intention to further optimize them in my experimental system.
The RNP-based approach is the one preferentially used to deliver Cas9 *in vivo*, constituting a therapeutic relevant alternative to the lentiviral system.

4.3.1 RNP delivered by transfection

To extend my observations by the use of RNP delivered by transfection, I used a synthetic gRNA against the GFP sequence ready-to-use, because the crRNA and tracrRNA were already combined together. The sgRNA is 20 nt long; it binds and cuts the same region of the GFP gene that is recognized by the guide of the lentiviral approach. The PAM sequence is TGG. I incubated the sgRNA and the Cas9 protein and I delivered the complex into the cells by using the lipofectamine CRISPRMAX Cas9 transfection reagent. I plated HeLa WT and GFP cells in 6 multiwell plates and, as soon as they attached to the plate, I prepared the reagents for Cas9 transfection. The conditions that I compared were: lipofectamine only, RNP without any guide, RNP associated with the GFP guide. I performed a time course for DDR activation and I analyzed coverslips every day. I identified that the 44 hours time point was the best one for appreciating a difference between the HeLa GFP cells transfected with the GFP Cas9 compared to the empty Cas9 and to HeLa WT cells, in terms of γH2AX and 53BP1 foci formation (figures 33-34).

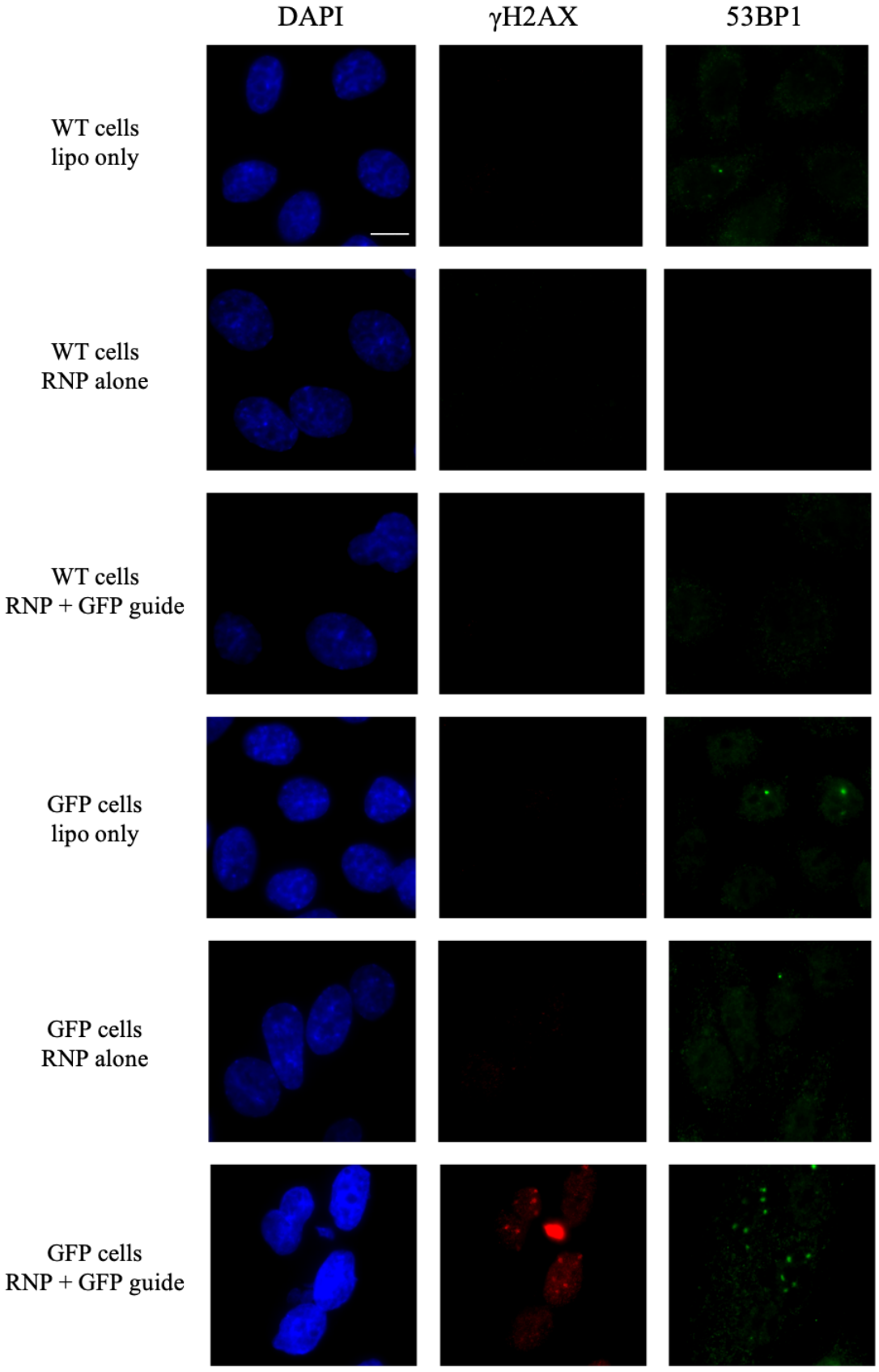

Figure 33. The transfected RNP complex induces DNA damage in Hela GFP cells only.
Representative immunofluorescence images showing γH2AX and 53BP1 stainings in HeLa WT and GFP cells 44 hours upon RNP transfection. Original magnification 60x, scale bar 10 μm.

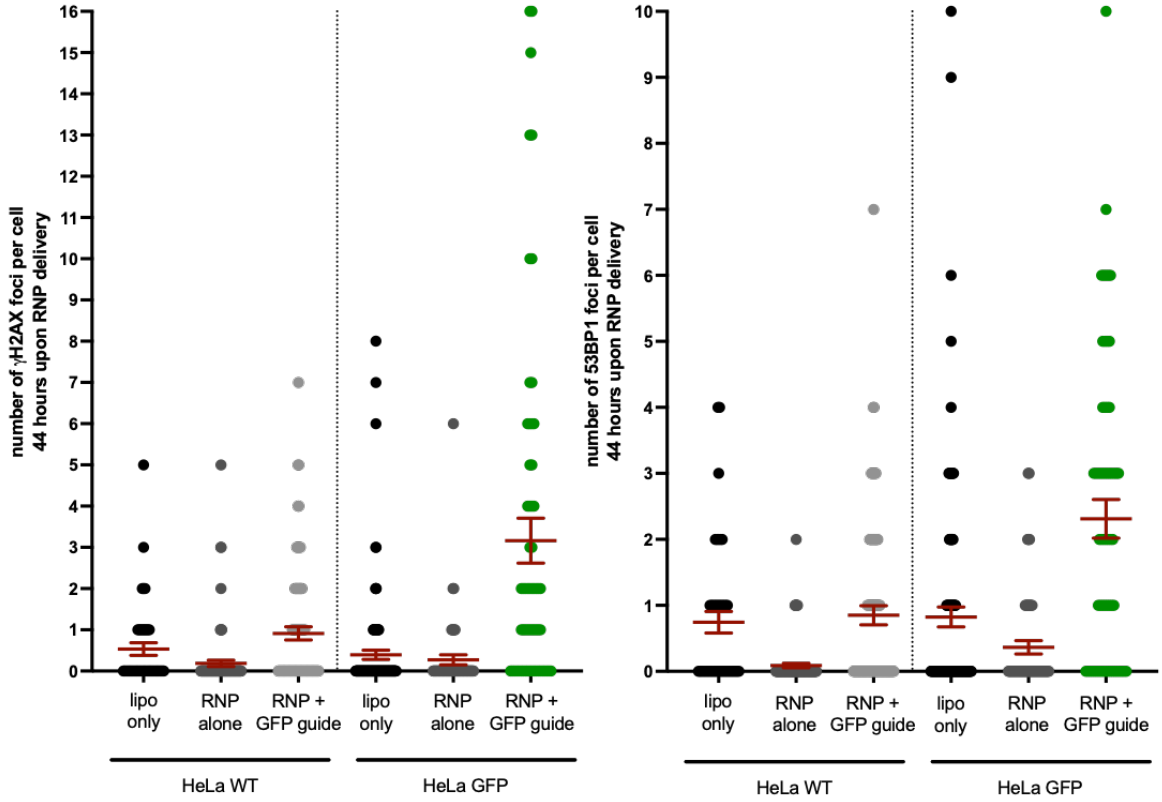

Figure 34. DNA damage induction upon RNP delivery by lipofection.
Quantitative analyses of γH2AX and 53BP1 foci in HeLa WT and GFP cells 44 hours upon RNP treatment. N=1 experiment. At least 50 cells per condition were analysed.

In addition, at this time point, I also observed a strong induction of micronuclei formation in HeLa GFP cells upon DNA damage generation, with more than 80% of cells displaying at least 1 micronucleus in the cytoplasm (figure 35A).

The presence of cytosolic DNA activated, also in this context, the expression of inflammatory genes since, 92 hours upon RNP transfection, I was able to detect an increase of IL-6 and IL-8 mRNA levels (figure 35B). I detected a small percentage of micronuclei and the expression of IL-6 also in HeLa WT cells treated with the GFP Cas9, suggesting that the RNP treatment could lead to a stress, which however remains lower compared to the response of GFP cells harboring DNA damage. This result can be improved and the viability of RNP treated cells remains to be checked, but these preliminary observations suggest that the RNP complex could be a valid alternative to the lentiviral system in inducing sequence-specific DSBs and recapitulating the events that I observed upon DSB induction in HeLa GFP cells.

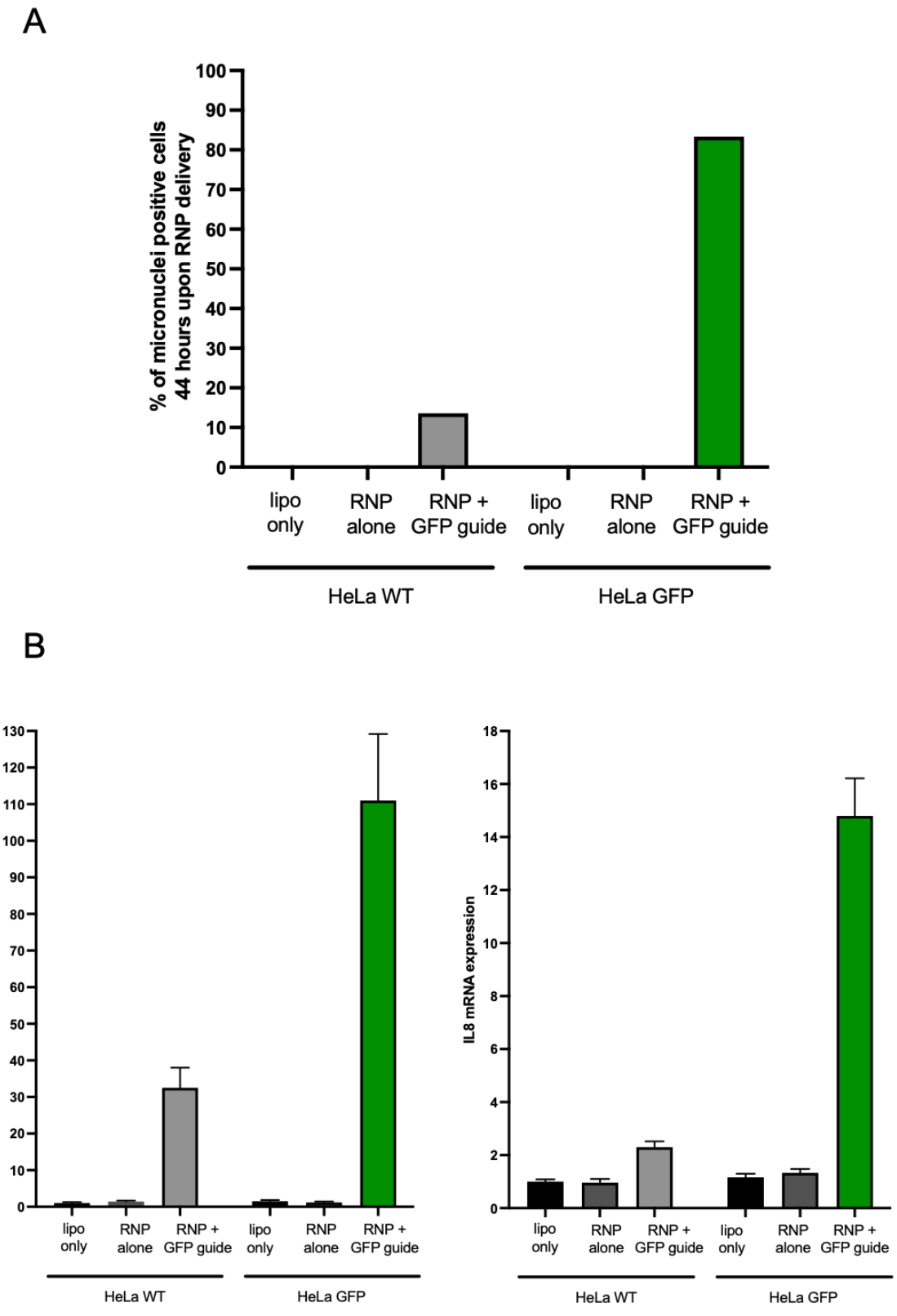

Figure 35. Micronuclei generation and expression of inflammatory genes upon RNP delivery by lipofection.

(A) Quantitative analyses of micronuclei formation in HeLa WT and GFP cells 44 hours upon RNP treatment. N=1 experiment. At least 50 cells per condition were analysed. **(B)** RT-qPCR for IL6 and IL8 mRNA expression levels in HeLa WT and GFP cells 92 hours after RNP transfection. N=3 technical experiments.

4.3.2 RNP delivered by electroporation

To compare the efficiency of different delivery methods, I also treated HeLa WT and GFP cells with the RNP complex provided by electroporation, in collaboration with the group of Raffaella Di Micco at the San Raffaele Telethon Institute for Gene Therapy. I electroporated cells in order to study the following conditions: not treated cells, electroporated only, RNP without any guide, RNP associated with the GFP guide (figure 36). Upon electroporation, I plated cells on coverslips and I checked DNA damage 20 hours afterwards. I observed that electroporation *per se* was not inducing significant amounts of DNA damage, compared to the not treated cells. This delivery method was even more efficient than transfection since I have observed a better induction of DNA damage, in terms of γH2AX and 53BP1 foci formation, in HeLa GFP cells treated with the RNP associated with the GFP guide, compared to the RNP only condition and to WT cells (figure 37). Also this experimental setup needs to be validated by further analyses, but it seems to indicate the possibility of using the RNP approach as a faster and possibly more efficient alternative to induce DNA damage than the lentiviral system.

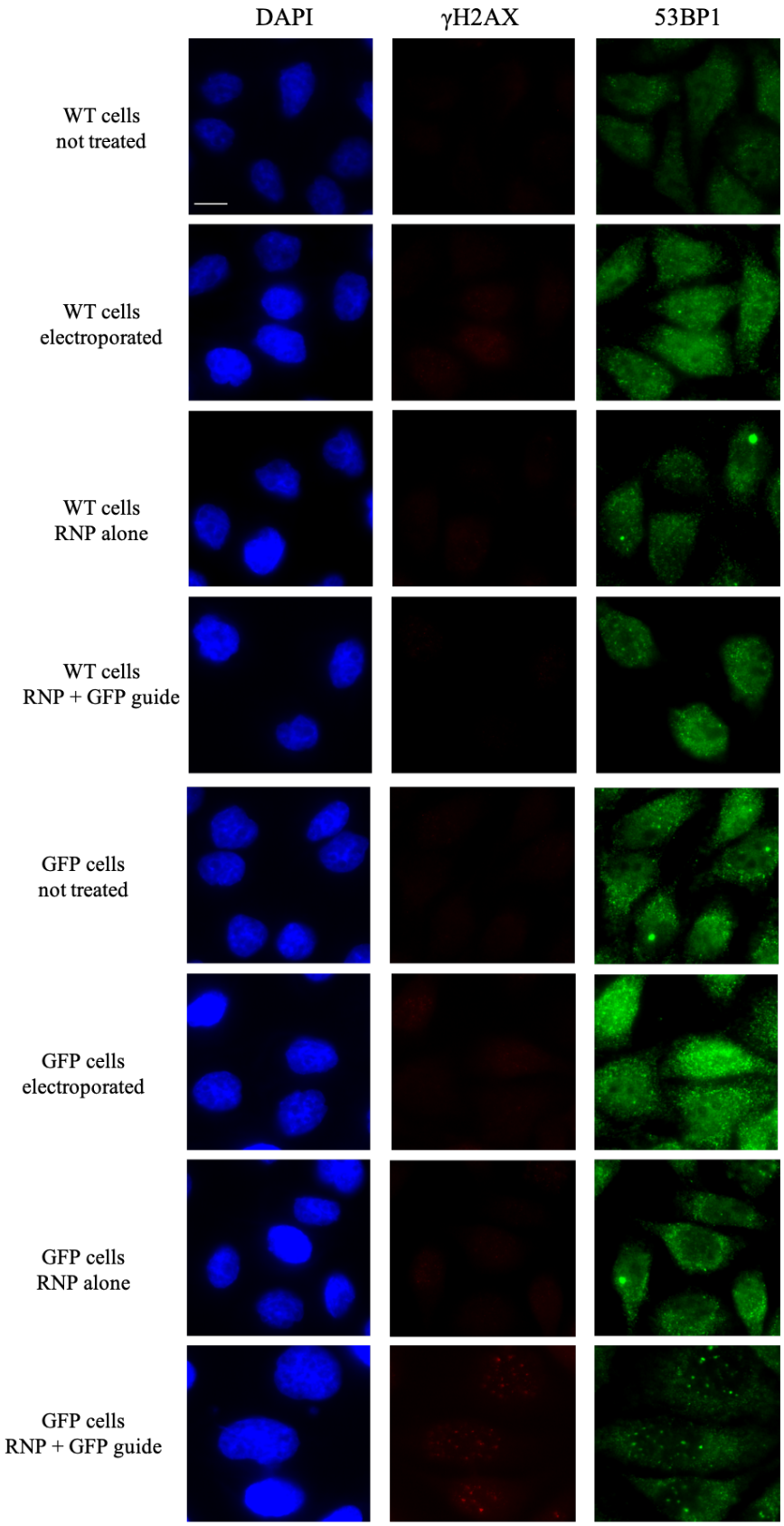

Figure 36. The electroporated RNP complex induces DNA damage in Hela GFP cells only. Representative immunofluorescence images showing γH2AX and 53BP1 stainings in HeLa WT and GFP cells 20 hours upon RNP electroporation. Original magnification 60x, scale bar 10 μm.

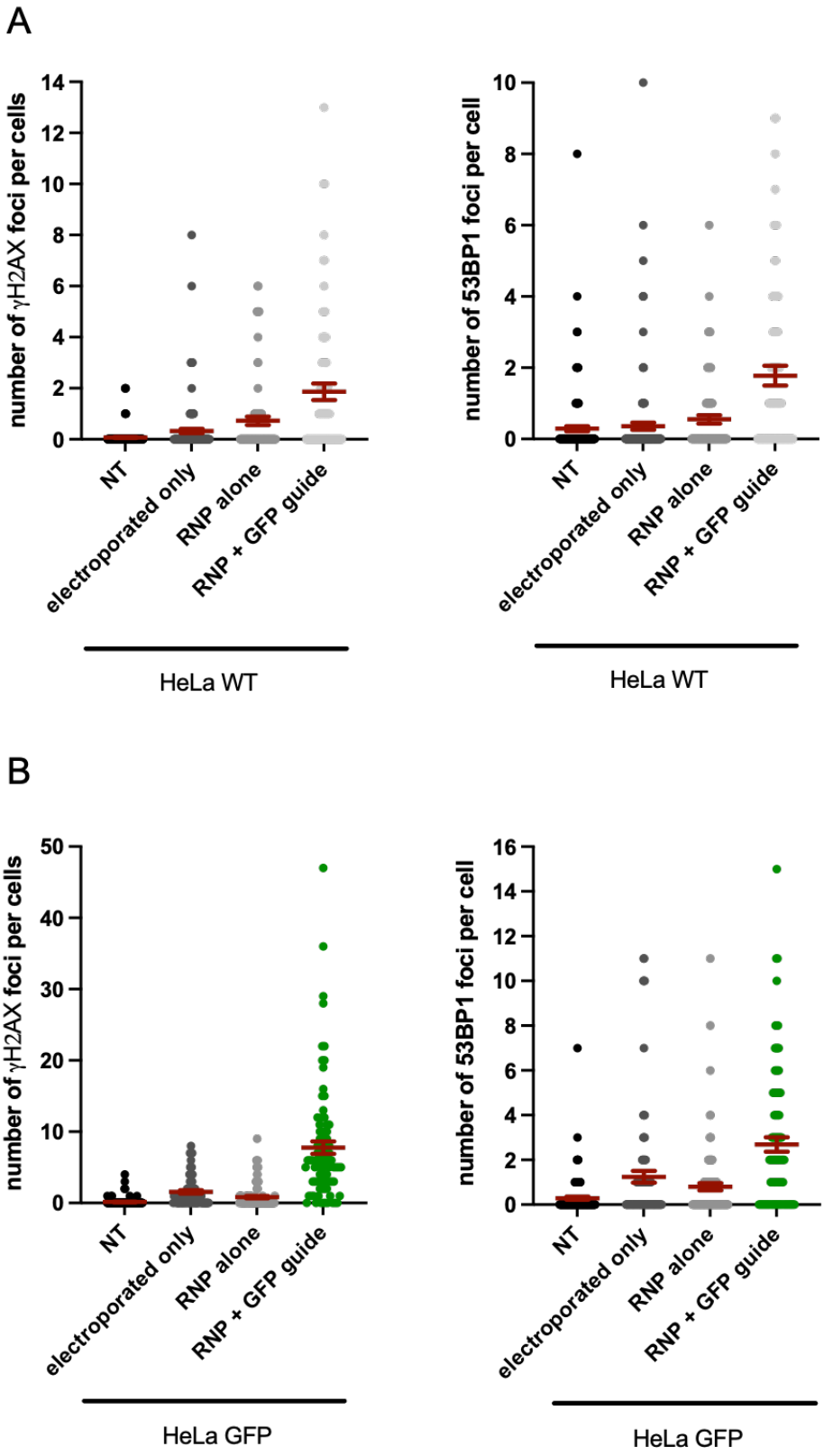

Figure 37. DNA damage induction upon RNP delivery by electroporation.
(A) Quantitative analyses of γH2AX and 53BP1 foci in HeLa WT cells 20 hours upon RNP treatment. N=1 experiment. At least 50 cells per condition were analysed. **(B)** Quantitative analyses of γH2AX and 53BP1 foci in HeLa GFP cells 20 hours upon RNP treatment. N=1 experiment. At least 50 cells per condition were analysed.

5 Discussion

5.1 The Cas9 system as a sequence-specific DNA damaging agent

It has been reported in literature that CRISPR/Cas9 screenings can give false positive results when DSBs are generated in highly amplified genes (Doench 2018). In loss-of-function screens carried out in different cancer cells, two independent groups identified a correlation between gene copy number and DNA damage-induced cell death (Aguirre et al. 2017; de Weck et al. 2018). Here it was shown that RNA guides targeting amplified regions in the genome of cancer cells induced a reproducible decrease in proliferation that strongly correlates with the number of target loci and authors hypothesized that the gene-independent anti-proliferative effect of CRISPR/Cas9 could be the consequence of several on-target DSB. Of course, these results have important implications for interpreting CRISPR/Cas9 screening data, but at the same time they suggest an amazing purposeful potential of CRISPR/Cas9.

Indeed, I was interested in investigating the possibility of using the CRISPR/Cas9 tools to inflict a sequence-specific DNA damage with the aim of impacting on the proliferation and survival of cells carrying an aberrant genome, while sparing normal cells because of the lack of the DNA target sequence.

5.1.1 The CRISPR/Cas9 system in cancer research

The CRISPR/Cas9 technology is presently being exploited the cancer research for different purposes; examples include to probe the causes of oncogenesis by inactivating genes involved in tumorigenesis (Zhang et al. 2021), by combining high-throughput screens with small molecules to find novel druggable targets (Lord, Quinn, and Ryan 2020) and by testing new cell-based therapies (Banerjee, Malonia, and Dutta 2021).

Another use of the CRISPR/Cas9 system in the cancer field is to engineer T cells in order to make them express synthetic receptors to recognize malignant cells: the results of these modifications are named chimeric antigen receptor (CAR) T cells (Cook and Ventura 2019). However, so far, only few approaches have been proposed to treat cancer cells with Cas9 targeting chromosomal rearrangements. Chromosomal rearrangements are the consequence of two DSBs generated in different regions of the genome that are joined together by NHEJ; these events can promote cancer development (Maddalo and Ventura 2016). In particular, fusion oncogenes (FOs) are the result of the fusions between two genes that are generally transcription factors or tyrosine kinases (Martinez-Lage et al. 2020). Since such fusion products are expressed only in cancer cells, their disruption constitutes an attractive therapeutic target. An example of such fusions is the Philadelphia chromosome in patients affected by leukemia. This rearrangement is the result of the joining of the c-abl proto-

oncogene tyrosine kinase (ABL1) on chromosome 9 to the breakpoint cluster region (BCR) on chromosome 22; the translocation results in the formation of the BCR-ABL fusion protein that consists in an active tyrosine kinase that can transform cells (Rowley 1973; Klein et al. 1982; Shtivelman et al. 1985; Maddalo and Ventura 2016). It has been shown that the genetic deletion of FOs can be achieved by introducing two DSBs in an intronic region of the two genes involved in the rearrangement and this is sufficient to kill target cells, with no evident effects on viability of normal cells (Martinez-Lage et al. 2020). While this approach highlights the power of the CRISPR/Cas9 technology in targeting genomic sites with unprecedented precision, a potential limitation is the fact that the CRISPR/Cas9 employed is expected to introduce DSBs also in the introns of the individual genes expressed in the healthy tissues, which might deregulate their expression.

5.1.2 **The CRISPR/Cas9 system as an antiviral therapy**

Other possible opportunities for the use of the CRISPR/Cas9 system can be the treatment of cells infected with an integrated proviral genome**.** Notably, CRISPR/Cas9 systems can be effective also in cells in which the integrated provirus is silent and not expressing its genes. Current antiviral therapies target virally-encoded gene products, thus they are inherently unable to eradicate latent infections. Indeed, a cell harboring a silent integrated provirus not expressing viral gene products presently cannot be targeted in any way.

The CRISPR/Cas technology has already been proposed as a strategy against viral infections in humans; however, the endonuclease is used to introduce DSBs in the dsDNA genome of the virus, either integrated or not, or in dsDNA intermediates to impede the expression of key factors for viral replication and propagation (Soppe and Lebbink 2017). For example, herpesviruses are dsDNA viruses that cause lifelong infections because of their ability to establish latent infections and they are associated with different human diseases (Paludan et al. 2011). Cas9 was used to target two essential genes for herpes simplex virus (HSV-1) replication *in vitro*, in mouse models and in human-derived corneas, where the virus can cause blindness (Yin et al. 2021). However, the survival of the edited cells was not investigated. The approach of knocking-out genes essential for viral replication was also tested in cells infected with the Epstein-Barr Virus (EBV), where it was observed not only a reduction in the viral load but also an increased cell death by apoptosis of Cas9-treated cells. The explanation of the authors is that the suppression of the viral activity can restore apoptosis in the infected cells; indeed, it has been shown that EBV infection increases the levels of Bcl-2, an anti-apoptotic gene, and decreases the levels of MYC (Ruf et al. 1999; Wang and Quake 2014).

The human papilloma virus (HPV) is a dsDNA virus that can frequently integrate into the host genome and cause different types of cancers (Williams et al. 2011). Cas9 was used against the two viral oncogenes E6 and E7 to restore the levels of p53 and p21 and induce apoptosis of the infected cells, in order to interfere with the cancer progression mediated by the virus (Zhen et al. 2014; Soppe and Lebbink 2017).

The hepatitis B virus has a partial dsDNA genome that is converted into double-stranded covalently closed circular DNA molecules (cccDNA) in the nucleus of the host cells; upon chronic infection it can lead to liver cirrhosis and cancer (Soppe and Lebbink 2017). Cas9 was used to target and disrupt the ORFs of essential viral genes both on the integrated viral genome and on the cccDNA, with consequent reduction of the viral genomes and protein levels in the infected cells (Lin, Zhang, and Li 2015).

The human immunodeficiency virus (HIV) is an example of a RNA virus with a dsDNA intermediate that can integrate in the form of a provirus in the genome of the host cells; it mainly infects CD4+ T cells leading to their depletions and causes the chronic disease of the acquired immunodeficiency syndrome (AIDS) (Soppe and Lebbink 2017). Cas9 was used to target the integrated provirus to knock out genes essential for viral replication, to induce multiple cuts to excise the viral genome (Dash et al. 2019) or to mutate the host genes expressing the receptors required for the viral entry into the cells, like CCR5 and CXCR4 (Atkins et al. 2021).

Cas nucleases targeting RNA have also been used against RNA viruses. For example, Cas13 or other Cas variants engineered to target RNA instead of DNA can act against the SARS-CoV-2 RNA genome (Soppe and Lebbink 2017; Luthra, Kaur, and Bhandari 2021; Baddeley and Isalan 2021).

Many progresses have been made with the use of Cas nucleases in targeting an infected cell, but the possible effects of DSBs on cell viability have not always been investigated.

Therefore, our approach seems to be novel and distinct from what has been previously proposed as it aims at impacting on cell viability rather than altering viral genes expression.

5.1.3 The combinatory effect of sequence-specific DSB induced by Cas9 and inhibition of its repair

The approach that I am proposing here can represent a valid strategy to kill cells with an aberrant genome by designing sequence-specific RNA guides for Cas9, avoiding the targeting of normal cells that miss the DNA sequence recognized by the endonuclease. Any sequence of a viral or cancer genome can be targeted, independently from its function. Indeed, Cas9 is not used to disrupt the expression of a gene product necessary for the survival

of the malignant cell but it is the DSB *per se* that is able to induce a cascade of events that lead to selective cell death.

Moreover, I am also proposing that the combination of sequence-specific DSB generation with its repair inhibition boosts the toxicity of Cas9-induced DNA damage. I tested the use of a pharmacological inhibitor of DNA PK, a key factor in the NHEJ pathway, that, however is not a sequence-specific treatment because it can also inhibit the repair of endogenous DNA damage. For this reason, sequence-specific DNA repair inhibition could be achieved by the use of ASO against the dilncRNAs transcribed upon DSB generation.

5.1.4 The GFP system as a proof of concept

I created two experimental model systems by infecting HeLa and RKO WT cells with a lentivirus carrying the promoterless GFP open reading frame (ORF) sequence. In this way I obtained two sets of isogenic cell lines that simulate a cell system in which a silent proviral genome is integrated in multiple copies and I have named them HeLa GFP and RKO GFP cells. I selected these two cell lines because, upon irradiation, they were the ones most sensitive to DNA damage among all those tested (figure 5).

The insertion of the GFP sequence did not alter the response of HeLa and RKO to DNA damage induction, as I validated by irradiation. Indeed, I observed a statistically significant reduction in proliferation mirrored by an increase of cell death in the irradiated HeLa and RKO cells, compared to the undamaged conditions, independently from the presence, or not, of the GFP sequence (figures 7-8).

I then characterized the CRISPR/Cas9 system in the HeLa experimental model and I validated key experiments in RKO cell lines. The experiments were carried out by delivering Cas9 by lentiviral infection to allow the expression of the endonuclease in all cells and the introduction of DSBs in a persistent manner.

I selected a GFP guide able to induce sequence-specific DSBs, as validated by BLESS, compared to a Cas9 expressing a scramble guide with no match in the genome and for this reason used as a negative control (figure 9).

DNA damage caused by Cas9 and the GFP guide activated DDR, as shown by γH2AX and 53BP1 foci formation, in HeLa GFP cells, compared to cells treated with the Cas9 expressing the scramble guide (figures 10-11). In addition to DDR activation, I also observed an increase in the formation of micronuclei, the majority of which were positive to cGAS staining (figures 15-16). A link between DNA damage, micronuclei formation and cGAS accumulation has been previously reported (MacKenzie et al. 2017; Harding et al. 2017; Glück et al. 2017). Indeed, different groups have demonstrated that upon induction of DSBs,

DNA can be released in the form of micronuclei in the cytoplasm, where cGAS can sense the cytosolic dsDNAs and accumulate in their proximity. They have also shown that the recognition of micronuclei by cGAS can induce the expression of inflammatory genes through the stimulator of interferon genes (STING), indicating that the cGAS-STING pathway can act as cellular surveillance mechanism (MacKenzie et al. 2017; Harding et al. 2017; Glück et al. 2017).

Since I observed cGAS positive micronuclei induction upon DSBs generation by Cas9, I studied the expression of inflammatory genes that are the target of the cGAS-STING pathway, (Dou et al. 2017) and indeed I demonstrated the induction of IL-6, IL-8, CXCL10 and TNF by qPCR in HeLa GFP cells treated with the Cas9 carrying the GFP guide, compared to the uncut condition (figure 17).

The induction of micronuclei observed upon Cas9-induced DNA damage is consistent with previous published results. Leibowitz et al demonstrated, by single-cell whole-genome sequencing in RPE-1 and BJ-5ta cells, that editing mediated by the CRISPR-Cas9 system generates micronuclei and chromosome bridges, which can initiate a process named chromothripsis, where one or few chromosomes can be involved to produce large rearrangements (Leibowitz et al. 2021). This phenomenon could give rise to concerns in the use of CRISPR for gene editing, but the generation of DSBs by Cas9 can instead be a good activator of a cascade of events that leads to the death of aberrant cells that have to be eliminated, supporting the use of weaponized CRISPR/cas9 system. Moreover, Cas9-induced DNA damage elicits an inflammatory response, activating the expression of cytokines and chemokines. It has been reported that these molecules, once released, can attract immune cells that eliminate the inflamed cells (Serhan and Savill 2005; L. Chen et al. 2017). The data that I am presenting here show a link between the damage induced by Cas9 and an inflammatory response activation in the cells that are damaged by the endonuclease, through the generation of micronuclei and the activation of the cGAS/STING pathway, that can potentially recruit immune cells at the site of inflammation.

To further support the results of my analyses by RT-qPCR of individual genes, I also performed a RNA-seq analysis on HeLa GFP cells treated with Cas9 carrying either the GFP or the scramble guide. The sequencing highlighted the activation of several pathways that lead to an inflammatory response in the damaged condition compared to the undamaged one, like the IL17 pathway, the TNF signaling pathaway and the cytokine and inflammatory response pathways. The IL-17 signaling pathway, for example, is the most upregulated pathway, accordingly to the BioCarta Gene Set. The Interleukin-17 is a key player in the

mammalian immune system and it is responsible for the expression of genes as IL-6, IL-8, TNF and CXCL10, confirming the results of my RT-qPCRs (figure 18).
These results not only show that Cas9 can be proposed as a novel sequence-specific DNA damaging agent, but confirm the possibility to engage immune cells that can further remove malignant cells, by inducing an inflammatory response, amplifying the effect of Cas9.

Since DNA damage can have an impact on cell cycle progression, I characterized the distribution of cells in the different phases of cell cycle by FACS, by staining cells with PI. I observed an increase of HeLa GFP cells in the G2 phase upon treatment with the Cas9 carrying the GFP guide, compared to the scramble condition (figure 14). This is consistent with the observations published by Aguirre and colleagues, that have demonstrated the accumulation of cells in G2 upon Cas9-induced DNA damage in amplified regions (Aguirre et al. 2017). However, a percentage of HeLa GFP cells, upon DNA damage generated by Cas9, increased their size and presented more that one nucleus per cell, suggesting problems in cell division, probably due to unrepaired damage. Cell multinucleation can cause a misinterpretation of FACS, because PI staining alone does not allow the discrimination between normal G2 cells and cells with multiple G1 nuclei. For this reason, I plan to further characterize cell cycle distribution by combining the analysis of cellular DNA content with the staining for cyclins, whose amounts vary during cell cycle, in order to distinguish cells that have different DNA content and are in different phases of cell cycle.

It is known that DNA damage induction causes a delay in cell cycle progression to allow for DNA repair; if this is not happening, cells are generally eliminated. However, if the checkpoints are compromised, cells can enter mitosis before completing DNA repair and they can undergo mitotic catastrophe (MC) (Surova and Zhivotovsky 2013). MC is the consequence of failed or dysregulated mitosis and it is connected to some morphological alterations like micronuclei and multinucleation that can cause cell death (Surova and Zhivotovsky 2013).
DNA damaging agents, like ionizing radiation and radiotherapy, can induce MC. In fact, it has been shown that damaged cells can arrest in G2/M but, if this arrest is overcome because of checkpoint adaptation, they can enter mitosis. This leads to chromosomal abnormalities as micronuclei and anaphase bridges and consequent cell death (Swift and Golsteyn 2016; Ko et al. 2020). Also multinucleated giant cells were observed upon ionizing radiations and were connected to MC (Vakifahmetoglu, Olsson, and Zhivotovsky 2008; Mirzayans et al. 2017). Moreover, the abrogation of the G2/M checkpoint upon DNA damage seems to be

related to the activation of the inflammatory signaling pathways through micronuclei generation and cGAS/STING activation (J. Chen et al. 2020).
Albeit speculatively, these results could suggest that Cas9-induced DNA damage could cause MC in cells that overcome the G2/M checkpoint through the formation of micronuclei that activate the cGAS/STING pathway and an inflammatory response; moreover, mitotic defects can generate multinucleated cells, recapitulating the events already observed upon DNA damage caused by ionizing radiations.

After the characterization of the effects induced by DSBs generated by Cas9, I was excited to observe that the DNA damage caused by the endonuclease was sufficient to halve the proliferation rate of HeLa GFP cells and increase cell death compared to cells treated with the Cas9 carrying the scramble guide or the WT conditions, demonstrating the therapeutic potential of the nuclease in targeting and killing cells with an integrated proviral genome (figure 19). The long-term effects of Cas9-induced DNA damage in HeLa GFP cells were even more evident by colony formation assay where I observed a two-third reduction in the number of colonies obtained by cells treated with the GFP guide, compared to the scramble condition (figure 20).
Importantly, my conclusions are not restricted to one cell type only but they were also validated in RKO cells, where I observed a similar reduction of proliferation and increase of cell death in RKO GFP cells treated with the Cas9 expressing the GFP guide, compared to GFP cells treated with the Cas9 carrying the scramble guide and the WT conditions, further supporting the possibility of weaponizing the CRISPR/Cas9 system (figure 21).

I also attempted to improve this result by designing nine additional distinct individual RNA guides spanning the entire GFP sequence to use in addition to the one already tested; the aim was to increase the number of Cas9 targets and consequently increase the impact of Cas9 in affecting the viability of the target cells. Moreover, since a Cas9-induced DSB is mainly repaired by the error-prone NHEJ pathway (Bothmer et al. 2017) thus generating potential resistant cell clones, multiple sites increase the possibility to keep inducing DSBs in the target cells. I compared three different conditions: cells treated with the Cas9 carrying the scramble guide, cells treated with Cas9 and only one GFP guide and cells treated with Cas9 and the pool of GFP guides. What I observed both in HeLa and RKO cells was that the GFP cell lines were sensitive to DSBs induced by the single GFP guide as I previously demonstrated, while the treatment with the pool of GFP guides was not causing further toxicity. The approach based on the use of multiple guides was still inducing a reduction in proliferation and an increase death in the target cells, but the impact was comparable with

the one obtained by using only a guide. This result must be interpreted after verifying that all the guides are equally efficient in inducing a DSB in the target sequence by BLESS as the single one I compare them to; anyway, it could be possible that different Cas9 proteins carrying different sgRNAs compete to bind and cut the target sequence, impeding multiple simultaneous cuts in the GFP sequence. In addition, to deliver 10 different sgRNAs in WT and GFP cells, I had to decrease the concentration of individual guides in order to provide the same amount of plasmids of the other two conditions, possibly impacting on the expression levels, and consequentially on the efficiency, of the different GFP guides. In any case, the use of a pool of guides was not affecting at all the proliferation of the WT cells, exactly like the scramble guide and the single GFP guide, showing the absence of off-target effects: this bodes well for their use once increased efficacy is ascertained (figure 22).

5.2 Repair inhibition of Cas9-induced DSB to increase cell death

A powerful potential way to increase the effects of the Cas9-induced DNA damage in the GFP cells is DSB repair inhibition.

5.2.1 DNA PK inhibitor to inhibit DSB repair

There are different ways to inhibit the repair of a DSB, and one of the most powerful ones is the use of pharmacological inhibitors of DNA PK. DNA PK is a key protein in the NHEJ repair pathway and it is considered a possible therapeutic target to treat several tumors, especially if combined with chemotherapy or ionizing radiation (Lord, Garrett, and Ashworth 2006). Different inhibitors of DNA PK have been developed and it has been shown that the combination of these inhibitors with DNA-damaging agents like IR or doxorubicin increases the accumulation pATM, γH2AX and 53BP1 foci that persist in time causing genomic instability and reduced cell survival (Fok et al. 2019).

Before testing the combination of Cas9-induced DSB and DNA PKi NU7441, I validated the combinatory effect of DSB generation by IR and inhibition of the repair by DNA PKi in killing treated cells. I irradiated cells with 1Gy in order to induce an amount of damage that is comparable with the one induced by Cas9. Even if I have observed an average of 3 foci of γH2AX and 53BP1 per cell upon Cas9 treatment, GFP cells have integrated around 16 copies of the GFP sequence, indicating that in principle cells could exhibit up to 16 DSBs at the same time. It has been reported that around 12 γH2AX foci are detectable 30 minutes upon 1Gy irradiation (Redon et al. 2009). This value can vary according to the cell line, but it indicates that 1Gy could be the correct positive control for my experiments. I have compared not irradiated and irradiated cells that were treated with either DNA PKi or DMSO as control.

As expected, both HeLa and RKO cells responded similarly to the treatments, independently from the presence of the GFP sequence: irradiation alone is sufficient to reduce proliferation and kill cells, but the combination of IR and DNA PK inhibition abrogated almost completely cell proliferation (figures 23-24).

Also the combination of sequence-specific DSBs induction by Cas9 and inhibition of their repair by DNA PKi increased cell death, but only in HeLa GFP cells, that contain the DNA target sequence of Cas9. DDR, checked by IF in terms of γH2AX and 53BP1 foci formation, was activated only in HeLa GFP cells treated with the Cas9 expressing the GFP guide, compared to HeLa GFP cells treated with the Cas9 expressing the scramble guide and the WT cells (figures 25-26). I characterized DDR in HeLa cells because RKO cells tend to die faster upon DNA damage induction, making the analyses for DDR markers more difficult. Instead, impaired proliferation upon the two treatments was validated both in HeLa and RKO GFP cells, strengthening the result and showing the specificity of Cas9, combined with DNA PKi, in killing only the cells with the target sequence (figure 27).
Researches have already combined Cas9 and DNA PKi; indeed, as already mentioned, the main pathway involved in the repair of a Cas9-induced DSB is NHEJ, even in the presence of a donor template used for gene editing. To increase the rates of HR-mediated repair of the DSBs generated by Cas9, DNA PK was transiently inhibited, facilitating the incorporation, in the target genome, of the desired modification (Robert et al. 2015). In this case, instead, I am showing for the first time the potential of combining the generation of sequence-specific DSBs with the inhibition of their repair by using DNA PKi in selectively killing only HeLa GFP and RKO GFP cells, that simulate a cell system where several copies of a viral genome are integrated.
I followed the behavior of the different cell lines for 5 days in Incucyte and I observed an almost completely abrogation of viability of the damaged GFP cells, especially in RKO GFP cells (figure 28). Anyway, it will be interesting to understand if the toxicity of the treatments can be stronger either with multiple administrations of DNA PKi or by studying the long-term effects of the DSB repair inhibition by performing colony formation assays.
I focused on the use of DNA PKi to impede the repair of the DSBs caused by Cas9 because NHEJ is the major pathway involved in DSB repair, but it would be interesting understanding if the inhibition of the HR pathway could lead to the same toxicity too. For example, Cas9 could be combined with an inhibitor of RAD51. Indeed, molecules have been reported to disrupt, by different mechanisms, HR and potentiate DNA damage induced cell death caused by either chemotherapy or IR (Scott et al. 2021).

However, these treatments are not specific because they can interfere also with the repair of endogenous DNA damage. Indeed, in the experiments performed using DNA PKi, I observed a slight non-specific toxicity of this molecule also in the undamaged conditions. For this reason, a sequence-specific DSB repair inhibitor would be ideal.

5.2.2 Sequence-specific DNA repair inhibition by antisense oligonucleotides

The generation of a DSB results in the recruitment of the RNA polymerase II complex that triggers the bi-directional transcription of dilncRNAs (Francia et al. 2012; Michelini et al. 2017; Pessina et al. 2019). These RNA molecules are essential for the recruitment of downstream DDR factors like 53BP1, with which they interact. ASOs against dilncRNAs disrupt their function by inhibiting the assembly of a proper DDR focus and thus the repair of DSBs (Michelini et al. 2017; D'Alessandro et al. 2018). For this reason, ASOs are the only candidates as sequence-specific DSBs repair inhibitors. The possible combinatory effect of sequence-specific DSB induction by Cas9 and the sequence-specific inhibition of its repair by ASOs would kill only cells with the target of the treatments, while sparing all the other cells.

I tested in HeLa GFP cells different ASOs against the dilncRNAs transcribed upon Cas9-induced DNA damage in the GFP sequence to define the maximum concentration that can be used without detrimental effects on the control conditions (figure 30). I then validated their function by looking at 53BP1 foci formation upon Cas9-induced DSBs in HeLa GFP cells. Also in this system, as the others previously characterized in the lab, ASOs against the dilncRNAs transcribed from the GFP DSBs reduced the number of 53BP1 foci, compared to GFP cells treated with a control ASO and the uncut conditions (figure 31).

I obtained only few preliminary data that suggest the synthetic lethality of the sequence-specific DNA damage induction in the GFP sequence by Cas9 and the sequence-specific repair inhibition by GFP ASOs. These results need to be optimized but, if validated, they could have an impact in clinical applications, since they could open the possibility to explore the effectiveness of this therapeutic approach to any type of genomic aberrations, while sparing normal cells.

5.2.2.1 Antisense oligonucleotides as a tool to cure diseases and ageing

Antisense oligonucleotides against RNA molecules are a promising tool to treat diseases. Nine ASOs have been approved and are on the market to cure human diseases; in addition, nearly fifty additional ASOs are in clinical trials for the treatment of many human diseases (Crooke et al. 2021).

Our group showed the potential of ASOs in treating pathological conditions that involve telomeres. Indeed, we reported that uncapped/damaged telomeres induce the synthesis, accumulation, and processing of telomeric damage-induced long non coding RNAs (tdilncRNAs) arising from telomeric DNA ends (Nguyen et al. 2018; Rossiello et al. 2017) in a manner similar to what we showed at DSBs (Michelini et al. 2017). These RNA molecules are transcribed both at the G-rich and C-rich strands of dysfunctional telomeres of mammalian cells and then processed by DROSHA and DICER to produce short RNAs, named telomeric DNA damage response RNAs (tDDRNAs). The pairing between dilncRNAs and tDDRNAs allows the recruitment of DDR proteins, such as 53BP1, into DDR foci. This process is essential for the full activation of DDR signalling and repair at dysfunctional telomeres.

The Hutchinson-Gilford progeria syndrome (HGPS) is a genetic disorder characterized by premature ageing features and caused by mutations in the Lamin A gene, which encodes a truncated lamin A protein called progerin, that lead to genome instability (De Sandre-Giovannoli et al. 2003; Eriksson et al. 2003). Our laboratory identified a role for telomere dysfunction in driving HGPS pathology (Aguado et al. 2019), demonstrating that patients-derived human primary fibroblasts and a HGPS mouse model present telomeric dysfunction, DDR activation and transcription of tdilncRNAs and tDDRNAs. ASOs against these RNA molecules block DDR activation at telomeres, reduce the proliferative defects caused by the expression of progerin and the entry into cellular senescence *in vitro*. Treatment with telomeric ASOs had a relevant effect also *in vivo*: indeed, they increased the proliferative capacity of HGPS patients' fibroblasts and significantly extended lifespan of the HGPS mice by improving tissue homeostasis and reducing inflammation (Aguado et al. 2019).

Telomeres can accumulate unrepaired DNA damage also during physiological aging (Fumagalli et al. 2012; Hewitt et al. 2012), that lead to persistent DDR activation and cellular senescence (Fumagalli et al. 2012; Rossiello et al. 2014). For this reason, we tested tASOs in a mouse model of accelerated ageing, which recapitulates many age-related conditions (Jaskelioff et al. 2011), because mice progressively shorten their telomeres at each generation due to the lack of Terc, the RNA component of telomerase (Blasco et al. 1997), a large ribonucleoprotein DNA polymerase, that elongates telomeres by *de novo* addition of TTAGGG DNA repeats at the chromosome ends (Greider and Blackburn 1985).

Two months old Terc $^{-/-}$ mice were systemically treated with intraperitoneal injections of tASOs, or an ASO with a control sequence, two times a week for one month in order to inhibit telomeric DDR. Mice were then sacrificed at 12 months of age and their organs were collected for analyses. The Terc$^{-/-}$ tissues from tASOs-treated mice were compared with mice treated with control-ASOs and with age-matched wild type mice. We focused our attention

on the analysis of lungs, bone marrow and spleen, since these mice recapitulate several features of human ageing, such as pulmonary fibrosis and anemia. The histochemical analysis on lung sections revealed that the control ASO-treated mice are characterized by increased markers of DNA damage, as γH2AX and 53BP1, and DDR activation, as the ATM substrate pKap1; tASOs treatment leaves unaffected the levels of γH2AX but causes a significant decrease of 53BP1 and pKap1, similarly to the wild type control animals. tASOs against the telomeric RNA transcripts not only prevent DDR activation at dysfunctional telomeres, but also structural degeneration and inflammation of tissues associated with ageing, ameliorating the phenotype of both pulmonary fibrosis and peripheral blood anemia. Taken together, these results make tASOs a powerful therapeutic tool to inhibit DDR in vivo and for the treatment of human ageing and age-related pathologies, due to their high sequence specificity in targeting tncRNAs.

5.2.3 The RNP approach as an alternative to the Cas9 lentiviral system

Finally, I have also optimized the protocols to deliver the RNP complex in my experimental model. The RNP complex is composed by the Cas9 endonuclease already assembled with the sgRNA targeting the GFP sequence. The advantage of using this system is the very fast DSB generation because it avoids the delay due to the integration, transcription and translation of the lentiviral system, allowing the introduction of a DSB in the sequence of interest within few minutes after the treatment. In addition, RNP seems to be the most attractive way to use Cas9 *in vivo* because it has been shown that its use further reduces the risks of insertional mutagenesis and it has a high efficiency and low off-targets (Mout et al. 2017). I have delivered the RNP complex both by transfection and electroporation in HeLa WT and GFP cells, but I was not able to detect the presence of the Cas9 protein by IF, probably because it is degraded very quickly (S. Kim et al. 2014). However, I was able to demonstrate the efficient delivery of the complex in the target cells following the induction of DNA damage, in terms of γH2AX and 53BP1 foci formation, in HeLa GFP cells treated with the GFP Cas9 (figures 33-34). In addition, I have also recapitulated some of the consequences of the DSBs generated with the lentiviral system: damaged HeLa GFP cells showed an increase in micronuclei production and in IL-6/IL-8 mRNA expression, suggesting an activation of inflammatory pathways. Even if I have detected a small percentage of micronuclei and the expression of IL-6 also in HeLa WT cells treated with the GFP Cas9, the effect is not comparable with the response of GFP cells to DNA damage generation, indicating a prompter reaction in the target cells, compared to controls (figure 35).

DNA damage induction, through γH2AX and 53BP1 foci formation, was achieved in HeLa GFP cells also by electroporating the RNP + GFP sgRNA complex, indicating that both the delivery methods are effectively transporting the endonuclease in the target cells (figure 36). These results have to be improved and the viability of RNP treated cells has to be studied, but these data suggest that the RNP complex could be a valid alternative to the lentiviral system in inducing sequence-specific DSBs and recapitulating the events that I have observed upon cut in HeLa GFP cells. Moreover, the rapidity by which the RNP complex can be delivered into the cells and starts cutting makes it a good candidate for being combined with the ASO treatment to characterize the effects of a sequence-specific DSB induction and repair inhibition.

5.2.4 Senolytics in combination with sequence-specific DSB induction

The generation of DSBs into the genome can induce a transient cell cycle arrest to allow the repair. If the damage is particularly severe, cells can undergo cell death or cellular senescence (d'Adda di Fagagna 2008).

In particular, senescence is a permanent arrest in proliferation caused by different cellular stresses, such as persistent DDR activation (Fumagalli et al. 2014). Senescent cells release inflammatory factors (SASP) and it has been shown that this can be due to the sensing by cGAS of cytosolic DNA that activates the stimulator of interferon genes (STING), supporting paracrine senescence (Glück et al. 2017).

I discovered that DSB generation by Cas9 induces the expression of inflammatory cytokines and chemokines through the cGAS pathway, similarly to senescent cells. It would be interesting to to test if also senescence markers like SA-β-galactosidase, p21 and p16 are expressed (Di Micco et al. 2021) and study if the combination of Cas9 with a senolytic like navitoclax, a Bcl-2 family protein inhibitor that binds to multiple anti-apoptotic Bcl-2 family proteins (Zhu et al. 2016), can further kill persistent damaged cells, compared to Cas9 treatment alone.

This could open two interesting biological questions: the first one is the possible synergy between the DSBs generated by Cas9 and the use of senolytics to kill damaged and senescent cells; the second one is the potential of Cas9 in inducing DNA damage in malignant cells and a consequent senescence state *in vivo*. In this case, senescent cells could release inflammatory factors that could attract immune cells for the clearance of the cells that are the target of the therapy (Childs et al. 2014).

To better characterize the possible effects of Cas9 in inducing senescence, I created another cell line named MCF10A GFP. Indeed, it is known that this cell line can enter in a senescence-like phenotype upon genotoxic stress (Maya-Mendoza et al. 2014). I infected MCF10A cells with the the pLenti-CMV-MCS-GFP-SV-puro lentiviral vector in order to introduce the promoterless GFP sequence and establish a stable cell line.

To have an estimate of how many copies of the GFP sequence have been integrated into the genome of these infected cells, I extracted genomic DNA MCF10A, both the WT and the GFP cell lines. I designed primers against the GFP sequence and I performed a real time-qPCR to detect the relative amounts of the GFP gene DNA compared to a single-copy gene as actin (figure 38A). Comparing the Ct of the GFP gene with the Ct of the actin gene, I estimated that around 16 copies of the pLenti-CMV-MCS-GFP-SV-puro Δpromoter lentiviral vector have been integrated per cell. FISH has validated this number also in MCF10A GFP cells, like in HeLa and RKO cells (see the results section). Also in this case the GFP copies seem to have been integrated at individual sites into the genome and not in cluster (figure 38B).

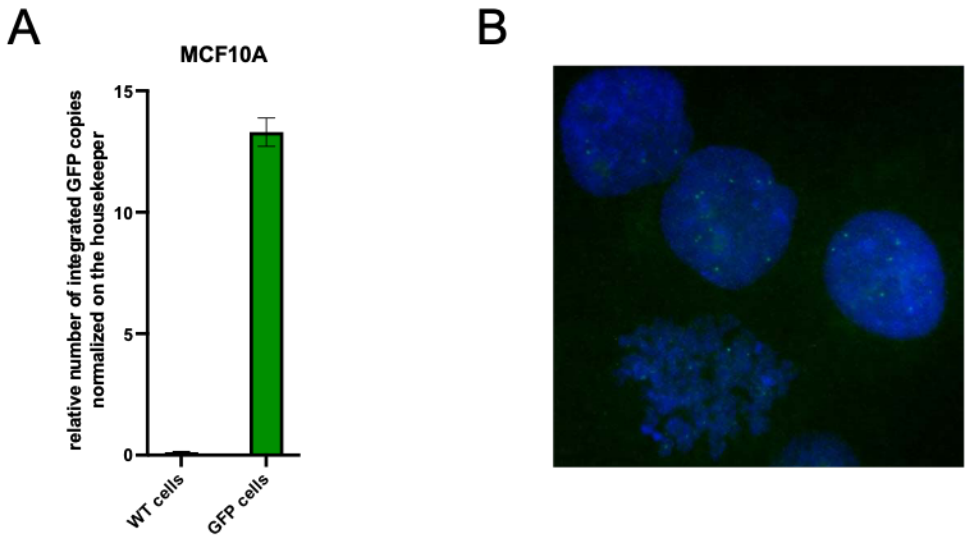

Figure 38. Generation of the MCF10A experimental system.
(A) Relative number of integrated GFP copies in MCF10A cells detected by qPCR, compared to actin. (B) A representative image of FISH signals showing the single integrations of the GFP sequence in the genome of MCF10A cells.

5.2.5 Immune checkpoint inhibitors in combination with Cas9-induced DSB

Chemotherapy is one of the main treatments against cancer and it includes DNA damaging drugs. Immunotherapy has recently emerged as an additional approach which include the use of inhibitors of immune checkpoint proteins like the programmed cell death protein-1

(PD-1) and the programmed death ligand-1 (PD-L1) (Sriram et al. 2021). PD-1 is a receptor commonly found on the surface of T cells and it involved in the regulation of autoimmunity; PDL-1, instead, it is found on different cells like macrophages, activated T and B cells, but it is also often overexpressed in tumor cells (Han, Liu, and Li 2020). The binding between PD-1 and PDL-1 allows the immune evasion of malignant cells; the blockage of the interaction between the two receptors by using specific antibodies is used as an antitumor activity because it enhances T cells response (Liu et al. 2021).

The upregulation of PDL-1 in cancer cells can be the consequence of the accumulation of somatic mutations due to defects in the DDR genes, thus generating neoantigens (Kakoti et al. 2020); other studies indicated that the overexpression is due to the DSBs generated by the DNA damaging agents used for the therapy because of the activation of DDR and the consequent stimulation of the STAT1/3-IRF1 pathways. It could explain why the combination of IR and immune checkpoint inhibitors promotes immunity against the tumor (Sato et al. 2017).

Another study has associated the effects of DNA damaging agents and immune checkpoint inhibitors to stimulate the immune system in killing cancer cells. DSBs induced in the tumor cells activate pathways like the DNA-PK, ATR, p38 signaling pathways that cause, together with other cellular processes not yet identified, the release of cytokines that boost the antitumor response by activating T cells (Sriram et al. 2021).

In addition to the pathways already cited, PD-L1 expression is controlled by the activator protein-1, a group of transcription factors that control a wide range of cellular processes and play an important role in different aspects of T cell activation and differentiation (Zerdes et al. 2018; Atsaves et al. 2019).

I observed, in the RNA-seq experiments, the activation of the AP-1 transcription factor in HeLa GFP cells upon Cas9-induced DNA damage. Indeed, it has been shown that cytokines like TNFα can activate AP-1 (Qiao et al. 2016). It would be interesting to validate if the inflammatory response caused by the DNA damage generated by Cas9 is sufficient to stimulate the AP-1 transcription factor and the consequent transcription of PD-L1. In that case, Cas9 could represent a novel DNA damaging agent that can induce the transcription of PD-L1 and can be combined with immune checkpoint inhibitors to kill malignant cells.

5.3 Future perspectives

Taken together, my experiments suggest the possibility of weaponizing the CRISPR/Cas9 system to selectively eliminate cells that have an aberrant genomic sequence. As a proof of concept, I created two model systems, based on the GFP sequence, to simulate cells infected

with multiple copies of an integrated proviral genome. I showed, in HeLa GFP cells, that the Cas9 cutting within the GFP sequence selectively kill cells with the target DNA sequence. Moreover, it activates DDR, generates cGAS-positive micronuclei that elicit an inflammatory response. Cas9-induced cell death was observed in both HeLa GFP and RKO GFP systems, strengthening my conclusions. In order to prove that this cascade of events is the consequence of the DNA damage induced by Cas9, I am planning to perform the same experiment by using a dead Cas9 able to bind the GFP sequence but not to cut it. In this way, I am expecting to demonstrate that cell death of target cells is not due to a Cas9 association with the target sequence, but to the effects caused by the actual DNA damage introduced by the nuclease.

Cas9-induced DSBs elicit an inflammatory response in HeLa GFP cells. Since cytokines and chemokines are molecules secreted by the cells in response to a stimulus, I am planning to further validate the expression of these molecules by performing a Bio-Plex assay, a bead-based multiplex immunoassay that allows the quantification of different cytokines simultaneously starting from few microliters of the supernatant of Cas9 treated cells.

The sequence-specific generation of DNA damage by Cas9 is able to reduce the proliferation of HeLa GFP cells and increase their death, compared to the undamaged conditions. I demonstrated that Cas9 produces a similar impact on the viability of RKO GFP cells; however, RKO cells express cGAS but they are defective for STING (Goedegebuure et al. 2021). It would be interesting investigating which mechanisms are stimulated in RKO GFP cells upon DSB induction by the endonuclease. It would help also in understanding which is the main type of programmed cell death that is activated upon Cas9-induced DNA damage. Indeed, I monitored cell viability and mortality in Incucyte, taking advantage of a dye that enters in cells that have lost membrane integrity; it allowed me to distinguish between alive and dead cells, but without providing indications about the cell death pathway involved.

I also observed that cells start dying three days upon lentivirally-delivered Cas9. To accelerate Cas9-induced cell death, I am testing if the RNP complex can be an alternative to the viral system: I delivered in HeLa cells the Cas9 endonuclease already assembled with the sgRNA targeting the GFP sequence by both transfection and electroporation; in this way, Cas9 can start introducing DSBs as soon as it enters the nucleus. DNA damage, in terms of γH2AX and 53BP1 foci formation, was efficiently generated in HeLa GFP cells treated with Cas9 and the GFP guide. I am planning to monitor if this system is able to recapitulate the effects caused by the DSBs generated with the lentiviral system.

Anyway, DSBs can be repaired with the insertion of mutations and the target site of Cas9 can be lost. I am investigating two possible ways to overcome this limitation. The first one is to increase the number of Cas9 targets. Indeed, I designed nine additional RNA guides

against different sites of the GFP sequence, in order to exacerbate the effects of Cas9-induced DNA damage. I monitored cell viability and mortality and I observed that the approach based on multiple guides did not implement the results obtained by using only one GFP guide. However, this system has to be further characterized: I have to verify if all the guides are cutting the GFP sequence with the same efficiency and if the different Cas9 associated with different RNA guides compete to bind and cut the DNA target.

The second way that I am investigating to increase the toxicity caused by the DNA damage induced by Cas9 is the combination of this DNA damaging agent with an inhibitor of DSB repair. I first demonstrated, both in HeLa and RKO GFP cells, combinatory effect of sequence-specific DSB induction by Cas9 and repair inhibition by DNA PKi. However, since DNA PKi is not a specific treatment because it can inhibit the repair of endogenous DNA damage, a sequence-specific DSB repair inhibitor is needed. For this reason, I started testing ASO against dilncRNAs transcribed from the break generated by Cas9 in the GFP sequence. I validated ASOs function in HeLa GFP cells by looking at 53BP1 foci formation upon Cas9-induced DNA damage. Excitingly, GFP ASO reduced the number of 53BP1 foci in cells treated with the Cas9 expressing the GFP guide, compared to cells treated with a control ASO and cells treated with the Cas9 expressing the scramble guide, showing that they can efficiently switch off DDR signaling. I am planning to investigate if the sequence-specific DSBs generation in the GFP sequence by Cas9 and the sequence-specific repair inhibition by GFP ASO can work together to kill GFP cells. If validated, these results could open the possibility to explore the therapeutic potential of a sequence-specific approach to kill cells carrying a genomic aberration that is the target of the treatments, while sparing normal cells.

6 Appendix

Impact of SARS-CoV-2 on DNA damage and repair

The severe acute respiratory syndrome coronavirus 2 (SARS-CoV-2) is the virus responsible for the coronavirus disease 2019 (COVID-19) pandemic and it is still affecting people's health after two years. Although vaccines are helping in containing the spreading of the virus and reducing the most severe symptoms of the disease, to date there are no treatments to cure the pathology and for this reason a better characterization of the mechanisms of action of the virus in human cells is necessary.

It has been reported that the coronavirus infectious bronchiolitis virus (IBV) activates the DNA damage response and arrests cell cycle of the host cells, because it causes replication stress due to the interaction of the viral protein NSP13 with the cellular DNA polymerase δ (Xu et al. 2011). Inspired by this study, in this last year and a half I worked to elucidate the impact of SARS-CoV-2 on DNA damage and DDR and I contributed to identify at least two ways by which the virus threatens genome integrity: it reduces dNTP levels and impairs DNA repair. Indeed, we discovered that SARS-CoV-2 infection is sufficient to cause DNA damage. We demonstrated it in two independent cell lines and in primary human nose epithelial cells infected with actual SARS-CoV-2 virus. We detected DNA damage by performing comet assays and analysing an extensive set of markers of DDR activation by quantitative immunoblots and at the single-cell level by immunofluorescence.

We investigated the possible mechanisms that lead to DNA damage generation and we demonstrated that SARS-CoV-2 cause the degradation of the CHK1 protein, and consequently of the ribonucleoside-diphosphate reductase subunit M2 (RRM2), involved in the conversion of rNTPs in dNTPs, and whose expression is controlled by CHK1.

I demonstrated the accumulation of γH2AX, $pRPA^{S4/8}$ and $pKAP1^{S824}$ foci, and the loss of CHK1 and RRM2 in infected cells, compared to controls, by immunofluorescence studies. Moreover, the decreased availability of dNTPs, that suggests an accumulation of rNTPs necessary to the virus for its own replication, leads to an altered S-phase progression, as I showed by flow cytometry. In addition, I observed induction of micronuclei, often stained positive for cGAS by IF, that triggers the expression of inflammatory cytokines.

I also noticed that, upon SARS-CoV-2 infection, the accumulation of γH2AX foci was not accompanied by colocalizing 53BP1 foci. We discovered that the SARS-CoV-2 N protein sequesters the cellular RNAs transcribed upon damage, impeding the recruitment of 53BP1 at the damaged DNA sites and interfering with their repair.

Most importantly, we recapitulated the main findings *in vivo*: in a SARS-CoV-2-infected mouse model (expressing the human ACE2) and in autoptic material from a cohort of human patients in which we analysed DDR events both in the lungs and in nose epithelia.
Taken together, these results can explain the inflammatory response observed in patients and complement the recent findings that indicate viral-induced cellular senescence (Lee et al. 2021).

SARS-CoV-2 infection causes DNA damage and an altered DNA damage response

Ubaldo Gioia[1,$], Sara Tavella[1,$], Pamela Martínez-Orellana[2], Andrea Colliva[2], Alessia Paldino[2], Marta Ceccon[1], Ettore Presot[3], Valeria Fumagalli[4], Matteo Cabrini[1], Valentina Matti[1], Federica Pisati[5], Giada Cicio[1,6], Sreejith Rajasekharan[2,#], Sara Sepe[1], Matilde Conte[1], Sara Barozzi[1], Zeno Lavagnino[1], Tea Carletti[2], Maria Concetta Volpe[2], Matteo Iannacone[4], Claudio Tripodo[1,6], Chiara Rampazzo[3], Rossana Bussani[7], Serena Zacchigna[2,7], Alessandro Marcello[2] and Fabrizio d'Adda di Fagagna[1,8].

[1]IFOM – the FIRC Institute of Molecular Oncology – 20139 Milan, Italy
[2]International Centre for Genetic Engineering and Biotechnology – 34149 Trieste, Italy
[3]University of Padova – Padova, Italy
[4]IRCCS San Raffaele Scientific Institute & University – 20132 Milan, Italy
[5]Cogentech Società Benefit srl –20139 Milan, Italy
[6]University of Palermo – 90133 Palermo, Italy
[7]University of Trieste – 34149 Trieste, Italy
[8]Institute of Molecular Genetics, National Research Institute (CNR) – Pavia, Italy.

[$]these authors contributed equally
[#]present address: Leibniz Institute for Experimental Virology (HPI) - 20251 Hamburg, Germany.

ABSTRACT

SARS-CoV-2 is the RNA virus responsible for the COVID-19 pandemic. Although several cellular pathways have been shown to be altered by SARS-CoV-2 infection, its impact on DNA integrity and the mechanisms involved are yet to be determined. Here we show that SARS-CoV-2 infection causes DNA damage and elicits a non-canonical activation of the damage response (DDR). SARS-CoV-2 gene products cause the reduction of the DDR kinase CHK1 and the consequent decrease of RRM2, part of the ribonucleotide reductase complex. This causes dNTP shortage and altered S-phase progression leading to DNA damage accumulation, cGAS activation and expression of proinflammatory cytokines. In addition, we show that SARS-CoV-2 N-protein, an abundant RNA binding protein, by competing with 53BP1 for the association with damage-induced long non-coding RNAs (dilncRNAs), impairs 53BP1 foci formation and reduces DNA repair by non-homologous end joining (NHEJ). Markers of DDR activation, in their altered form, are observed in the lungs of SARS-CoV-2-infected mice expressing human ACE2 and of COVID-19 patients.

We propose that SARS-CoV-2 infection, by boosting rNTP levels to promote its own replication at the expenses of dNTP, and by interfering with dilncRNAs biology, impacts on genome integrity causing DDR activation, activation of proinflammatory pathways and promoting cellular senescence.

INTRODUCTION

Severe acute respiratory syndrome coronavirus 2 (SARS-CoV-2) is a highly transmissible single-stranded RNA virus, responsible for the ongoing coronavirus disease 2019 (COVID-19) pandemic (V'kovski et al. 2021). Its 30 kb genome encodes for 26 polypeptides (SARS-CoV-2 reference genome, NC_045512.2) which include 16 non-structural proteins (NSPs) necessary for viral replication and transcription, 4 structural proteins like the nucleocapsid (N) and the spike (S) proteins required for virion assembly, and 6 accessory proteins involved in viral replication (Yang and Rao 2021).

Virus infections can impact several cellular pathways including the DNA damage response (DDR). While the interplay between DNA viruses and DDR has been studied in some detail (Lilley, Schwartz, and Weitzman 2007), the impact of RNA viruses is less known (Ryan, Hollingworth, and Grand 2016). For example, the coronavirus infectious bronchiolitis virus (IBV) was shown to activate DDR in a manner mediated by the viral protein NSP13 leading to cell cycle arrest (Xu et al. 2011). Although SARS-CoV-2 infection has been suggested to engage some components of the DDR machinery (Bouhaddou et al. 2020; Victor et al. 2021; Lipskaia et al. 2021; D'Agnillo et al. 2021), a thorough characterization and a mechanistic understanding of the interplay between SARS-CoV-2 and DDR is lacking.

The DDR is a network of pathways that sense DNA lesions, signal their presence and coordinate their repair (Jackson and Bartek 2009). Ruptures in the DNA, single-strand and double-strand breaks (SSBs and DSBs), are detected by replication protein A (RPA) and by the MRE11-RAD50-NBS1 (MRN) complex, respectively (Polo and Jackson 2011). Such factors guide the recruitment of the apical DDR kinases ataxia telangiectasia and Rad3-related (ATR) or ataxia-telangiectasia mutated (ATM) at SSBs or DSBs, respectively (Polo and Jackson 2011). ATR and ATM undergo autophosphorylation and, once activated, they phosphorylate several DDR factors, including the effector kinases CHK1 and CHK2, which, together with their phosphorylated targets, ultimately enforce cell-cycle arrest (Polo and Jackson 2011). DDR activation can cause cell death, cellular senescence (d'Adda di Fagagna 2008; Di Micco et al. 2021), inflammation (Rodier et al. 2009) and genome instability, which in turn can promote tumorigenesis (Jackson and Bartek 2009).

We have recently demonstrated that the induction of a DSB results in the local recruitment of a functional RNA Polymerase II complex that triggers the bi-directional transcription of a novel class of RNA molecules named damage-induced long non-coding RNAs (dilncRNAs) (Michelini et al. 2017; Pessina et al. 2019). These RNAs are necessary for the stable recruitment of DDR factors like p53-binding protein 1 (53BP1), with whom they interact, at the DSB in the form of foci (Michelini et al. 2017; Pessina et al. 2019). Inhibiting the synthesis or functions of dilncRNAs disrupts the assembly of DDR foci and impairs DNA repair by homologous recombination (HR) and non-homologous end-joining (NHEJ) (Michelini et al. 2017; Pessina et al. 2019; D'Alessandro et al. 2018). dilncRNAs support 53BP1 foci formation by promoting its liquid-liquid phase separation (LLPS) (Kilic et al. 2019; Pessina et al. 2019). Interestingly, also SARS-CoV-2 N-protein has been shown to phase-separate in a RNA-dependent manner (Savastano et al. 2020; Perdikari et al. 2020).

In the present study we show that SARS-CoV-2 infection causes DNA damage and the activation of a non-canonical DDR. This is associated with the degradation of the DDR kinase CHK1 and the loss of RRM2, a component of the ribonucleotide reductase complex (Naruyama et al. 2008), which leads to dNTP shortage and impaired S-phase progression, with consequent DNA damage accumulation, DDR activation and induction of inflammatory cytokines. In addition, we demonstrate that SARS-CoV-2 N-protein impairs 53BP1 recruitment at DSB by competing with dilncRNAs binding, ultimately reducing DNA repair by NHEJ. Finally, we show that these events occur *in vivo* in a mouse model of SARS-CoV-2 infection and in COVID-19 patients.

Overall our results may provide a mechanism for the inflammatory response observed in COVID-19 patients and the recently reported virus-induced cellular senescence (Lee et al. 2021).

RESULTS

SARS-CoV-2 infection causes DNA damage and non-canonical DDR activation in cultured human cells.

We studied the potential engagement of the DDR pathways at different time points upon infection by SARS-CoV-2 of human Huh7 cells by immunoblotting of whole cell lysates. As reference we used mock-infected cells and as positive controls we used cells treated either with hydroxyurea (HU), which induces DNA replication stress and activates the ATR-CHK1 axis (Koç et al. 2004; Shechter, Costanzo, and Gautier 2004), or with ionizing radiation (IR) that causes the formation of DSBs and mainly activates the ATM-CHK2 pathway (Jackson and Bartek 2009) (Fig. 1A). By the use of different phospho-specific antibodies, we observed

that SARS-CoV-2 infection triggered the autophosphorylation, and thus activation, of the master kinases DNA-PK (pDNA-PK^{S2056} – involved in DNA repair) and ATM (pATM^{S1981}) but not ATR (pATR^{T1989}) (Fig. 1A,B). Surprisingly however, CHK2, the direct downstream target of ATM kinase activity, was neither phosphorylated on its activating site (T68) nor showed an electrophoretic shift: this suggests an impaired signal transduction along the ATM-CHK2 axis (Fig. 1A,B). Similarly, CHK1, a kinase acting downstream of ATR, was not phosphorylated on S317. Differently, KAP1 (also known as TRIM28), a chromatin-bound ATM target, was strongly phosphorylated (pKAP1^{S824}) in SARS-CoV-2 infected cells (Fig. 1A,B). Also, P53 was not significantly phosphorylated on S15, a target site of ATM- and ATR-mediated phosphorylation (Fig. 1A,B). In addition, SARS-CoV-2 caused the robust phosphorylation of H2AX (γH2AX) and RPA (pRPA$^{S4/8}$), markers of DSB and SSB, respectively (Jackson and Bartek 2009) (Fig. 1A,B). All this was not associated with significant rates of apoptosis in these settings (Fig. S1A). Similar conclusions were reached upon a parallel analysis of Calu-3 human lung epithelial cells infected by SARS-CoV-2 (Fig. S1B,C).

To confirm and extend at single-cell resolution the impact of SARS-CoV-2 infection on DDR activation, we performed quantitative immunofluorescence analyses of the same samples described above. We observed increased numbers of DDR foci per cell of γH2AX, pRPA$^{S4/8}$ and pKAP1^{S824} in infected compared to mock-infected cells (Fig. 1C,D).

Elevated pRPA$^{S4/8}$ and γH2AX signals observed in infected cells is a strong indication of DNA damage accumulation. To directly monitor the impact of SARS-CoV-2 on physical DNA integrity, we performed comet assays in infected or mock-infected Huh7 cells. We observed more DNA fragmentation in SARS-CoV-2-infected cells compared to control cells, as measured by tail moment analyses (Fig. 1E,F).

Nuclear DNA damage released in the cytoplasm can be sensed by the cGAS-STING pathway that, when activated, triggers an inflammatory response (Harding et al. 2017). We therefore investigated whether cGAS-STING and the inflammatory pathways were elicited in cultured cells upon SARS-CoV-2 infection. To do so, we used SARS-CoV-2 infected or mock-infected Calu-3 cells, as the Huh7 cell line does not express neither cGAS or STING (Thomsen et al. 2016). By immunofluorescence analyses, we appreciated increased cGAS dotted signals in infected Calu-3, indicating that the cGAS-STING pathway was indeed engaged by SARS-CoV-2 infection (Fig. S1D,E). In addition, infected cells exhibited a higher number of micronuclei, which also stained positive for cGAS (Fig. S1D,E), suggestive of the release of damaged nuclear DNA in the cytosol following infection.

Next, we monitored by RT-qPCR the impact of DNA damage accumulation and cGAS-STING activation on the transcriptional induction of pro-inflammatory response genes in

SARS-CoV-2-infected or mock-infected Calu-3. Our analyses revealed a significant upregulation of mRNA expression of *IL6*, *IL8*, *CXCL10* and *TNFα* genes in the infected samples (Fig. S1F).

In sum, these results indicate that SARS-CoV-2 infection generates nuclear DNA damage that activates different components of the DDR pathways, however in a non-canonical manner, suggesting a potential interference by viral gene products in this process. Such virus-induced genome instability engages the cGAS-STING pathway and promotes pro-inflammatory cytokines expression.

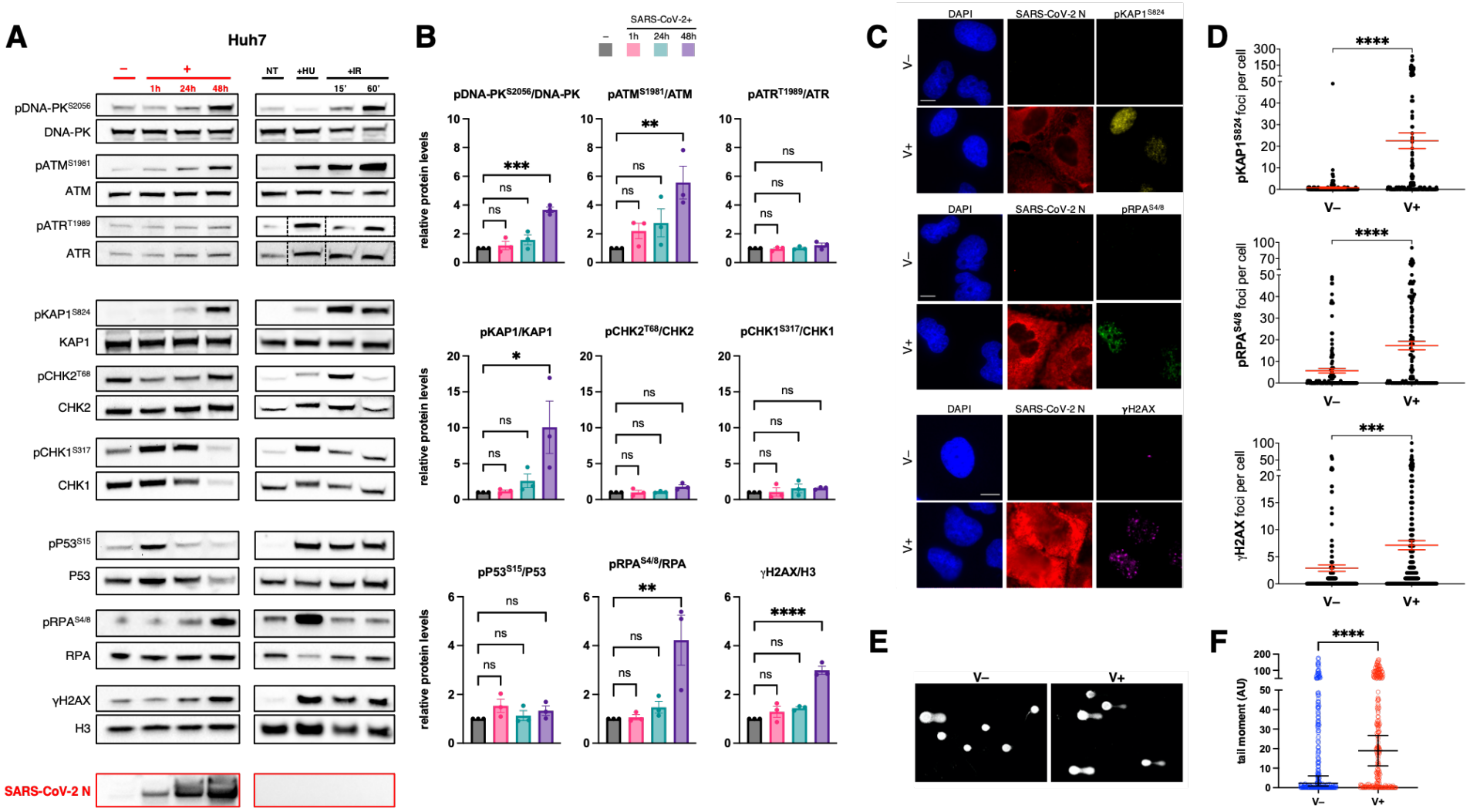
A
Huh7
–
+
1h
24h
48h
NT
+HU
+IR
15'
60'
pDNA-PK S2056
DNA-PK
pATM S1981
ATM
pATR T1989
ATR
pKAP1 S824
KAP1
pCHK2 T68
CHK2
pCHK1 S317
CHK1
pP53 S15
P53
pRPA S4/8
RPA
γH2AX
H3
SARS-CoV-2 N
B
SARS-CoV-2+
–
1h
24h
48h
pDNA-PK S2056/DNA-PK
pATM S1981/ATM
pATR T1989/ATR
pKAP1/KAP1
pCHK2 T68/CHK2
pCHK1 S317/CHK1
pP53 S15/P53
pRPA S4/8/RPA
γH2AX/H3
relative protein levels
ns
C
DAPI
SARS-CoV-2 N
pKAP1 S824
pRPA S4/8
γH2AX
V–
V+
D
pKAP1 S824 foci per cell
pRPA S4/8 foci per cell
γH2AX foci per cell
****
***
E
F
tail moment (AU)

Figure 1

SARS-CoV-2 infection causes DNA damage and non-canonical DDR activation. A) Immunoblotting of whole cell lysates of Huh7 cells infected, or not, with SARS-CoV-2 analyzed by immunoblotting at different time points post-infection for markers of DDR activation. Lysates from Huh7 cells not-treated (NT) or treated with 6 mM hydroxyurea (HU) or exposed to 2 Gy ionizing radiation (IR) and collected at different time points were used as positive controls. Viral replication was monitored by probing for SARS-CoV-2 N protein. **B**) Quantification of activated protein levels shown in A. Values are means ± s.e.m. of three independent infections and normalized to mock-infected samples. **C**) Representative immunofluorescence (IF) images of SARS-CoV-2 infected (V+) or mock-infected (V-) Huh7 cells fixed at 48 h post-infection and stained for DDR markers. SARS-CoV-2 N protein was used to label infected cells. Nuclei were stained with DAPI. Scale bar = 10 μm. **D**) Quantification of DDR activation shown in C. Each dot is a nucleus. Horizontal red bars are the means ± s.e.m. of three independent infections – at least 100 cells per condition were scored. **E**) Images of comet assays of mock- and virus-infected Huh7 cells. **F**) Quantification of comet tail moment shown in E. Horizontal black bars represent the median values ± 95% CI of three independent infections – at least 80 cells per condition for each biological replicate were scored.

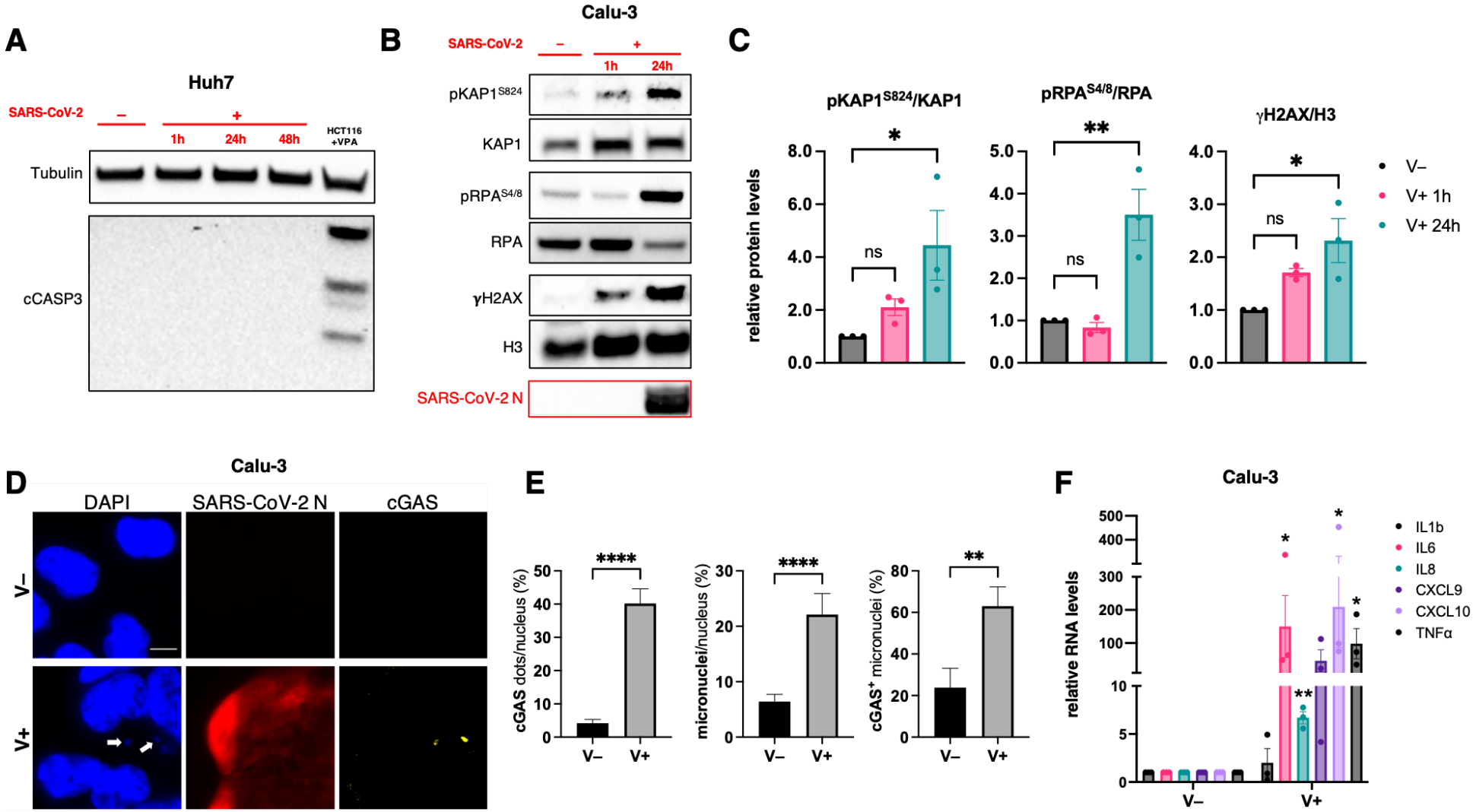
A
Huh7
SARS-CoV-2
–
+
1h
24h
48h
HCT116 +VPA
Tubulin
cCASP3
B
Calu-3
SARS-CoV-2
–
+
1h
24h
pKAP1S824
KAP1
pRPAS4/8
RPA
γH2AX
H3
SARS-CoV-2 N
C
pKAP1S824/KAP1
pRPAS4/8/RPA
γH2AX/H3
relative protein levels
ns
*
**
V–
V+ 1h
V+ 24h
D
Calu-3
DAPI
SARS-CoV-2 N
cGAS
V–
V+
E
cGAS dots/nucleus (%)
micronuclei/nucleus (%)
cGAS+ micronuclei (%)
****
**
V–
V+
F
Calu-3
relative RNA levels
IL1b
IL6
IL8
CXCL9
CXCL10
TNFα
V–
V+

Figure S1

A) Cleaved Caspase-3 (cCASP3) analysis by immunoblotting of whole lysates of Huh7 cells infected or not with SARS-CoV-2 at different time points. Lysates from HCT116 treated with valproic acid (VPA) were analyzed as a positive control for apoptosis activation. Probing for tubulin was used as a loading control. **B**) Validation of the activation of the key DDR markers by immunoblotting of whole lysates of Calu-3 cells infected or not with SARS-CoV-2 at different time points. Viral replication was monitored by probing for SARS-CoV-2 N protein. **C**) Quantification of protein levels from infected Calu-3 shown in B; values are the means ± s.e.m. of three independent infections and shown as relative to mock-infected samples. **D**) Representative images of 24 h infected or mock-infected Calu-3 cells stained for cGAS and N-protein. **E**) Quantification of cGAS activation and micronuclei induction shown in D: values are the means ± s.e.m. of three independent experiments; at least 100 cells were scored for each sample; arrows point to $cGAS^+$ micronuclei (scale bar = 10 μm). **F**) Analysis of the expression of pro-inflammatory cytokines by RT-qPCR in total RNA from 24 h infected (V+) or mock-infected (V-) Calu-3 cells. Values are the averages ± s.e.m. of three independent experiments and shown as relative to mock-infected samples.

SARS-CoV-2 infection causes decreased CHK1 and RRM2 protein levels and dNTPs shortage.

While studying individual DDR proteins activation, we noticed that CHK1 protein amounts progressively decreased upon infection in both Huh7 and Calu-3 cells (Fig. 1A, 2A-C and S2A,B). CHK1 protein level was affected mainly post-transcriptionally, as its mRNA did not decrease significantly (Fig. S2C,D). CHK1 loss has been shown to be sufficient to cause DNA replication stress and DNA damage accumulation (González Besteiro et al. 2019). Noteworthy, besides its functions in DDR, CHK1 has been reported to control the expression of the Ribonucleoside-diphosphate Reductase Subunit M2 (RRM2), the small subunit of the ribonucleotide reductase (RNR) enzyme that converts rNTPs into dNTPs, which are necessary for DNA synthesis (Naruyama et al. 2008; Zhang et al. 2009). We thus tested RRM2 mRNA and protein levels by RT-qPCR, immunoblotting and immunofluorescence. We consistently observed that RRM2 mRNA and protein levels progressively and significantly decreased following SARS-CoV-2 infection in all our tests (Fig. 2A-C and S2A-D).

Then, to address if RRM2 loss observed in infected cells caused an actual decrease in dNTP availability, we directly measured individual dNTP concentrations in SARS-CoV-2 infected or mock-infected Huh7 and Calu-3 cell lines. Our analyses revealed that SARS-CoV-2 infection indeed reduces the levels of cellular dNTPs (Fig. 2D).

Inhibition or depletion of RRM2 and the consequent dNTP shortage can prevent DNA synthesis, ultimately hampering S-phase progression (Koç et al. 2004; Naruyama et al. 2008). To monitor cell cycle progression following SARS-CoV-2 infection, we measured DNA content in infected or mock-infected cells by propidium iodide staining followed by

flow cytometry analysis. Interestingly, we observed that the percentage of cells in S-phase significantly increased in SARS-CoV-2-infected cells with respect to control samples (Fig. 2E,F) – this was confirmed by strongly reduced levels of CDT1, a marker of G1-phase which is rapidly degraded in S-phase (Higa et al. 2003; Hu et al. 2004; Sansam et al. 2006) (Fig. S2E,F). We additionally pulse-labelled cells with BrdU for 1 h prior to flow cytometry. We observed an increased percentage of BrdU-negative cells in S-phase in SARS-CoV-2-infected samples (Fig. 2G). These results demonstrate an impaired S-phase progression following infection.

We then probed which viral gene product could be responsible for CHK1 downregulation. We therefore individually expressed in Huh7 cells 24 of the 26 annotated SARS-CoV-2 proteins (Gordon et al. 2020) (SARS-CoV-2 reference genome, NC_045512.2) and analysed their impact on CHK1 levels by immunoblotting and immunofluorescence. Among the SARS-CoV-2 gene products tested, ORF6 and NSP13 were the factors with the strongest impact on CHK1 protein levels (Fig. 2H,I and S2G). Of note, the expression of these viral factors also reduced RRM2 levels and caused increased γH2AX and RPA phosphorylation (S4/8) (Fig. 2J,K).

Overall, these results are consistent with a model in which SARS-CoV-2 gene products cause CHK1 loss, which reduces RRM2 levels and consequently the pool of available dNTPs, impairing DNA replication and proper S-phase progression. Defects in DNA replication following SARS-CoV-2 infection may subsequently lead to DNA damage accumulation, ultimately exacerbating the inflammatory response.

CHK1 loss is sufficient to reduce RRM2 levels, cause DNA damage and contribute to inflammation.

To determine a causative role of CHK1 for RRM2 altered expression and DNA replication defects, we depleted CHK1 in Huh7 cells by RNA interference and studied their cell-cycle profile by flow cytometry. Consistent with previous reports (Naruyama et al. 2008), we observed that cells knocked down for CHK1 accumulate in S-phase (Fig. 3A,B and S3A). Moreover, by pulse-labelling CHK1-depleted cells with BrdU for 1 h prior to flow cytometry analysis, we observed a much higher fraction of BrdU-negative cells compared to control samples (Fig. 3C). This indicates that CHK1-depleted cells fail to complete S-phase, recapitulating the phenotypes observed in SARS-CoV-2 infected cells (Fig. 2G).

Next, we examined RRM2 protein levels in CHK1 knocked-down (siCHK1) and control (siCTRL) cells. We observed that CHK1 depletion was sufficient to reduce RRM2 levels and cause DNA damage, as indicated by increased $pRPA^{S4/8}$ and γH2AX signals, and

activation of P38/MAPK and STAT1 pathways (Fig. 3D,E). Notably, SARS-CoV-2 infection also strongly elicited both P38 and STAT1 cascades (Bouhaddou et al. 2020) (Fig. S3B). These results suggest that CHK1 depletion, by triggering P38/MAPK and STAT1 signalling, could contribute to the activation of the pro-inflammatory pathways. Therefore, to investigate the effects of CHK1 loss on inflammation, we transfected Calu-3 cells with siCHK1 or siCTRL and analysed by RT-qPCR the mRNA levels of pro-inflammatory cytokines. We observed that CHK1-depleted Calu-3 cells displayed higher levels of *IL1b, IL6*, *CXCL9, CXCL10* and *TNFα* mRNAs (Fig. 3F), indicating that lack of CHK1 may be sufficient to trigger an inflammatory response.

In sum, CHK1 loss is sufficient to recapitulate some events observed in SARS-CoV-2-infecetd cells such as RRM2 reduction and impaired S-phase progression, and to activate inflammatory pathways.

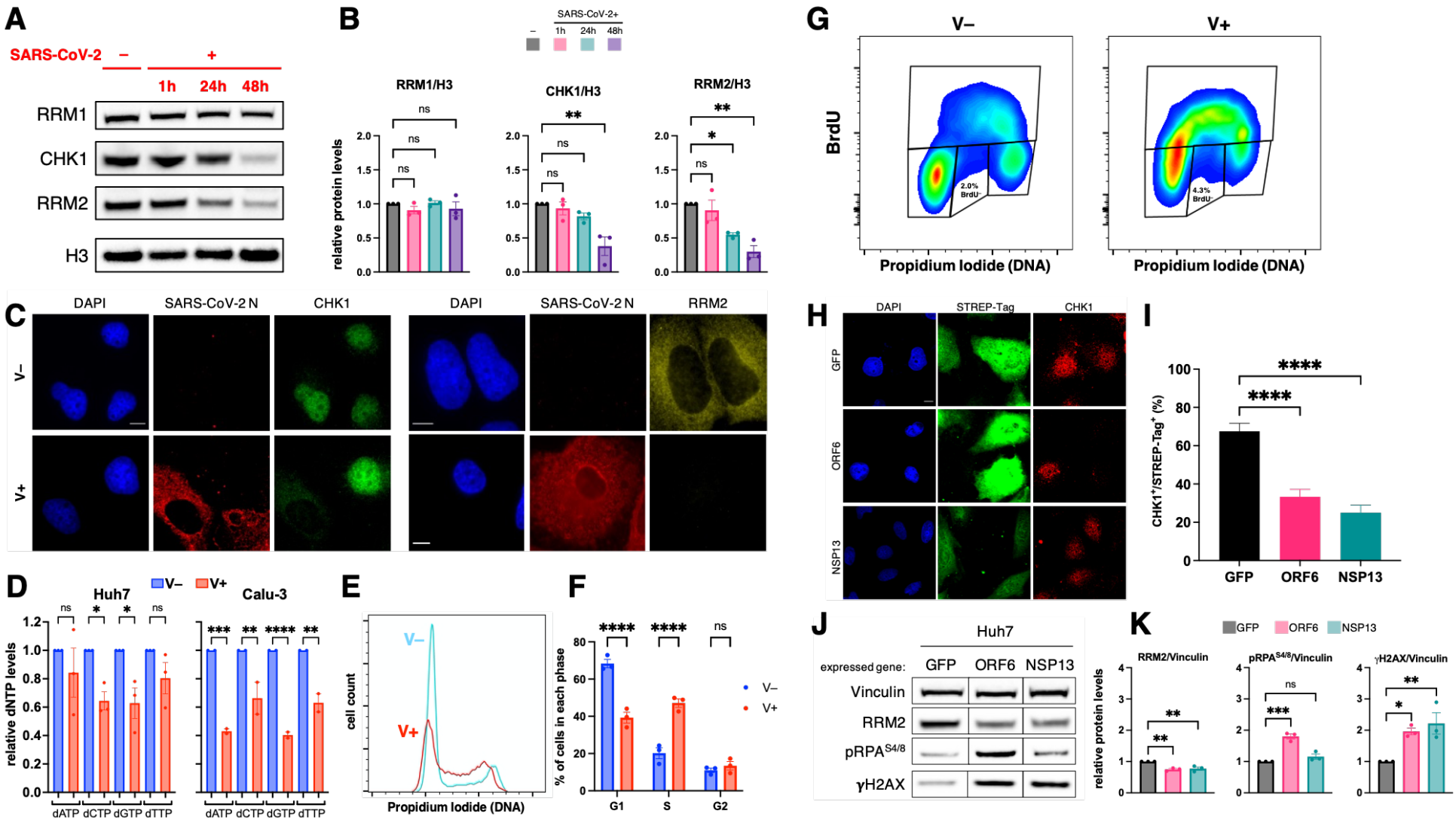
A
SARS-CoV-2 – +
1h 24h 48h
RRM1
CHK1
RRM2
H3
B
SARS-CoV-2+
– 1h 24h 48h
RRM1/H3
CHK1/H3
RRM2/H3
relative protein levels
ns
**
*
C
DAPI
SARS-CoV-2 N
CHK1
RRM2
V–
V+
D
Huh7
Calu-3
V–
V+
relative dNTP levels
dATP dCTP dGTP dTTP
E
cell count
V–
V+
Propidium Iodide (DNA)
F
% of cells in each phase
G1
S
G2
G
V–
V+
BrdU
Propidium Iodide (DNA)
2.0% BrdU+
4.3% BrdU+
H
DAPI
STREP-Tag
CHK1
GFP
ORF6
NSP13
I
CHK1+/STREP-Tag+ (%)
GFP
ORF6
NSP13
****
J
Huh7
expressed gene:
GFP
ORF6
NSP13
Vinculin
RRM2
pRPA S4/8
γH2AX
K
GFP
ORF6
NSP13
RRM2/Vinculin
pRPA S4/8/Vinculin
γH2AX/Vinculin
relative protein levels

Figure 2

SARS-CoV-2 infection reduces CHK1 and RRM2 levels ultimately leading to dNTP shortage. **A**) Representative immunoblots on total protein lysates of SARS-CoV-2 infected Huh7 cells collected at the indicated time points post-infection. **B**) Histograms show the densitometric analyses of RRM1, CHK1 and RRM2 protein amounts normalized on H3 levels; values are the averages ± s.e.m. of three independent infections and shown as relative to mock-infected cells. **C**) Selected images of SARS-CoV-2 (V+) infected or mock-infected (V-) Huh7 cells fixed at 48 h post-infection and stained for CHK1 (green), RRM2 (yellow) and SARS-CoV-2 N protein (red); nuclei were counter-stained with DAPI (blue) (scale bar = 10 μm). **D**) dNTP concentration was measured in 48 h and 24 h infected or mock-infected Huh7 (left) and Calu-3 (right) cell lines, respectively. Values are the means ± s.e.m. of at least two independent infections and shown as relative to mock-infected samples. **E**) cellular DNA content measured by flow cytometry in propidium iodide (PI)-stained infected- or mock-infected Huh7 cells fixed 48 h post-infection. **F**) Graphical representation of cell cycle phase distributions shown in E; values are the means ± s.e.m. of three independent infections. **G**) Bivariate plot showing DNA content (PI staining) and BrdU incorporation measured by flow cytometry in infected- or mock-infected Huh7 cells fixed at 48 h post-infection. **H**) Representative images of Huh7 cells expressing 2xStrep-tagged SARS-CoV-2 ORF6, NSP13 or GFP as a control, fixed at 48 h post-transfection and stained with anti-Strep-tag (green) and anti-CHK1 (red) antibodies; nuclei were stained with DAPI (blue) (scale bar = 10 μm). **I**) Histograms showing the percentage of CHK1-expressing cells ($CHK1^{+}$) among transfected ones (STREP-Tag+) as determined in H; values are the averages ± s.e.m. of three independent experiments; at least 75 cells were scored for each condition. **J**) Analysis of RRM2, $pRPA^{S4/8}$ and γH2AX levels by immunoblotting of whole lysates obtained from Huh7 cells transfected with plasmids expressing the indicated SARS-CoV-2 proteins. **K**) Quantification of protein amounts shown in J and normalized over vinculin: values are the means ± s.e.m. of three independent transfections; cells expressing GFP were used as a reference.

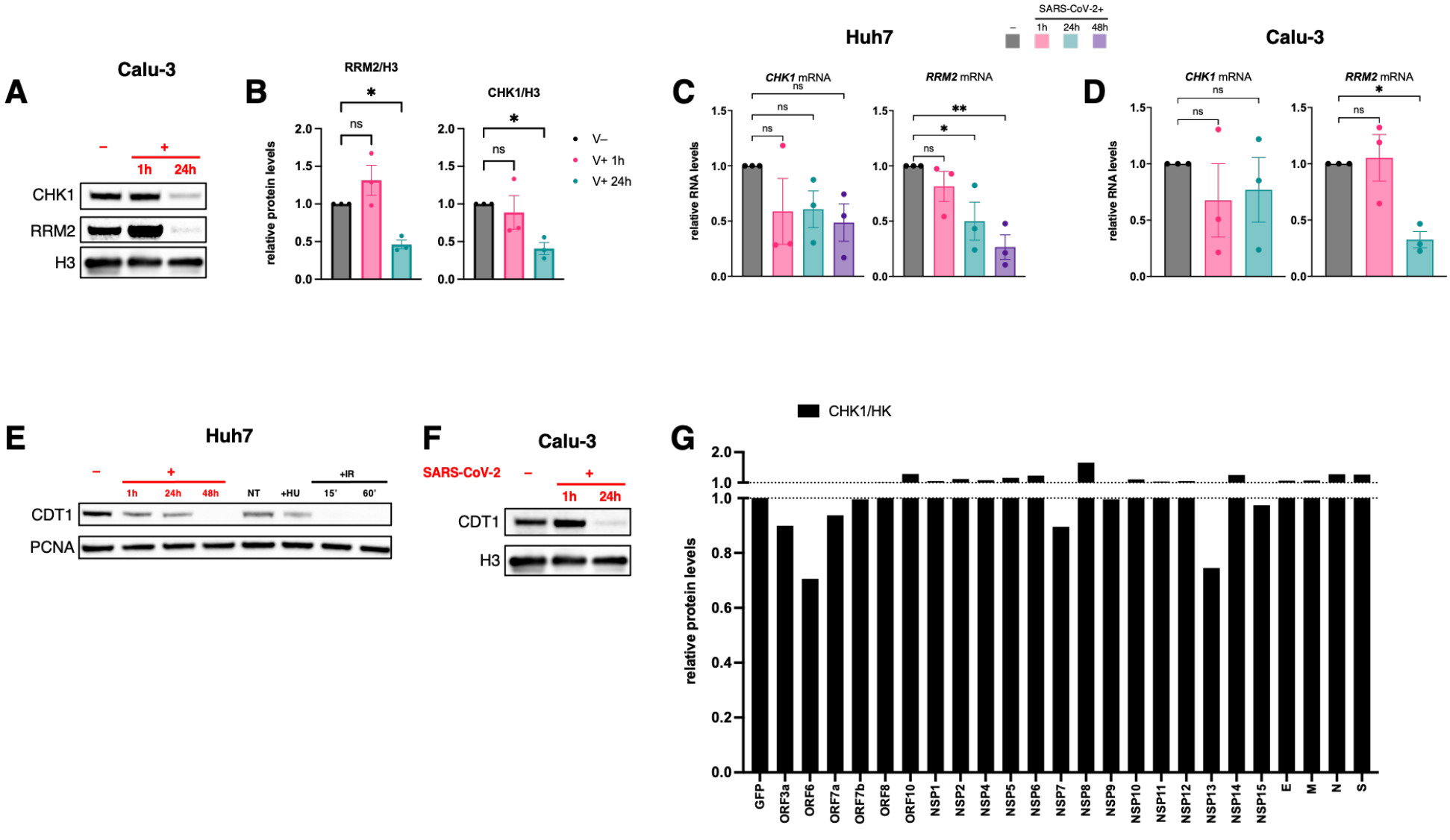
A
Calu-3
–
+
1h
24h
CHK1
RRM2
H3
B
RRM2/H3
CHK1/H3
relative protein levels
ns
*
V–
V+ 1h
V+ 24h
C
Huh7
SARS-CoV-2+
1h
24h
48h
CHK1 mRNA
RRM2 mRNA
relative RNA levels
**
D
Calu-3
E
Huh7
NT
+HU
+IR
15'
60'
CDT1
PCNA
F
Calu-3
SARS-CoV-2
H3
G
CHK1/HK
relative protein levels
GFP
ORF3a
ORF6
ORF7a
ORF7b
ORF8
ORF10
NSP1
NSP2
NSP4
NSP5
NSP6
NSP7
NSP8
NSP9
NSP10
NSP11
NSP12
NSP13
NSP14
NSP15
E
M
N
S

Figure S2

A) Representative immunoblots of protein lysates from Calu-3 cells infected with SARS-CoV-2 at the indicated time points (hours). **B**) Histograms show the densitometric analysis of the protein amounts normalized over H3 levels; values are relative to mock-infected cells and represented as the averages ± s.e.m. of three independent infections. **C,D**) Profiling of *CHK1* and *RRM2* mRNA expression by RT-qPCR in infected (V+) or mock-infected (V-) Huh7 and Calu-3 cells, respectively, at the indicated time points post-infection; values are the means ± s.e.m. of three independent infections. **E**) CDT1 analysis by immunoblotting of the samples shown in Figure 1A. **F**) CDT1 analysis by immunoblotting of the samples shown in A. **G**) Histograms represent the densitometric analysis of CHK1 protein levels as detected by immunoblots of Huh7 cells transfected with the plasmids encoding for the indicated SARS-CoV-2 proteins; values are normalized to either vinculin or β-actin protein amounts (house-keeper, HK) and shown as relative to the control-sample expressing GFP.

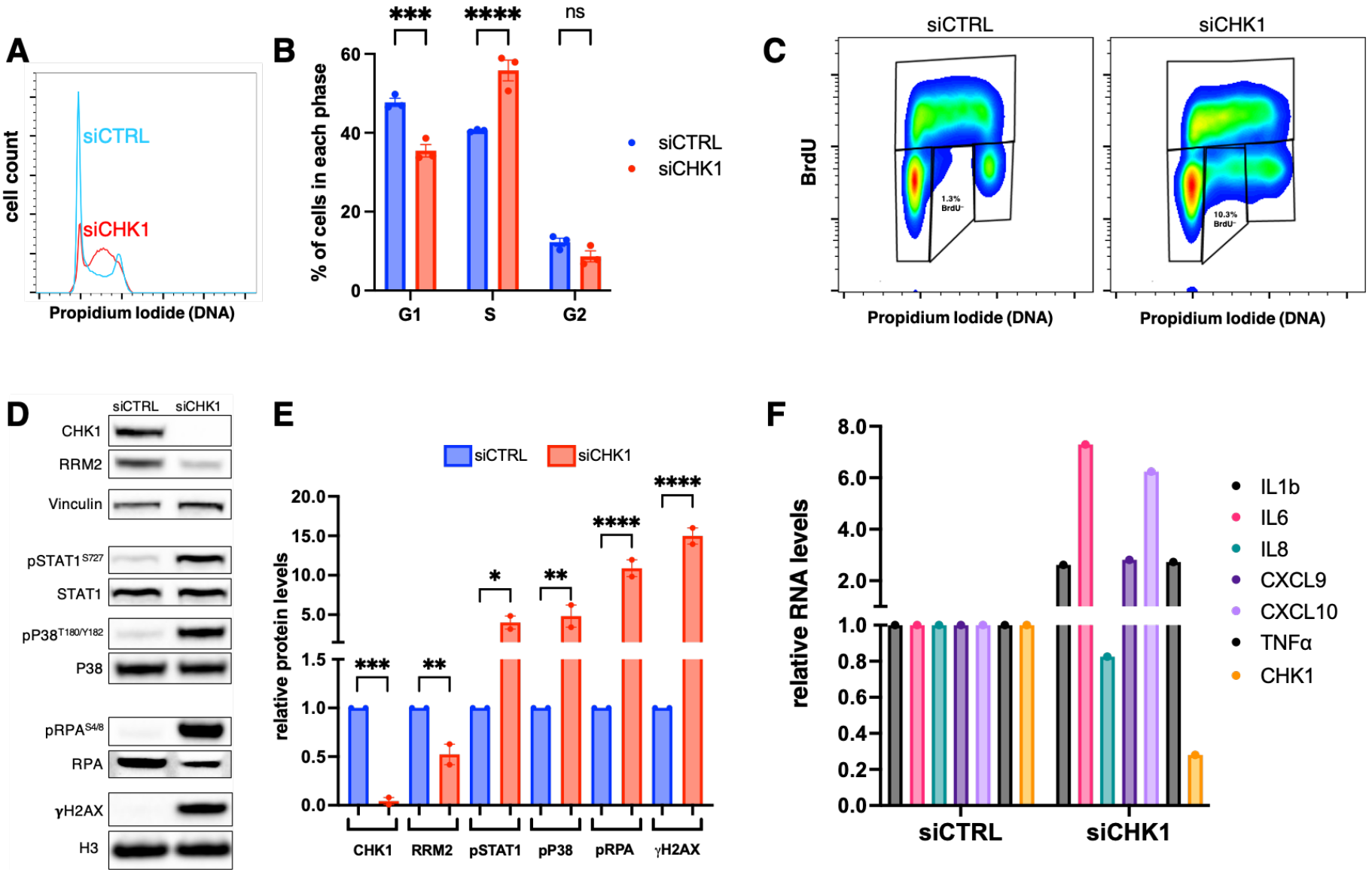
A
cell count
siCTRL
siCHK1
Propidium Iodide (DNA)
B
***
****
ns
% of cells in each phase
60
40
20
0
G1
S
G2
siCTRL
siCHK1
C
siCTRL
siCHK1
BrdU
1.3%
BrdU-
10.3%
BrdU-
Propidium Iodide (DNA)
Propidium Iodide (DNA)
D
siCTRL
siCHK1
CHK1
RRM2
Vinculin
pSTAT1 S727
STAT1
pP38 T180/Y182
P38
pRPA S4/8
RPA
γH2AX
H3
E
siCTRL
siCHK1
relative protein levels
20.0
15.0
10.0
5.0
1.5
1.0
0.5
0.0
***
**
*
**
****
****
CHK1
RRM2
pSTAT1
pP38
pRPA
γH2AX
F
relative RNA levels
8.0
6.0
4.0
2.0
1.0
0.8
0.6
0.4
0.2
0.0
siCTRL
siCHK1
IL1b
IL6
IL8
CXCL9
CXCL10
TNFα
CHK1

Figure 3

CHK1 loss is sufficient to reduce RRM2 levels, cause DNA damage and induce pro-inflammatory cytokines expression. A) Huh7 cells were transfected with siRNAs against *CHK1* mRNA (siCHK1) or with a non-targeting siRNA (siCTRL) and stained for propidium iodide prior to flow cytometry analysis. **B**) Histograms show the percentage of cells in each phase of the cell cycle; values are the means ± s.e.m. of three independent experiments. **C**) Samples in A were pulse-labelled with BrdU for 1 hour prior to bivariate analysis by flow cytometry. **D**) Representative immunoblots of protein lysates from Huh7 cells transfected with siCHK1 or siCTRL. **E**) Densitometric analyses of the protein levels shown in D. Values are the means ± s.e.m. of two independent experiments and shown as relative to the siCTRL-transfected sample. **F**) Study by RT-qPCR of the expression of the indicated pro-inflammatory cytokines in Calu-3 depleted for CHK1 (siCHK1). Values are relative to siCTRL-transfected cells.

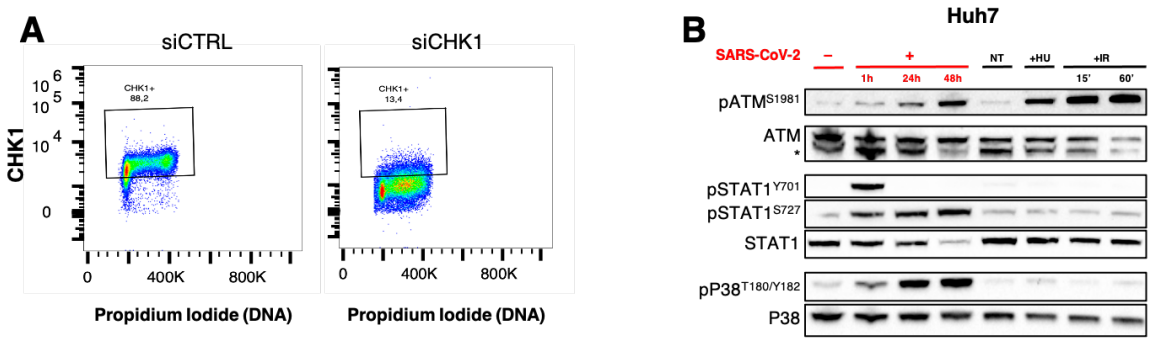

Figure S3

A) Samples described in Figure 3A were stained for CHK1 and propidium iodide prior to flow cytometry analysis. **B**) Immunoblots for the indicated proteins and protein phosphorylation events from samples described in Figure 1A. The asterisk marks an unspecific signal.

SARS-CoV-2 N disrupts 53BP1 recruitment at DSB and inhibits DNA repair by NHEJ.

While characterizing the non-canonical DDR triggered by SARS-CoV-2 infection (Fig. 1A-D), we noticed that γH2AX foci accumulation was not accompanied by co-localizing 53BP1 foci in both Huh7 and Calu-3 cell lines (Fig. 4A-B and S4A,B) – despite unaltered protein levels (Fig. S4C). To strengthen this conclusion, we infected human primary nasal epithelial cells (HNEpC). We confirmed that SARS-CoV-2 infection causes γH2AX foci accumulation, supporting the notion of DNA damage generation also in primary cells setting; however, also here we did not observe 53BP1 foci formation (Fig. 4C-D).

SARS-CoV-2 nucleocapsid (N) protein is an RNA-binding protein that plays critical roles in viral replication and it is capable to undergo RNA-dependent liquid-liquid phase separation (LLPS) (Chen et al. 2020; Perdikari et al. 2020; Savastano et al. 2020; S. Wang et al. 2021; Jia Wang et al. 2021). Intriguingly, 53BP1 also phase-separates in an RNA-dependent manner (Pessina et al. 2019). We thus transiently expressed the viral N-protein gene (Gordon et al. 2020) into Huh7 cells and 48 h later we exposed them to ionizing radiations. We observed that irradiated cells expressing SARS-CoV-2 N, despite increased numbers of γH2AX foci per cell had fewer 53BP1 foci compared to control cells (Fig. 4E,F). To reduce the possibility of an indirect effect of N-protein mediated by altered gene expression, we generated purified recombinant SARS-CoV-2 N-protein and micro-injected it into the nuclei of irradiated U2OS cells that stably express 53BP1-GFP (Bekker-Jensen et al. 2005) to study the kinetics of 53BP1 foci by live-imaging within minutes after injection. We observed 53BP1 foci number decreasing with a faster (~8.5-fold) kinetic in cells injected with the N-protein compared to control cells injected with BSA (Fig. 4G and S4D), strongly

indicating that viral N-protein directly impairs 53BP1 focal accumulation at DNA damage sites.

Next, we sought to elucidate the molecular mechanisms underlying N-protein impact on 53BP1 functions. In co-immunoprecipitation experiments 53BP1 did not seem to biochemically interact with N-protein (Fig. S4E). Damage-induced long non-coding RNAs (dilncRNAs) generated at DSB drive LLPS of 53BP1 (Michelini et al. 2017; Pessina et al. 2019). Intriguingly, both viral and cellular RNAs have been reported to associate with SARS-CoV-2 N-protein and promote its phase separation (Jia Wang et al. 2021) – indeed we observed that recombinant N-protein undergoes LLPS *in vitro* with RNA from uninfected or SARS-CoV-2 infected cells to a similar extent, as determined in turbidity assays (Fig. S4F). We therefore asked if SARS-CoV-2 N associates with cellular dilncRNAs. To test this, we performed RNA immuno-precipitation (RIP) against the N-protein in NIH2/4 cells which we previously characterized for the expression of dilncRNAs upon site-specific DSB induction by expression of I-SceI endonuclease and can be profiled by RT-qPCR(F Michelini et al. 2017). Therefore, following SARS-CoV-2 N gene expression into NIH2/4 cells and DSB induction through I-SceI expression, we immunoprecipitated the N-protein and analysed the associated RNAs by RT-qPCR. We observed that immunoprecipitated SARS-CoV-2 N-protein was associated with dilncRNA upon DSB generation, but not with the mRNA encoding for H2AX used as a negative control (Fig. 4H). Next, we immunoprecipitated endogenous 53BP1 in cut (+ I-SceI) NIH2/4 cells expressing or not the viral N-protein, and monitored dilncRNAs association to 53BP1. We observed that 53BP1 association with dilncRNAs was significantly reduced in cells expressing SARS-CoV-2 N protein, compared to cells transfected with an empty vector (Fig. 4I). Notably, such reduced binding was not due to reduced 53BP1 protein levels or its immunoprecipitation efficiency following N-protein overexpression (Fig. S4G). Since 53BP1 plays important DNA repair functions through non-homologous end-joining (NHEJ) (Zimmermann and De Lange 2014), we tested the impact of SARS-CoV-2 N protein in NHEJ. To study that, we took advantage of a U2OS cell line bearing an integrated GFP construct flanked by two I-SceI recognition sites (EJ5-GFP) (Gunn and Stark 2009). Following I-SceI expression, DSBs are generated at these sequences and repair through NHEJ can be examined by qPCR on genomic DNA (gDNA) with primers flanking the re-joined site (Gioia et al. 2019). Thus, EJ5-GFP U2OS were transfected with a plasmid expressing a HA-tagged version of I-SceI together with a vector encoding for the N-protein or an empty control vector. 72 hours post-transfection, gDNA was collected and analysed by qPCR. We observed that NHEJ efficiency in cells expressing SARS-CoV-2 N-protein was decreased compared to control samples (Fig. 4J). Such reduction was comparable to that previously observed by depleting 53BP1 in similar

settings (Shamanna et al. 2016; Gioia et al. 2019; Pessina et al. 2019). Importantly, the expression of SARS-CoV-2 N did not affect I-SceI levels (Fig. S4H). Overall, these results show that SARS-CoV-2 N-protein interferes with 53BP1 focus formation at DSBs and impairs DNA repair by NHEJ.

In sum, these results indicate that SARS-CoV-2 N competes with 53BP1 for dilncRNAs binding, and thus reduces 53BP1 focus forming ability at sites of DNA damage, ultimately hampering DNA damage repair.

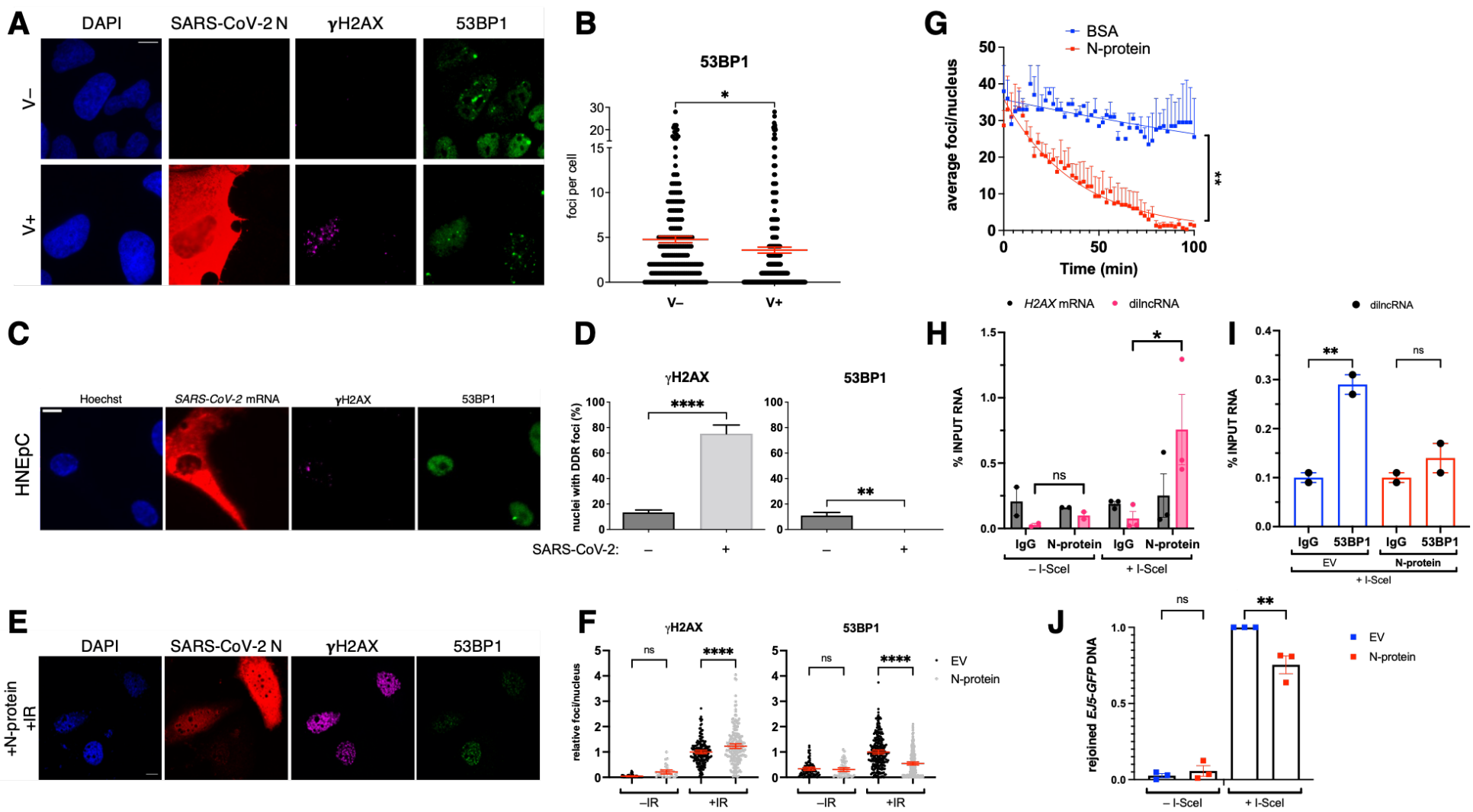
A
DAPI
SARS-CoV-2 N
γH2AX
53BP1
V–
V+
B
53BP1
foci per cell
V–
V+
G
BSA
N-protein
average foci/nucleus
Time (min)
C
Hoechst
SARS-CoV-2 mRNA
γH2AX
53BP1
HNEpC
D
γH2AX
53BP1
nuclei with DDR foci (%)
SARS-CoV-2:
H
H2AX mRNA
dilncRNA
% INPUT RNA
IgG
N-protein
– I-SceI
+ I-SceI
I
dilncRNA
% INPUT RNA
IgG
53BP1
EV
N-protein
+ I-SceI
E
DAPI
SARS-CoV-2 N
γH2AX
53BP1
+N-protein +IR
F
γH2AX
53BP1
relative foci/nucleus
–IR
+IR
EV
N-protein
J
rejoined EJ5-GFP DNA
– I-SceI
+ I-SceI
EV
N-protein

Figure 4

SARS-CoV-2 N protein suppresses 53BP1 activation and inhibits repair by NHEJ. A) Representative immunofluorescence images of SARS-CoV-2 infected (V+) or mock-infected (V–) Huh7 cells stained for N-protein (red), γH2AX (magenta) and 53BP1 (green); nuclei were counter-stained with DAPI (blue) (scale bar = 10 μm). **B**) Quantification of 53BP1 foci pictured in A: each dot represents the number of 53BP1 foci per nucleus; horizontal red bars are the averages ± s.e.m. of three independent infections; at least 100 cells were scored in each condition. **C**) Image of infected cultured primary nasal epithelial cells in which SARS-CoV-2 mRNA detected by FISH is shown in red and DDR foci are detected by immunostaining against γH2AX (magenta) and 53BP1 (green); nuclei were counter-stained with Hoechst (blue). **D**) Quantification of DDR activation shown in C: the histograms show the percentage of nuclei with DDR foci (> 1) in cells expressing (+) or not (–) SARS-CoV-2 mRNA. **E**) Images of irradiated Huh7 cells expressing the viral N-protein: samples were stained for N-protein (red), γH2AX (magenta) and 53BP1 (green) at 1 h post-IR; nuclei were counter-stained with DAPI (blue) (scale bar = 10 μm). **F**) Quantification of DDR foci shown in E: the dot-plots show the number of γH2AX or 53BP1 foci per nucleus in samples transfected with a plasmid expressing N-protein (grey dots) or with an empty vector (EV) as control (black dots). Values are relative to irradiated cells transfected with EV; red bars represent the averages ± 95% CI of three independent experiments; at least 100 cells were scored for sample. **G**) Purified recombinant viral N-protein or BSA were microinjected into the nuclei of irradiated 53BP1-GFP U2OS cells. 53BP1 focus formation over time were visualized and quantified in injected cells. The graph shows the foci count per nucleus over time in the presence of N-protein or BSA as a control; error bars represent s.e.m.; the experiment was repeated three times with similar results. **H**) NIH2/4 cells expressing or not I-SceI were transfected with a vector encoding for the viral N-protein. Whole cell lysates were incubated with anti-N-protein or with normal rabbit IgG and co-precipitated RNA analyzed by strand-specific RT-qPCR. *H2AX* mRNA was used as an unrelated transcript. Values are shown as percentage of input RNA and represent the means ± s.e.m. of at least two independent experiments. **I**) Endogenous 53BP1 was immunoprecipitated from cut NIH2/4 cells (+ I-SceI) transfected with a plasmid expressing the N-protein or with an empty vector (EV) as a control. The levels of transcripts bound to 53BP1 were monitored as in H and shown as percentage of input RNA. Values are the average ± s.e.m. of two independent experiments. **J**) EJ5-GFP U2OS cells were transfected with a plasmid expressing N-protein or with an empty vector (EV) along with or without a construct expressing I-SceI (± I-SceI). DSB re-joining events were evaluated by qPCR with primers spanning I-SceI cut sites carried out on gDNA isolated at 72 h post-transfection. Values are relative to I-SceI transfected cells not expressing N-protein and represented as the means ± s.e.m. of three independent experiments.

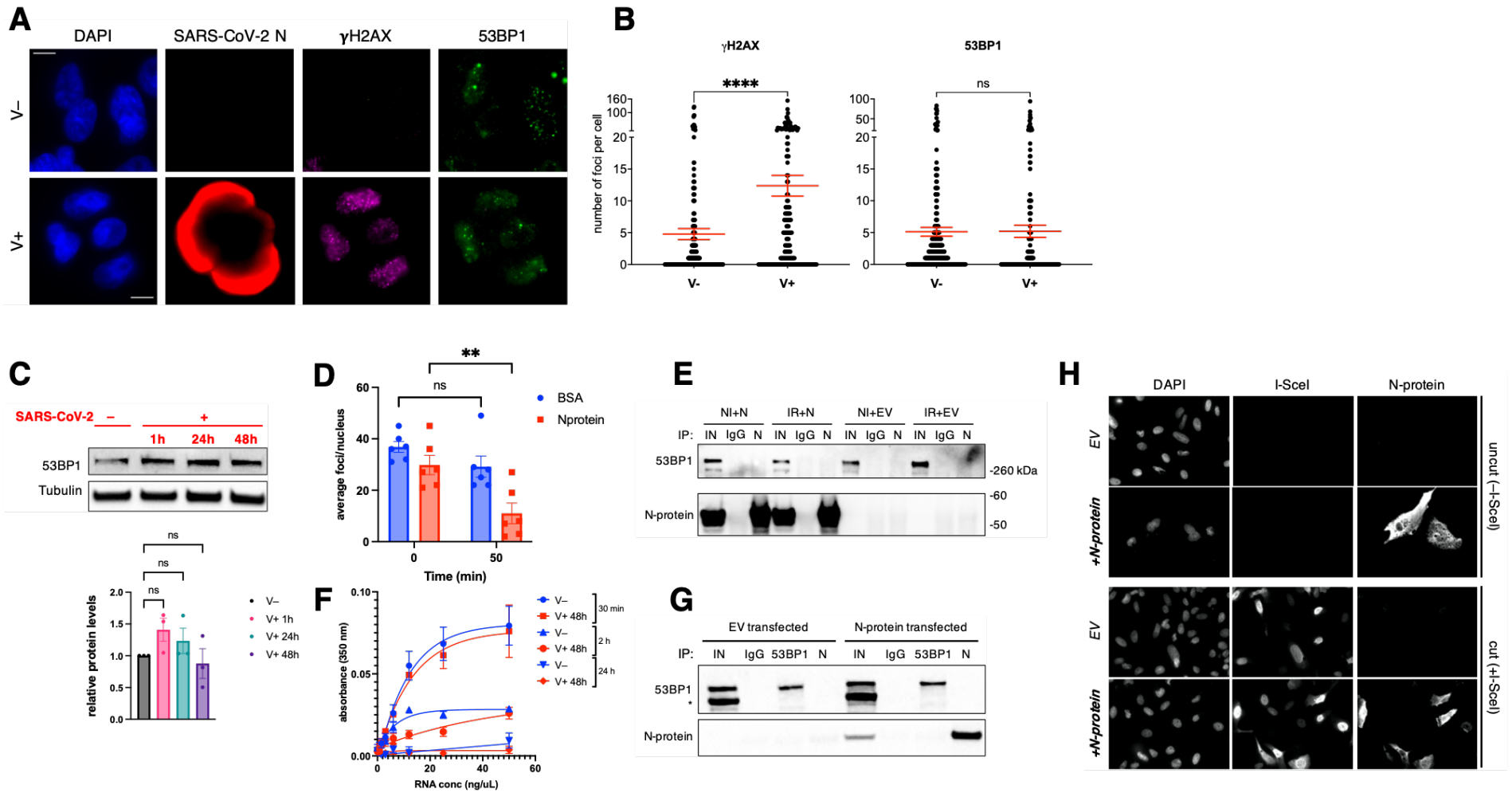
A
DAPI
SARS-CoV-2 N
γH2AX
53BP1
V–
V+
B
γH2AX
53BP1
****
ns
number of foci per cell
V-
V+
C
SARS-CoV-2
1h
24h
48h
53BP1
Tubulin
ns
relative protein levels
V–
V+ 1h
V+ 24h
V+ 48h
D
**
ns
BSA
Nprotein
average foci/nucleus
Time (min)
E
NI+N
IR+N
NI+EV
IR+EV
IP:
IN IgG N
53BP1
N-protein
-260 kDa
-60
-50
F
absorbance (350 nm)
RNA conc (ng/uL)
30 min
2 h
24 h
G
EV transfected
N-protein transfected
IP:
IN IgG 53BP1 N
53BP1
N-protein
H
DAPI
I-SceI
N-protein
EV
+N-protein
uncut (–I-SceI)
cut (+I-SceI)

Figure S4

A) Selected immunofluorescence images of SARS-CoV-2 infected (V+) or mock-infected (V–) Calu-3 cells; cells were stained for N-protein (red), γH2AX (magenta) and 53BP1 (green); nuclei were counter-stained with DAPI (blue) (scale bar = 10 μm). **B**) Quantification of DDR foci represented in A: the dot-plots show the number of γH2AX or 53BP1 foci per nucleus; horizontal red bars are the averages ± s.e.m. of three independent infections; at least 100 cells were scored in each sample. **C**) Analysis of 53BP1 protein expression by immunoblot on whole lysates from infected Huh7 samples shown in Figure 1A; tubulin was used as a loading control. The histograms below show the quantification of total 53BP1 levels; values are the means ± s.e.m. of three independent infections and shown as relative to mock-infected samples. **D**) Quantification of 53BP1 foci in irradiated 53BP1-GFP U2OS cells upon micro-injection of purified recombinant N-protein or BSA as control: the graph shows 53BP1 foci number per nucleus immediately (0 min) or 50 min after micro-injection; bars represent the means ± s.e.m. of three independent experiments. **E**) Total protein lysates of Huh7 cells transfected with a plasmid encoding SARS-CoV-2 N or with an empty vector (EV), which were either irradiated (IR) or not irradiated (NI), were incubated with an anti-N-protein antibody (IP: N) or with normal rabbit IgGs (IgG) and analysed by immunoblotting for the presence of 53BP1; samples were fractionated along with 1% of input lysates (IN). **F**) Turbidity associated with N-protein phase separation in presence of increasing concentrations of RNA from SARS-CoV-2 infected (V+ 48 h) or mock-infected (V–) Huh7 cells: the graph shows quantifications of solution's turbidity, measured by absorbance at 350 nm, upon incubation at RT for 30 min, 2 h, or 24 h; data points represent the means ± s.e.m. of three replicates. **G**) Evaluation of immunoprecipitation efficiency of the RIP experiments shown in Figure 4H,I: 10% of lysates, incubated with either an anti-53BP1 (IP: 53BP1), -N-protein (N) or with normal rabbit IgGs (IgG), was analyzed by immunoblot for 53BP1 or N-protein levels along with 1% input lysates (IN). **H**) Representative immunofluorescence images of samples described in Figure 4J: fixed cells were stained for viral N-protein and for I-SceI using an anti-HA-tag antibody; nuclei were counter-stained with DAPI.

SARS-CoV-2 infection causes DNA damage *in vivo* in mouse models and in COVID-19 patients.

We next sought to validate and extend our conclusions *in vivo*. We thus investigated markers of DDR activation in lung tissues of mice expressing human ACE2 (hACE2) upon infection by intranasal administration of SARS-CoV-2 (Fig. S5A,B) – wild type mice treated with PBS or exposed to IR were used as negative and positive control for DDR activation, respectively. Lung tissues from infected mice were stained for γH2AX and 53BP1 and showed strong γH2AX focal signals compared to mock-infected subjects. Instead, 53BP1 foci did not augment (Fig. 5). These results, consistent with our observations in cultured cells (Fig. 4A-D), indicate that SARS-CoV-2 infection causes DNA damage accumulation but, differently from IR (Fig. 5), does not lead to 53BP1 focal accumulation.

As SARS-CoV-2 infection has been recently shown to induce cellular senescence and contribute to inflammation *in vivo* (D'Agnillo et al. 2021; Lee et al. 2021; Lipskaia et al. 2021), we asked if DNA damage accumulation observed in infected mice correlated with the

induction of senescence markers in their lungs. We therefore probed the same tissues for p16 and p21, two markers of senescence, and found that both factors increased in infected murine lungs (Fig. S5C,D). Interestingly however, induced p21 expression was detected almost exclusively in pneumocytes and in the bronchial epithelium of the infected lungs, while p16 induction was associated with inflammatory cells populating the lung parenchyma of SARS-CoV-2 infected mice (Fig. S5C,D).

We also analyzed human samples from postmortem lungs and nasal mucosa of COVID-19 patients for γH2AX signals. We first considered a series of 31 lungs from patients who died with a clinical diagnosis of COVID-19, determined as a positive naso-pharyngeal swab or bronchoalveolar lavage during their last hospitalization (Bussani et al. 2020). In these samples we performed fluorescence in situ hybridization (FISH) or immunohistochemistry (IHC) to confirm the presence of SARS-CoV-2 mRNA and proteins (N and S), respectively. Out of 31 patients, 17 turned positive for either viral mRNA or viral proteins, while 14 were negative. We observed that the presence of γH2AX nuclear foci was significantly higher in lung epithelial cells of COVID-19 individuals that stained positive by either FISH or IHC for SARS-CoV-2 (COVID-19+), compared to patients that stained negative for the presence of SARS-CoV-2, or to subjects not diagnosed for the pathology (non-COVID) (Fig. 6A and S6A). We also performed the same analyses in samples of nasal mucosa from the same patients. We analyzed 29 samples (2 mucosae could not be harvested), out of which 18 reacted positively for SARS-CoV-2. In this case, the presence of γH2AX nuclear foci was almost exclusively detected in the nasal epithelium infected by SARS-CoV-2, as very few foci were detected in samples that scored negative for viral RNA and proteins, and no foci were evident in non-COVID mucosae (Fig. 6B and S6B). Then, to probe at the cell level the correlation between γH2AX levels and viral infection, we extended the analyses in the lung and nasal mucosa tissues of COVID-19 patients by probing for both γH2AX and the presence of SARS-CoV-2 genome. We observed that epithelial cells positive for SARS-CoV-2 mRNA exhibited a much higher number of γH2AX foci with respect to cells not infected by the virus (Fig. 6C-D), providing an additional strong correlation between viral infection and DNA damage generation.

Furthermore, we monitored the levels of RRM2 in three lung and three nasal mucosal tissues of patients who scored positive for SARS-CoV-2 mRNA and we observed that RRM2 expression was invariably and significantly lower in the infected epithelial cells compared to the not infected ones, consistent with our observations in cultured cells (Fig. 6E,F and Fig. 2C).

Overall, these results indicate that SARS-CoV-2 infection causes an altered DDR activation in both mouse and human lungs and in human nasal mucosae.

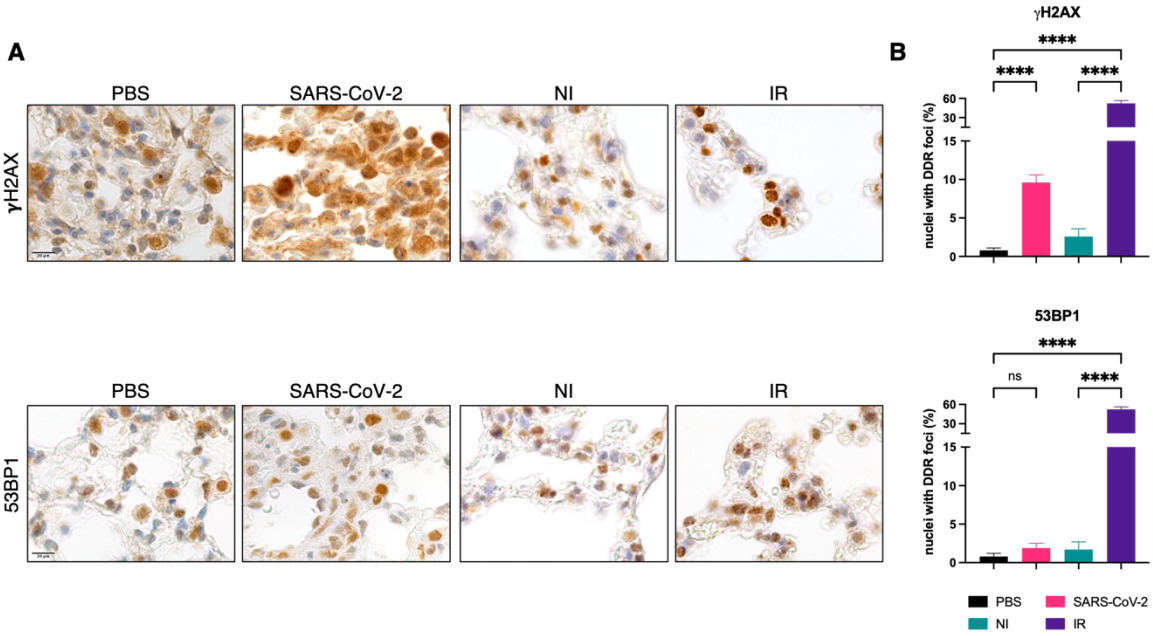

Figure 5

SARS-CoV-2 infection causes DNA damage in *hACE2*-mouse lungs. A) Representative immunohistochemical images of lungs from SARS-CoV-2 infected *hACE2*-mice or mock-infected (PBS) wild-type mice that were stained for either γH2AX or 53BP1; lungs from irradiated (IR) or not irradiated (NI) wild-type mice were analyzed as controls of DDR activation. Scale bar = 20 μm. **B**) Quantification of cells with DDR foci (>1) as in A: values are the means ± s.e.m.; at least 500 cells were scored for each set.

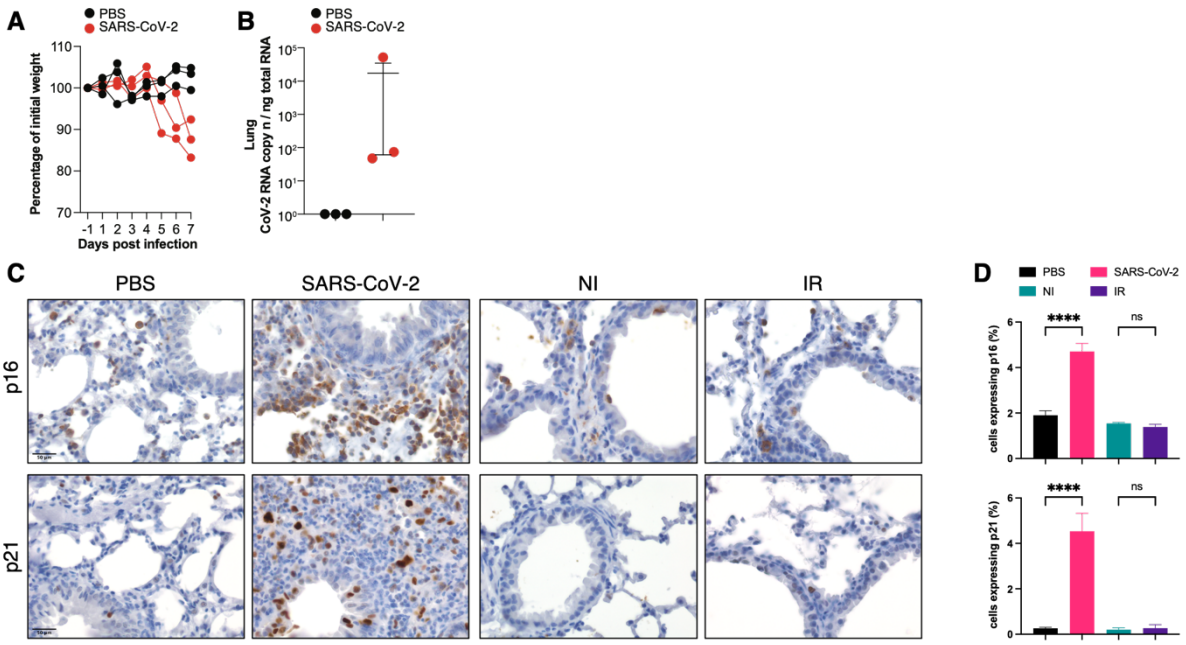

Figure S5

SARS-CoV-2 infection triggers markers of cellular senescence in *hACE2*-mouse lungs. A) Mouse body weight was monitored daily for up to 7 days and expressed as the percentage of weight relative to the initial weight on day 0. Single values of PBS-control mice (black dots) and infected mice (red dots) are represented. **B**) Quantification of SARS-CoV-2 RNA in the lung of PBS control mice and infected mice measured 7 days post infection. RNA values are expressed as copy number per ng of total RNA. Data are expressed as means ± s.e.m. **C**) Selected immunohistochemical images of lungs from SARS-CoV-2 infected *hACE2*-mice or mock-infected (PBS) wild-type mice probed for p16 or p21; lungs from irradiated (IR) or not (NI) wild-type mice were also analyzed. **D**) Quantification of the fraction of p16 or p21 positive cells determined in C. Scale bar = 50 µm. Statistics as in Figure 5B.

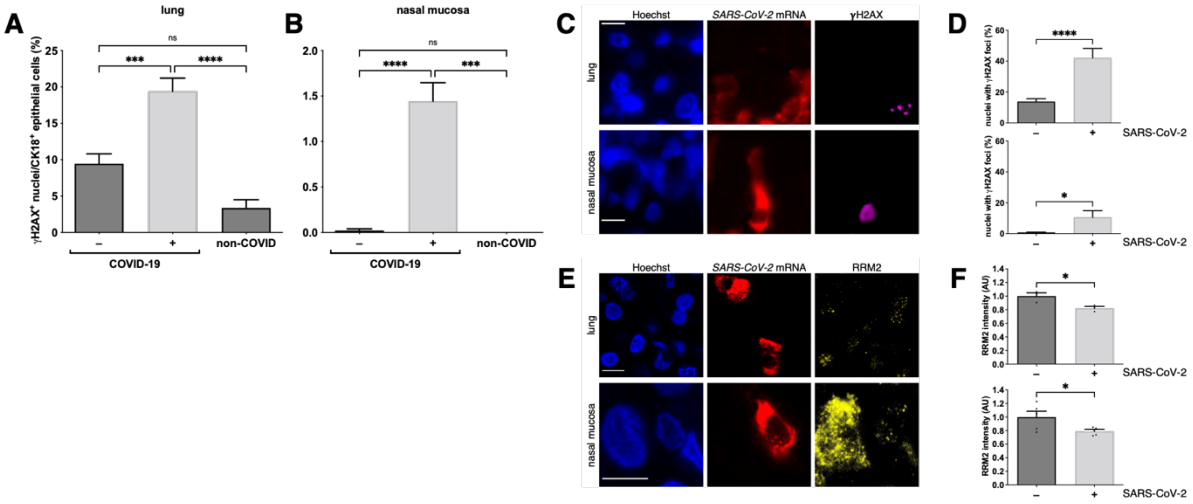

Figure 6

SARS-CoV-2 infection induces DNA damage in COVID-19 patients. A) Quantification of DNA damage in COVID-19 patients: histograms show the percentage of epithelial cells bearing γH2AX foci (> 1) in lungs of patients diagnosed for COVID-19 detected negative (–, n = 14) or positive (+, n = 17) for the presence of SARS-CoV-2; the same tissues from patients with no diagnosis of COVID-19 (non-COVID, n = 9) were analyzed as controls. **B**) Quantification of DNA damage as in A in the nasal tissue; between 5 and 18 individuals were studied per each group. **C**) Selected images of lung and nasal mucosal tissues of COVID-19 patients stained for SARS-CoV-2 mRNA (red) and γH2AX (magenta). Nuclei were counter-stained with Hoechst (blue). **D**) Quantification of γH2AX foci as in C: the histograms show the percentage of nuclei with γH2AX foci (> 1) in epithelial cells containing (+) or not (–) SARS-CoV-2 mRNA; n = 17. **E**) Representative images of lung and nasal tissues of COVID-19 patients stained for SARS-CoV-2 mRNA (red) and RRM2 (yellow). Nuclei were counter-stained with Hoechst (blue). **F**) Quantification of RRM2 levels determined in E: the graph shows the intensity of RRM2 signal in epithelial cells non-infected (-) or infected (+) with SARS-CoV-2; values are relative to uninfected cells; n = 18.

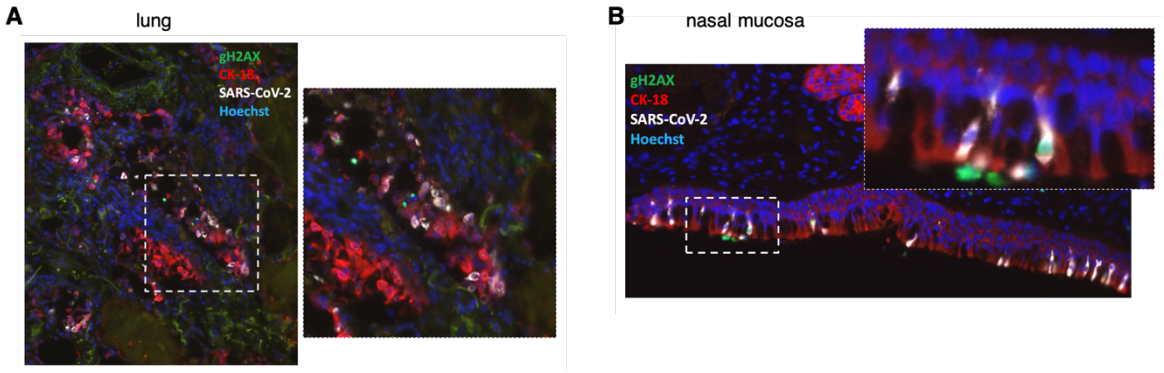

Figure S6

A,B) Representative images of lung and nasal mucosal tissues, respectively, of COVID-19 patients stained for γH2AX (green), CK-18 (red) and SARS-CoV-2 mRNA (white). Nuclei were counter-stained with Hoechst (blue).

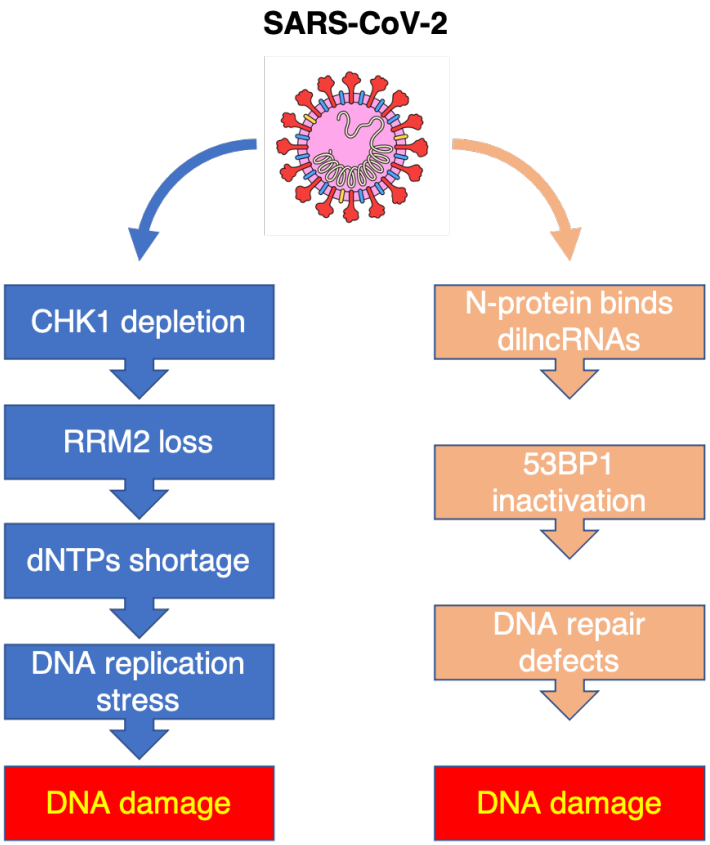

Figure 7

Schematic model of the impact of SARS-CoV-2 infection on genome integrity.

DISCUSSION

Viruses are known to hijack cellular activities, including the DNA damage signalling and repair pathways as a strategy to promote their replication (Weitzman, Lilley, and Chaurushiya 2010; Ryan, Hollingworth, and Grand 2016). This may have deleterious effects on the cell, including its DNA, potentially leading to genome instability (Weitzman, Lilley, and Chaurushiya 2010). SARS-CoV-2 infection has been reported to alter different host pathways (Banerjee et al. 2020; Blanco-Melo et al. 2020; Bouhaddou et al. 2020) and to correlate with the activation of some DDR markers and senescence (Ren et al. 2021; Zhou et al. 2021; Jiang and Mei 2021; Lipskaia et al. 2021; D'Agnillo et al. 2021; Lee et al. 2021; Bouhaddou et al. 2020; Victor et al. 2021). However, when studied, a correlation of DNA damage has been mainly drawn with reactive oxygen species (D'Agnillo et al. 2021; Lee et al. 2021), although likely only partly contributing (Lee et al. 2021). The observation that some DDR inhibitors could reduce SARS-CoV-2 replication (Garcia et al. 2021) further hints at a mutual interplay.

Here, we show that SARS-CoV-2 causes DNA damage (Fig. 1E,F) and triggers DDR activation (Fig. 1A-D and S1B,C). However, the DDR pathways are engaged in a non-canonical manner. For instance, although the master kinase ATM is activated by viral infection, its downstream effector kinase CHK2 is not (Fig. 1A,B); instead KAP1, another ATM target that plays multiple roles besides DDR (Cheng 2014), is strongly phosphorylated (Fig. 1A,B). This indicates that SARS-CoV-2 interferes with ATM target selection, and the mechanisms and viral product involved will need to be further probed.

Our study revealed at least two potential mechanisms leading to DNA damage accumulation following SARS-CoV-2 infection: one impacting on cellular dNTP metabolism, which leads to DNA replication defects; another impeding 53BP1 activation and causing reduced DNA repair (Fig. 7)

Although SARS-CoV-2 infection has been shown to influence negatively the expression of several cellular proteins in different ways (Stukalov et al. 2021; Burke et al. 2021; Blanco-Melo et al. 2020; Banerjee et al. 2020; Bouhaddou et al. 2020), the abundance of most of the DDR proteins tested was unaffected (Fig. 1A and S4C). An interesting exception is CHK1, that, together with P53, decreases following SARS-CoV-2 infection (Fig. 1A; 2A-D and S2A-D). Degradation of factors involved in DDR is a strategy shared by different viruses to override host defences for their advantage (Turnell and Grand 2012; Ma-Lauer et al. 2016; Lilley et al. 2010; Weitzman, Lilley, and Chaurushiya 2010). Notably, suppression of P53 activity has been also observed following infection with SARS-CoV, whereas overexpressing P53 in infected cells significantly reduced viral replication (Ma-Lauer et al. 2016).

CHK1 is known to control the expression of different members of the E2F family of transcription factors, which are important regulators of cell cycle progression (Trimarchi and Lees 2002) and control the transcription of the *RRM2* gene, ultimately allowing cells to accomplish DNA synthesis in S-phase (Gong et al. 2016; Zhang et al. 2009; Naruyama et al. 2008). Here, we demonstrated that SARS-CoV-2 infection, likely through the viral factors ORF6 and NSP13, leads to CHK1 loss and consequent RRM2 decrease (Fig. 1A and 2A-C,H-K), causing dNTP shortage and a prolonged S-phase (Fig. 2D-G), consistent with the generation of DNA replication stress and eventually DNA damage accumulation. What would be the advantage for a virus to cause all that? We propose that this is likely an unmeant consequence of the dire need for rNTP of SARS-CoV-2. The observation that a staggering two-thirds of the total RNA in SARS-CoV-2 infected cells is of viral origin (Kim et al. 2020) indicate that an infected cell needs to triple its normal RNA synthesis capacity. Thus, the virus has been under selective pressure to boost rNTP levels. Apparently, one way evolution found was to reduce CHK1 levels, causing decreased RRM2 activity and consequent accumulation of rNTP at the expenses of dNTP. Thus, a drop in dNTP is likely the unmeant consequence ("collateral damage") of the viral need for rNTP. Viruses are not new to hijack the NTP machinery. For instance, a similar yet opposite mechanism was observed in the DNA virus HPV31 which was reported to boost the function of RRM2 by stimulating the ATR-CHK1-E2F1 signalling axis to increase dNTPs levels and favour its genome replication (Anacker et al. 2016).

In addition to the induction of DNA damage by the above-described mechanism, we provide evidence that SARS-CoV-2 inhibits DNA repair. We observed a strikingly reduced ability of 53BP1 to form DDR foci, despite unaltered protein levels, in infected cells (Fig. 4). We propose that SARS-CoV-2 N, an avid RNA binding protein, impairs 53BP1 condensation at DSB by competing for dilncRNAs binding. Indeed, both 53BP1 and N protein are known to undergo LLPS in an RNA-dependent manner and here we demonstrate that N-protein, just like 53BP1(F Michelini et al. 2017) binds to dilncRNA. The observation that microinjected purified recombinant N protein quickly disassembles 53BP1 foci supports its direct role this model (Fig. 4G).

Intriguingly, enoxacin, a small molecule that we previously showed to boost RNA-mediated 53BP1 foci assembly and DNA repair through NHEJ (Gioia et al. 2019), has been recently proposed to reduce SARS-CoV-2 infection (Ahmadi and Moradi 2021). It is therefore tempting to speculate that enoxacin, by enhancing 53BP1 activities, could reduce the negative impact of SARS-CoV-2 N protein on DNA damage repair.

Also, to the best of our knowledge, this represents the first evidence of a nuclear role of SARS-CoV-2 N-protein. Although both SARS-CoV and SARS-CoV-2 N-proteins are

equipped with functional nuclear localization signals (NLSs), they localize to the nucleus only in part (Timani et al. 2005; Rowland et al. 2005; Gussow et al. 2020) (e.g., Fig. 1C, S1D and 4A,E). Interestingly however, recent phylogenetic studies have correlated the enhancement of motifs that promote nuclear localization of viral N-proteins with the pathogenicity and virulence of coronaviruses (Gussow et al. 2020).

Hyperactivation of the inflammatory pathways is responsible for fatal COVID-19 cases worldwide(P. Mehta et al. 2020). DNA damage accumulation and chronic DDR activation are potent inducers of inflammation in both cell autonomous and non-autonomous manners (Li and Chen 2018). Consistent with previous studies (Zhou et al. 2021; Ren et al. 2021), we observed that SARS-CoV-2 infection of cultured lung epithelial cells activates the cGAS/STING pathway, which senses damaged DNA and triggers the expression of inflammatory cytokines (Fig. S1D-F).

We also show that CHK1 loss is sufficient to activate stress and inflammatory cascades (Fig. 3). Since disruption of the CHK1-RRM2 pathway was previously reported to trigger cellular senescence (Aird et al. 2013), we propose that SARS-CoV-2-mediated CHK1 loss may promote a pro-inflammatory transcriptional program akin to the so called senescence-associated secretory phenotype (SASP), which includes the production of pro-inflammatory cytokines like IL6 (Fig. 3F), ultimately able to spark the cell extrinsic inflammation (Rodier et al. 2009).

In this regard, a role for SARS-CoV-2 induced senescence in promoting macrophage infiltration and inflammation *in vivo* has been recently proposed (Lee et al. 2021). Here, we observed that SARS-CoV-2 infection causes DNA damage accumulation that correlates with markers of cellular senescence (Fig. 5, 6 and S5). In particular, infected pneumocytes express high levels of p21, while polymorphonuclear and monocytoid inflammatory elements have elevated amounts of p16, consistent with a model of two waves of inflammatory response: an initial cell-intrinsic one and a second triggered by the host immune system.

Taken together, our results suggest that SARS-CoV-2 infection-induced DNA damage can trigger a cell-intrinsic pro-inflammatory program that, in concert with the known activation of the immune response system, causes the strong inflammatory response observed in COVID-19 disease.

Finally, by generating the evidence and proposing an underlying mechanism for the generation of DNA damage, the activation of DDR pathways and of a pro-inflammatory programme, we provide a model to support the notion of SARS-CoV-2 induced cellular senescence (Lee et al. 2021; Lipskaia et al. 2021). In this regard, it will be interesting to determine if persistent DNA damage and DDR activation, feature of cellular senescence (Fumagalli et al. 2012; Rossiello et al. 2014), following SARS-CoV-2 infection may be

responsible for the chronic manifestations of the pathology known as long COVID (Nalbandian et al. 2021).

METHODS

Cell culture and treatments. Vero E6 cells (ATCC-1586), human hepatocarcinoma Huh7 cells (kindly provided by Ralf Bartenschlager, University of Heidelberg, Germany) and lung adenocarcinoma Calu-3 (ATCC HTB-55), were cultured in Dulbecco's modified Eagle's medium (DMEM, ThermoFisher, Paisley, UK) supplemented with 10% foetal bovine serum (FBS, ThermoFisher, Paisley, UK) and 50 µg/mL gentamicin. 53BP1-GFP U2OS, EJ5-GFP U2OS and NIH2/4 cell lines were cultured as already described(Gioia et al. 2019; Pessina et al. 2019; F Michelini et al. 2017). Cell cultures were maintained at 37°C under 5% CO_2. Cells were routinely tested for mycoplasma contamination. DNA damage was induced in cultured cells by 6 mM hydroxyurea (HU) treatment for 4 hours, or by exposure to ionizing radiation (IR: 2 Gy) and analyses 15 or 60 min post-IR.

SARS-CoV-2 propagation and *in vitro* infection. Working stocks of SARS-CoV-2 ICGEB-FVG_5 isolated and sequenced in Trieste, Italy(Danilo Licastro, Sreejith Rajasekharan, Simeone Dal Monego, Ludovica Segat and Alessandro Marcello 2020), were propagated on semiconfluent Vero E6 cells. Plaque assay was performed by incubating dilutions of SARS-CoV-2 on Vero E6 monolayers at 37°C for 1 h, which were then washed with phosphate buffered saline (PBS) and overlaid with DMEM 2% FBS containing 1.5% carboxymethylcellulose (CMC, Sigma-Aldrich, St Louis, USA) for 3 days. Cells were then fixed with 3.7% paraformaldehyde (PFA, Sigma-Aldrich, St Louis, MO, USA) and stained with crystal violet 1%. Cultured Huh7 and Calu-3 cells were infected at 0.1 MOI, after 1 h the non-bound virus was rinsed off with PBS 1X and fresh DMEM containing 2% of heat-inactivated FBS was added to the cells. Mock-infected cells were included in all experiments. Uniformity of viral infection in all experiments was confirm by viral titration, RNA detection and IF. At different hours post-infection, cell supernatants were collected and used for virus titration by plaque assay as described above and for viral RNA quantification as previously described(Rajasekharan et al. 2021).

Immunoblotting. Whole cell extracts were obtained by lysing Huh7 and Calu-3 cell lines in 1X Laemmli Buffer (2% SDS, 10% glycerol, 60 mM Tris pH 6.8). Prior to fractionation on 4-12% gradient SDS-PAGE (Thermo Fisher), whole extracts were sonicated 10 times for 30 sec ON and 30 sec OFF at high intensity using Bioruptor™ Next Gen (Diagenode) in a

water bath at 4 °C. Proteins were then transferred onto nitrocellulose membrane and analyzed as described before(Gioia et al. 2019) with the antibodies listed in Supplementary Table 1.

Quantitative immuno-fluorescence analysis in cultured cells. Quantitative immuno-fluorescence assays were carried out in cultured cells as described(Gioia et al. 2019), with minor modifications. Specifically, Calu-3 cells were fixed with 4% PFA and permeabilized first with methanol/acetone (1:1) for 2 min at RT and then with Triton 0.2% in PBS 1X for 10 min at RT The antibodies used are listed in Supplementary Table 1.

RNA extraction and RT-qPCR analysis. SARS-CoV-2 infected or mock-infected Huh7 and Calu-3 cells were harvested in TriFast™ (EMR507100, Euroclone) and total RNA extracted using RNeasy™ Kit (Qiagen). RNA from siRNA-transfected Calu-3 was purified with Maxwell® RSC miRNA Tissue Kit (Promega). DNase I was added during RNA purification, following manufacturers' protocols. Purified total RNA was reverse transcribed with SuperScript™ VILO™ cDNA Synthesis Kit (Thermo Fisher) and cDNA analyzed by qPCR using SYBR Green I Master Mix (Roche) with the primers listed in Supplementary Table 2.

Comet assay. Alkaline comet assay was performed on 48 h SARS-CoV-2 infected or mock-infected Huh7 cells using CometAssay Reagent Kit for Single Cell Gel Elec- trophoresis Assay (Trevigen, 4250-050-K), following manufacturer's instructions. Tail moment was measured using CometScore 2.0 software.

dNTP quantification. dNTP pools were extracted from mock-infected and infected cell cultures. Briefly, cell plates were carefully washed free of medium with cold PBS and extracted with ice-cold 60 % methanol. Methanolic extract was centrifuged, boiled for 3 min, brought to dryness by centrifugal evaporation (Savant, SC100 SpeedVac Concentrator and RT100A Refrigerated Condensation Trap) and stored at -80°C until use. Cells left on the plate were dried and dissolved on 0.3 M NaOH and the absorbance at 260 nm of the lysates was used as an index of cell mass, in turn an approximation for cell number(Frangini et al. 2013). The dry residue was dissolved in water and used to determine the size of dNTP pools by the DNA polymerase-based assay as described(Ferraro et al. 2010). Two different aliquots of each pool extract were analyzed and pool sizes were normalized by the A_{260} nm of the NaOH lysates.

BrdU staining and flow cytometry analysis. For cell-cycle analysis, cells were fixed first in formaldehyde 2% and then in 75% ethanol. Cells were probed with anti-BrdU primary antibody (Supplementary Table 1) diluted in PBS 1% BSA at RT for 1h. After washing, cells were incubated with the secondary antibody, diluted 1:400, at RT for 1h in the same buffer. Finally, cells were stained with Propidium Iodide (PI) (Sigma-Aldrich, 50 $\mu g\ ml^{-1}$) in PBS 1% BSA and RNase A (Sigma-Aldrich, 250 $\mu g\ ml^{-1}$). Samples were acquired with Attune NxT (Thermofisher) using a 561 nm laser and 695/40 filter for PI; 488 nm laser and 530/30 filter for BrdU. Analysis was carried out using FlowJo 10.7.1 (BD Biosciences). At least 10^4 events were analyzed for each sample.

Plasmid and siRNA transfection. pLVX-EF1α-2xStrep-IRES-Puro vectors encoding for SARS-CoV-2 proteins are a kind gift from Professor Nevan J. Krogan(Gordon et al. 2020). pcDNA™3.1 (+) Mammalian Expression Vector (Thermo Fisher) was used as a control empty vector where indicated. Plasmids were transfected with Lipofectamine™ 2000 Transfection Reagent (Thermo Fisher) in Opti-MEM™ (Thermo Fisher). Short-interfering RNAs (siRNAs) were purchased from Dharmacon™ (Horizon) and transfected into Huh7 or Calu-3 cells with Lipofectamine RNAiMAX Transfection Reagent (Thermo Fisher) in Opti-MEM™. Cells were harvested for analyses at 48 hours post-transfection.

Isolation and SARS-CoV-2 infection of human primary nasal epithelial cells (HNEpC). HNEpC were harvested from healthy adult volunteers. Nasal cavities were anesthetized using lidocaine and nasal epithelial cells were harvested by repeatedly scraping turbinates with a disposable bronchial cytology brush (CONMED). The tissue was resuspended in DMEM supplemented with 10% fetal bovine serum (FBS) and centrifuged at 300 x g for 5 minutes. The pellet was digested in a solution containing 1000 U of Accutase (Sigma, A6964), 5000 U of Dispase (Corning, 354235) and 1 mg/ml DNAse II (Sigma, D8764) for 8 minutes at 37°C. The digestion was stopped by adding an equal volume of Pneumacult medium (Stem Cell technologies, 5050) supplemented with 10% FBS and filtered through a 100 µm cell strainer. The cell suspension was centrifuged at 300 x g for 5 minutes and the pellet resuspended in red blood cell lysis solution (150 mM NH_4Cl and 10 mM $KHCO_3$) for 2 minutes. Cells were centrifuged at 300 x g for 5 minutes, resuspended in medium and seeded on 8-well chambers (Ibidi) at a concentration of $5*10^5$ cells per well. After 48 hours, cells were infected with SARS-CoV-2(Danilo Licastro, Sreejith Rajasekharan, Simeone Dal Monego, Ludovica Segat and Alessandro Marcello 2020) at 1 MOI as described above. Cells were cultured for 48 hours and fixed in 4% PFA for 15 minutes at room temperature for staining.

Immunofluorescence and fluorescence in situ hybridization on HNEpC. Fixed HNEpC were washed once with PBS and permeabilized with 0.5% Triton X-100 (Sigma, T8787) in PBS for 15 minutes at room temperature. Fluorescence in situ hybridization (FISH) to detect SARS-CoV-2 genome was performed using a kit by Molecular Instruments, following manufacturer instruction. After FISH, samples were incubated with a blocking solution (0.5% Triton X-100, 10% horse serum in PBS) for 30 minutes and incubated with the following primary antibodies diluted 1:100 in blocking solution for 16 hours at 4°C: anti-γH2AX and anti-53BP1 (Supplementary Table 1). After three washes in PBS, samples were incubated with the appropriate alexa-fluor© conjugated secondary antibody (Invitrogen) diluted 1:500 in blocking solution. After three washes in PBS, nuclei were counterstained using Hoechst 33342 thrihydrochloride (Invitrogen, h3570) and samples mounted using Mowiol© (Sigma, 81381).

SARS-CoV-2 Nucleocapsid (N) protein expression and purification. pET28 plasmid bearing SARS-CoV-2 N-protein fused to a C-terminal His_6-tag was a kind gift from S. Pasqualato (European Institute of Oncology, Milan). N-protein was expressed in E. coli BL21-CodonPlus (DE3)-RP (Agilent) upon induction with 500 µM isopropyl-ß-D-1-thiogalactopyranoside (IPTG) for 16 h at 18 °C. Harvested cells were resuspended in resuspension buffer (25 mM Tris pH 8, 500 mM NaCl, 5% glycerol, 2 mM ß-mercaptoethanol, 10 mM imidazole), supplemented with protease inhibitors and TurboNuclease, and then disrupted by sonication. Polyethyleneimine (PEI) was added dropwise to the lysate (final 0.2%) in order to get rid of nucleic acids. After centrifugation, the clarified supernatant was applied onto Ni-NTA Agarose beads (Qiagen) and the His_6-Nucleocapsid protein was eluted in elution buffers containing 250 mM and 500 mM imidazole. The eluted protein was applied on a HiTrap Heparin HP column (Cytiva), eluted using a salt gradient, concentrated and then loaded on a Superdex 200 Increase 10/300 GL (Cytiva) pre-equilibrated in SEC buffer (25 mM Tris pH 8, 500 mM NaCl, 2 mM ß-mercaptoethanol). Protein-containing fractions were pooled, concentrated and stored in SEC buffer. Protein purity was assessed by Comassie blue SDS-PAGE and resulted in > 90%.

Micro-injection and live imaging analysis. Before micro-injection experiments, the purified viral N-protein was dialyzed overnight against microinjection buffer (25 mM Tris pH 8, 150 mM NaCl) in order to remove ß-mercaptoethanol and decrease NaCl concentration to the physiological value. Acetylated-BSA (Thermofisher) that was used as a control for microinjection, was dialyzed as well against microinjection buffer. Micro-

injection experiments were performed as already described(Pessina et al. 2019), with some minor changes. An UltraVIEW VoX spinning-disk confocal system (PerkinElmer) equipped with a motorized Luigs & Neumann SM7 micromanipulator was used. Glass borosilicate capillaries were pulled to a diameter of 0.7 mm and loaded with 6 mg/mL Nucleocapsid protein solution or BSA solution as a control, in presence of Rhodamine B Dextran (Thermofisher) as a marker for microinjected cells. Samples were injected into U2OS cell nuclei 30 min after irradiation (2 Gy) using a FemtoJet pump (Eppendorf) at a constant pressure of 20 hPa. Immediately after injection, a z-stack was acquired every minute for 100 min total using a X60 oil-immersion objective (Nikon Plan Apo VC, 1.4 NA). 488 nm and 561 nm lasers were used to excite GFP and Rhodamine B respectively. Quantification of 53BP1-GFP foci per nucleus per single frame was performed using the software Cell Profiler. Foci number per nucleus was plotted along time and the corresponding curve was fitted to an exponential function to determine the decay rate (k) using Prism software. Statistical analysis on k values was performed using t-test.

Turbidity assay. Purified recombinant N-protein (5 mM) in micro-injection buffer (25 mM Tris pH 8, 150 mM NaCl) was mixed *in vitro* with increasing concentrations of RNA extracted from SARS-CoV-2 infected (48 hpi) or mock-infected Huh7 cells. Turbidity of the solutions was measured at 350 nm using a Nanovue plus Spectrophotometer (Cytiva) after 30 min, 2 h and 24 h of incubation at RT. The obtained values were plotted versus the RNA concentration using the software Prism.

SARS-CoV-2 N immuno-precipitation. Huh7 cells were transfected with the plasmid encoding for SARS-CoV-2 N protein(Gordon et al. 2020) or with an empty vector as a control. 48 h post-transfection, cells were irradiated or not. 1 h post-IR, cells were harvested by trypsinization and washed twice in ice-cold 1X PBS. Cell pellets were lysed in IP Buffer (25 mM Tris-HCl, pH 7.4; 150 mM KCl; 5% Glycerol; 0.5% NP40; 10 mM $MgCl_2$; 1 mM $CaCl_2$) supplemented with 1X Protease Inhibitors (Roche), 0.5 mM DTT, 40 U ml^{-1} RNaseOUT and 1000 U ml^{-1} DNase I (Roche), and incubated at RT for 15 min and at 4 °C for extra 15 min with gentle rotation. Lysates were cleared by centrifugation at max speed for 20 min at 4 °C. After addition of 5 mM EDTA (pH 8), lysates were incubated overnight at 4 °C with 5 μg of anti-N-protein (40588-T62 Sino Biological) or with normal rabbit IgGs (Cell Signaling), which were previously bound to Dynabeads™ Protein G (Thermo Fisher). After 5 washes with 1 ml of IP Buffer, immuno-precipitated proteins were analyzed by immunoblotting.

RNA immuno-precipitation and analysis. RNA immuno-precipitation (RIP) and dilncRNA analysis was carried out in NIH2/4 cells as previously described(F Michelini et al. 2017), with minor modifications. Briefly, I-SceI-GR-expressing NIH2/4 cells were transfected with the plasmid encoding for SARS-CoV-2 N or with an empty vector as a control at 24 hours prior to triamcinolone acetonide 0.1 μM (TAA, Sigma-Aldrich) administration. Immuno-precipitation was performed using 5 μg of anti-N-protein (40588-T62 Sino Biological), or 10 μg of anti-53BP1 (Novus), or with normal rabbit IgGs (Cell Signaling).

Non-homologous end-joining (NHEJ) repair assay. Evaluation of repair efficiency by NHEJ following viral N-protein expression was conducted as shown previously(Gioia et al. 2019), with minor modification: HA-I-SceI expressing plasmid was transfected along with the plasmid encoding for SARS-CoV-2 N-protein.

Mice and *in vivo* SARS-CoV-2 infection and treatments. Experiments involving animals have been carried out in accordance with the Italian Laws (D.lgs. 26/2014), which enforce Directive 2010/63/EU (Directive 2010/63/EU of the European Parliament and of the Council of 22 September 2010 on the protection of animals used for scientific purposes). Accordingly, the project has been authorized by the Italian Competent Authority (Ministry of Health). B6.Cg-Tg(K18-ACE2)$^{2Prlmn/}$J mice were purchased from The Jackson Laboratory. Mice were housed under specific pathogen-free conditions and K18-hACE2 heterozygous mice were used at 6-10 weeks of age. All infectious work was performed in designed BSL-3 workspaces. The SARS-CoV-2/human/ITA/Milan-UNIMI-1/2020 (GenBank: MT748758.1) isolation was carried out in BSL-3 workspace and performed in Vero E6 cells, which were cultured at 37°C, 5% CO_2 in complete medium (DMEM supplemented with 10% FBS, MEM non-essential amino acids, 100 U/ml penicillin, 100 U/ml streptomycin, 2 mM L-glutamine). Virus stocks were titrated using Endpoint Dilutions Assay (EDA, $TCID_{50}$/ml). Vero E6 cells were seeded into 96 wells plates and infected at 95% of confluency with base 10 dilutions of virus stock. After 1 h of adsorption at 37°C, the cell-free virus was removed, cells were washed with PBS 1X, and complete medium was added to cells. After 48h, plates were evaluated for the presence of a cytopathic effect (CPE). $TCID_{50}$/ml of viral stocks were then determined by applying the Reed–Muench formula. Virus infection of K18-hACE2 mice was performed via intranasal administration of 1 x 10^5 $TCID_{50}$ per mouse under Isoflurane 2% (# IsoVet250) anesthesia. Mice were monitored to record body weight, clinical and respiratory parameters. Mice were euthanized by cervical

dislocation. At the time of autopsy, mice were perfused through the right ventricle with PBS. Lung tissues were collected in liquid nitrogen or in Zn-formalin and transferred into 70% ethanol 24 h later. For irradiation experiments, an eleven-month-old C57BL/6 J mouse was irradiated with 2 Gy TBI using GADGIL– X Ray irradiator. An age and sex matched mice were used as control. Mice were euthanized by CO_2 inhalation at 1 h post-IR and lungs collected for fixation in 10% neutral buffered formalin overnight, washed in water and paraffin-embedded for histological analysis.

Immunohistochemical (IHC) staining of murine lungs. Haematoxylin/Eosin (Diapath) staining was performed to assess histological features according to standard protocol and samples were mounted in Eukitt (Bio-Optica). For IHC analysis, paraffin was removed with xylene and the sections were rehydrated in graded alcohol. Antigen retrieval was carried out using pH6 preheated target retrieval solution for 30 minutes. Tissue sections were blocked with FBS serum in PBS for 60 min and incubated overnight with the primary antibodies (Supplementary Table1). The antibody binding was detected using a polymer detection kit (GAR-HRP, Microtech) followed by a diaminobenzidine chromogen reaction (Peroxidase substrate kit, DAB, SK-4100; Vector Lab). All sections were counterstained with Mayer's hematoxylin and visualized using a bright-field microscope.

Patients diagnosed for COVID-19 and subjects without COVID-19. Histological analysis was performed by expert technicians and pathologists at the Pathology Unit of Trieste University Hospital. The same pathologists analyzed all samples considered in this study, excluding operator-dependent biases. This study was approved by the Joint Ethical Committee of the Regione Friuli Venezia Giulia, Italy (re. 0019072/P/GEN/ARCS).

Immunofluorescence, fluorescence in situ hybridization on human paraffin-embedded tissue and imaging analysis. Paraffin-embedded tissues from biopsies of lung and nasal mucosae of COVID-19 patients were cut in 4 μm-thick sections. To remove paraffin, sections were kept at 60°C for 30 minutes, then in Xylene for 15 minutes and rehydrated using serial dilutions of water:ethanol (0:100, 10:90, 30:70, 50:50 and 100:0), for 3 minutes each. For antigen retrieval, samples were boiled for 20 minutes in a basic pH solution (10 mM Tris, 0.05% Tween20© pH 9.0) and cooled down in ice for 1 hour. Sections were then permeabilized with 0.5% Triton X-100 in PBS for 15 minutes at RT, followed by FISH, as described before. After FISH, samples were incubated with a blocking solution (0.5% Triton X-100, 10% horse serum in PBS) for 30 minutes and then with the following primary antibodies diluted 1:100 in blocking solution for 16 hours at 4°C: anti-γH2AX, anti-RRM2

(Supplementary Table 1) and anti-Human Cytokeratin 8/18 (Dako, Clone EP17/EP30, M3652). After three washes in PBS, samples were incubated with the appropriate Alexa-fluor© conjugated secondary antibody (Invitrogen) diluted 1:200 in blocking solution. After three washes in PBS, nuclei were counterstained using Hoechst 33342 thrihydrochloride (Invitrogen, h3570) and samples were mounted using Mowiol© (Sigma, 81381). Tissues were imaged using a Nikon Ti-Eclipse fluorescence microscope using a 20X objective. Images were analyzed using ImageJ (NIH). To evaluate DNA damage in tissue samples, epithelial cells with γH2AX nuclear foci were manually counted using the cell counter plugin of ImageJ. Cells displaying a cytoplasmic staining positive for both cytokeratin and SARS-CoV-2 mRNA were considered as infected epithelial cells. The remaining cytokeratin-18 positive cells were considered as non-infected epithelial cells. To evaluate the levels of RRM2 expression in the same tissues, the signal was quantifying by manually drawing cellular masks around FISH signal. RRM2 levels were calculated upon application of a common threshold, obtained in unstained samples, to remove any unspecific signal.

Statistical Analysis.

One-way or two-way ANOVA was used for multiple comparisons between samples, unless stated otherwise. *$p < 0.05$, **$p < 0.01$, ***$p < 0.001$, ****$p < 0.0001$.

Supplementary Table 1

Antibody	Company	Catalogue number
γH2AX (Ser139)	Millipore	05-636
53BP1	Bethyl	A303-906A
Cleaved Caspase-3 (Asp 175)	Cell Signaling	9661
pDNA PKcs (Ser2056) (EPR5670)	Abcam	ab124918
ATM	Abcam	ab32420
pATM (Ser1981)	Rockland	200-301-400
ATR	Santa Cruz	sc-1887
pATR (T1989)	Abcam	ab223258
KAP1	Abcam	ab10484
pKAP1 (S824)	Bethyl	A300-767A
CHK1 (2G1D5)	Cell Signaling	#2360
CHK1 (ST57-09)	ThermoFisher	MA532180
pCHK1 (S317)	Cell Signaling	#2344
CHK2	Millipore	05-649
pCHK2 (Thr68)	Cell Signaling	#2661
P53	Abcam	ab1101
pP53 (Ser15)	Cell Signaling	#9284
RPA	Calbiochem	NA18-100UG
pRPA (S4/S8)	Bethyl	A300-245A
Histone H3	Abcam	ab10799
SARS-CoV2 nucleocapsid (1A6)	ThermoFisher	MA5-35941
SARS-CoV2 nucleocapsid	Sino Biological	40588-T62
Tubulin	Sigma-Aldrich	T5168
STAT1 (9H2)	Cell Signaling	#9176
pSTAT1 (Tyr 701) (58D6)	Cell Signaling	#9167
RRM1	Santa Cruz	sc-11733
RRM2	Santa Cruz	sc-10844
BrdU	BDbioscience	347580
CDT1	Cell Signaling	#8064
PCNA	Bio Rad	MCA1558
P38 MAPK	Cell Signaling	#9212
pP38 MAPK (Thr180/Tyr182)	Cell Signaling	#9211
Strep-tag II epitope	Qiagen	34850
ISceI (FL-86)	Santa Cruz	sc-98269
Human Cytokeratin 8/18 (EP17/EP30)	Dako	M3652
p16	Abcam	ab51243
p21	Abcam	ab188224

Supplementary Table 2

primer name	primer sequence
Human RPLP0 FW	TTCATTGTGGGAGCAGAC
Human RPLP0 RV	CAGCAGTTTCTCCAGAGC
Human CXCL9 FW	GGACTATCCACCTACAATCCTTG
Human CXCL9 RV	TTTTAATCAGTTCCTTCACATCTGC
Human CXCL10 FW	GCATCAGCATTAGTAATCAACCTG
Human CXCL10 RV	TGGCCTTCGATTCTGGATTC
Human TNF FW	ACCTCTCTCTAATCAGCCCTC
Human TNF RV	CTACAGGCTTGTCACTCGG
Human IL-1B FW	ATGCACCTGTACGATCACTG
Human IL-1B RV	ACAAAGGACATGGAGAACACC
Human IL-6 FW	CCACTCACCTCTTCAGAACG
Human IL-6 RV	CATCTTTGGAAGGTTCAGGTTG
Human IL8 FW	TTGGCAGCCTTCCTGATTTC
Human IL8 RV	TCTTTAGCACTCCTTGGCAAAAC
Human CHK1 FW	CAACAAACCCCTCAAGAAAGG
Human CHK1 RV	TGGATTGAATGTGCTTAGAAAATC
Human RRM2 FW	AAGGACATTCAGCACTGGG
Human RRM2 RV	AGCGGGCTTCTGTAATCTG

ACKNOWLEDGEMENTS

We would like to thank: N. J. Krogan (UCSC, San Francisco, CA, USA) and S. Pasqualato (IEO, Milan, Italy) for providing plasmids; Maria Grazia Totaro and Sara Martone (IFOM, Milan, Italy) for technical support with flow cytometry analyses; Serena Magni, Emanuele Martini and D. Parazzoli (IFOM, Milan, Italy) for support with imaging analyses; L. Falbo (IFOM, Milan, Italy) for providing antibodies; F. Giavazzi (Università degli Studi di Milano, Segrate, Italy) for helpful advice. F.d'A.d.F laboratory is supported by: ERC advanced grant (TELORNAGING—835103); AIRC-IG (21762); Telethon (GGP17111); AIRC 5X1000 (21091); ERC PoC grant (FIREQUENCER—875139); Progetti di Ricerca di Interesse Nazionale (PRIN) 2015 "ATR and ATM-mediated control of chromo- some integrity and cell plasticity"; Progetti di Ricerca di Interesse Nazionale (PRIN) 2017 "RNA and genome Instability"; Progetto AriSLA 2021 "DDR & ALS"; POR FESR 2014-2020 Regione Lombardia (InterSLA project); FRRB—Fondazione Regionale per la Ricerca Biomedica—under the frame of EJP RD, the European Joint Programme on Rare Diseases with funding from the European Union's Horizon 2020 research and innovation program under the EJP RD COFUND-EJP NO 825575.

AUTHOR CONTRIBUTIONS

U.G. wrote the manuscript, conceived, conducted and analyzed the RIP, co-IP, comet and NHEJ repair assays; performed the immunoblot analyses; expressed the individual SARS-CoV-2 proteins in cultured cells and analyzed their impact on DDR activation by immunoblot and immunostaining; designed, carried out and analyzed the experiments of CHK1 knockdown by RNAi; analyzed all of the remaining data. **S.T.** wrote and edited the manuscript, performed immunofluorescence in infected cultured cells and carried out the immunostaining for flow-cytometry analyses; generated cDNA from infected cultured cells. **P.M.O.** and **S.R.** performed all the SARS-CoV-2 infection assays, measured virus by WB, IF, plaque assay and RT-PCR and prepared the samples for analysis. **A.C.** and **A.P.** performed the analysis of DDR activation in infected primary nasal epithelial cells and carried out FISH, IHC and immunofluorescence analyses in human lung and nasal mucosa tissues. **M.Ce.** produced recombinant SARS-CoV-2 N and performed micro-injection experiments and turbidity assays. **E.P.** conducted the analysis of dNTP levels in infected cultured cells. **V.F.** propagated SARS-CoV-2, infected *hACE2*-mice and generated lung tissues from such animals. **M.Ca.** purified and analyzed by RT-qPCR the RNA of infected cultured cells and CHK1-depleted Calu-3 cells. **V.M.** contributed to analyzing by RT-qPCR the RNA of infected cultured cells. **F.P.** and **G.C.** conducted the IHC analyses on mouse lungs. **S.S.** generated lung samples from irradiated or not wild type mice. **M.Co.** analyzed the flow cytometry experiments. **S.B.** and **Z.L.** assisted M.Ce. in conducting and analyzing micro-injection experiments. **T.C.** assisted in the management of the BSL3 facility and virus stock preparation. **M.C.V.** prepared and characterized nasal primary cells. **M.I.** supervised V.F. **C.T.** supervised G.C. and edited the manuscript. **C.R.** designed the quantification of dNTP levels, supervised E.P. and edited the manuscript. **R.B.** performed post-mortem pathology on human lungs. **S.Z.** coordinated the analysis of human tissues, supervised A.C., A.P. and M.C.V., and edited the manuscript. **A.M.** coordinated the virology aspects of the work, supervised P.M.O., S.R. and T.C., and edited the manuscript. **F.d'A.d.F.** conceived the study, assembled and revised the manuscript.

CONFLICT OF INTEREST

The authors declare no competing financial interests.

7 References

Aguado, Julio, Agustin Sola-Carvajal, Valeria Cancila, Gwladys Revêchon, Peh Fern Ong, Corey Winston Jones-Weinert, Emelie Wallén Arzt, et al. 2019. “Inhibition of DNA Damage Response at Telomeres Improves the Detrimental Phenotypes of Hutchinson–Gilford Progeria Syndrome.” *Nature Communications* 10 (1): 1–11. https://doi.org/10.1038/s41467-019-13018-3.

Aguirre, Andrew J, Robin M Meyers, Barbara A Weir, Francisca Vazquez, Cheng-zhong Zhang, Uri Ben-david, April Cook, et al. 2017. “Genomic Copy Number Dictates a Gene-Independent Cell Response to CRISPR-Cas9 Targeting” 6 (8): 914–29. https://doi.org/10.1158/2159-8290.CD-16-0154.Genomic.

Ahmadi, Amirhossein, and Sharif Moradi. 2021. “In Silico Analysis Suggests the RNAi-Enhancing Antibiotic Enoxacin as a Potential Inhibitor of SARS-CoV-2 Infection.” *Scientific Reports* 11 (10271). https://doi.org/10.1038/s41598-021-89605-6.

Aird, Katherine M., Gao Zhang, Hua Li, Zhigang Tu, Benjamin G. Bitler, Azat Garipov, Hong Wu, et al. 2013. “Suppression of Nucleotide Metabolism Underlies the Establishment and Maintenance of Oncogene-Induced Senescence.” *Cell Reports* 3 (4): 1252–65. https://doi.org/10.1016/j.celrep.2013.03.004.

Alberto Ciccia and Stephen J Elledge. 2010. “The DNA Damage Response: Making It Safe to Play with Knives.” *Molecular Cell* 40 (2): 179–204. https://doi.org/10.1016/j.molcel.2010.09.019.The.

Anacker, Daniel C., Heather L. Aloor, Caitlin N. Shepard, Gina M. Lenzi, Bryan A. Johnson, Baek Kim, and Cary A. Moody. 2016. “HPV31 Utilizes the ATR-Chk1 Pathway to Maintain Elevated RRM2 Levels and a Replication-Competent Environment in Differentiating Keratinocytes.” *Virology* 499 (October): 383–96. https://doi.org/10.1016/j.virol.2016.09.028.

Ansari, Amir Mehdi, A. Karim Ahmed, Aerielle E. Matsangos, Frank Lay, Louis J. Born, Guy Marti, John W. Harmon, and Zhaoli Sun. 2016. “Cellular GFP Toxicity and Immunogenicity: Potential Confounders in in Vivo Cell Tracking Experiments.” *Stem Cell Reviews and Reports* 12 (5): 553–59. https://doi.org/10.1007/s12015-016-9670-8.

Anzalone, Andrew V., Luke W. Koblan, and David R. Liu. 2020. “Genome Editing with CRISPR–Cas Nucleases, Base Editors, Transposases and Prime Editors.” *Nature Biotechnology* 38 (7): 824–44. https://doi.org/10.1038/s41587-020-0561-9.

Arnoult, Nausica, Ma Correia, Adriana, Anna Merlo, Sara Garcia-Gomez, Marija Maric, Marco Tognetti, Christopher W Benner, Simon J Boulton, Alan Saghatelian, and Jan Karlseder. 2017. “Regulation of DNA Repair Pathway Choice in S/G2 by the NHEJ Inhibitor CYREN Europe PMC Funders Group.” *Nature* 549 (7673): 548–52. https://doi.org/10.1038/nature24023.Regulation.

Atkins, Andrew, Cheng-Han Chung, Alexander G. Allen, Will Dampier, Theodore E. Gurrola, Ilker K. Sariyer, Michael R. Nonnemacher, and Brian Wigdahl. 2021. “Off-Target Analysis in Gene Editing and Applications for Clinical Translation of CRISPR/Cas9 in HIV-1 Therapy.” *Frontiers in Genome Editing* 3 (August): 1–26. https://doi.org/10.3389/fgeed.2021.673022.

Atsaves, Vasileios, Vasiliki Leventaki, George Z. Rassidakis, and Francois X. Claret. 2019. “AP-1 Transcription Factors as Regulators of Immune Responses in Cancer.” *Cancers* 11 (7). https://doi.org/10.3390/cancers11071037.

Baddeley, Helen J. E., and Mark Isalan. 2021. “The Application of CRISPR/Cas Systems for Antiviral Therapy.” *Frontiers in Genome Editing* 3 (October): 1–8. https://doi.org/10.3389/fgeed.2021.745559.

Banerjee, Abhik K., Mario R. Blanco, Emily A. Bruce, Drew D. Honson, Linlin M. Chen, Amy Chow, Prashant Bhat, et al. 2020. “SARS-CoV-2 Disrupts Splicing, Translation, and Protein Trafficking to Suppress Host Defenses.” *Cell* 183 (5): 1325-1339.e21. https://doi.org/10.1016/j.cell.2020.10.004.

Banerjee, Anamika, Sunil Kumar Malonia, and Shubham Dutta. 2021. “Frontiers of CRISPR-Cas9 for Cancer Research and Therapy.” *Journal of Exploratory Research in Pharmacology* 6 (3): 96–104. https://doi.org/10.14218/jerp.2020.00033.

Barrangou, Rodolphe, Christophe Fremaux, Hélène Deveau, Melissa Richards, Patrick Boyaval, Sylvain Moineau, Dennis A. Romero, and Philippe Horvath. 2007. “CRISPR Provides Acquired Resistance Against Viruses in Prokaryotes Rodolphe.” *Science* 315 (March): 1709–12. https://doi.org/10.1126/science.1138140.

Bartek, Jiri, Claudia Lukas, and Jiri Lukas. 2004. “Checking on DNA Damage in S Phase.” *Nature Reviews Molecular Cell Biology* 5 (10): 792–804. https://doi.org/10.1038/nrm1493.

Behr, Matthew, Jing Zhou, Bing Xu, and Hongwei Zhang. 2021. “In Vivo Delivery of CRISPR-Cas9 Therapeutics: Progress and Challenges.” *Acta Pharmaceutica Sinica B* 11 (8): 2150–71. https://doi.org/10.1016/j.apsb.2021.05.020.

Bekker-Jensen, Simon, Claudia Lukas, Fredrik Melander, Jiri Bartek, and Jiri Lukas. 2005. “Dynamic Assembly and Sustained Retention of 53BP1 at the Sites of DNA Damage Are Controlled by Mdc1/NFBD1.” *Journal of Cell Biology* 170 (2): 201–11. https://doi.org/10.1083/jcb.200503043.

Bekker-Jensen, Simon, and Niels Mailand. 2010. “Assembly and Function of DNA Double-Strand Break Repair Foci in Mammalian Cells.” *DNA Repair* 9 (12): 1219–28. https://doi.org/10.1016/j.dnarep.2010.09.010.

Beth Levine, and John Abrams. 2008. “P53: The Janus of Autophagy?” *Nature Cell Biology* 10 (6): 637–39. https://doi.org/10.1038/ncb0608-637.

Blackford, Andrew N., and Stephen P. Jackson. 2017. “ATM, ATR, and DNA-PK: The Trinity at the Heart of the DNA Damage Response.” *Molecular Cell* 66 (6): 801–17. https://doi.org/10.1016/j.molcel.2017.05.015.

Blanco-Melo, Daniel, Benjamin E. Nilsson-Payant, Wen Chun Liu, Skyler Uhl, Daisy Hoagland, Rasmus Møller, Tristan X. Jordan, et al. 2020. “Imbalanced Host Response to SARS-CoV-2 Drives Development of COVID-19.” *Cell* 181 (5): 1036-1045.e9. https://doi.org/10.1016/j.cell.2020.04.026.

Blasco, María A., Han Woong Lee, M. Prakash Hande, Enrique Samper, Peter M. Lansdorp, Ronald A. DePinho, and Carol W. Greider. 1997. “Telomere Shortening and Tumor Formation by Mouse Cells Lacking Telomerase RNA.” *Cell* 91 (1): 25–34. https://doi.org/10.1016/S0092-8674(01)80006-4.

Boch, Jens, Heidi Scholze, Sebastian Schornack, Angelika Landgraf, Simone Hahn, Sabine Kay, Thomas Lahaye, Anja Nickstadt, and Ulla Bonas. 2009. “Breaking the Code of DNA Binding Specificity of TAL-Type III Effectors.” *Science* 326 (5959): 1509–12.

https://doi.org/10.1126/science.1178811.

Boehning, Marc, Claire Dugast-Darzacq, Marija Rankovic, Anders S. Hansen, Taekyung Yu, Herve Marie-Nelly, David T. McSwiggen, et al. 2018. “RNA Polymerase II Clustering through Carboxy-Terminal Domain Phase Separation.” *Nature Structural and Molecular Biology* 25 (9): 833–40. https://doi.org/10.1038/s41594-018-0112-y.

Boijja, Ann, Isaac A Klein, Benjamin R Sabari, Alessandra Dall Agnese, L Eliot, Alicia V Zamudio, Charles H Li, et al. 2018. “Transcription Factors Activate Genes through the Phase Separation Capacity of Their Activation Domains.” *Cell* 175 (7): 1842–55. https://doi.org/10.1016/j.cell.2018.10.042.Transcription.

Bolotin, Alexander, Benoit Quinquis, Alexei Sorokin, and S. Dusko Ehrlich. 2005. “Clustered Regularly Interspaced Short Palindrome Repeats (CRISPRs) Have Spacers of Extrachromosomal Origin.” *Microbiology* 151 (8): 2551–61. https://doi.org/10.1099/mic.0.28048-0.

Bonilla, Braulio, Sarah R. Hengel, McKenzie K. Grundy, and Kara A. Bernstein. 2020. “RAD51 Gene Family Structure and Function.” *Annual Review of Genetics* 54 (91): 25–46. https://doi.org/10.1146/annurev-genet-021920-092410.

Bont, Rinne De, and Nik van Larebeke. 2004. “Endogenous DNA Damage in Humans: A Review of Quantitative Data.” *Mutagenesis* 19 (3): 169–85. https://doi.org/10.1093/mutage/geh025.

Borde, Valérie, and Bernard de Massy. 2013. “Programmed Induction of DNA Double Strand Breaks during Meiosis: Setting up Communication between DNA and the Chromosome Structure.” *Current Opinion in Genetics and Development* 23 (2): 147–55. https://doi.org/10.1016/j.gde.2012.12.002.

Bothmer, Anne, Tanushree Phadke, Luis A. Barrera, Carrie M. Margulies, Christina S. Lee, Frank Buquicchio, Sean Moss, et al. 2017. “Characterization of the Interplay between DNA Repair and CRISPR/Cas9-Induced DNA Lesions at an Endogenous Locus.” *Nature Communications* 8 (May 2016): 1–12. https://doi.org/10.1038/ncomms13905.

Bouhaddou, Mehdi, Danish Memon, Bjoern Meyer, Kris M. White, Veronica V. Rezelj, Miguel Correa Marrero, Benjamin J. Polacco, et al. 2020. “The Global Phosphorylation Landscape of SARS-CoV-2 Infection.” *Cell* 182 (3): 685-712.e19. https://doi.org/10.1016/j.cell.2020.06.034.

Branzei, Dana, and Marco Foiani. 2008. “Regulation of DNA Repair throughout the Cell Cycle.” *Nature Reviews Molecular Cell Biology* 9 (4): 297–308. https://doi.org/10.1038/nrm2351.

Brinkman, Eva K., Tao Chen, Marcel de Haas, Hanna A. Holland, Waseem Akhtar, and Bas van Steensel. 2018. “Kinetics and Fidelity of the Repair of Cas9-Induced Double-Strand DNA Breaks.” *Molecular Cell* 70 (5): 801-813.e6. https://doi.org/10.1016/j.molcel.2018.04.016.

Burke, James M., Laura A. St Clair, Rushika Perera, and Roy Parker. 2021. “SARS-CoV-2 Infection Triggers Widespread Host MRNA Decay Leading to an MRNA Export Block.” *Rna*, rna.078923.121. https://doi.org/10.1261/rna.078923.121.

Bussani, Rossana, Edoardo Schneider, Lorena Zentilin, Chiara Collesi, Hashim Ali, Luca

Braga, Maria Concetta Volpe, et al. 2020. “Persistence of Viral RNA, Pneumocyte Syncytia and Thrombosis Are Hallmarks of Advanced COVID-19 Pathology.” *EBioMedicine* 61. https://doi.org/10.1016/j.ebiom.2020.103104.

Bussel, Mark T.J. van, Ahmad Awada, Maja J.A. de Jonge, Morten Mau-Sørensen, Dorte Nielsen, Patrick Schöffski, Henk M.W. Verheul, et al. 2021. “A First-in-Man Phase 1 Study of the DNA-Dependent Protein Kinase Inhibitor Peposertib (Formerly M3814) in Patients with Advanced Solid Tumours.” *British Journal of Cancer* 124 (4): 728–35. https://doi.org/10.1038/s41416-020-01151-6.

Cabrini, Matteo, Marco Roncador, Alessandro Galbiati, Lina Cipolla, Antonio Maffia, Fabio Iannelli, Simone Sabbioneda, Fabrizio d’Adda di Fagagna, and Sofia Francia. 2021. “DROSHA Is Recruited to DNA Damage Sites by the MRN Complex to Promote Non-Homologous End Joining.” *Journal of Cell Science* 134 (6). https://doi.org/10.1242/jcs.249706.

Certo, Michael T., Byoung Y. Ryu, James E. Annis, Mikhail Garibov, Jordan Jarjour, David J. Rawlings, and Andrew M. Scharenberg. 2011. “Tracking Genome Engineering Outcome at Individual DNA Breakpoints.” *Nature Methods* 8 (8): 671–76. https://doi.org/10.1038/nmeth.1648.

Chang, Howard H.Y., Nicholas R. Pannunzio, Noritaka Adachi, and Michael R. Lieber. 2017. “Non-Homologous DNA End Joining and Alternative Pathways to Double-Strand Break Repair.” *Nature Reviews Molecular Cell Biology* 18 (8): 495–506. https://doi.org/10.1038/nrm.2017.48.

Charlesworth, Carsten T., Priyanka S. Deshpande, Daniel P. Dever, Joab Camarena, Viktor T. Lemgart, M. Kyle Cromer, Christopher A. Vakulskas, et al. 2019. “Identification of Preexisting Adaptive Immunity to Cas9 Proteins in Humans.” *Nature Medicine* 25 (2): 249–54. https://doi.org/10.1038/s41591-018-0326-x.

Chatterjee, Nimrat, and Graham C. Walker. 2017. “Mechanisms of DNA Damage, Repair, and Mutagenesis.” *Environmental and Molecular Mutagenesis* 58 (5): 235–63. https://doi.org/10.1002/em.22087.

Chen, Hui, Yang Cui, Xuling Han, Wei Hu, Min Sun, Yong Zhang, Pei Hui Wang, Guangtao Song, Wei Chen, and Jizhong Lou. 2020. “Liquid–Liquid Phase Separation by SARS-CoV-2 Nucleocapsid Protein and RNA.” *Cell Research*, 1–3. https://doi.org/10.1038/s41422-020-00408-2.

Chen, Jie, Shane M. Harding, Ramakrishnan Natesan, Lei Tian, Joseph L. Benci, Weihua Li, Andy J. Minn, Irfan A. Asangani, and Roger A. Greenberg. 2020. “Cell Cycle Checkpoints Cooperate to Suppress DNA- and RNA-Associated Molecular Pattern Recognition and Anti-Tumor Immune Responses.” *Cell Reports* 32 (9): 108080. https://doi.org/10.1016/j.celrep.2020.108080.

Chen, Linlin, Huidan Deng, Hengmin Cui, Jing Fang, Zhicai Zuo, Junliang Deng, Yinglun Li, Xun Wang, and Ling Zhao. 2017. “Inflammatory Responses and Inflammation-Associated Diseases in Organs.” *Oncotarget* 9 (6): 7204–18. https://doi.org/10.18632/oncotarget.23208.

Chen, Minjiang, Aiwu Mao, Min Xu, Qiaoyou Weng, Jianting Mao, and Jiansong Ji. 2019. “CRISPR-Cas9 for Cancer Therapy: Opportunities and Challenges.” *Cancer Letters* 447 (December 2018): 48–55. https://doi.org/10.1016/j.canlet.2019.01.017.

Chen, Zhang Hui, Yan P. Yu, Ze Hua Zuo, Joel B. Nelson, George K. Michalopoulos, Satdatshan Monga, Silvia Liu, George Tseng, and Jian Hua Luo. 2017. "Targeting Genomic Rearrangements in Tumor Cells through Cas9-Mediated Insertion of a Suicide Gene." *Nature Biotechnology* 35 (6): 543–50. https://doi.org/10.1038/nbt.3843.

Cheng, Chun-Ting. 2014. "KAPtain in Charge of Multiple Missions: Emerging Roles of KAP1." *World Journal of Biological Chemistry* 5 (3): 308. https://doi.org/10.4331/wjbc.v5.i3.308.

Cheng, Hao, Feng Zhang, and Yang Ding. 2021. "Crispr/Cas9 Delivery System Engineering for Genome Editing in Therapeutic Applications." *Pharmaceutics* 13 (1649). https://doi.org/10.3390/pharmaceutics13101649.

Childs, Bennett G, Darren J Baker, James L Kirkland, Judith Campisi, and Jan M Deursen. 2014. "Senescence and Apoptosis: Dueling or Complementary Cell Fates?" *EMBO Reports* 15 (11): 1139–53. https://doi.org/10.15252/embr.201439245.

Cho, Won Ki, Jan Hendrik Spille, Micca Hecht, Choongman Lee, Charles Li, Valentin Grube, and Ibrahim I. Cisse. 2018. "Mediator and RNA Polymerase II Clusters Associate in Transcription-Dependent Condensates." *Science* 361 (6400): 412–15. https://doi.org/10.1126/science.aar4199.Mediator.

Christian, Michelle, Tomas Cermak, Erin L. Doyle, Clarice Schmidt, Feng Zhang, Aaron Hummel, Adam J. Bogdanove, and Daniel F. Voytas. 2010. "Targeting DNA Double-Strand Breaks with TAL Effector Nucleases." *Genetics* 186 (2): 756–61. https://doi.org/10.1534/genetics.110.120717.

Clarke, Ryan, Robert Heler, Matthew S. MacDougall, Nan Cher Yeo, Alejandro Chavez, Maureen Regan, Leslyn Hanakahi, George M. Church, Luciano A. Marraffini, and Bradley J. Merrill. 2018. "Enhanced Bacterial Immunity and Mammalian Genome Editing via RNA-Polymerase-Mediated Dislodging of Cas9 from Double-Strand DNA Breaks." *Molecular Cell* 71 (1): 42-55.e8. https://doi.org/10.1016/j.molcel.2018.06.005.

Collins, Patrick L., Caitlin Purman, Sofia I. Porter, Vincent Nganga, Ankita Saini, Katharina E. Hayer, Greer L. Gurewitz, et al. 2020. "DNA Double-Strand Breaks Induce H2Ax Phosphorylation Domains in a Contact-Dependent Manner." *Nature Communications* 11 (1). https://doi.org/10.1038/s41467-020-16926-x.

Cong, Le, F Ann Ran, David Cox, Shuailiang Lin, Robert Barretto, Patrick D Hsu, Xuebing Wu, Wenyan Jiang, and Luciano a Marraffini. 2013. "Cong, L., Ran, F. A., Cox, D., Lin, S., Barretto, R., Habib, N., … Zhang, F. (2013). Multiplex Genome Engineering Using CRISPR/Cas Systems. Science (New York, N.Y.)." *Science (New York, N.Y.)* 339 (6121): 819–23. https://doi.org/10.1126/science.1231143.Multiplex.

Conti, Anastasia, and Raffaella Di Micco. 2018. "P53 Activation: A Checkpoint for Precision Genome Editing?" *Genome Medicine* 10 (66). https://doi.org/10.1186/s13073-018-0578-6.

Cook, Peter J., and Andrea Ventura. 2019. "Cancer Diagnosis and Immunotherapy in the Age of CRISPR." *Genes Chromosomes and Cancer* 58 (4): 233–43. https://doi.org/10.1002/gcc.22702.

Crasta, Karen, Neil J. Ganem, Regina Dagher, Alexandra B. Lantermann, Elena V.

Ivanova, Yunfeng Pan, Luigi Nezi, Alexei Protopopov, Dipanjan Chowdhury, and David Pellman. 2012. “DNA Breaks and Chromosome Pulverization from Errors in Mitosis.” *Nature* 482 (7383): 53–58. https://doi.org/10.1038/nature10802.

Crooke, Stanley T., Brenda F. Baker, Rosanne M. Crooke, and Xue hai Liang. 2021. “Antisense Technology: An Overview and Prospectus.” *Nature Reviews Drug Discovery* 20 (6): 427–53. https://doi.org/10.1038/s41573-021-00162-z.

Crosetto, Nicola, Abhishek Mitra, Maria Joao Silva, Magda Bienko, Norbert Dojer, Qi Wang, Elif Karaca, et al. 2013. “Nucleotide-Resolution DNA Double-Strand Breaks Mapping by next-Generation Sequencing” 10 (4): 361–65. https://doi.org/10.1038/nmeth.2408.

Cruz-García, Andrés, Ana López-Saavedra, and Pablo Huertas. 2014. “BRCA1 Accelerates CtIP-Ediated DNA-End Resection.” *Cell Reports* 9 (2): 451–59. https://doi.org/10.1016/j.celrep.2014.08.076.

d’Adda di Fagagna, Fabrizio. 2008. “Living on a Break: Cellular Senescence as a DNA-Damage Response.” *Nature Reviews Cancer* 8 (7): 512–22. https://doi.org/10.1038/nrc2440.

———. 2014. “A Direct Role for Small Non-Coding RNAs in DNA Damage Response.” *Trends in Cell Biology* 24 (3): 171–78. https://doi.org/10.1016/j.tcb.2013.09.008.

d’Adda di Fagagna, Fabrizio, Philip M Reaper, Lorena Clay-Farrace, Heike Fiegler, Philippa Carr, Thomas Von Zglinicki, Gabriele Saretzki, Nigel P Carter, and Stephen P Jackson. 2003. “A DNA Damage Checkpoint Response in Telomere-Initiated Senescence.” *Nature* 426 (November): 194–98.

D’Agnillo, Felice, Kathie-Anne Walters, Yongli Xiao, Zong-Mei Sheng, Kelsey Scherler, Jaekeun Park, Sebastian Gygli, et al. 2021. “Lung Epithelial and Endothelial Damage, Loss of Tissue Repair, Inhibition of Fibrinolysis, and Cellular Senescence in Fatal COVID-19.” *Science Translational Medicine* 13 (620): 1–18. https://doi.org/10.1126/scitranslmed.abj7790.

D’Alessandro, Giuseppina, Donna Rose Whelan, Sean Michael Howard, Valerio Vitelli, Xavier Renaudin, Marek Adamowicz, Fabio Iannelli, et al. 2018. “BRCA2 Controls DNA:RNA Hybrid Level at DSBs by Mediating RNase H2 Recruitment.” *Nature Communications* 9 (1). https://doi.org/10.1038/s41467-018-07799-2.

Danilo Licastro, Sreejith Rajasekharan, Simeone Dal Monego, Ludovica Segat, Pierlanfranco D’Agaro, and The Regione FVG Laboratory Group on COVID-19 Alessandro Marcello. 2020. “Isolation and Full-Length Genome Characterization of SARSCoV- 2 from COVID-19 Cases in Northern Italy,” 9–12.

Danilo Maddalo and Andrea Ventura. 2016. “Somatic Engineering of Oncogenic Chromosomal Rearrangements: A Perspective.” *Cancer Res* 76 (17): 4918–23. https://doi.org/10.1158/0008-5472.CAN-16-0726.Somatic.

Dash, Prasanta K., Rafal Kaminski, Ramona Bella, Hang Su, Saumi Mathews, Taha M. Ahooyi, Chen Chen, et al. 2019. “Sequential LASER ART and CRISPR Treatments Eliminate HIV-1 in a Subset of Infected Humanized Mice.” *Nature Communications* 10 (1): 1–20. https://doi.org/10.1038/s41467-019-10366-y.

Dash, Radha Charan, and Kyle Hadden. 2021. “Protein–Protein Interactions in Translesion

Synthesis." *Molecules* 26 (18). https://doi.org/10.3390/molecules26185544.

Deltcheva, Elitza, Krzysztof Chylinski, Cynthia M. Sharma, Karine Gonzales, Yanjie Chao, Zaid A. Pirzada, Maria R. Eckert, Jörg Vogel, and Emmanuelle Charpentier. 2011. "CRISPR RNA Maturation by Trans-Encoded Small RNA and Host Factor RNase III." *Nature* 471 (7340): 602–7. https://doi.org/10.1038/nature09886.

Demin, Annie A., Kouji Hirota, Masataka Tsuda, Marek Adamowicz, Richard Hailstone, Jan Brazina, William Gittens, et al. 2021. "XRCC1 Prevents Toxic PARP1 Trapping during DNA Base Excision Repair." *Molecular Cell* 81 (14): 3018–30. https://doi.org/10.1016/j.molcel.2021.05.009.

Dev, Harveer, Ting Wei Will Chiang, Chloe Lescale, Inge de Krijger, Alistair G. Martin, Domenic Pilger, Julia Coates, et al. 2018. "Shieldin Complex Promotes DNA End-Joining and Counters Homologous Recombination in BRCA1-Null Cells." *Nature Cell Biology* 20 (8): 954–65. https://doi.org/10.1038/s41556-018-0140-1.

Doench, John G. 2018. "Am i Ready for CRISPR? A User's Guide to Genetic Screens." *Nature Reviews Genetics* 19 (2): 67–80. https://doi.org/10.1038/nrg.2017.97.

Dou, Zhixun, Kanad Ghosh, Maria Grazia Vizioli, Jiajun Zhu, Payel Sen, Kirk J. Wangensteen, Johayra Simithy, et al. 2017. "Cytoplasmic Chromatin Triggers Inflammation in Senescence and Cancer." *Nature* 550 (7676): 402–6. https://doi.org/10.1038/nature24050.

Doudna, Jennifer A., and Emmanuelle Charpentier. 2014. "The New Frontier of Genome Engineering with CRISPR-Cas9." *Science* 346 (6213). https://doi.org/10.1126/science.1258096.

Eid, Wassim, Martin Steger, Mahmoud El-Shemerly, Lorenza P. Ferretti, Javier Peña-Diaz, Christiane König, Emanuele Valtorta, Alessandro A. Sartori, and Stefano Ferrari. 2010. "DNA End Resection by CtIP and Exonuclease 1 Prevents Genomic Instability." *EMBO Reports* 11 (12): 962–68. https://doi.org/10.1038/embor.2010.157.

Evan, Gerard I., and Fabrizio d'Adda di Fagagna. 2009. "Cellular Senescence: Hot or What?" *Current Opinion in Genetics and Development* 19 (1): 25–31. https://doi.org/10.1016/j.gde.2008.11.009.

Fajrial, Apresio K., Qing Qing He, Nurul I. Wirusanti, Jill E. Slansky, and Xiaoyun Ding. 2020. "A Review of Emerging Physical Transfection Methods for CRISPR/Cas9-Mediated Gene Editing." *Theranostics* 10 (12): 5532–49. https://doi.org/10.7150/thno.43465.

Ferraro, Paola, Elisa Franzolin, Giovanna Pontarin, Peter Reichard, and Vera Bianchi. 2010. "Quantitation of Cellular Deoxynucleoside Triphosphates." *Nucleic Acids Research* 38 (6): e85–e85. https://doi.org/10.1093/nar/gkp1141.

Ferreira da Silva, Joana, Mathilde Meyenberg, and Joanna I. Loizou. 2021. "Tissue Specificity of DNA Repair: The CRISPR Compass." *Trends in Genetics* 37 (11): 958–62. https://doi.org/10.1016/j.tig.2021.07.010.

Fok, Jacqueline H.L., Antonio Ramos-Montoya, Mercedes Vazquez-Chantada, Paul W.G. Wijnhoven, Valeria Follia, Neil James, Paul M. Farrington, et al. 2019. "AZD7648 Is a Potent and Selective DNA-PK Inhibitor That Enhances Radiation, Chemotherapy and Olaparib Activity." *Nature Communications* 10 (1): 1–15.

https://doi.org/10.1038/s41467-019-12836-9.

Francia, Sofia; Michelini, Flavia; Saxena, Alka; Tang, Dave; de Hoon, Michiel; Anelli, Viviana; Mione, Marina; Carninci, Piero; d'Adda di Fagagna, Fabrizio. 2012. "Site-Specific DICER & DROSHA RNA Products Contrl DDR." *Nature* 488 (7410): 231–35. https://doi.org/10.1038/nature11179.Site-specific.

Francia, Sofia, Matteo Cabrini, Valentina Matti, Amanda Oldani, and Fabrizio d'Adda di Fagagna. 2016. "DICER, DROSHA and DNA Damage Response RNAs Are Necessary for the Secondary Recruitment of DNA Damage Response Factors." *Journal of Cell Science* 129 (7): 1468–76. https://doi.org/10.1242/jcs.182188.

Francia, Sofia, Flavia Michelini, Alka Saxena, Dave Tang, Michiel De Hoon, Viviana Anelli, Marina Mione, Piero Carninci, and Fabrizio D'adda Di Fagagna. 2012. "Site-Specific DICER and DROSHA RNA Products Control the DNA-Damage Response." *Nature* 488 (7410): 231–35. https://doi.org/10.1038/nature11179.

Frangini, Miriam, Elisa Franzolin, Francesco Chemello, Paolo Laveder, Chiara Romualdi, Vera Bianchi, and Chiara Rampazzo. 2013. "Synthesis of Mitochondrial DNA Precursors during Myogenesis, an Analysis in Purified C2C12 Myotubes*." *Journal of Biological Chemistry* 288 (8): 5624–35. https://doi.org/10.1074/jbc.M112.441147.

Franken, Nicolaas A.P., Hans M. Rodermond, Jan Stap, Jaap Haveman, and Chris van Bree. 2006. "Clonogenic Assay of Cells in Vitro." *Nature Protocols* 1 (5): 2315–19. https://doi.org/10.1038/nprot.2006.339.

Fu, Yanfang, Jeffry D. Sander, Deepak Reyon, Vincent M. Cascio, and J. Keith Joung. 2014. "Improving CRISPR-Cas Nuclease Specificity Using Truncated Guide RNAs." *Nature Biotechnology* 32 (3): 279–84. https://doi.org/10.1038/nbt.2808.

Fumagalli, Marzia, Francesca Rossiello, Michela Clerici, Sara Barozzi, Davide Cittaro, Jessica M Kaplunov, Gabriele Bucci, et al. 2012. "Telomeric DNA Damage Is Irreparable and Causes Persistent DNA-Damage-Response Activation." *Nature Cell Biology* 14 (4): 355. https://doi.org/10.1038/ncb2466.

Fumagalli, Marzia, Francesca Rossiello, Chiara Mondello, and Fabrizio d'Adda di Fagagna. 2014. "Stable Cellular Senescence Is Associated with Persistent DDR Activation." *PLoS ONE* 9 (10): 44–46. https://doi.org/10.1371/journal.pone.0110969.

Garcia, Gustavo, Arun Sharma, Arunachalam Ramaiah, Chandani Sen, Arunima Purkayastha, Donald B. Kohn, Mark S. Parcells, et al. 2021. "Antiviral Drug Screen Identifies DNA-Damage Response Inhibitor as Potent Blocker of SARS-CoV-2 Replication." *Cell Reports* 35 (1). https://doi.org/10.1016/j.celrep.2021.108940.

Gasparini, Patrizia, Giulia Bertolini, Mara Binda, Alessandra Magnifico, Luisa Albano, Monica Tortoreto, Graziella Pratesi, et al. 2010. "Molecular Cytogenetic Characterization of Stem-like Cancer Cells Isolated from Established Cell Lines." *Cancer Letters* 296 (2): 206–15. https://doi.org/10.1016/j.canlet.2010.04.009.

Gekara, Nelson O. 2017. "DNA Damage-Induced Immune Response: Micronuclei Provide Key Platform." *Journal of Cell Biology* 216 (10): 2999–3001. https://doi.org/10.1083/jcb.201708069.

Gilbert, Luke A, Max A Horlbeck, Britt Adamson, E Jacqueline, Yuwen Chen, Evan H Whitehead, Carla Guimaraes, et al. 2014. "Genome-Scale CRISPR-Mediated Control

of Gene Repression and Activation." *Cell* 159 (3): 647–61. https://doi.org/10.1016/j.cell.2014.09.029.

Gilbert, Luke A, Matthew H Larson, Leonardo Morsut, Zairan Liu, A Gloria, Sandra E Torres, Noam Stern-ginossar, et al. 2013. "CRISPR-Mediated Modular RNA-Guided Regulation of Transcription in Eukaryotes." *Cell* 154 (2): 442–51. https://doi.org/10.1016/j.cell.2013.06.044.

Gioia, U, S Francia, M Cabrini, S Brambillasca, F Michelini, C W Jones-Weinert, and F d'Adda di Fagagna. 2019. "Pharmacological Boost of DNA Damage Response and Repair by Enhanced Biogenesis of DNA Damage Response RNAs." *Sci Rep* 9 (1): 6460. https://doi.org/10.1038/s41598-019-42892-6.

Glück, Selene, Baptiste Guey, Muhammet Fatih Gulen, Katharina Wolter, Niklas Arndt Schmacke, Anne Bridgeman, Jan Rehwinkel, Lars Zender, and Andrea Ablasser. 2017. "Innate Immune Sensing of Cytosolic Chromatin Fragments through CGAS Promotes Senescence." *Nat Cell Biol* 19 (9): 1061–70. https://doi.org/10.1038/ncb3586.Innate.

Goedegebuure, Ruben S.A., Esther A. Kleibeuker, Francesca M. Buffa, Kitty C.M. Castricum, Syed Haider, Iris A. Schulkens, Luuk ten Kroode, et al. 2021. "Interferon- and STING-Independent Induction of Type I Interferon Stimulated Genes during Fractionated Irradiation." *Journal of Experimental and Clinical Cancer Research* 40 (1): 1–14. https://doi.org/10.1186/s13046-021-01962-2.

Gong, Chaoju, Hong Liu, Rui Song, Tingting Zhong, Meng Lou, Tingyang Wang, Hongyan Qi, Jing Shen, Lijun Zhu, and Jimin Shao. 2016. "ATR-CHK1-E2F3 Signaling Transactivates Human Ribonucleotide Reductase Small Subunit M2 for DNA Repair Induced by the Chemical Carcinogen MNNG." *Biochimica et Biophysica Acta* 1859: 612–26. https://doi.org/10.1016/j.bbagrm.2016.02.012.

González Besteiro, Marina A, Nicolás L Calzetta, Sofía M Loureiro, Martín Habif, Rémy Bétous, Marie-Jeanne Pillaire, Antonio Maffia, Simone Sabbioneda, Jean-Sébastien Hoffmann, and Vanesa Gottifredi. 2019. "Chk1 Loss Creates Replication Barriers That Compromise Cell Survival Independently of Excess Origin Firing." *The EMBO Journal* 38 (16): 1–16. https://doi.org/10.15252/embj.2018101284.

Gordon, David E., Gwendolyn M. Jang, Mehdi Bouhaddou, Jiewei Xu, Kirsten Obernier, Kris M. White, Matthew J. O'Meara, et al. 2020. "A SARS-CoV-2 Protein Interaction Map Reveals Targets for Drug Repurposing." *Nature* 583 (7816): 459–68. https://doi.org/10.1038/s41586-020-2286-9.

Greider, Carol W., and Elizabeth H. Blackburn. 1985. "Identification of a Specific Telomere Terminal Transferase Activity in Tetrahymena Extracts." *Cell* 43 (2): 405–13. https://doi.org/10.1016/0092-8674(85)90170-9.

Guilinger, John P., David B. Thompson, and David R. Liu. 2014. "Fusion of Catalytically Inactive Cas9 to FokI Nuclease Improves the Specificity of Genome Modification" 32 (6): 577–82. https://doi.org/10.1038/nbt.2909.

Gunn, Amanda, and Jeremy M. Stark. 2009. "I-SceI-Based Assays to Examine Distinct Repair Outcomes of Mammalian Chromosomal Double Strand Breaks." *Life Sciences* 531: 588. https://doi.org/10.1006/cbir.1999.0447.

Guo, Xiaogang, Tiejun Zhang, Zheng Hu, Yanqi Zhang, Zhaoying Shi, Qinhu Wang, Yan

Cui, Fengqin Wang, Hui Zhao, and Yonglong Chen. 2014. “Efficient RNA/Cas9-Mediated Genome Editing in Xenopus Tropicalis.” *Development* 141: 707–14. https://doi.org/10.1242/dev.099853.

Guo, Xihan, Xueqin Dai, Xue Wu, Neng Cao, and Xu Wang. 2020. “Small but Strong: Mutational and Functional Landscapes of Micronuclei in Cancer Genomes.” *International Journal of Cancer* 148 (4): 812–24. https://doi.org/10.1002/ijc.33300.

Gupta, Darshana, Oindrila Bhattacharjee, Drishti Mandal, Madhab Kumar Sen, Dhritiman Dey, Adhiraj Dasgupta, Tawsif Ahmed Kazi, et al. 2019. “CRISPR-Cas9 System: A New-Fangled Dawn in Gene Editing.” *Life Sciences* 232 (April): 116636. https://doi.org/10.1016/j.lfs.2019.116636.

Gussow, Ayal B., Noam Auslander, Guilhem Faure, Yuri I. Wolf, Feng Zhang, and Eugene V. Koonin. 2020. “Genomic Determinants of Pathogenicity in SARS-CoV-2 and Other Human Coronaviruses.” *Proceedings of the National Academy of Sciences* 117 (26): 15193–99. https://doi.org/10.1073/pnas.2008176117.

Haapaniemi, Emma, Sandeep Botla, Jenna Persson, Bernhard Schmierer, and Jussi Taipale. 2018. “CRISPR-Cas9 Genome Editing Induces a P53-Mediated DNA Damage Response.” *Nature Medicine* 24 (7): 927–30. https://doi.org/10.1038/s41591-018-0049-z.

Haeussler, Maximilian. 2020. “CRISPR Off-Targets: A Question of Context.” *Cell Biology and Toxicology* 36 (1): 5–9. https://doi.org/10.1007/s10565-019-09497-1.

Hakem, Razqallah. 2008. “DNA-Damage Repair; the Good, the Bad, and the Ugly.” *EMBO Journal* 27 (4): 589–605. https://doi.org/10.1038/emboj.2008.15.

Han, Yanyan, Dandan Liu, and Lianhong Li. 2020. “PD-1/PD-L1 Pathway: Current Researches in Cancer.” *American Journal of Cancer Research* 10 (3): 727–42. http://www.ncbi.nlm.nih.gov/pubmed/32266087.

Hanahan, Douglas, and Robert A. Weinberg. 2011. “Hallmarks of Cancer: The next Generation.” *Cell* 144 (5): 646–74. https://doi.org/10.1016/j.cell.2011.02.013.

Harding, Shane M., Joseph L. Benci, Jerome Irianto, Dennis E. Discher, Andy J. Minn, and Roger A. Greenberg. 2017. “Mitotic Progression Following DNA Damage Enables Pattern Recognition within Micronuclei.” *Nature* 548 (7668): 466–70. https://doi.org/10.1038/nature23470.

Hart, Madeleine, Sophie D. Adams, and Viji M. Draviam. 2021. “Multinucleation Associated DNA Damage Blocks Proliferation in P53-Compromised Cells.” *Communications Biology* 4 (1): 1–11. https://doi.org/10.1038/s42003-021-01979-5.

Hayflick, L., and P. S. Moorhead. 1961. “The Serial Cultivation of Human Diploid Cell Strains.” *Experimental Cell Research* 25 (3): 585–621. https://doi.org/10.1016/0014-4827(61)90192-6.

Hendel, Ayal, Rasmus O. Bak, Joseph T. Clark, Andrew B. Kennedy, Daniel E. Ryan, Subhadeep Roy, Israel Steinfeld, et al. 2015. “Chemically Modified Guide RNAs Enhance CRISPR-Cas Genome Editing in Human Primary Cells.” *Nature Biotechnology* 33 (9): 985–89. https://doi.org/10.1038/nbt.3290.

Herbig, Utz, Wendy A. Jobling, Benjamin P.C. Chen, David J. Chen, and John M. Sedivy.

2004. “Telomere Shortening Triggers Senescence of Human Cells through a Pathway Involving ATM, P53, and P21CIP1, but Not P16INK4a.” *Molecular Cell* 14 (4): 501–13. https://doi.org/10.1016/S1097-2765(04)00256-4.

Hewitt, Graeme, Diana Jurk, Francisco D.M. Marques, Clara Correia-Melo, Timothy Hardy, Agata Gackowska, Rhys Anderson, Morgan Taschuk, Jelena Mann, and João F. Passos. 2012. “Telomeres Are Favoured Targets of a Persistent DNA Damage Response in Ageing and Stress-Induced Senescence.” *Nature Communications* 3. https://doi.org/10.1038/ncomms1708.

Higa, Leigh Ann A., Ivailo S. Mihaylov, Damon P. Banks, Jianyu Zheng, and Hui Zhang. 2003. “Radiation-Mediated Proteolysis of CDT1 by CUL4-ROC1 and CSN Complexes Constitutes a New Checkpoint.” *Nature Cell Biology* 5 (11): 1008–15. https://doi.org/10.1038/ncb1061.

Hintzsche, Henning, Ulrike Hemmann, Albrecht Poth, Dietmar Utesch, Jasmin Lott, and Helga Stopper. 2017. “Fate of Micronuclei and Micronucleated Cells.” *Mutation Research - Reviews in Mutation Research* 771: 85–98. https://doi.org/10.1016/j.mrrev.2017.02.002.

Holoch and Moazed. 2015. “RNA-Mediated Epigenetic Regulation of Gene Expression Daniel.” *Nat Rev Genet* 16 (2): 71–84. https://doi.org/10.1038/nrg3863.RNA-mediated.

Hsu, Patrick D., Eric S. Lander, and Feng Zhang. 2014. “Development and Applications of CRISPR-Cas9 for Genome Engineering.” *Cell* 157 (6): 1262–78. https://doi.org/10.1016/j.cell.2014.05.010.

Hsu, Patrick D., David A. Scott, Joshua A. Weinstein, F. Ann Ran, Silvana Konermann, Vineeta Agarwala, Yinqing Li, et al. 2013. “DNA Targeting Specificity of RNA-Guided Cas9 Nucleases.” *Nature Biotechnology* 31 (9): 827–32. https://doi.org/10.1038/nbt.2647.

Hu, Jian, Chad M. McCall, Tomohiko Ohta, and Yue Xiong. 2004. “Targeted Ubiquitination of CDT1 by the DDB1-CUL4A-ROC1 Ligase in Response to DNA Damage.” *Nature Cell Biology* 6 (10): 1003–9. https://doi.org/10.1038/ncb1172.

Huang, Ruixue, and Ping Kun Zhou. 2021. *DNA Damage Repair: Historical Perspectives, Mechanistic Pathways and Clinical Translation for Targeted Cancer Therapy*. *Signal Transduction and Targeted Therapy*. Vol. 6. Springer US. https://doi.org/10.1038/s41392-021-00648-7.

Hui Yang, Haoyi Wang, Chikdu S. Shivalila, Albert W. Cheng, Linyu Shi, and Rudolf Jaenisch. 2013. “One-Step Generation of Mice Carrying Reporter and Conditional Alleles by CRISPR/Cas Mediated Genome Engineering.” *Cell* 154 (6): 1370–79. https://doi.org/10.1016/j.cell.2013.08.022.

Hustedt, Nicole, and Daniel Durocher. 2017. “The Control of DNA Repair by the Cell Cycle.” *Nature Cell Biology* 19 (1): 1–9. https://doi.org/10.1038/ncb3452.

Iacovoni, Jason S., Pierre Caron, Imen Lassadi, Estelle Nicolas, Laurent Massip, Didier Trouche, and Gaëlle Legube. 2010. “High-Resolution Profiling of Γh2AX around DNA Double Strand Breaks in the Mammalian Genome.” *EMBO Journal* 29 (8): 1446–57. https://doi.org/10.1038/emboj.2010.38.

Iannelli, Fabio, Alessandro Galbiati, Ilaria Capozzo, Quan Nguyen, Brian Magnuson, Flavia Michelini, Giuseppina D'Alessandro, et al. 2017. "A Damaged Genome's Transcriptional Landscape through Multilayered Expression Profiling around in Situ-Mapped DNA Double-Strand Breaks." *Nature Communications* 8 (May): 1–7. https://doi.org/10.1038/ncomms15656.

Ihry, Robert J., Kathleen A. Worringer, Max R. Salick, Elizabeth Frias, Daniel Ho, Kraig Theriault, Sravya Kommineni, et al. 2018. "P53 Inhibits CRISPR-Cas9 Engineering in Human Pluripotent Stem Cells." *Nature Medicine* 24 (7): 939–46. https://doi.org/10.1038/s41591-018-0050-6.

Ishino, Y., H. Shinagawa, K. Makino, M. Amemura, and A. Nakatura. 1987. "Nucleotide Sequence of the Iap Gene, Responsible for Alkaline Phosphatase Isoenzyme Conversion in Escherichia Coli, and Identification of the Gene Product." *Journal of Bacteriology* 169 (12): 5429–33. https://doi.org/10.1128/jb.169.12.5429-5433.1987.

Iyer, Divya Ramalingam, and Nicholas Rhind. 2017. "The Intra-S Checkpoint Responses to DNA Damage." *Genes* 8 (2). https://doi.org/10.3390/genes8020074.

Jackson, Stephen P., and Jiri Bartek. 2009. "The DNA-Damage Response in Human Biology and Disease." *Nature* 461 (7267): 1071–78. https://doi.org/10.1038/nature08467.

Jackson, Stephen P., and Daniel Durocher. 2013. "Regulation of DNA Damage Responses by Ubiquitin and SUMO." *Molecular Cell* 49 (5): 795–807. https://doi.org/10.1016/j.molcel.2013.01.017.

Jansen, Ruud, Jan D.A. Van Embden, Wim Gaastra, and Leo M. Schouls. 2002. "Identification of Genes That Are Associated with DNA Repeats in Prokaryotes." *Molecular Microbiology* 43 (6): 1565–75. https://doi.org/10.1046/j.1365-2958.2002.02839.x.

Jao, Li En, Susan R. Wente, and Wenbiao Chen. 2013. "Efficient Multiplex Biallelic Zebrafish Genome Editing Using a CRISPR Nuclease System." *Proceedings of the National Academy of Sciences of the United States of America* 110 (34): 13904–9. https://doi.org/10.1073/pnas.1308335110.

Jarrett, Kelsey E., Ciaran Lee, Marco De Giorgi, Ayrea Hurley, Baiba K. Gillard, Alexandria M. Doerfler, Ang Li, Henry J. Pownall, Gang Bao, and William R. Lagor. 2018. "Somatic Editing of Ldlr with AAV-CRISPR Is an Efficient Tool for Atherosclerosis Research." *Arterioscler Thromb Vasc Biol* 38 (9): 1997–2006. https://doi.org/10.1161/ATVBAHA.

Jasin, Maria, and Rodney Rothstein. 2013. "Repair of Strand Breaks by Homologous Recombination." *Cold Spring Harbor Perspectives in Biology* 5 (11): 1–18. https://doi.org/10.1101/cshperspect.a012740.

Jaskelioff, Mariela, Florian L. Muller, Ji Hye Paik, Emily Thomas, Shan Jiang, Andrew C. Adams, Ergun Sahin, et al. 2011. "Telomerase Reactivation Reverses Tissue Degeneration in Aged Telomerase-Deficient Mice." *Nature* 469 (7328): 102–7. https://doi.org/10.1038/nature09603.

Jiang, Hui, and Ya Fang Mei. 2021. "SARS – CoV – 2 Spike Impairs DNA Damage Repair and Inhibits V (D) J Recombination In Vitro."

Jinek, Martin, Krzysztof Chylinski, Ines Fonfara, Michael Hauer, Jennifer A. Doudna, and Emmanuelle Charpentier. 2012. “A Programmable Dual-RNA-Guided DNA Endonuclease in Adaptive Bacterial Immunity.” *Science* 337 (6096): 816–21. https://doi.org/10.1126/science.1225829.

Jinek, Martin, Alexandra East, Aaron Cheng, Steven Lin, Enbo Ma, and Jennifer Doudna. 2013. “RNA-Programmed Genome Editing in Human Cells.” *ELife* 2013 (2): 1–9. https://doi.org/10.7554/eLife.00471.

Jinek, Martin, Fuguo Jiang, David W. Taylor, Samuel H. Sternberg, Emine Kaya, Enbo Ma, Carolin Anders, et al. 2014. “Structures of Cas9 Endonucleases Reveal RNA-Mediated Conformational Activation.” *Science* 343 (6176): 1–28. https://doi.org/10.1126/science.1247997.

Kakoti, Sangeeta, Hiro Sato, Siddhartha Laskar, Takaaki Yasuhara, and Atsushi Shibata. 2020. “DNA Repair and Signaling in Immune-Related Cancer Therapy.” *Frontiers in Molecular Biosciences* 7 (September): 1–11. https://doi.org/10.3389/fmolb.2020.00205.

Kastan, Michael B., and Jiri Bartek. 2004. “Cell-Cycle Checkpoints and Cancer.” *Nature* 432 (7015): 316–23. https://doi.org/10.1038/nature03097.

Kenjo, Eriya, Hiroyuki Hozumi, Yukimasa Makita, Kumiko A. Iwabuchi, Naoko Fujimoto, Satoru Matsumoto, Maya Kimura, et al. 2021. “Low Immunogenicity of LNP Allows Repeated Administrations of CRISPR-Cas9 MRNA into Skeletal Muscle in Mice.” *Nature Communications* 12 (7101). https://doi.org/10.1038/s41467-021-26714-w.

Khvorova, Anastasia, and Jonathan K. Watts. 2017. “The Chemical Evolution of Oligonucleotide Therapies of Clinical Utility.” *Nature Biotechnology* 35 (3): 238–48. https://doi.org/10.1038/nbt.3765.

Kilic, Sinan, Aleksandra Lezaja, Marco Gatti, Eliana Bianco, Jone Michelena, Ralph Imhof, and Matthias Altmeyer. 2019. “Phase Separation of 53 BP 1 Determines Liquid-like Behavior of DNA Repair Compartments,” 1–17. https://doi.org/10.15252/embj.2018101379.

Kim, Dongwan, Joo Yeon Lee, Jeong Sun Yang, Jun Won Kim, V. Narry Kim, and Hyeshik Chang. 2020. “The Architecture of SARS-CoV-2 Transcriptome.” *Cell* 181 (4): 914-921.e10. https://doi.org/10.1016/j.cell.2020.04.011.

Kim, Hyongbum, and Jin Soo Kim. 2014. “A Guide to Genome Engineering with Programmable Nucleases.” *Nature Reviews Genetics* 15 (5): 321–34. https://doi.org/10.1038/nrg3686.

Kim, Sojung, Daesik Kim, Seung Woo Cho, Jungeun Kim, and Jin-Soo Kim. 2014. “Highly Efficient RNA-Guided Genome Editing in Human Cells via Delivery of Purified Cas9 Ribonucleoproteins.” *Genome Research* 24: 1012–19. https://doi.org/10.1101/gr.171322.113.

Kim, Yang Gyun, Jooyeun Cha, and Srinivasan Chandrasegaran. 1996. “Hybrid Restriction Enzymes: Zinc Finger Fusions to Fok I Cleavage Domain.” *Proceedings of the National Academy of Sciences of the United States of America* 93 (3): 1156–60. https://doi.org/10.1073/pnas.93.3.1156.

Klein, Annelies De, Ad Geurts Van Kessel, Gerard Grosveld, Claus R. Bartram, Anne Hagemeijer, Dirk Bootsma, Nigel K. Spurr, Nora Heisterkamp, John Groffen, and John R. Stephenson. 1982. "A Cellular Oncogene Is Translocated to the Philadelphia Chromosome in Chronic Myelocytic Leukaemia." *Nature* 300: 765–67. https://doi.org/10.1038/300765a0.

Ko, Huaising C., Pippa F. Cosper, Randall J. Kimple, and Matthew E. Witek. 2020. *Combining Radiation and Chemotherapy to Improve the Therapeutic Ratio*. *Improving the Therapeutic Ratio in Head and Neck Cancer*. Elsevier Inc. https://doi.org/10.1016/b978-0-12-817868-3.00003-2.

Koblan, Luke W, Michael R Erdos, Christopher Wilson, Wayne A Cabral, Jonathan M Levy, Zheng-mei Xiong, Urraca L Tavarez, et al. 2021. "In Vivo Base Editing Rescues Hutchinson-Gilford Progeria Syndrome in Mice Luke" 589 (7843): 608–14. https://doi.org/10.1038/s41586-020-03086-7.

Koç, Ahmet, Linda J. Wheeler, Christopher K. Mathews, and Gary F. Merrill. 2004. "Hydroxyurea Arrests DNA Replication by a Mechanism That Preserves Basal DNTP Pools." *Journal of Biological Chemistry* 279 (1): 223–30. https://doi.org/10.1074/jbc.M303952200.

Konermann, Silvana, Mark D Brigham, Alexandro E Trevino, Omar O Abudayyeh, Clea Barcena, Patrick D Hsu, Jonathan S Gootenberg, Hiroshi Nishimasu, Osamu Nureki, and Feng Zhang. 2015. "Genome-Scale Transcriptional Activation by an Engineered CRISPR-Cas9 Complex." *Nature* 517 (7536): 583–88. https://doi.org/10.1038/nature14136.

Krokan, Hans E, and Magnar Bjoras. 2013. "Base Excision Repair." *Cold Spring Harb Perspect Biol.* 5 (4): a012583. http://www.ncbi.nlm.nih.gov/pubmed/23545420%0Ahttp://www.pubmedcentral.nih.gov/articlerender.fcgi?artid=PMC3683898%0Apapers://a0f45058-72ca-4dc9-be03-e459899c7713/Paper/p615.

Krupina, Ksenia, Alexander Goginashvili, and Don W. Cleveland. 2021. "Causes and Consequences of Micronuclei." *Current Opinion in Cell Biology* 70: 91–99. https://doi.org/10.1016/j.ceb.2021.01.004.

Kunkel, Thomas A., and Dorothy A. Erie. 2005. "DNA Mismatch Repair." *Annual Review of Biochemistry* 74: 681–710. https://doi.org/10.1146/annurev.biochem.74.082803.133243.

Kuscu, Cem, Sevki Arslan, Ritambhara Singh, Jeremy Thorpe, and Mazhar Adli. 2014. "Genome-Wide Analysis Reveals Characteristics of off-Target Sites Bound by the Cas9 Endonuclease." *Nature Biotechnology* 32 (7): 677–83. https://doi.org/10.1038/nbt.2916.

Lee, Ji Hoon, and Tanya T. Paull. 2005. "ATM Activation by DNA Double-Strand Breaks through the Mre11-Rad50-Nbs1 Complex." *Science* 308 (5721): 551–54. https://doi.org/10.1126/science.1108297.

Lee, Soyoung, Yong Yu, Jakob Trimpert, Fahad Benthani, Mario Mairhofer, Paulina Richter-Pechanska, Emanuel Wyler, et al. 2021. "Virus-Induced Senescence Is Driver and Therapeutic Target in COVID-19." *Nature* 599 (November). https://doi.org/10.1038/s41586-021-03995-1.

Leibowitz, Mitchell L., Stamatis Papathanasiou, Phillip A. Doerfler, Logan J. Blaine, Lili Sun, Yu Yao, Cheng Zhong Zhang, Mitchell J. Weiss, and David Pellman. 2021. "Chromothripsis as an On-Target Consequence of CRISPR–Cas9 Genome Editing." *Nature Genetics* 53 (6): 895–905. https://doi.org/10.1038/s41588-021-00838-7.

Li, Guo Min. 2008. "Mechanisms and Functions of DNA Mismatch Repair." *Cell Research* 18 (1): 85–98. https://doi.org/10.1038/cr.2007.115.

Li, Tuo, and Zhijian J. Chen. 2018. "The CGAS–CGAMP–STING Pathway Connects DNA Damage to Inflammation, Senescence, and Cancer." *Journal of Experimental Medicine* 215 (5): 1287–99. https://doi.org/10.1084/jem.20180139.

Liang, Xiquan, Jason Potter, Shantanu Kumar, Yanfei Zou, Rene Quintanilla, Mahalakshmi Sridharan, Jason Carte, et al. 2015. "Rapid and Highly Efficient Mammalian Cell Engineering via Cas9 Protein Transfection." *Journal of Biotechnology* 208: 44–53. https://doi.org/10.1016/j.jbiotec.2015.04.024.

Liao, Hsin Kai, Ying Gu, Arturo Diaz, John Marlett, Yuta Takahashi, Mo Li, Keiichiro Suzuki, et al. 2015. "Use of the CRISPR/Cas9 System as an Intracellular Defense against HIV-1 Infection in Human Cells." *Nature Communications* 6: 1–10. https://doi.org/10.1038/ncomms7413.

Lilley, Caroline E., Mira S. Chaurushiya, Chris Boutell, Sebastien Landry, Junghae Suh, Stephanie Panier, Roger D. Everett, Grant S. Stewart, Daniel Durocher, and Matthew D. Weitzman. 2010. "A Viral E3 Ligase Targets RNF8 and RNF168 to Control Histone Ubiquitination and DNA Damage Responses." *EMBO Journal* 29 (5): 943–55. https://doi.org/10.1038/emboj.2009.400.

Lilley, Caroline E., Rachel A. Schwartz, and Matthew D. Weitzman. 2007. "Using or Abusing: Viruses and the Cellular DNA Damage Response." *Trends in Microbiology* 15 (3): 119–26. https://doi.org/10.1016/j.tim.2007.01.003.

Lin, Guigao, Kuo Zhang, and Jinming Li. 2015. "Application of CRISPR/Cas9 Technology to HBV." *International Journal of Molecular Sciences* 16 (11): 26077–86. https://doi.org/10.3390/ijms161125950.

Lino, Christopher A., Jason C. Harper, James P. Carney, and Jerilyn A. Timlin. 2018. "Delivering Crispr: A Review of the Challenges and Approaches." *Drug Delivery* 25 (1): 1234–57. https://doi.org/10.1080/10717544.2018.1474964.

Lipskaia, Larissa, Pauline Maisonnasse, Charles Fouillade, Valentin Sencio, Quentin Pascal, Jean-Michel Flaman, Emmanuelle Born, et al. 2021. "Evidence That SARS-CoV-2 Induces Lung-Cell Senescence: Potential Impact on COVID-19 Lung Disease." *American Journal of Respiratory Cell and Molecular Biology*, 1–21. https://doi.org/10.1165/rcmb.2021-0205le.

Liu, Jinhua, Zichao Chen, Yaqun Li, Wenjie Zhao, Jibiao Wu, and Zhen Zhang. 2021. "PD-1/PD-L1 Checkpoint Inhibitors in Tumor Immunotherapy." *Frontiers in Pharmacology* 12. https://doi.org/10.3389/fphar.2021.731798.

Livak, Kenneth J., and Thomas D. Schmittgen. 2001. "Analysis of Relative Gene Expression Data Using Real-Time Quantitative PCR and the 2-ΔΔCT Method." *Methods* 25 (4): 402–8. https://doi.org/10.1006/meth.2001.1262.

Long, Chengzu, Leonela Amoasii, Alex A. Mireault, John R. McAnally1, Hui Li, Efrain

Sanchez-Ortiz, Samadrita Bhattacharyya, John M. Shelton, Rhonda Bassel-Duby, and Eric N. Olson. 2016. “Postnatal Genome Editing Partially Restores Dystrophin Expression in a Mouse Model of Muscular Dystrophy Chengzu.” *Science* 351 (6271): 400–403. https://doi.org/10.1126/science.aad5725.

Lord, Christopher J., Michelle D. Garrett, and Alan Ashworth. 2006. “Targeting the Double-Strand DNA Break Repair Pathway as a Therapeutic Strategy.” *Clinical Cancer Research* 12 (15): 4463–68. https://doi.org/10.1158/1078-0432.CCR-06-1269.

Lord, Christopher J., Niall Quinn, and Colm J. Ryan. 2020. “Integrative Analysis of Large-Scale Loss-of-Function Screens Identifies Robust Cancer-Associated Genetic Interactions.” *ELife* 9: 1–37. https://doi.org/10.7554/eLife.58925.

Lou, Zhenkun, Claudia Christiano Silva Chini, Katherine Minter-Dykhouse, and Junjie Chen. 2003. “Mediator of DNA Damage Checkpoint Protein 1 Regulates BRCA1 Localization and Phosphorylation in DNA Damage Checkpoint Control.” *Journal of Biological Chemistry* 278 (16): 13599–602. https://doi.org/10.1074/jbc.C300060200.

Lu, Huasong, Dan Yu, Anders S. Hansen, Sourav Ganguly, Rongdiao Liu, Alec Heckert, Xavier Darzacq, and Qiang Zhou. 2018. “Phase-Separation Mechanism for C-Terminal Hyperphosphorylation of RNA Polymerase II.” *Nature* 558 (7709): 318–23. https://doi.org/10.1038/s41586-018-0174-3.

Lu, Wei Ting, Ben R. Hawley, George L. Skalka, Robert A. Baldock, Ewan M. Smith, Aldo S. Bader, Michal Malewicz, Felicity Z. Watts, Ania Wilczynska, and Martin Bushell. 2018. “Drosha Drives the Formation of DNA:RNA Hybrids around DNA Break Sites to Facilitate DNA Repair.” *Nature Communications* 9 (1). https://doi.org/10.1038/s41467-018-02893-x.

Ludovic C. J. Gillet and Orlando D. Scharer. 2006. “Molecular Mechanism of Global Genome Nucleotide Excision Repair.” *Chem Rev* 106: 253–76. https://doi.org/10.1021/cr040483f.

Lukas, Claudia, Velibor Savic, Simon Bekker-Jensen, Carsten Doil, Beate Neumann, Ronni Sølvhøj Pedersen, Merete Grøhfte, et al. 2011. “53BP1 Nuclear Bodies Form around DNA Lesions Generated by Mitotic Transmission of Chromosomes under Replication Stress.” *Nature Cell Biology* 13 (3): 243–53. https://doi.org/10.1038/ncb2201.

Lukas, Jiri, Claudia Lukas, and Jiri Bartek. 2011. “More than Just a Focus: The Chromatin Response to DNA Damage and Its Role in Genome Integrity Maintenance.” *Nature Cell Biology* 13 (10): 1161–69. https://doi.org/10.1038/ncb2344.

Luther, D. C., Y. W. Lee, H. Nagaraj, F. Scaletti, and V. M. Rotello. 2018. “Delivery Approaches for CRISPR/Cas9 Therapeutics in Vivo: Advances and Challenges.” *Expert Opinion on Drug Delivery* 15 (9): 905–13. https://doi.org/10.1080/17425247.2018.1517746.

Luthra, Ritika, Simran Kaur, and Kriti Bhandari. 2021. “Applications of CRISPR as a Potential Therapeutic.” *Life Sciences* 284 (August): 119908. https://doi.org/10.1016/j.lfs.2021.119908.

Ma-Lauer, Yue, Javier Carbajo-Lozoya, Marco Y. Hein, Marcel A. Müller, Wen Deng, Jian Lei, Benjamin Meyer, et al. 2016. “P53 Down-Regulates SARS Coronavirus Replication and Is Targeted by the SARS-Unique Domain and PLpro via E3

Ubiquitin Ligase RCHY1." *Proceedings of the National Academy of Sciences of the United States of America* 113 (35): E5192–5201. https://doi.org/10.1073/pnas.1603435113.

MacKenzie, Karen J., Paula Carroll, Carol Anne Martin, Olga Murina, Adeline Fluteau, Daniel J. Simpson, Nelly Olova, et al. 2017. "CGAS Surveillance of Micronuclei Links Genome Instability to Innate Immunity." *Nature* 548 (7668): 461–65. https://doi.org/10.1038/nature23449.

Maddalo, Danilo, Eusebio Manchado, Carla P. Concepcion, Ciro Bonetti, Joana A. Vidigal, Yoon Chi Han, Paul Ogrodowski, et al. 2014. "In Vivo Engineering of Oncogenic Chromosomal Rearrangements with the CRISPR/Cas9 System." *Nature* 516 (7531): 423–28. https://doi.org/10.1038/nature13902.

Mailand, Niels, Alexandre V. Podtelejnikov, Anja Groth, Matthias Mann, Jiri Bartek, and Jiri Lukas. 2002. "Regulation of G2/M Events by Cdc25A through Phosphorylation-Dependent Modulation of Its Stability." *EMBO Journal* 21 (21): 5911–20. https://doi.org/10.1093/emboj/cdf567.

Makarova, Kira S., Daniel H. Haft, Rodolphe Barrangou, Stan J.J. Brouns, Emmanuelle Charpentier, Philippe Horvath, Sylvain Moineau, et al. 2011. "Evolution and Classification of the CRISPR-Cas Systems." *Nature Reviews Microbiology* 9 (6): 467–77. https://doi.org/10.1038/nrmicro2577.

Mali, Prashant, Luhan Yang, Kevin M. Esvelt, John Aach, Marc Guell, James E. DiCarlo, Julie E. Norville, and George M. Church. 2013. "RNA-Guided Human Genome Engineering via Cas9." *Science* 339 (6121): 823–26. https://doi.org/10.1126/science.1232033.

Manfredi, James J. 2003. "P53 and Apoptosis: It's Not Just in the Nucleus Anymore." *Molecular Cell* 11 (3): 552–54. https://doi.org/10.1016/S1097-2765(03)00106-0.

Maria Eriksson, W. Ted Brown, Leslie B. Gordon, Michael W. Glynn, Joel Singer, Laura Scott, Michael R. Erdos, et al. 2003. "Recurrent de Novo Point Mutations in Lamin A Cause Hutchinson–Gilford Progeria Syndrome." *Nature* 423: 293–98. https://doi.org/doi:10.1038/nature01629.

Marnef, Aline, Sarah Cohen, and Gaëlle Legube. 2017. "Transcription-Coupled DNA Double-Strand Break Repair: Active Genes Need Special Care." *Journal of Molecular Biology* 429 (9): 1277–88. https://doi.org/10.1016/j.jmb.2017.03.024.

Marteijn, Jurgen A., Hannes Lans, Wim Vermeulen, and Jan H.J. Hoeijmakers. 2014. "Understanding Nucleotide Excision Repair and Its Roles in Cancer and Ageing." *Nature Reviews Molecular Cell Biology* 15 (7): 465–81. https://doi.org/10.1038/nrm3822.

Martinez-Lage, M., R. Torres-Ruiz, P. Puig-Serra, P. Moreno-Gaona, M. C. Martin, F. J. Moya, O. Quintana-Bustamante, et al. 2020. "In Vivo CRISPR/Cas9 Targeting of Fusion Oncogenes for Selective Elimination of Cancer Cells." *Nature Communications* 11 (1). https://doi.org/10.1038/s41467-020-18875-x.

Matthews, Helen K., Cosetta Bertoli, and Robertus A.M. de Bruin. 2021. "Cell Cycle Control in Cancer." *Nature Reviews Molecular Cell Biology* 23 (January). https://doi.org/10.1038/s41580-021-00404-3.

Maya-Mendoza, A., J. M. Merchut-Maya, J. Bartkova, J. Bartek, C. H. Streuli, and D. A. Jackson. 2014. “Immortalised Breast Epithelia Survive Prolonged DNA Replication Stress and Return to Cycle from a Senescent-Like State.” *Cell Death and Disease* 5 (7). https://doi.org/10.1038/cddis.2014.315.

Mcvey, Mitch, Sang Eun Lee, Harrison Avenue, and San Antonio. 2017. “MMEJ Repair of Double-Strand Breaks: Deleted Sequences and Alternative Endings.” *Trends Genet.* 24 (11): 529–38. https://doi.org/10.1016/j.tig.2008.08.007.MMEJ.

Meador, J. A., M. Zhao, Y. Su, G. Narayan, C. R. Geard, and A. S. Balajee. 2008. “Histone H2AX Is a Critical Factor for Cellular Protection against DNA Alkylating Agents.” *Oncogene* 27 (43): 5662–71. https://doi.org/10.1038/onc.2008.187.

Mehta, Anuja, and James E. Haber. 2014. “Sources of DNA Double-Strand Breaks and Models of Recombinational DNA Repair.” *Cold Spring Harbor Perspectives in Biology* 6 (9): 1–17. https://doi.org/10.1101/cshperspect.a016428.

Mehta, Puja, Daniel F McAuley, Michael Brown, Emilie Sanchez, Rachel S Tattersall, and Jessica J Manson. 2020. “COVID-19: Consider Cytokine Storm Syndromes and Immunosuppression.” *The Lancet* 395 (March): 1033–34. https://doi.org/10.1016/S0140-6736(20)30628-0.

Micco, Raffaella Di, Marzia Fumagalli, Angelo Cicalese, Sara Piccinin, Patrizia Gasparini, Chiara Luise, Catherine Schurra, et al. 2006. “Oncogene-Induced Senescence Is a DNA Damage Response Triggered by DNA Hyper-Replication.” *Nature* 444 (7119): 638–42. https://doi.org/10.1038/nature05327.

Micco, Raffaella Di, Valery Krizhanovsky, Darren Baker, and Fabrizio d’Adda di Fagagna. 2021. “Cellular Senescence in Ageing: From Mechanisms to Therapeutic Opportunities.” *Nature Reviews Molecular Cell Biology* 22 (2): 75–95. https://doi.org/10.1038/s41580-020-00314-w.

Michelini, F, S Pitchiaya, V Vitelli, S Sharma, U Gioia, F Pessina, M Cabrini, et al. 2017. “Damage-Induced LncRNAs Control the DNA Damage Response through Interaction with DDRNAs at Individual Double-Strand Breaks.” *Nat Cell Biol* 19 (12): 1400–1411. https://doi.org/10.1038/ncb3643.

Michelini, Flavia, Ameya P. Jalihal, Sofia Francia, Chance Meers, Zachary T. Neeb, Francesca Rossiello, Ubaldo Gioia, et al. 2018. “From ‘Cellular’ RNA to ‘Smart’ RNA: Multiple Roles of RNA in Genome Stability and Beyond.” *Chemical Reviews* 118 (8): 4365–4403. https://doi.org/10.1021/acs.chemrev.7b00487.

Miller, J., A. D. McLachlan, and A. Klug. 1985. “Repetitive Zinc-Binding Domains in the Protein Transcription Factor IIIA from Xenopus Oocytes.” *The EMBO Journal* 4 (6): 1609–14. https://doi.org/10.1002/j.1460-2075.1985.tb03825.x.

Miller, Jeffrey C., Siyuan Tan, Guijuan Qiao, Kyle A. Barlow, Jianbin Wang, Danny F. Xia, Xiangdong Meng, et al. 2011. “A TALE Nuclease Architecture for Efficient Genome Editing.” *Nature Biotechnology* 29 (2): 143–50. https://doi.org/10.1038/nbt.1755.

Mirman, Zachary, and Titia de Lange. 2020. “53BP1: A DSB Escort.” *Genes & Development* 34 (1–2): 7–23. https://doi.org/10.1101/gad.333237.119.

Mirman, Zachary, Francisca Lottersberger, Hiroyuki Takai, Tatsuya Kibe, Yi Gong, Kaori

Takai, Alessandro Bianchi, Michal Zimmermann, Daniel Durocher, and Titia de Lange. 2018. “53BP1–RIF1–Shieldin Counteracts DSB Resection through CST- and Polα-Dependent Fill-In.” *Nature* 560 (7716): 112–16. https://doi.org/10.1038/s41586-018-0324-7.

Mirzayans, Razmik, Bonnie Andrais, April Scott, Ying W. Wang, Piyush Kumar, and David Murray. 2017. “Multinucleated Giant Cancer Cells Produced in Response to Ionizing Radiation Retain Viability and Replicate Their Genome.” *International Journal of Molecular Sciences* 18 (2). https://doi.org/10.3390/ijms18020360.

Mojica, Francisco J.M., César Díez-Villaseñor, Jesús García-Martínez, and Elena Soria. 2005. “Intervening Sequences of Regularly Spaced Prokaryotic Repeats Derive from Foreign Genetic Elements.” *Journal of Molecular Evolution* 60 (2): 174–82. https://doi.org/10.1007/s00239-004-0046-3.

Moscou, Matthew J., and Adam J. Bogdanove. 2009. “A Simple Cipher Governs DNA Recognition by TAL Effectors.” *Science* 326 (5959): 1501. https://doi.org/10.1126/science.1178817.

Mout, Rubul, Moumita Ray, Yi-Wei Lee, Federica Scaletti, and Vincent M Rotello. 2017. “In Vivo Delivery of CRISPR/Cas9 for Therapeutic Gene Editing: Progress and Challenges.” *Bioconjug Chem* 28 (4): 880–84. https://doi.org/10.1021/acs.bioconjchem.7b00057.

Nalbandian, Ani, Kartik Sehgal, Aakriti Gupta, Mahesh V. Madhavan, Claire McGroder, Jacob S. Stevens, Joshua R. Cook, et al. 2021. “Post-Acute COVID-19 Syndrome.” *Nature Medicine* 27 (4): 601–15. https://doi.org/10.1038/s41591-021-01283-z.

Narasimha, Anil M, Manuel Kaulich, Gary S Shapiro, Yoon J Choi, Piotr Sicinski, and Steven F Dowdy. 2014. “Cyclin D Activates the Rb Tumor Suppressor by Mono-Phosphorylation.” *ELife* 3: 1–21. https://doi.org/10.7554/elife.02872.

Naruyama, Hiromichi, Midori Shimada, Hiroyuki Niida, Doaa H. Zineldeen, Yoshihiro Hashimoto, Kenjiro Kohri, and Makoto Nakanishi. 2008. “Essential Role of Chk1 in S Phase Progression through Regulation of RNR2 Expression.” *Biochemical and Biophysical Research Communications* 374 (1): 79–83. https://doi.org/10.1016/j.bbrc.2008.06.112.

Nguyen, Quan, Julio Aguado, Fabio Iannelli, Ana Maria Suzuki, Francesca Rossiello, Fabrizio D’Adda Di Fagagna, and Piero Carninci. 2018. “Target-Enrichment Sequencing for Detailed Characterization of Small RNAs.” *Nature Protocols* 13 (4): 768–86. https://doi.org/10.1038/nprot.2018.001.

Nimonkar, Amitabh V., Jochen Genschel, Eri Kinoshita, Piotr Polaczek, Judith L. Campbell, Claire Wyman, Paul Modrich, and Stephen C. Kowalczykowski. 2011. “BLM-DNA2-RPA-MRN and EXO1-BLM-RPA-MRN Constitute Two DNA End Resection Machineries for Human DNA Break Repair.” *Genes and Development* 25 (4): 350–62. https://doi.org/10.1101/gad.2003811.

Niu, Yuyu, Bin Shen, Yiqiang Cui, Yongchang Chen, Jianying Wang, Lei Wang, Yu Kang, et al. 2014. “Generation of Gene-Modified Cynomolgus Monkey via Cas9/RNA-Mediated Gene Targeting in One-Cell Embryos.” *Cell* 156 (4): 836–43. https://doi.org/10.1016/j.cell.2014.01.027.

Noordermeer, Sylvie M., Salomé Adam, Dheva Setiaputra, Marco Barazas, Stephen J.

Pettitt, Alexanda K. Ling, Michele Olivieri, et al. 2018. “The Shieldin Complex Mediates 53BP1-Dependent DNA Repair.” *Nature* 560 (7716): 117–21. https://doi.org/10.1038/s41586-018-0340-7.

Northall, Sarah J., Ivana Ivančić-Baće, Panos Soultanas, and Edward L. Bolt. 2016. “Remodeling and Control of Homologous Recombination by DNA Helicases and Translocases That Target Recombinases and Synapsis.” *Genes* 7 (8): 1–12. https://doi.org/10.3390/genes7080052.

O’Connor, M. J., N. M.B. Martin, and G. C.M. Smith. 2007. “Targeted Cancer Therapies Based on the Inhibition of DNA Strand Break Repair.” *Oncogene* 26 (56): 7816–24. https://doi.org/10.1038/sj.onc.1210879.

O’Connor, Mark J. 2015. “Targeting the DNA Damage Response in Cancer.” *Molecular Cell* 60 (4): 547–60. https://doi.org/10.1016/j.molcel.2015.10.040.

Ogrunc, Müge, and Fabrizio d’Adda di Fagagna. 2011. “Never-Ageing Cellular Senescence.” *European Journal of Cancer* 47 (11): 1616–22. https://doi.org/10.1016/j.ejca.2011.04.003.

Ohle, Corina, Rafael Tesorero, Géza Schermann, Nikolay Dobrev, Irmgard Sinning, and Tamás Fischer. 2016. “Transient RNA-DNA Hybrids Are Required for Efficient Double-Strand Break Repair.” *Cell* 167 (4): 1001-1013.e7. https://doi.org/10.1016/j.cell.2016.10.001.

Paludan, Søren R., Andrew G. Bowie, Kristy A. Horan, and Katherine A. Fitzgerald. 2011. “Recognition of Reovirus RNAs by the Innate Immune System.” *Nat Rev Immunol* 11 (2): 143–54. https://doi.org/10.1038/nri2937.

Panier, Stephanie, and Daniel Durocher. 2009. “Regulatory Ubiquitylation in Response to DNA Double-Strand Breaks.” *DNA Repair* 8 (4): 436–43. https://doi.org/10.1016/j.dnarep.2009.01.013.

Pankotai, Tibor, Céline Bonhomme, David Chen, and Evi Soutoglou. 2012. “DNAPKcs-Dependent Arrest of RNA Polymerase II Transcription in the Presence of DNA Breaks.” *Nature Structural and Molecular Biology* 19 (3): 276–82. https://doi.org/10.1038/nsmb.2224.

Paquet, Dominik, Dylan Kwart, Antonia Chen, Andrew Sproul, Samson Jacob, Shaun Teo, Kimberly Moore Olsen, Andrew Gregg, Scott Noggle, and Marc Tessier-Lavigne. 2016. “Efficient Introduction of Specific Homozygous and Heterozygous Mutations Using CRISPR/Cas9.” *Nature* 533 (7601): 125–29. https://doi.org/10.1038/nature17664.

Parrilla-Castellar, Edgardo R., Sonnet J.H. Arlander, and Larry Karnitz. 2004. “Dial 9-1-1 for DNA Damage: The Rad9-Hus1-Rad1 (9-1-1) Clamp Complex.” *DNA Repair* 3 (8–9): 1009–14. https://doi.org/10.1016/j.dnarep.2004.03.032.

Perdikari, Theodora Myrto, Anastasia C Murthy, Veronica H Ryan, Scott Watters, Mandar T Naik, and Nicolas L Fawzi. 2020. “SARS-CoV-2 Nucleocapsid Protein Phase-Separates with RNA and with Human HnRNPs.” *The EMBO Journal*, e106478. https://doi.org/10.15252/embj.2020106478.

Pessina, Fabio, Fabio Giavazzi, Yandong Yin, Ubaldo Gioia, Valerio Vitelli, Alessandro Galbiati, Sara Barozzi, et al. 2019. “Functional Transcription Promoters at DNA

Double-Strand Breaks Mediate RNA-Driven Phase Separation of Damage-Response Factors." *Nature Cell Biology* 21 (10): 1286–99. https://doi.org/10.1038/s41556-019-0392-4.

Pessina, Fabio, Ubaldo Gioia, Ornella Brandi, Stefania Farina, Marta Ceccon, Sofia Francia, and Fabrizio d'Adda di Fagagna. 2021. "DNA Damage Triggers a New Phase in Neurodegeneration." *Trends in Genetics* 37 (4): 337–54. https://doi.org/10.1016/j.tig.2020.09.006.

Peter, Marcus E. 2011. "Apoptosis Meets Necrosis." *Nature* 471 (7338): 310–12. https://doi.org/10.1038/471310a.

Peterson, Shaun E., Yinyin Li, Foon Wu-Baer, Brian T. Chait, Richard Baer, Hong Yan, Max E. Gottesman, and Jean Gautier. 2013. "Activation of DSB Processing Requires Phosphorylation of CtIP by ATR." *Molecular Cell* 49 (4): 657–67. https://doi.org/10.1016/j.molcel.2012.11.020.

Pickar-Oliver, Adrian, and Charles A. Gersbach. 2019. "The next Generation of CRISPR–Cas Technologies and Applications." *Nature Reviews Molecular Cell Biology* 20 (8): 490–507. https://doi.org/10.1038/s41580-019-0131-5.

Polo, Sophie E., and Stephen P. Jackson. 2011. "Dynamics of DNA Damage Response Proteins at DNA Breaks: A Focus on Protein Modifications." *Genes and Development* 25 (5): 409–33. https://doi.org/10.1101/gad.2021311.

Pourcel, C., G. Salvignol, and Gilles Vergnaud. 2005. "CRISPR Elements in Yersinia Pestis Acquire New Repeats by Preferential Uptake of Bacteriophage DNA, and Provide Additional Tools for Evolutionary Studies." *Microbiology* 151 (3): 653–63. https://doi.org/10.1099/mic.0.27437-0.

Qi, Lei S., Matthew H. Larson, Luke A. Gilbert, Jennifer A. Doudna, Jonathan S. Weissman, Adam P. Arkin, and Wendell A. Lim. 2013. "Repurposing CRISPR as an RNA-Γuided Platform for Sequence-Specific Control of Gene Expression." *Cell* 152 (5): 1173–83. https://doi.org/10.1016/j.cell.2013.02.022.

Qi, Yiping, Yong Zhang, Joshua A. Baller, and Daniel F. Voytas. 2016. "Histone H2AX and the Small RNA Pathway Modulate Both Non-Homologous End-Joining and Homologous Recombination in Plants." *Mutation Research - Fundamental and Molecular Mechanisms of Mutagenesis* 783: 9–14. https://doi.org/10.1016/j.mrfmmm.2015.12.002.

Qiao, Yichun, Huan He, Philip Jonsson, Indranil Sinha, Chunyan Zhao, and Karin Dahlman-Wright. 2016. "AP-1 Is a Key Regulator of Proinflammatory Cytokine TNFα-Mediated Triple-Negative Breast Cancer Progression." *Journal of Biological Chemistry* 291 (10): 5068–79. https://doi.org/10.1074/jbc.M115.702571.

Rajasekharan, Sreejith, Rafaela Milan Bonotto, Lais Nascimento Alves, Yvette Kazungu, Monica Poggianella, Pamela Martinez-Orellana, Natasa Skoko, Sulena Polez, and Alessandro Marcello. 2021. "Inhibitors of Protein Glycosylation Are Active against the Coronavirus Severe Acute Respiratory Syndrome Coronavirus Sars-Cov-2." *Viruses* 13 (5). https://doi.org/10.3390/v13050808.

Ran, F Ann, Patrick D Hsu, Chie-yu Lin, Jonathan S Gootenberg, Alexandro Trevino, David a Scott, Azusa Inoue, Shogo Matoba, Yi Zhang, and Feng Zhang. 2013. "Double Nicking by RNA-Guided CRISPR Cas9 for Enhanced Genome Editing

Specificity." *Cell* 154 (6): 1380–89. https://doi.org/10.1016/j.cell.2013.08.021..

Ran, F Ann, Patrick D Hsu, Jason Wright, Vineeta Agarwala, David A Scott, and Feng Zhang. 2013. "Genome Engineering Using the CRISPR-Cas9 System." *Nature Protocols* 8 (11): 2281–2308. https://doi.org/10.1038/nprot.2013.143.

Redon, Christophe E., Jennifer S. Dickey, William M. Bonner, and Olga A. Sedelnikova. 2009. "γ-H2AX as a Biomarker of DNA Damage Induced by Ionizing Radiation in Human Peripheral Blood Lymphocytes and Artificial Skin." *Advances in Space Research* 43 (8): 1171–78. https://doi.org/10.1016/j.asr.2008.10.011.

Ren, He, Chaobing Ma, Haoran Peng, Bo Zhang, Lulin Zhou, Yan Su, Xiaoyan Gao, and Hongyan Huang. 2021. "Micronucleus Production, Activation of DNA Damage Response and CGAS-STING Signaling in Syncytia Induced by SARS-CoV-2 Infection." *Biology Direct* 16 (1): 1–10. https://doi.org/10.1186/s13062-021-00305-7.

Richardson, Christopher D., Graham J. Ray, Mark A. DeWitt, Gemma L. Curie, and Jacob E. Corn. 2016. "Enhancing Homology-Directed Genome Editing by Catalytically Active and Inactive CRISPR-Cas9 Using Asymmetric Donor DNA." *Nature Biotechnology* 34 (3): 339–44. https://doi.org/10.1038/nbt.3481.

Riley, Todd, Eduardo Sontag, Patricia Chen, and Arnold Levine. 2008. "Transcriptional Control of Human P53-Regulated Genes." *Nature Reviews Molecular Cell Biology* 9 (5): 402–12. https://doi.org/10.1038/nrm2395.

Rinaldi, Carlo, and Matthew J.A. Wood. 2018. "Antisense Oligonucleotides: The next Frontier for Treatment of Neurological Disorders." *Nature Reviews Neurology* 14 (1): 9–22. https://doi.org/10.1038/nrneurol.2017.148.

Robert, Francis, Mathilde Barbeau, Sylvain Éthier, Josée Dostie, and Jerry Pelletier. 2015. "Pharmacological Inhibition of DNA-PK Stimulates Cas9-Mediated Genome Editing." *Genome Medicine* 7 (1): 1–11. https://doi.org/10.1186/s13073-015-0215-6.

Rodier, Francis, Jean-philippe Coppé, Christopher K Patil, Wieteke A M Hoeijmakers, Denise P Muñoz, Saba R Raza, Adam Freund, Eric Campeau, Albert R Davalos, and Judith Campisi. 2009. "Persistent DNA Damage Signalling Triggers Senescence-Associated Inflammatory Cytokine Secretion" 11 (8). https://doi.org/10.1038/ncb1909.

Roh, Jae Il, Junghoon Lee, Seong Uk Park, Young Shin Kang, Jaehoon Lee, Ah Reum Oh, Dong Joon Choi, Ji Young Cha, and Han Woong Lee. 2018. "CRISPR-Cas9-Mediated Generation of Obese and Diabetic Mouse Models." *Experimental Animals* 67 (2): 229–37. https://doi.org/10.1538/expanim.17-0123.

Roidos, Paris, Stephanie Sungalee, Salvatore Benfatto, Özdemirhan Serçin, Adrian M. Stütz, Amir Abdollahi, Jan Mauer, Frank T. Zenke, Jan O. Korbel, and Balca R. Mardin. 2020. "A Scalable CRISPR/Cas9-Based Fluorescent Reporter Assay to Study DNA Double-Strand Break Repair Choice." *Nature Communications* 11 (1). https://doi.org/10.1038/s41467-020-17962-3.

Rosenblum, Daniel, Anna Gutkin, Ranit Kedmi, Srinivas Ramishetti, Nuphar Veiga, Ashley M. Jacobi, Mollie S. Schubert, et al. 2020. "CRISPR-Cas9 Genome Editing Using Targeted Lipid Nanoparticles for Cancer Therapy." *Science Advances* 6 (47). https://doi.org/10.1126/sciadv.abc9450.

Rossiello, Francesca, Julio Aguado, Sara Sepe, Fabio Iannelli, Quan Nguyen, Sethuramasundaram Pitchiaya, Piero Carninci, and Fabrizio D.Adda Di Fagagna. 2017. "DNA Damage Response Inhibition at Dysfunctional Telomeres by Modulation of Telomeric DNA Damage Response RNAs." *Nature Communications* 8 (May 2016). https://doi.org/10.1038/ncomms13980.

Rossiello, Francesca, Utz Herbig, Maria Pia Longhese, Marzia Fumagalli, and Fabrizio d'Adda di Fagagna. 2014. "Irreparable Telomeric DNA Damage and Persistent DDR Signalling as a Shared Causative Mechanism of Cellular Senescence and Ageing." *Current Opinion in Genetics and Development* 26: 89–95. https://doi.org/10.1016/j.gde.2014.06.009.

Rowland, Raymond R. R., Vinita Chauhan, Ying Fang, Andrew Pekosz, Maureen Kerrigan, and Miriam D. Burton. 2005. "Intracellular Localization of the Severe Acute Respiratory Syndrome Coronavirus Nucleocapsid Protein: Absence of Nucleolar Accumulation during Infection and after Expression as a Recombinant Protein in Vero Cells." *Journal of Virology* 79 (17): 11507–12. https://doi.org/10.1128/jvi.79.17.11507-11512.2005.

Rowley, Janet D. 1973. "A New Consistent Chromosomal Abnormality in Chronic Myelogenous Leukaemia Identified by Quinacrine Fluorescence and Giemsa Staining." *Nature* 243: 290–93. https://doi.org/https://doi.org/10.1038/243290a0.

Ruf, Ingrid K., Paul W. Rhyne, Hui Yang, Corina M. Borza, Lindsey M. Hutt-Fletcher, John L. Cleveland, and Jeffery T. Sample. 1999. "Epstein-Barr Virus Regulates c-MYC, Apoptosis, and Tumorigenicity in Burkitt Lymphoma." *Molecular and Cellular Biology* 19 (3): 1651–60. https://doi.org/10.1128/mcb.19.3.1651.

Ryan, Ellis L., Robert Hollingworth, and Roger J. Grand. 2016. "Activation of the DNA Damage Response by RNA Viruses." *Biomolecules* 6 (1): 2–24. https://doi.org/10.3390/biom6010002.

Sabari, Benjamin R, Alessandra Dall Agnese, Ann Boija, Isaac A Klein, L Eliot, Krishna Shrinivas, Brian J Abraham, et al. 2018. "Coactivator Condensation at Super-Enhancers Links Phase Separation and Gene Control" 361 (6400): 1–24. https://doi.org/10.1126/science.aar3958.Coactivator.

San Filippo, Joseph, Patrick Sung, and Hannah Klein. 2008. "Mechanism of Eukaryotic Homologous Recombination." *Annual Review of Biochemistry* 77: 229–57. https://doi.org/10.1146/annurev.biochem.77.061306.125255.

Sancar, Aziz, Laura A. Lindsey-Boltz, Keziban Ünsal-Kaçmaz, and Stuart Linn. 2004. "Molecular Mechanisms of Mammalian DNA Repair and the DNA Damage Checkpoints." *Annual Review of Biochemistry* 73: 39–85. https://doi.org/10.1146/annurev.biochem.73.011303.073723.

Sandre-Giovannoli, Annachiara De, Rafaëlle Bernard, Pierre Cau, Claire Navarro, Jeanne Amiel, Irène Boccaccio, Stanislas Lyonnet, et al. 2003. "Lamin A Truncation in Hutchinson-Gilford Progeria." *Science* 300 (5628): 2055. https://doi.org/10.1126/science.1084125.

Sansam, Christopher L., Jennifer L. Shepard, Kevin Lai, Alessandra Ianari, Paul S. Danielian, Adam Amsterdam, Nancy Hopkins, and Jacqueline A. Lees. 2006. "DTL/CDT2 Is Essential for Both CDT1 Regulation and the Early G2/M Checkpoint." *Genes and Development* 20 (22): 3117–29.

https://doi.org/10.1101/gad.1482106.

Santaguida, Stefano, and Angelika Amon. 2015. “Short- and Long-Term Effects of Chromosome Mis-Segregation and Aneuploidy.” *Nature Reviews Molecular Cell Biology* 16 (8): 473–85. https://doi.org/10.1038/nrm4025.

Sartori, Alessandro A., Claudia Lukas, Julia Coates, Martin Mistrik, Shuang Fu, Jiri Bartek, Richard Baer, Jiri Lukas, and Stephen P. Jackson. 2007. “Human CtIP Promotes DNA End Resection.” *Nature* 450 (7169): 509–14. https://doi.org/10.1038/nature06337.

Sato, Hiro, Atsuko Niimi, Takaaki Yasuhara, Tiara Bunga Mayang Permata, Yoshihiko Hagiwara, Mayu Isono, Endang Nuryadi, et al. 2017. “DNA Double-Strand Break Repair Pathway Regulates PD-L1 Expression in Cancer Cells.” *Nature Communications* 8 (1). https://doi.org/10.1038/s41467-017-01883-9.

Savastano, Adriana, Alain Ibáñez de Opakua, Marija Rankovic, and Markus Zweckstetter. 2020. “Nucleocapsid Protein of SARS-CoV-2 Phase Separates into RNA-Rich Polymerase-Containing Condensates.” *Nature Communications* 11 (6041). https://doi.org/10.1038/s41467-020-19843-1.

Schep, Ruben, Eva K. Brinkman, Christ Leemans, Xabier Vergara, Robin H. van der Weide, Ben Morris, Tom van Schaik, et al. 2021. “Impact of Chromatin Context on Cas9-Induced DNA Double-Strand Break Repair Pathway Balance.” *Molecular Cell* 81 (10): 2216-2230.e10. https://doi.org/10.1016/j.molcel.2021.03.032.

Schiroli, Giulia, Anastasia Conti, Samuele Ferrari, Lucrezia della Volpe, Aurelien Jacob, Luisa Albano, Stefano Beretta, et al. 2019. “Precise Gene Editing Preserves Hematopoietic Stem Cell Function Following Transient P53-Mediated DNA Damage Response.” *Cell Stem Cell* 24: 551–65. https://doi.org/10.1016/j.stem.2019.02.019.

Schumann, Kathrin, Steven Lin, Eric Boyer, Dimitre R. Simeonov, Meena Subramaniam, Rachel E. Gate, Genevieve E. Haliburton, et al. 2015. “Generation of Knock-in Primary Human T Cells Using Cas9 Ribonucleoproteins.” *Proceedings of the National Academy of Sciences* 112 (33): 10437–42. https://doi.org/10.1073/pnas.1512503112.

Scott, Duncan E., Nicola J. Francis-Newton, May E. Marsh, Anthony G. Coyne, Gerhard Fischer, Tommaso Moschetti, Andrew R. Bayly, et al. 2021. “A Small-Molecule Inhibitor of the BRCA2-RAD51 Interaction Modulates RAD51 Assembly and Potentiates DNA Damage-Induced Cell Death.” *Cell Chemical Biology* 28 (6): 835-847.e5. https://doi.org/10.1016/j.chembiol.2021.02.006.

Serhan, Charles N., and John Savill. 2005. “Resolution of Inflammation: The Beginning Programs the End.” *Nature Immunology* 6 (12): 1191–97. https://doi.org/10.1038/ni1276.

Shalem, Ophir, Neville E Sanjana, Ella Hartenian, Xi Shi, David A Scott, Dirk Heckl, Benjamin L Ebert, David E Root, John G Doench, and Feng Zhang. 2014. “Genome-Scale CRISPR-Cas9 Knockout Screening in Human Cells.” *Science* 343 (6166): 84–87. https://doi.org/10.1126/science.1247005.

Shamanna, Raghavendra A., Huiming Lu, Jessica K. De Freitas, Jane Tian, Deborah L. Croteau, and Vilhelm A. Bohr. 2016. “WRN Regulates Pathway Choice between Classical and Alternative Non-Homologous End Joining.” *Nature Communications* 7

(May): 1–12. https://doi.org/10.1038/ncomms13785.

Shanbhan, Niraj M., Ilona U. Rafalska-Metcalf, Carlo Balane- Bolivar, Susan M. Janicki, and Roger A Greenberg. 2010. “An ATM-Dependent Transcriptional Silencing Program Is Transmitted Through Chromatin in Cis to DNA Double Strand Breaks.” *Cell* 141 (6): 970–81. https://doi.org/10.1016/j.cell.2010.04.038.An.

Sharma, Sheetal, Roopesh Anand, Xuzhu Zhang, Sofia Francia, Flavia Michelini, Alessandro Galbiati, Hannah Williams, et al. 2021. “MRE11-RAD50-NBS1 Complex Is Sufficient to Promote Transcription by RNA Polymerase II at Double-Strand Breaks by Melting DNA Ends.” *Cell Reports* 34 (1): 108565. https://doi.org/10.1016/j.celrep.2020.108565.

Shechter, David, Vincenzo Costanzo, and Jean Gautier. 2004. “Regulation of DNA Replication by ATR: Signaling in Response to DNA Intermediates.” *DNA Repair* 3 (8–9): 901–8. https://doi.org/10.1016/j.dnarep.2004.03.020.

Shibata, Mikihiro, Hiroshi Nishimasu, Noriyuki Kodera, Seiichi Hirano, Toshio Ando, Takayuki Uchihashi, and Osamu Nureki. 2017. “Real-Space and Real-Time Dynamics of CRISPR-Cas9 Visualized by High-Speed Atomic Force Microscopy.” *Nature Communications* 8 (1): 1–9. https://doi.org/10.1038/s41467-017-01466-8.

Shiloh, Yosef. 2006. “The ATM-Mediated DNA-Damage Response: Taking Shape.” *Trends in Biochemical Sciences* 31 (7): 402–10. https://doi.org/10.1016/j.tibs.2006.05.004.

Shtivelman, E, B Lifshitz, Robert P Gale, and Eli Cananni. 1985. “Fused Transcript of Abl and Bcr Genes in Chronic Myelogenous Leukaemia.” *Nature* 315: 550–54. https://doi.org/https://doi.org/10.1038/315550a0.

Smith, Cory, Athurva Gore, Wei Yan, Leire Abalde-Atristain, Zhe Li, Chaoxia He, Ying Wang, et al. 2014. “Whole-Genome Sequencing Analysis Reveals High Specificity of CRISPR/Cas9 and TALEN-Based Genome Editing in Human IPSCs.” *Cell Stem Cell* 15 (1): 12–13. https://doi.org/10.1016/j.stem.2014.06.011.

Soppe, Jasper Adriaan, and Robert Jan Lebbink. 2017. “Antiviral Goes Viral: Harnessing CRISPR/Cas9 to Combat Viruses in Humans.” *Trends in Microbiology* 25 (10): 833–50. https://doi.org/10.1016/j.tim.2017.04.005.

Soulas-Sprauel, P., P. Rivera-Munoz, L. Malivert, G. Le Guyader, V. Abramowski, P. Revy, and J. P. De Villartay. 2007. “V(D)J and Immunoglobulin Class Switch Recombinations: A Paradigm to Study the Regulation of DNA End-Joining.” *Oncogene* 26 (56): 7780–91. https://doi.org/10.1038/sj.onc.1210875.

Spycher, Christoph, Edward S. Miller, Kelly Townsend, Lucijana Pavic, Nicholas A. Morrice, Pavel Janscak, Grant S. Stewart, and Manuel Stucki. 2008. “Constitutive Phosphorylation of MDC1 Physically Links the MRE11-RAD50-NBS1 Complex to Damaged Chromatin.” *Journal of Cell Biology* 181 (2): 227–40. https://doi.org/10.1083/jcb.200709008.

Sriram, Ganapathy, Lauren E. Milling, Jung Kuei Chen, Yi Wen Kong, Brian A. Joughin, Wuhbet Abraham, Susanne Swartwout, Erika D. Handly, Darrell J. Irvine, and Michael B. Yaffe. 2021. “The Injury Response to DNA Damage in Live Tumor Cells Promotes Antitumor Immunity.” *Science Signaling* 14 (705): eabc4764. https://doi.org/10.1126/scisignal.abc4764.

Staahl, Brett T., Madhurima Benekareddy, Claire Coulon-Bainier, Ashwin A. Banfal, Stephen N. Floor, Jennifer K. Sabo, Cole Urnes, Gabriela Acevedo Munares, Anirvan Ghosh, and Jennifer A. Doudna. 2017. "Efficient Genome Editing in the Mouse Brain by Local Delivery of Engineered Cas9 Ribonucleoprotein Complexes." *Nature Biotechnology* 35 (5): 431–34. https://doi.org/10.1038/nbt.3806.

Sternberg, Samuel H., and Jennifer A. Doudna. 2015. "Expanding the Biologist's Toolkit with CRISPR-Cas9." *Molecular Cell* 58 (4): 568–74. https://doi.org/10.1016/j.molcel.2015.02.032.

Stewart, Grant S., Bin Wang, Colin R. Bigneli, A. Malcolm R. Taylor, and Stephen J. Elledge. 2003. "MDC1 Is a Mediator of the Mammalian DNA Damage Checkpoint." *Nature* 421 (6926): 961–66. https://doi.org/10.1038/nature01446.

Stringer, Brett W., Bryan W. Day, Rochelle C.J. D'Souza, Paul R. Jamieson, Kathleen S. Ensbey, Zara C. Bruce, Yi Chieh Lim, et al. 2019. "A Reference Collection of Patient-Derived Cell Line and Xenograft Models of Proneural, Classical and Mesenchymal Glioblastoma." *Scientific Reports* 9 (1): 1–14. https://doi.org/10.1038/s41598-019-41277-z.

Stukalov, Alexey, Virginie Girault, Vincent Grass, Ozge Karayel, Valter Bergant, Christian Urban, Darya A. Haas, et al. 2021. *Multilevel Proteomics Reveals Host Perturbations by SARS-CoV-2 and SARS-CoV*. *Nature*. https://doi.org/10.1038/s41586-021-03493-4.

Sturzenegger, Andreas, Kamila Burdova, Radhakrishnan Kanagaraj, Maryna Levikova, Cosimo Pinto, Petr Cejka, and Pavel Janscak. 2014. "DNA2 Cooperates with the WRN and BLM RecQ Helicases to Mediate Long-Range DNA End Resection in Human Cells." *Journal of Biological Chemistry* 289 (39): 27314–26. https://doi.org/10.1074/jbc.M114.578823.

Sun, Yueru, Thomas J. McCorvie, Luke A. Yates, and Xiaodong Zhang. 2020. "Structural Basis of Homologous Recombination." *Cellular and Molecular Life Sciences* 77 (1): 3–18. https://doi.org/10.1007/s00018-019-03365-1.

Surova, O., and B. Zhivotovsky. 2013. "Various Modes of Cell Death Induced by DNA Damage." *Oncogene* 32 (33): 3789–97. https://doi.org/10.1038/onc.2012.556.

Swastika Sur and Devendra K. Agrawal. 2016. "Phosphatases and Kinases Regulating CDC25 Activity in the Cell Cycle: Clinical Implications of CDC25 Overexpression and Potential Treatment Strategies Swastika." *Mol Cell Biochem* 416 (1–2): 33–46. https://doi.org/10.1007/s11010-016-2693-2.Phosphatases.

Swift, L. H., and R. M. Golsteyn. 2016. *The Relationship Between Checkpoint Adaptation and Mitotic Catastrophe in Genomic Changes in Cancer Cells*. *Genome Stability: From Virus to Human Application*. Elsevier Inc. https://doi.org/10.1016/B978-0-12-803309-8.00022-7.

Swift, Michelle L., Kate Beishline, Samuel Flashner, and Jane Azizkhan-Clifford. 2021. "DSB Repair Pathway Choice Is Regulated by Recruitment of 53BP1 through Cell Cycle-Dependent Regulation of Sp1." *Cell Reports* 34 (11): 108840. https://doi.org/10.1016/j.celrep.2021.108840.

Symington, Lorraine S., and Jean Gautier. 2011. "Double-Strand Break End Resection and Repair Pathway Choice." *Annual Review of Genetics* 45: 247–71.

https://doi.org/10.1146/annurev-genet-110410-132435.

Taylor, Martin R.G., Mário Špírek, Kathy R. Chaurasiya, Jordan D. Ward, Raffaella Carzaniga, Xiong Yu, Edward H. Egelman, et al. 2015. “Rad51 Paralogs Remodel Pre-Synaptic Rad51 Filaments to Stimulate Homologous Recombination.” *Cell* 162 (2): 271–86. https://doi.org/10.1016/j.cell.2015.06.015.

Thomsen, Martin K., Ramya Nandakumar, Daniela Stadler, Antje Malo, Roser Marin Valls, Fan Wang, Line S. Reinert, et al. 2016. “Lack of Immunological DNA Sensing in Hepatocytes Facilitates Hepatitis B Virus Infection.” *Hepatology* 64 (3): 746–59. https://doi.org/10.1002/hep.28685.

Timani, Khalid Amine, Qingjiao Liao, Linbai Ye, Yingchun Zeng, Jing Liu, Yi Zheng, Li Ye, et al. 2005. “Nuclear/Nucleolar Localization Properties of C-Terminal Nucleocapsid Protein of SARS Coronavirus.” *Virus Research* 114 (1–2): 23–34. https://doi.org/10.1016/j.virusres.2005.05.007.

Trimarchi, Jeffrey M., and Jacqueline A. Lees. 2002. “Sibling Rivalry in the E2F Family.” *Nature Reviews Molecular Cell Biology* 3 (1): 11–20. https://doi.org/10.1038/nrm714.

Tsai, Shengdar Q, Nicolas Wyvekens, Cyd Khayter, Jennifer A Foden, Vishal Thapar, Deepak Reyon, Mathew J Goodwin, Martin J Aryee, and Keith Joung. 2014. “Dimeric CRISPR RNA-Guided FokI Nucleases for Highly Specific Genome Editing.” *Nat Biotechnol* 32 (6): 569–76. https://doi.org/10.1038/nbt.2908.

Turnell, Andrew S., and Roger J. Grand. 2012. “DNA Viruses and the Cellular DNA-Damage Response.” *Journal of General Virology* 93 (PART 10): 2076–97. https://doi.org/10.1099/vir.0.044412-0.

Urnov, Fyodor D. 2021. “Imagine CRISPR Cures.” *Molecular Therapy* 29 (11): 3103–6. https://doi.org/10.1016/j.ymthe.2021.10.019.

Urnov, Fyodor D., Edward J. Rebar, Michael C. Holmes, H. Steve Zhang, and Philip D. Gregory. 2010. “Genome Editing with Engineered Zinc Finger Nucleases.” *Nature Reviews Genetics* 11 (9): 636–46. https://doi.org/10.1038/nrg2842.

V’kovski, Philip, Annika Kratzel, Silvio Steiner, Hanspeter Stalder, and Volker Thiel. 2021. “Coronavirus Biology and Replication: Implications for SARS-CoV-2.” *Nature Reviews Microbiology* 19 (3): 155–70. https://doi.org/10.1038/s41579-020-00468-6.

Vakifahmetoglu, H., M. Olsson, and B. Zhivotovsky. 2008. “Death through a Tragedy: Mitotic Catastrophe.” *Cell Death and Differentiation* 15 (7): 1153–62. https://doi.org/10.1038/cdd.2008.47.

Vanamee, Éva Scheuring, Sandro Santagata, and Aneel K. Aggarwal. 2001. “FokI Requires Two Specific DNA Sites for Cleavage.” *Journal of Molecular Biology* 309 (1): 69–78. https://doi.org/10.1006/jmbi.2001.4635.

Ventura, Andrea, and Lukas E. Dow. 2017. “Modeling Cancer in the CRISPR Era.” *Annual Review of Cancer Biology* 2: 111–31. https://doi.org/10.1146/annurev-cancerbio-030617-050455.

———. 2018. “Modeling Cancer in the CRISPR Era.” *Annual Review of Cancer Biology* 2: 111–31. https://doi.org/10.1146/annurev-cancerbio-030617-050455.

Veres, Adrian, Bridget S. Gosis, Qiurong Ding, Ryan Collins, Ashok Ragavendran, Harrison Brand, Serkan Erdin, Michael E. Talkowski, and Kiran Musunuru. 2014. "Low Incidence of Off-Target Mutations in Individual CRISPR-Cas9 and TALEN Targeted Human Stem Cell Clones Detected by Whole-Genome Sequencing." *Cell Stem Cell* 15 (1): 27–30. https://doi.org/10.1016/j.stem.2014.04.020.

Victor, Joshua, Jamie Deutsch, Annalis Whitaker, Erica N. Lamkin, Anthony March, Pei Zhou, Jason W. Botten, and Nimrat Chatterjee. 2021. "SARS-CoV-2 Triggers DNA Damage Response in Vero E6 Cells." *Biochemical and Biophysical Research Communications* 579: 141–45. https://doi.org/10.1016/j.bbrc.2021.09.024.

Vitale, Ilio, Lorenzo Galluzzi, Maria Castedo, and Guido Kroemer. 2011. "Mitotic Catastrophe: A Mechanism for Avoiding Genomic Instability." *Nature Reviews Molecular Cell Biology* 12 (6): 385–92. https://doi.org/10.1038/nrm3115.

Vitelli, Valerio, Alessandro Galbiati, Fabio Iannelli, Fabio Pessina, Sheetal Sharma, and Fabrizio D'Adda di Fagagna. 2017. "Recent Advancements in DNA Damage-Transcription Crosstalk and High-Resolution Mapping of DNA Breaks." *Annual Review of Genomics and Human Genetics* 18: 87–113. https://doi.org/10.1146/annurev-genom-091416-035314.

Waldman, Todd, Christoph Lengauer, Kenneth W. Kinzler, and Bert Vogelstein. 1996. "Uncoupling of S Phase and Mitosis Induced by Anticancer Agents in Cells Lacking P21." *Nature* 381 (6584): 713–16. https://doi.org/10.1038/381713a0.

Wang, Jia, Chengrui Shi, Qun Xu, and Hang Yin. 2021. "SARS-CoV-2 Nucleocapsid Protein Undergoes Liquid–Liquid Phase Separation into Stress Granules through Its N-Terminal Intrinsically Disordered Region." *Cell Discovery* 7 (1): 3–7. https://doi.org/10.1038/s41421-020-00240-3.

Wang, Jianbin, and Stephen R. Quake. 2014. "RNA-Guided Endonuclease Provides a Therapeutic Strategy to Cure Latent Herpesviridae Infection." *Proceedings of the National Academy of Sciences of the United States of America* 111 (36): 13157–62. https://doi.org/10.1073/pnas.1410785111.

Wang, Qinhong, and Michael Goldstein. 2016. "Molecular and Cellular Pathobiology Small RNAs Recruit Chromatin-Modifying Enzymes MMSET and Tip60 to Reconfigure Damaged DNA upon Double-Strand Break and Facilitate Repair." https://doi.org/10.1158/0008-5472.CAN-15-2334.

Wang, Shuai, Tong Dai, Ziran Qin, Ting Pan, Feng Chu, Lingfeng Lou, Long Zhang, et al. 2021. "Targeting Liquid–Liquid Phase Separation of SARS-CoV-2 Nucleocapsid Protein Promotes Innate Antiviral Immunity by Elevating MAVS Activity." *Nature Cell Biology* 23 (7): 718–32. https://doi.org/10.1038/s41556-021-00710-0.

Wang, Tim, Jenny J. Wei, David M. Sabatini, and Eric S. Lander. 2014. "Genetic Screens in Human Cells Using the CRISPR/Cas9 System." *Science* 343 (6166): 80–84. https://doi.org/10.1126/science.1246981.

Waters, Lauren S., Brenda K. Minesinger, Mary Ellen Wiltrout, Sanjay D'Souza, Rachel V. Woodruff, and Graham C. Walker. 2009. "Eukaryotic Translesion Polymerases and Their Roles and Regulation in DNA Damage Tolerance." *Microbiology and Molecular Biology Reviews* 73 (1): 134–54. https://doi.org/10.1128/mmbr.00034-08.

Weck, Antoine de, Javad Golji, Michael D. Jones, Joshua M. Korn, Eric Billy, E. Robert

McDonald, Tobias Schmelzle, Hans Bitter, and Audrey Kauffmann. 2018. "Correction of Copy Number Induced False Positives in CRISPR Screens." *PLoS Computational Biology* 14 (7): 1–12. https://doi.org/10.1371/journal.pcbi.1006279.

Wei, Tuo, Qiang Cheng, Yi Li Min, Eric N. Olson, and Daniel J. Siegwart. 2020. "Systemic Nanoparticle Delivery of CRISPR-Cas9 Ribonucleoproteins for Effective Tissue Specific Genome Editing." *Nature Communications* 11 (3232). https://doi.org/10.1038/s41467-020-17029-3.

Wei, Wei, Zhaoqing Ba, Min Gao, Yang Wu, Yanting Ma, Simon Amiard, Charles I. White, Jannie Michaela Rendtlew Danielsen, Yun Gui Yang, and Yijun Qi. 2012. "A Role for Small RNAs in DNA Double-Strand Break Repair." *Cell* 149 (1): 101–12. https://doi.org/10.1016/j.cell.2012.03.002.

Weitzman, Matthew D., Caroline E. Lilley, and Mira S. Chaurushiya. 2010. "Genomes in Conflict: Maintaining Genome Integrity during Virus Infection." *Annual Review of Microbiology* 64: 61–81. https://doi.org/10.1146/annurev.micro.112408.134016.

Williams, Vonetta M., Maria Filippova, Ubaldo Soto, and Penelope J. Duerksen-Hughes. 2011. "HPV-DNA Integration and Carcinogenesis: Putative Roles for Inflammation and Oxidative Stress." *Future Virology* 6 (1): 45–57. https://doi.org/10.2217/fvl.10.73.

Witwicka, Hanna, Sung Yong Hwang, Pablo Reyes-Gutierrez, Hong Jia, Paul E. Odgren, Leah Rae Donahue, Mark J. Birnbaum, and Paul R. Odgren. 2015. "Studies of OC-STAMP in Osteoclast Fusion: A New Knockout Mouse Model, Rescue of Cell Fusion, and Transmembrane Topology." *PLoS ONE* 10 (6): 1–25. https://doi.org/10.1371/journal.pone.0128275.

Wu, Shao Shuai, Qing Cui Li, Chang Qing Yin, Wen Xue, and Chun Qing Song. 2020. "Advances in CRISPR/Cas-Based Gene Therapy in Human Genetic Diseases." *Theranostics* 10 (10): 4374–82. https://doi.org/10.7150/thno.43360.

Xu, Christine L., Merry Z.C. Ruan, Vinit B. Mahajan, and Stephen H. Tsang. 2019. "Viral Delivery Systems for Crispr." *Viruses* 11 (1): 1–12. https://doi.org/10.3390/v11010028.

Xu, Ling Hui, Mei Huang, Shou Guo Fang, and Ding Xiang Liu. 2011. "Coronavirus Infection Induces DNA Replication Stress Partly through Interaction of Its Nonstructural Protein 13 with the P125 Subunit of DNA Polymerase δ." *Journal of Biological Chemistry* 286 (45): 39546–59. https://doi.org/10.1074/jbc.M111.242206.

Yan, Jingyue, Diana D. Kang, Gillian Turnbull, and Yizhou Dong. 2021. "Delivery of CRISPR-Cas9 System for Screening and Editing RNA Binding Proteins in Cancer." *Advanced Drug Delivery Reviews* 180: 114042. https://doi.org/10.1016/j.addr.2021.114042.

Yáñez-Muñoz, Rafael J., Kamaljit S. Balaggan, Angus MacNeil, Steven J. Howe, Manfred Schmidt, Alexander J. Smith, Prateek Buch, et al. 2006. "Effective Gene Therapy with Nonintegrating Lentiviral Vectors." *Nature Medicine* 12 (3): 348–53. https://doi.org/10.1038/nm1365.

Yang, Haitao, and Zihe Rao. 2021. "Structural Biology of SARS-CoV-2 and Implications for Therapeutic Development." *Nature Reviews Microbiology* 19 (11): 685–700. https://doi.org/10.1038/s41579-021-00630-8.

Yang, Yun Gui, and Yijun Qi. 2015. “RNA-Directed Repair of DNA Double-Strand Breaks.” *DNA Repair* 32: 82–85. https://doi.org/10.1016/j.dnarep.2015.04.017.

Yazdi, Parvin T., Yi Wang, Song Zhao, Nimitt Patel, Eva Y.H.P. Lee, and Jun Qin. 2002. “SMC1 Is a Downstream Effector in the ATM/NBS1 Branch of the Human S-Phase Checkpoint.” *Genes and Development* 16 (5): 571–82. https://doi.org/10.1101/gad.970702.

Yin, Di, Sikai Ling, Dawei Wang, Yao Dai, Hao Jiang, Xujiao Zhou, Soren R. Paludan, Jiaxu Hong, and Yujia Cai. 2021. “Targeting Herpes Simplex Virus with CRISPR–Cas9 Cures Herpetic Stromal Keratitis in Mice.” *Nature Biotechnology* 39 (5): 567–77. https://doi.org/10.1038/s41587-020-00781-8.

Zerdes, Ioannis, Alexios Matikas, Jonas Bergh, George Z. Rassidakis, and Theodoros Foukakis. 2018. “Genetic, Transcriptional and Post-Translational Regulation of the Programmed Death Protein Ligand 1 in Cancer: Biology and Clinical Correlations.” *Oncogene* 37 (34): 4639–61. https://doi.org/10.1038/s41388-018-0303-3.

Zhang, Huimin, Chunhong Qin, Changming An, Xiwang Zheng, Shuxin Wen, Wenjie Chen, Xianfang Liu, et al. 2021. “Application of the CRISPR/Cas9-Based Gene Editing Technique in Basic Research, Diagnosis, and Therapy of Cancer.” *Molecular Cancer* 20 (1): 1–22. https://doi.org/10.1186/s12943-021-01431-6.

Zhang, Yong Wei, Tamara L. Jones, Scott E. Martin, Natasha J. Caplen, and Yves Pommier. 2009. “Implication of Checkpoint Kinase-Dependent up-Regulation of Ribonucleotide Reductase R2 in DNA Damage Response.” *Journal of Biological Chemistry* 284 (27): 18085–95. https://doi.org/10.1074/jbc.M109.003020.

Zhao, W., J. B. Steinfeld, F. Liang, X. Chen, D. G. Maranon, C. J. Ma, Y. Kwon, et al. 2017. “Promotion of RAD51-Mediated Homologous DNA Pairing by BRCA1-BARD1.” *Nature.* 47 (3): 549–62. https://doi.org/10.1038/nature24060.Promotion.

Zhao, Yan, Huw D. Thomas, Michael A. Batey, Ian G. Cowell, Caroline J. Richardson, Roger J. Griffin, A. Hilary Calvert, David R. Newell, Graeme C.M. Smith, and Nicola J. Curtin. 2006. “Preclinical Evaluation of a Potent Novel DNA-Dependent Protein Kinase Inhibitor NU7441.” *Cancer Research* 66 (10): 5354–62. https://doi.org/10.1158/0008-5472.CAN-05-4275.

Zhen, Shuai, Ling Hua, Y. Takahashi, S. Narita, Yun Hui Liu, and Yan Li. 2014. “In Vitro and in Vivo Growth Suppression of Human Papillomavirus 16-Positive Cervical Cancer Cells by CRISPR/Cas9.” *Biochemical and Biophysical Research Communications* 450 (4): 1422–26. https://doi.org/10.1016/j.bbrc.2014.07.014.

Zhou, Zhuo, Xinyi Zhang, Xiaobo Lei, Xia Xiao, Tao Jiao, Ruiyi Ma, Xiaojing Dong, Qi Jiang, Wenjing Wang, and Yujin Shi. 2021. “Sensing of Cytoplasmic Chromatin by CGAS Activates Innate Immune Response in SARS-CoV-2 Infection,” no. May. https://doi.org/10.1038/s41392-021-00800-3.

Zhu, Haocheng, Chao Li, and Caixia Gao. 2020. “Applications of CRISPR–Cas in Agriculture and Plant Biotechnology.” *Nature Reviews Molecular Cell Biology* 21 (11): 661–77. https://doi.org/10.1038/s41580-020-00288-9.

Zhu, Yi, Tamara Tchkonia, Heike Fuhrmann-Stroissnigg, Haiming M. Dai, Yuanyuan Y. Ling, Michael B. Stout, Tamar Pirtskhalava, et al. 2016. “Identification of a Novel Senolytic Agent, Navitoclax, Targeting the Bcl-2 Family of Anti-Apoptotic Factors.”

Aging Cell 15 (3): 428–35. https://doi.org/10.1111/acel.12445.

Zimmermann, Michal, and Titia De Lange. 2014. "53BP1: Pro Choice in DNA Repair." *Trends in Cell Biology* 24 (2): 108–17. https://doi.org/10.1016/j.tcb.2013.09.003.

Zimmermann, Michal, Francisca Lottersberger, Sara B Buonomo, Agnel Sfeir, and Titia De Lange. 2013. "53BP1 Regulates DSB Repair Using Rif1 to Control 5′ End Resection." *Science* 339 (6120): 700–704. https://www.science.org.

Ziv, Yael, Dana Bielopolski, Yaron Galanty, Claudia Lukas, Yoichi Taya, David C. Schultz, Jiri Lukas, Simon Bekker-Jensen, Jiri Bartek, and Yosef Shiloh. 2006. "Chromatin Relaxation in Response to DNA Double-Strand Breaks Is Modulated by a Novel ATM-and KAP-1 Dependent Pathway." *Nature Cell Biology* 8 (8): 870–76. https://doi.org/10.1038/ncb1446.

Zou, Lee, and Stephen J. Elledge. 2003. "Sensing DNA Damage through ATRIP Recognition of RPA-SsDNA Complexes." *Science* 300 (5625): 1542–48. https://doi.org/10.1126/science.1083430.